UNIVERSIDAD COMPLUTENSE DE MADRID
FACULTAD DE CIENCIAS QUÍMICAS
Departamento de Química Orgánica I

TESIS DOCTORAL

Mechanically interlocked deriviatives of single walled carbon nanotubes

Derivados mecánicamente enlazados de nanotubos de carbono de pared sencilla

MEMORIA PARA OPTAR AL GRADO DE DOCTOR

PRESENTADA POR

Alberto de Juan Garrudo

Director

Emilio M. Pérez

Madrid, 2018

UNIVERSIDAD COMPLUTENSE DE MADRID

FACULTAD DE CIENCIAS QUÍMICAS

Departamento de Química Orgánica

MECHANICALLY INTERLOCKED DERIVATIVES OF SINGLE WALLED CARBON NANOTUBES

DERIVADOS MECÁNICAMENTE ENLAZADOS DE NANOTUBOS DE CARBONO DE PARED SENCILLA

TESIS DOCTORAL

Alberto de Juan Garrudo

Madrid, 2017

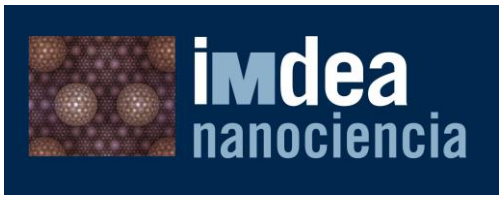

MECHANICALLY INTERLOCKED DERIVATIVES OF SINGLE WALLED CARBON NANOTUBES

DERIVADOS MECÁNICAMENTE ENLAZADOS DE NANOTUBOS DE CARBONO DE PARED SENCILLA

Director:

Dr. Emilio M. Pérez

Memoria que para optar al grado de

DOCTOR EN CIENCIAS QUÍMICAS

presenta

Alberto de Juan Garrudo

MADRID

Febrero, 2017

A mis padres, a mi hermano y a mi novia

Agradecimientos

En primer lugar, me gustaría agradecer a mi director de tesis Emilio M. Pérez, al centro IMDEA Nanociencia y a su director el Profesor Rodolfo Miranda la oportunidad de poder llevar a cabo mis estudios de doctorado en un ambiente científico puntero a nivel nacional. Agradecer también al Ministerio de Educación y al European Research Council la financiación recibida.

Un agradecimiento especial a todas las personas que han participado en mis trabajos de investigación. Pertenecientes al grupo de investigación de Emilio M. Pérez: Alejandro López, Mar Bernal y Belén Nieto. Al profesor Nazario Martín por su aportación a mis trabajos. A Joaquín Calbo, Yann Pouillon, Enrique Ortí y Ángel Rubio por los cálculos teóricos. A Volker Strauss, Christoph Schierl y Dirk M. Guldi por las medidas foto-físicas. A Emiliano Martínez y Encarnación Lorenzo por el extenso estudio electroquímico. Gracias a Santiago Casado, Luisa Ruiz y Almudena Torres por su ayuda en la caracterización microscópica de mis productos.

Gracias también al SIDI de la UAM, en especial a los laboratorios de RMN de líquidos y sólidos, y al laboratorio de Masas por sus servicios para la caracterización de las moléculas que aparecen en este trabajo. A nuestro antiguo técnico de RMN de IMDEA Javier López y a su relevo Zulay Pardo. Al centro nacional de microscopía electrónica y sus técnicos Adrián, J. Luis y Esteban. A Emilio, técnico del taller de vidrio de la facultad de químicas de la UCM.

Gracias a todos mis compañeros del grupo de Emilio M. Pérez por su ayuda y colaboración, en especial a Teresa, Emerson y Alex. Teresa, muchas gracias por todos los momentos locos y divertidos, por ser tan animada, por ayudar cuando fuera necesario y por el gran congreso que pasamos en Philadelphia. Mi querido francés-español, con un octavo de alemán, Emerson, eres una de las personas más inteligentes y eficientes con las que me he cruzado. Muchísimas gracias por toda la ayuda que me has prestado, gracias por ser un excelente guía tanto gastronómico como turístico en nuestro viaje a Estrasburgo y por muchas cosas más. En último lugar, muchísimas gracias Alex. En estos cuatro años realizando la tesis he aprendido muchas cosas de ti. Me has ayudado mucho tanto con tus conocimientos en síntesis, como con buenas ideas y consejos. Siempre has estado ahí tanto para lo bueno como para lo malo. Una de las cosas que me

llevo del doctorado es un gran amigo que creo que será para siempre, muchas gracias Alex.

También merecen un reconocimiento todas las personas de IMDEA que me han ayudado y apoyado. Gracias Juancar por animar el instituto y Antonio por mantenerlo como el primer día, gracias a todo el personal de administración por su gran trabajo y gracias a la señorita casi doctora Leonor de La Cueva por su ayuda científica, compañerismo y amistad.

Agradecer a mi director de tesis Emilio, todos los buenos ratos que hemos pasado y todo el conocimiento que me has transmitido. Gracias por formarme como investigador y darme la oportunidad de mostrar mi trabajo en tantos congresos complementando así mi formación. Agradecer también al Profesor Nazario Martín la oportunidad de acercarme a la ciencia acogiéndome desde muy "joven" en su grupo de investigación. Extender mi agradecimiento a todos los miembros del grupo del profesor Nazario Martín.

Muchas gracias a todos mis amigos, tanto químicos como no. Gracias Dani, Darío, Josu, Ramón, Santi, Chechu, Mercedes, Lydia, Sara bis, Miky, Mery, Simba, es imposible agradeceros todo lo que hacéis por mí en tan pocas líneas, gracias por ser grandes amigos y apoyarme durante todo este camino.

Finalmente, quiero aprovechar este trabajo para dar las gracias a las personas más importantes en mi vida y a las que quizás no se lo agradezca lo suficiente. Muchas gracias a toda mi familia, abuelos, tíos, primos, sobrinos gatunos, por cuidarme y hacerme pasar tan buenos momentos. A mis padres, Fernando y Charo sin los cuales, obviamente no estaría presentando este trabajo. Muchísimas gracias por todo lo que habéis hecho por mí en estos casi 29 años, gracias por la educación que me habéis dado y los valores que me habéis inculcado. A mi hermano Rubén, no creo que se pueda tener un hermano mejor, gracias por ser como eres chache. A mi cuñi Carol, una persona pequeñita pero con enorme corazón. Y por último, Sara, gracias por cambiar mi vida desde que puse un pie en la Universidad. Son ya muchos años a tu lado y no tengo palabras para agradecer todo lo que has hecho por mí. Muchísimas gracias por todo tu apoyo, ayuda, consejos, paciencia, alegría, cariño y diversión. Gracias por ser como eres y por estar siempre a mi lado, gracias Sara.

A todos y a todas, gracias.

References, abbreviations and acronyms

In this thesis only published work has been presented. Many projects and results have been left out.

Bibliographic citations have been placed as footnotes in the pages where they were first cited in the section and at the end of each section or chapter; they were added independently at every section or chapter, so they are duplicated in different chapters when necessary.

Throughout this manuscript, abbreviations and acronyms recommended by the American Chemical Society in the Organic Chemistry area (revised in the *Journal of Organic Chemistry* on January **2013**; http://pubs.acs.org/paragonplus/submission/joceah/joceah_authguide.pdf) have been employed. In addition, those indicated below have also been used.

A	Adenine
ADMP	Acyclic diene metathesis polymerization
AFM	Atomic force microscopy
AIBN	2,2′-Azobis(2-methylpropionitrile)
C	Cytosine
$CBPQT^{4+}$	Cyclobis(paraquat-*p*-phenylene)
CD	Cyclodextrin
CNTs	Carbon nanotubes
CP MAS	Cross-polarization magic-angle spinning
CV	Cyclic voltammetry
$DBA{\cdot}PF_6$	Dibenzylammonium hexafluorophosphate
DB24C8	Dibenzo [24]crown-8
DCM	Dichloromethane
DFT	Density functional theory
DMF	N,N-Dimethylformamide

DNA	Deoxyribonucleic acid
DTAB	Dodecyltrimethylammonium bromide
DTT	Dithiothreitol
EDX	Energy-dispersive X-ray spectroscopy
exTTF	π-extended tetrathiafulvalene
FMN	Flavin mononucleotide
G	Guest
GC	Glassy carbon
GPC	Gel permeation chromatography
H	Host
HG	Host-guest
HPLC	High pressure liquid chromatography
HR-TEM	High resolution-transmission electron microscopy
MeOH	Methanol
MINTs	Mechanically interlocked single wall carbon nanotubes
MIMs	Mechanically interlocked molecules
MM	Molecular mechanics
MOFs	Metal organic frameworks
MWNTs	Multi-walled carbon nanotubes
NMR	Nuclear magnetic resonance
NMP	N-methyl pyrrolidine
NT-FET	Nanotube field effect transistors
OLED	Organic light-emitting diode
PABS	poly(*m*-aminobenzene sulfonic acid)
PDI	Polydispersity index
PFO	Polyfluorene

PI	Polyimide
PLE	Photoluminescence emission
PmPV	Poly(*m*-phenylenevynilene)
PTFE	Polytetrafluoroethylene
QM	Quantum mechanical
RBM	Radial breathing modes
RCM	Ring closing metathesis
RRDE	Rotating ring-disc electrode
SAMs	Self-assembled monolayers
SCE	Specific calomel electrode
SDBS	Sodium dodecylbenzene sulfonate
SDS	Sodium dodecyl sulfate
SMFS	Single molecule force spectroscopy
ssDNA	Single strain deoxyribonucleic acid
STEM	Scanning transmission electron mode
SWNTs	Single walled carbon nanotubes
T	Thymine
TBAP	Tetrabutylammonium perchlorate
TCE	Tetrachloroethane
TEM	Transmission electron microscopy
TGA	Thermogravimetric analysis
THF	Tetrahydrofuran
TMEDA	N,N,N′,N′-tetramethylethylenediamine
TTF	Tetrathifulvalene
UV-vis-NIR	Ultraviolet-visible-near infrared
1D	Unidimensional

TABLE OF CONTENTS

SUMMARY

Summary

Introduction

Single walled carbon nanotubes (SWNTs) were discovered by Ijima[1] and Bethune [2] in 1993. They have been attracted a great deal of attention from the scientific community due to their extraordinary mechanical, [3,4,5] electrical[6,7,8] and optical properties.[9]

Currently, many research efforts are focused not only on the synthesis[10,11,12] of carbon nanotubes and their purification through physical methods,[13,14,15] but also on the chemical functionalization of SWNTs through covalent[16] or noncovalent methods[17]. The final objective of chemical modification is either to purify[18] the complex mixture of SWNTs or to modulate their interesting properties. The covalent modification of SWNTs leads to products with high kinetic stability, but it disrupts the sp^2 carbon network, so the native properties of the pristine material change. The noncovalent modification of SWNTs respects the structure and the interesting properties of pristine SWNTs, but the products usually show low kinetic stability.

1. S. Iijima and T. Ichihashi, *Nature*, 1993, **363**, 603-605.
2. D. S. Bethune, C. H. Klang, M. S. de Vries, G. Gorman, R. Savoy, J. Vázquez and R. Beyers, *Nature*, 1993, **363**, 605-607.
3. C. A. Cooper, R. J. Young and M. Halsall, *Composites Part A*, 2001, **32**, 401-411.
4. A. Krishnan, E. Dujardin, T. W. Ebbesen, P. N. Yianilos and M. M. J. Treacy, *Phys. Rev. B*, 1998, **58**, 14013-14019.
5. J.-P. Salvetat, G. A. D. Briggs, J.-M. Bonard, R. R. Bacsa, A. J. Kulik, T. Stöckli, N. A. Burnham and L. Forró, *Phys. Rev. Lett.*, 1999, **82**, 944-947.
6. J. W. Mintmire, B. I. Dunlap and C. T. White, *Phys. Rev. Lett*., 1992, **68**, 631-634.
7. M. Ouyang, J.-L. Huang, C. L. Cheung and C. M. Lieber, *Science*, 2001, **292**, 702.
8. M. Ouyang, J.-L. Huang and C. M. Lieber, *Acc. Chem. Res.*, 2002, **35**, 1018-1025.
9. Y. Saito and S. Uemura, *Carbon*, 2000, **38**, 169-182.
10. H. Dai, *Acc. Chem. Res.*, 2002, **35**, 1035-1044.
11. S. M. Bachilo, L. Balzano, J. E. Herrera, F. Pompeo, D. E. Resasco and R. B. Weisman, *J. Am. Chem. Soc.*, 2003, **125**, 11186-11187.
12. A. R. Harutyunyan, G. Chen, T. M. Paronyan, E. M. Pigos, O. A. Kuznetsov, K. Hewaparakrama, S. M. Kim, D. Zakharov, E. A. Stach and G. U. Sumanasekera, *Science*, 2009, **326**, 116.
13. R. Krupke, F. Hennrich, H. v. Löhneysen and M. M. Kappes, *Science*, 2003, **301**, 344.
14. M. S. Arnold, S. I. Stupp and M. C. Hersam, *Nano Lett.*, 2005, **5**, 713-718.
15. H. Liu, T. Tanaka, Y. Urabe and H. Kataura, *Nano Lett*., 2013, **13**, 1996-2003.
16. S. Banerjee, T. Hemraj-Benny and S. S. Wong, *Adv. Mater.*, 2005, **17**, 17-29.
17. Y.-L. Zhao and J. F. Stoddart, *Acc. Chem. Res.*, 2009, **42**, 1161-1171.
18. X. Tu, S. Manohar, A. Jagota and M. Zheng, *Nature*, 2009, **460**, 250-253.

Objectives

The present thesis has four main objectives:

1) To introduce the mechanical bond as a new tool for the chemical modification of SWNTs.
2) To optimize the MINT-forming reaction conditions and elucidate its mechanism.
3) To evaluate the effect of the mechanical bond on the physical properties of SWNTs.
4) To develop a new method to quantify the interactions between organic molecules and the sidewall of SWNTs.

Results

Mechanically Interlocked Single-Wall Carbon Nanotubes

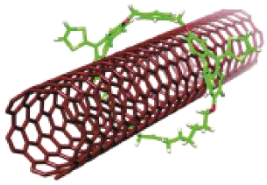

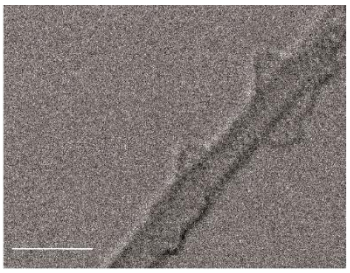

In the present work the mechanical bond is introduced as an alternative to modify SWNTs, producing SWNT derivatives that show high kinetic stability and preserve the native structure of pristine SWNTs. Therefore, this strategy combines the advantages of both covalent and noncovalent methods of functionalization of SWNTs. To synthetize the mechanically interlocked single wall carbon nanotubes derivatives (MINTs), a clipping protocol was followed. Macrocyclic precursors equipped with two exTTF units as recognition moiety linked by an aromatic spacer, and functionalized with two flexible alkyl chains decorated with terminal doubles bonds were closed around the nanotube though ring closing metathesis reaction (RCM). MINT derivatives were widely

characterized by analytical, spectroscopic, and microscopic techniques, as well as by appropriate control experiments, probing the mechanically interlocked nature of the derivatives.

Angew. Chem. Int. Ed., **2014**, *53*, 5394-5400.

Optimization and Insights into the Mechanism of Formation of Mechanically Interlocked Derivatives of Single-Walled Carbon Nanotubes

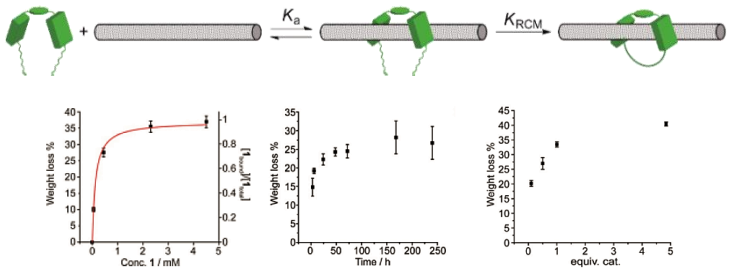

The optimal conditions for the synthesis of MINTs were studied systematically by variation of concentration of the U-shaped receptor, reaction time and catalyst concentration. The increase of the degree of functionalization with the relative concentration of the U-shape molecule resembles a 1:1 binding isotherm, revealing the formation of a **1**·SWNT complex. The kinetics data follow a pseudo-first order reaction in agreement with an intramolecular RCM, and discarding the formation of dimers or oligomers of the U-shaped receptor. Considering both results, the formation of **1**·SWNTs complex, followed by the RCM, was confirmed as the mechanism of the MINT-forming reaction.

ChemPlusChem, **2015**, *80*, 1153-1157.

The Mechanical Bond on Carbon Nanotubes: Diameter-Selective Functionalization and Effects on Physical Properties

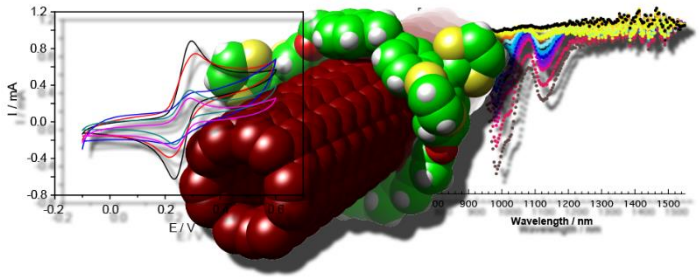

In this work, the synthesis of a new mechanical interlocked derivative of SWTNs based on exTTF macrocycles is described. Analysis of the extensive spectroscopic characterization (UV-vis-NIR, fluorescence, Raman) reveals a preferential functionalization of the smaller (6,5)-SWNTs vs the larger (7,6)-SWNTs. Upon photoexcitation, efficient charge-transfer was observed through transient absorption measures. Cyclic voltammetry experiments show differences between both supramolecular models and MINT derivative, observing greater reversibility and lower current intensity in MINT derivative due to the closer interactions between the exTTF electroactive species and the SWNT sidewall. Besides, different charge-transfer rate constants and diffusion coefficients for the MINT derivatives and supramolecular models were found, confirming that the interaction between the macrocycles and the nanotube is different in each case. Molecular mechanics and DFT calculations support the experimental findings.

Nanoscale, **2016**, *8*, 9254-9264.

Determination of association constants towards carbon nanotubes

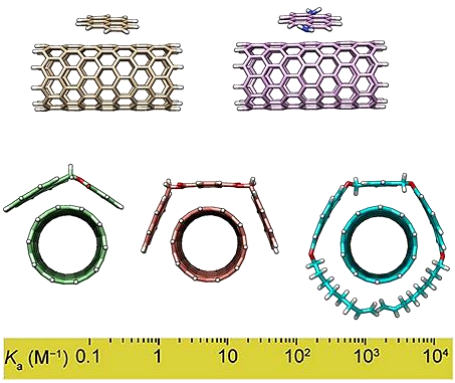

Supramolecular chemistry has been employed to modify SWNTs during the last decade. However, a standard method for the quantification of supramolecular interactions between small molecules and SWNTs in suspension/solution has not been reported. This work describes a simple method for the determination of binding constants (K_a) in heterogeneous supramolecular systems formed by soluble organic molecules and insoluble SWNTs. The insolubility of SWNTs allows separating the species present in the supramolecular equilibrium, from which we calculate the binding constant as a function of the concentration of the free species. The binding constants of five host molecules based on pyrene and two kinds of SWNTs were determined, showing the scope of the method. Numerically, values of K_a from 1 to 10^4 M^{-1} were obtained. Moreover, the method showed to be sensitive to structural changes in both host and guest molecules, as well as to solvent effects. The binding constants determined experimentally were corroborated through DFT calculation.

Chem. Sci., **2015**, *6*, 7008-7014.

Conclusions

i) We have introduced the mechanical bond as a new tool for the chemical manipulation of SWNTs and demonstrated that MINTs are kinetically stable and preserve the native structure of pristine SWNTs.

ii) MINT forming reaction mechanism, where the reaction follows two steps: formation of U-shaped receptor·SWNTs complex followed by RCM reaction, was confirmed by thermodynamic and kinetic experiments.

iii) The ideal conditions for MINTs synthesis are: concentrations of linear receptor greater or equal to 1 mM, 1 equivalent of Grubbs 2nd generation catalyst with respect to the linear receptor and reaction times of at least 48 hours.

iv) Efficient charge-transfer in the excited state between the electron donor exTTF macrocycles and electron acceptor SWNTs was observed by transient absorption spectroscopy.

v) The significantly different charge-transfer rate constants and diffusion coefficients between MINTs and supramolecular model reflect the influence of the mechanical bond on the properties of SWNTs.

vi) A simple method for the determination of association constants between soluble molecules and SWNTs has been developed. This method is sensitive to solvent effects as well as structure changes of host or/and guest, and is suitable for a wide range of binding constants.

References

1. S. Iijima and T. Ichihashi, *Nature*, 1993, **363**, 603-605.
2. D. S. Bethune, C. H. Klang, M. S. de Vries, G. Gorman, R. Savoy, J. Vázquez and R. Beyers, *Nature*, 1993, **363**, 605-607.
3. C. A. Cooper, R. J. Young and M. Halsall, *Composites Part A*, 2001, **32**, 401-411.
4. A. Krishnan, E. Dujardin, T. W. Ebbesen, P. N. Yianilos and M. M. J. Treacy, *Phys. Rev. B*, 1998, **58**, 14013-14019.
5. J.-P. Salvetat, G. A. D. Briggs, J.-M. Bonard, R. R. Bacsa, A. J. Kulik, T. Stöckli, N. A. Burnham and L. Forró, *Phys. Rev. Lett.*, 1999, **82**, 944-947.
6. J. W. Mintmire, B. I. Dunlap and C. T. White, *Phys. Rev. Lett.*, 1992, **68**, 631-634.
7. M. Ouyang, J.-L. Huang, C. L. Cheung and C. M. Lieber, *Science*, 2001, **292**, 702.
8. M. Ouyang, J.-L. Huang and C. M. Lieber, *Acc. Chem. Res.*, 2002, **35**, 1018-1025.
9. Y. Saito and S. Uemura, *Carbon*, 2000, **38**, 169-182.
10. H. Dai, *Acc. Chem. Res.*, 2002, **35**, 1035-1044.
11. S. M. Bachilo, L. Balzano, J. E. Herrera, F. Pompeo, D. E. Resasco and R. B. Weisman, *J. Am. Chem. Soc.*, 2003, **125**, 11186-11187.
12. A. R. Harutyunyan, G. Chen, T. M. Paronyan, E. M. Pigos, O. A. Kuznetsov, K. Hewaparakrama, S. M. Kim, D. Zakharov, E. A. Stach and G. U. Sumanasekera, *Science*, 2009, **326**, 116.
13. R. Krupke, F. Hennrich, H. v. Löhneysen and M. M. Kappes, *Science*, 2003, **301**, 344.
14. M. S. Arnold, S. I. Stupp and M. C. Hersam, *Nano Lett.*, 2005, **5**, 713-718.
15. H. Liu, T. Tanaka, Y. Urabe and H. Kataura, *Nano Lett.*, 2013, **13**, 1996-2003.
16. S. Banerjee, T. Hemraj-Benny and S. S. Wong, *Adv. Mater.*, 2005, **17**, 17-29.
17. Y.-L. Zhao and J. F. Stoddart, *Acc. Chem. Res.*, 2009, **42**, 1161-1171.
18. X. Tu, S. Manohar, A. Jagota and M. Zheng, *Nature*, 2009, **460**, 250-253.

RESUMEN

Resumen

Introducción

Los nanotubos de carbono de pared simple fueron descubiertos por Ijima[1] y Bethune[2] en 1993. Desde entonces han despertado un gran interés debido a sus extraordinarias propiedades mecánicas,[3,4,5] electrónicas[6,7,8] y ópticas.[9]

Actualmente, numerosas investigaciones se han centrado en la síntesis[10,11,12] y purificación[13,14,15] de nanotubos de carbono, así como en su funcionalización química mediante métodos covalentes[16] y no covalentes.[17] El objetivo final de la modificación química es tanto purificar[18] las complicadas mezclas de nanotubos de carbono como modular sus propiedades. Por un lado, la modificación covalente de nanotubos de carbono genera productos con alta estabilidad cinética, pero se modifica la red de carbonos sp^2 alterando las propiedades del material de partida. Por otro lado, la modificación no covalente de nanotubos de carbono permite mantener intactas la estructura y propiedades del material de partida, pero los productos obtenidos suelen presentar baja estabilidad cinética.

1. S. Iijima and T. Ichihashi, *Nature*, 1993, **363**, 603-605.
2. D. S. Bethune, C. H. Klang, M. S. de Vries, G. Gorman, R. Savoy, J. Vázquez and R. Beyers, *Nature*, 1993, **363**, 605-607.
3. C. A. Cooper, R. J. Young and M. Halsall, *Composites Part A*, 2001, **32**, 401-411.
4. A. Krishnan, E. Dujardin, T. W. Ebbesen, P. N. Yianilos and M. M. J. Treacy, *Phys. Rev. B*, 1998, **58**, 14013-14019.
5. J.-P. Salvetat, G. A. D. Briggs, J.-M. Bonard, R. R. Bacsa, A. J. Kulik, T. Stöckli, N. A. Burnham and L. Forró, *Phys. Rev. Lett.*, 1999, **82**, 944-947.
6. J. W. Mintmire, B. I. Dunlap and C. T. White, *Phys. Rev. Lett*., 1992, **68**, 631-634.
7. M. Ouyang, J.-L. Huang, C. L. Cheung and C. M. Lieber, *Science*, 2001, **292**, 702.
8. M. Ouyang, J.-L. Huang and C. M. Lieber, *Acc. Chem. Res.*, 2002, **35**, 1018-1025.
9. Y. Saito and S. Uemura, *Carbon*, 2000, **38**, 169-182.
10. H. Dai, *Acc. Chem. Res.*, 2002, **35**, 1035-1044.
11. S. M. Bachilo, L. Balzano, J. E. Herrera, F. Pompeo, D. E. Resasco and R. B. Weisman, *J. Am. Chem. Soc.*, 2003, **125**, 11186-11187.
12. A. R. Harutyunyan, G. Chen, T. M. Paronyan, E. M. Pigos, O. A. Kuznetsov, K. Hewaparakrama, S. M. Kim, D. Zakharov, E. A. Stach and G. U. Sumanasekera, *Science*, 2009, **326**, 116.
13. R. Krupke, F. Hennrich, H. v. Löhneysen and M. M. Kappes, *Science*, 2003, **301**, 344.
14. M. S. Arnold, S. I. Stupp and M. C. Hersam, *Nano Lett.*, 2005, **5**, 713-718.
15. H. Liu, T. Tanaka, Y. Urabe and H. Kataura, *Nano Lett*., 2013, **13**, 1996-2003.
16. S. Banerjee, T. Hemraj-Benny and S. S. Wong, *Adv. Mater.*, 2005, **17**, 17-29.
17. Y.-L. Zhao and J. F. Stoddart, *Acc. Chem. Res.*, 2009, **42**, 1161-1171.
18. X. Tu, S. Manohar, A. Jagota and M. Zheng, *Nature*, 2009, **460**, 250-253.

Objetivos

La presente tesis tiene cuatro objetivos principales:

1) Introducir el enlace mecánico como nueva herramienta para la modificación química de nanotubos de carbono.
2) Optimizar las condiciones de reacción para la obtención de derivados mecánicamente enlazados de nanotubos de carbono, así como elucidar el mecanismo de reacción.
3) Evaluar el efecto del enlace mecánico en las propiedades físicas de los derivados de nanotubos de carbono.
4) Desarrollar un método para cuantificar la fuerza de la interacción entre moléculas orgánicas (huésped) y las paredes de los nanotubos de carbono (anfitrión).

Resultados

Se resumen aquí los cuatro artículos que conforman los capítulos de la presente tesis.

Mechanically Interlocked Single-Wall Carbon Nanotubes

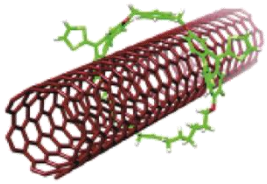

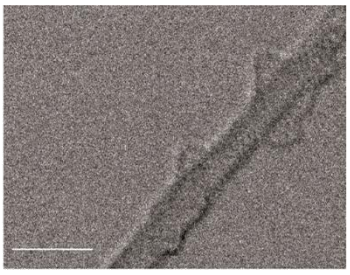

En este trabajo, se introdujo el enlace mecánico como alternativa para modificar nanotubos de carbono, dando lugar a derivados que no solo poseen alta estabilidad cinética, sino que también mantienen las extraordinarias propiedades del material de partida. Por lo tanto, esta estrategia combina las ventajas de los métodos previos de funcionalización de nanotubos de carbono:

covalente y no covalente. Para sintetizar los derivados mecánicamente enlazados de nanotubos de carbono de pared simple (MINTs de sus siglas en inglés), se siguió un protocolo denominado "clipping". Los precursores lineales de los macrociclos están formados por dos unidades de "exTTF" que actúan como motivos de reconocimiento de nanotubos de carbono, unidas entre sí por un espaciador aromático. Además, las unidades de "exTTF" están funcionalizadas por dos cadenas alquílicas flexibles decoradas con dobles enlaces terminales. Dichos dobles enlaces permitieron cerrar el precursor lineal alrededor del nanotubo mediante una reacción de metátesis de cierre de anillo. Los MINTs se caracterizaron ampliamente mediante técnicas analíticas, espectroscópicas y microscópicas, y se llevaron a cabo los correspondientes experimentos control, demostrando la naturaleza mecánicamente enlazada de los derivados.

Angew. Chem. Int. Ed., **2014**, *53*, 5394-5400.

Optimization and Insights into the Mechanism of Formation of Mechanically Interlocked Derivatives of Single-Walled Carbon Nanotubes

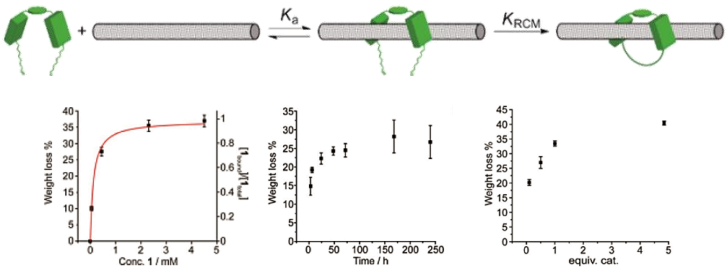

Las condiciones óptimas para la síntesis de MINTs se estudiaron de forma sistemática mediante la variación de concentración del receptor lineal, tiempo de reacción y concentración de catalizador. El incremento del grado de funcionalización al aumentar la concentración relativa de la molécula con forma de U recuerda a una isoterma de enlace 1:1, revelando la formación del complejo receptor lineal-nanotubo. El análisis de los datos cinéticos demostró que la reacción sigue una cinética de pseudo primer orden como corresponde a una reacción de metátesis de cierre de anillo, descartando así la formación de dímeros u oligómeros formados a partir del receptor lineal. Considerando ambos

resultados, la formación del complejo receptor lineal-nanotubo seguido por la reacción de cierre de anillo, fue confirmado como mecanismo de reacción en la síntesis de derivados mecánicamente enlazados de nanotubos de carbono.

ChemPlusChem, **2015**, *80*, 1153-1157.

The Mechanical Bond on Carbon Nanotubes: Diameter-Selective Functionalization and Effects on Physical Properties

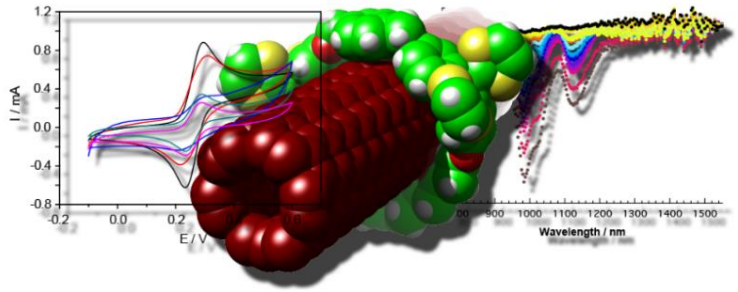

En este trabajo se describe la síntesis de un nuevo derivado mecánicamente enlazado de nanotubos de carbono basado en macrociclos de "exTTF". El análisis de la caracterización espectroscópica (UV-vis-IR, fluorescencia, Raman) reveló cierta selectividad en la funcionalización de los nanotubos (6,5) frente a los nanotubos (7,6) que presentan mayor diámetro. Mediante medidas de absorción transitoria, se observó una transferencia de carga eficiente después de foto-excitar los MINTs. Además, se realizaron experimentos de voltamperometría cíclica que mostraron diferencias entre el modelo supramolecular y el mecánicamente enlazado. Se observó mayor reversibilidad y menor intensidad de corriente en el derivado mecánicamente enlazado debido a la mayor proximidad entre las unidades de "exTTF" y la pared del nanotubo de carbono. Además, se observaron diferencias significativas en las constantes de velocidad de transferencia de carga y los coeficientes de difusión determinados para el modelo supramolecular y el mecánicamente enlazado, confirmando que la interacción entre el macrociclo y el nanotubo es diferente en ambos casos. Cálculos teóricos mediante mecánica molecular y la teoría del

funcional de la densidad (DFT de sus siglas en inglés) apoyan los resultados experimentales.

Nanoscale, **2016**, *8*, 9254-9264.

Determination of association constants towards carbon nanotubes

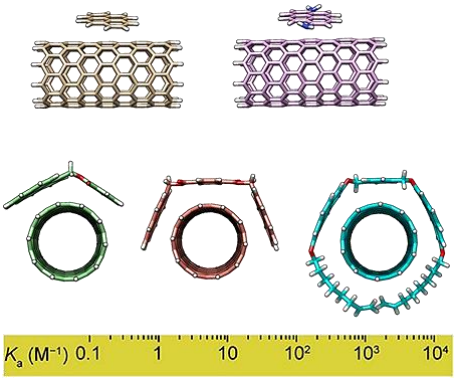

Durante la última década, la química supramolecular ha sido empleada para modificar nanotubos de carbono en numerosas ocasiones. Sin embargo, ningún método estándar para cuantificar la extensión de las interacciones supramoleculares de derivados no covalentes de nanotubos de carbono ha sido publicado. Este trabajo describe un método simple para la determinación de constantes de asociación (K_a) en sistemas supramoleculares heterogéneos formados por moléculas orgánicas solubles e insolubles nanotubos de carbono. Gracias a la insolubilidad de los nanotubos de carbono es posible separar físicamente las especies presentes en el equilibrio supramolecular, permitiendo calcular la constante de asociación en función de la concentración de una de dichas especies. Se determinó la constante de asociación de cinco moléculas con dos tipos de nanotubos de carbono en varios disolventes, demostrando el amplio rango de aplicación de este método. Se obtuvieron valores de K_a desde 1 a 10^3 M^{-1}. El método demostró ser sensible a cambios estructurales tanto del huésped como del anfitrión, así como a efectos del disolvente. Las constantes de asociación determinadas experimentalmente fueron corroboradas mediante cálculos basados en la teoría del funcional de la densidad (DFT).

Chem. Sci., **2015**, *6*, 7008-7014.

Conclusiones

i) Se ha introducido el enlace mecánico como una nueva herramienta para la manipulación química de nanotubos de carbono y se ha demostrado que los derivados obtenidos son estables cinéticamente y mantienen la integridad estructural de los nanotubos de partida.

ii) El mecanismo de la reacción de formación de los derivados mecánicamente enlazados de nanotubos de carbono, constituido por dos pasos: la formación del complejo receptor lineal-nanotubo seguido de la reacción de metátesis de cierre de anillo, ha sido confirmado mediante experimentos tanto termodinámicos como cinéticos.

iii) Las condiciones óptimas encontradas para la síntesis de los derivados mecánicamente enlazados son: concentración de receptor lineal igual o mayor a 1 mM, 1 equivalente molar de catalizador de Grubbs de segunda generación con respecto al receptor lineal y tiempos de reacción de al menos 48 horas.

iv) Un eficiente fenómeno de transferencia de carga en el estado excitado entre las unidades de "exTTF" (donador de electrones) presentes en los macrociclos y los nanotubos de carbono (aceptor de electrones) se ha observado mediante espectroscopía de absorción transitoria.

v) Las diferencias observadas entre las constantes de velocidad de transferencia de carga y los coeficientes de difusión determinados para el modelo supramolecular y el mecánicamente enlazado, reflejan la influencia del enlace mecánico en las propiedades de los nanotubos de carbono.

vi) Se ha desarrollado un método sencillo para la determinación de constantes de asociación entre moléculas solubles y nanotubos de carbono. Este método es sensible a cambios de disolvente, así como a cambios estructurales tanto en el huésped como en el anfitrión. Además, es adecuado para trabajar en un amplio rango de constantes de asociación.

Referencias

1. S. Iijima and T. Ichihashi, *Nature*, 1993, **363**, 603-605.
2. D. S. Bethune, C. H. Klang, M. S. de Vries, G. Gorman, R. Savoy, J. Vázquez and R. Beyers, *Nature*, 1993, **363**, 605-607.
3. C. A. Cooper, R. J. Young and M. Halsall, *Composites Part A*, 2001, **32**, 401-411.
4. A. Krishnan, E. Dujardin, T. W. Ebbesen, P. N. Yianilos and M. M. J. Treacy, *Phys. Rev. B*, 1998, **58**, 14013-14019.
5. J.-P. Salvetat, G. A. D. Briggs, J.-M. Bonard, R. R. Bacsa, A. J. Kulik, T. Stöckli, N. A. Burnham and L. Forró, *Phys. Rev. Lett.*, 1999, **82**, 944-947.
6. J. W. Mintmire, B. I. Dunlap and C. T. White, *Phys. Rev. Lett.*, 1992, **68**, 631-634.
7. M. Ouyang, J.-L. Huang, C. L. Cheung and C. M. Lieber, *Science*, 2001, **292**, 702.
8. M. Ouyang, J.-L. Huang and C. M. Lieber, *Acc. Chem. Res.*, 2002, **35**, 1018-1025.
9. Y. Saito and S. Uemura, *Carbon*, 2000, **38**, 169-182.
10. H. Dai, *Acc. Chem. Res.*, 2002, **35**, 1035-1044.
11. S. M. Bachilo, L. Balzano, J. E. Herrera, F. Pompeo, D. E. Resasco and R. B. Weisman, *J. Am. Chem. Soc.*, 2003, **125**, 11186-11187.
12. A. R. Harutyunyan, G. Chen, T. M. Paronyan, E. M. Pigos, O. A. Kuznetsov, K. Hewaparakrama, S. M. Kim, D. Zakharov, E. A. Stach and G. U. Sumanasekera, *Science*, 2009, **326**, 116.
13. R. Krupke, F. Hennrich, H. v. Löhneysen and M. M. Kappes, *Science*, 2003, **301**, 344.
14. M. S. Arnold, S. I. Stupp and M. C. Hersam, *Nano Lett.*, 2005, **5**, 713-718.
15. H. Liu, T. Tanaka, Y. Urabe and H. Kataura, *Nano Lett.*, 2013, **13**, 1996-2003.
16. S. Banerjee, T. Hemraj-Benny and S. S. Wong, *Adv. Mater.*, 2005, **17**, 17-29.
17. Y.-L. Zhao and J. F. Stoddart, *Acc. Chem. Res.*, 2009, **42**, 1161-1171.
18. X. Tu, S. Manohar, A. Jagota and M. Zheng, *Nature*, 2009, **460**, 250-253.

INTRODUCTION

1. Introduction

1.1 Mechanically Interlocked Molecules (MIMs)

Mechanically interlocked molecules (MIMs) are formed by two or more discrete components that are not connected directly by covalent bonds, but because of their topology, to separate them requires breaking a covalent bond.[1,2] Examples of MIMs are catenanes, rotaxanes, molecular knots, and molecular Borromean rings.

Mechanically interlocked structures have attracted a great deal of attention of many researchers, not only because of their extravagant topologies, but mostly as a consequence of the possibility to experiment submolecular movement. Because of the dynamic nature of the mechanical bond, MIMs are promising molecules for the fabrication of molecular shuttles,[3] rotors[4] and machines.[5] This has been recently recognized with the Nobel Prize in Chemistry 2016, which was awarded jointly to Jean-Pierre Sauvage, Sir J. Fraser Stoddart and Bernard L. Feringa "for the design and synthesis of molecular machines". That is 2/3 of the Nobel Prize awarded to MIMs.

1.1.1 Rotaxanes

The rotaxane concept appeared at the beginning of seventies with the seminal works of Schill *et al.*[6,7] Rotaxane architectures present one or more macrocycles trapped on a linear component (thread) by bulky substituents at its ends (stoppers) that prevent dissociation.

1. K. Kim, *Chem. Soc. Rev.*, 2002, **31**, 96-107.
2. J. F. Stoddart, *Chem. Soc. Rev*., 2009, **38**, 1802-1820.
3. J. D. Crowley, S. M. Goldup, A.-L. Lee, D. A. Leigh and R. T. McBurney, *Chem. Soc. Rev.*, 2009, **38**, 1530-1541.
4. D. A. Leigh, J. K. Y. Wong, F. Dehez and F. Zerbetto, *Nature*, 2003, **424**, 174-179.
5. B. Lewandowski, G. De Bo, J. W. Ward, M. Papmeyer, S. Kuschel, M. J. Aldegunde, P. M. E. Gramlich, D. Heckmann, S. M. Goldup, D. M. D'Souza, A. E. Fernandes and D. A. Leigh, *Science*, 2013, **339**, 189-193.
6. G. Schill and H. Zollenkopf, *Justus Liebigs Ann. Chem.*,1969, **721**, 53-74.
7. G. Schill and R. Henschel, *Justus Liebigs Ann. Chem.*, 1970, **731**, 113-119.

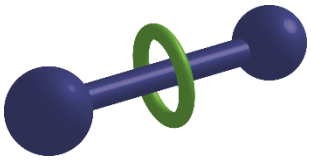

Figure 1. Cartoon of [2]rotaxane. Thread and stoppers components are in blue and ring component in green.

The synthesis of these structures can be carried through clipping, slipping or threading followed by stoppering strategies. We will focus on the first one because it is the synthetic method employed in the present thesis.

Clipping consists in the formation of the macrocyclic wheel through some chemical reaction around the preformed thread, decorated with stoppers at its ends. To form the ring around the linear component, a specific and relatively strong interaction (driving force) between some region of the ring precursor and the thread is necessary. Many examples of the synthesis of rotaxanes through clipping, based on different interactions between the macrocycle precursor and thread and chemical reactions to close the ring have been published. Sttodart *et al.*[8]synthetized a [2]rotaxane based on the charge-transfer interaction of π-electron donor tetrathifulvalene (TTF) unit with the π-electron accepting tetracationic cyclophane, cyclobis(paraquat-*p*-phenylene) ($CBPQT^{4+}$). This couple is widely employed in the synthesis of pseudorotaxanes, which are often precursors for rotaxanes and catenanes.

8. J. O. Jeppesen, J. Perkins, J. Becher and J. F. Stoddart, *Org. Lett.*, 2000, **2**, 3547-3550.

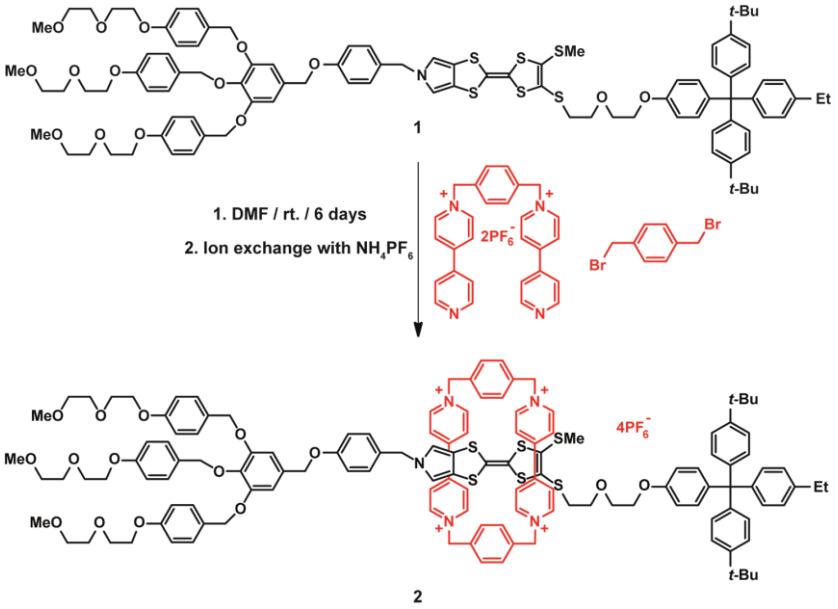

Scheme 1. Final step in the synthesis of the [2]rotaxane **2** based on the specific interaction between TTF subunit and $CBPQT^{4+}$ precursor.

The authors carried out the synthesis of an asymmetric dumbbell-shaped axle **1** thanks to the use of monopyrrole-TTF unit, which allows to the attachment in a stepwise manner of both hydrophobic and hydrophilic stopper. Axle **1** was subsequently used as a template for the formation of the macrocyclic wheel around it to yield molecule **2** through an N-alkylation reaction. The assembly of this rotaxane is governed by kinetic control, because the final step in the synthesis is an N-alkylation reaction, that is an irreversible reaction. The amphiphilic nature of the thread confers this rotaxane the ability to self-organize into monolayers as a prelude to their introduction into devices.

Another example of a thread-ring couple that shows strong supramolecular interactions is dialkylammonium ions with suitably large crown-ether macrocycles, such as dibenzo[24]crown-8 (DB24C8). This couple had been extensively used for the synthesis of rotaxanes through slipping or threading followed by stoppering strategies, but not by clipping protocol. One of the first examples where a [2]rotaxane based on this couple was synthetized through clipping method, was published by Williams *et al.*[9]

9. P. T. Glink, A. I. Oliva, J. F. Stoddart, A. J. P. White and D. J. Williams, *Angew. Chem. Int. Ed.*, 2001, **40**, 1870-1875.

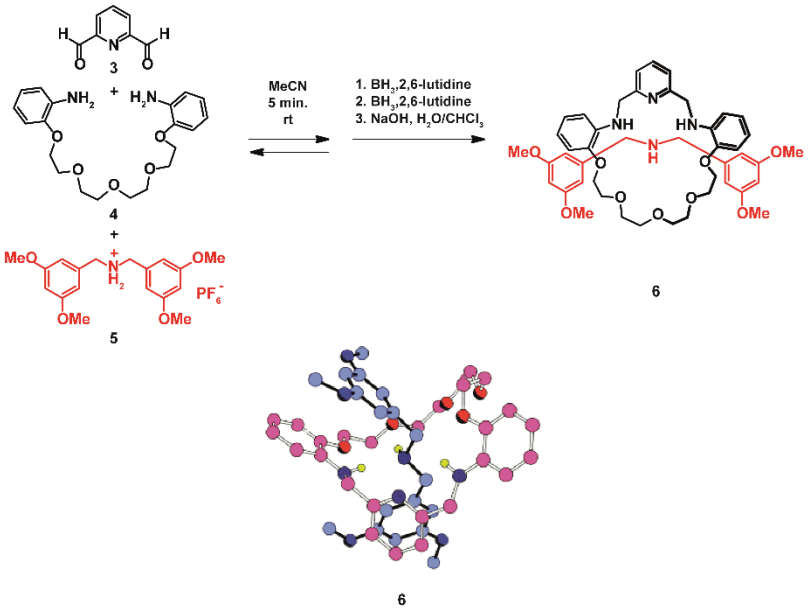

Scheme 2. Synthesis of molecule **6** by clipping of dialdehyde **3** and diamine **4** around the dialkylammonium ion **5**, followed by reduction of the imino bonds and deprotonation of dialkylammonium ion. Ball-and-stick representation of the solid-state structure of the neutral [2]rotaxane **6**. Carbon atoms are represented by pink and blue spheres, oxygen atoms by red spheres, nitrogen atoms by dark blue spheres and hydrogen atoms correspond to amine groups by yellow spheres.

The authors used an imine condensation reaction (dynamic reaction) from mixtures of aldehydes and amines, to synthetize the rotaxane **6**. They mixed 2,6-pyridinedicarboxaldehyde **3**, tetraethyleneglycol bis(2-aminophenyl)ether **4** and dialkylammonium ion derivative **5** in acetonitrile, isolating the mechanically interlocked form. This rotaxane is kinetically labile as a result of the presence of hydrolyzable imine groups. The authors increase the stability of the structure by reduction of the imine bounds with borane 2,6-lutidine complex, whose efficiency as reducing agent for this process was previously demonstrated by them.[10] Finally, rotaxane **6** was isolated after purification. The authors obtained a crystalline solid which was characterized by X-ray diffraction, revealing the formation of a [2]rotaxane in which the dumbbell-shaped component is threaded through the central cavity of the triaza crown ether.

Grubbs *el al.*[11]described the synthesis of [2]rotaxane based on the same type of interaction between a secondary dialkylammonium ions ($R_2NH_2^+$) and crown

10. S. J. Rowan and J. F. Stoddart, *Org. Lett.*, 1999, **1**, 1913-1916.
11. A. F. M. Kilbinger, S. J. Cantrill, A. W. Waltman, M. W. Day and R. H. Grubbs, *Angew. Chem. Int. Ed.*, 2003, **42**, 3281-3285.

ethers similar to DB24C8. Their objective was to combine the consistency of this supramolecular synthon with the versatile and reversible ring-closing-metathesis (RCM) reaction to form rotaxanes under thermodynamic control.

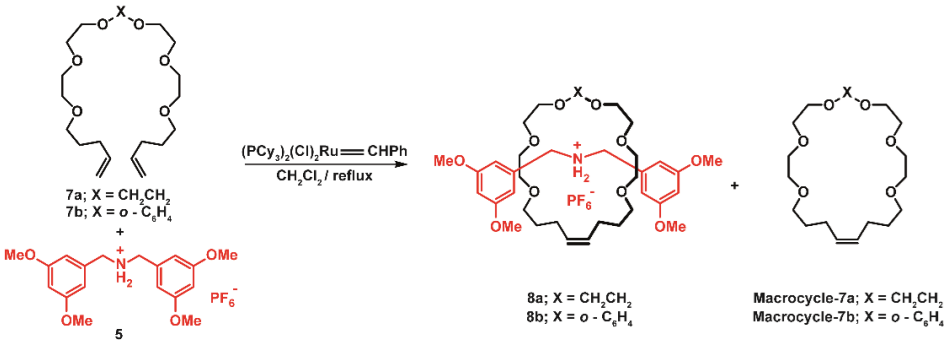

Scheme 3. Synthesis of the [2]rotaxane **8a** and **8b** from the corresponding di-olefin through RCM reaction.

To achieve their purpose, the authors designed both macrocyclic precursor **7a** and **7b**, isolating after RCM reaction in presence of Grubbs catalyst 1st generation the corresponding crown ether analogues. Once synthetized, the affinity of both macrocycles against dibenzylammonium hexafluorophosphate (DBA·PF_6) were calculated through ^{1}H-NMR titration experiments, obtaining a binding constant of 100 and 10 M^{-1} for the macrocycle derived from **7a** and **7b**, respectively. Although these association constants are smaller than that obtained for DB24C8 (K_a = 320 M^{-1}), they expected that it would be enough to guide the formation of the rotaxanes. When the RCM reaction of both precursors was carried out in presence of the corresponding dumbbell-shaped dialkylammonium ions **5**, rotaxanes **8a** and **8b** were isolated with yields of 73% and 30%, respectively. These results are in agreement with the different binding constants observed for both macrocycles. Finally, to check the dynamic nature of the RCM reaction, the authors mixed the preformed macrocycle-**7a** with the linear molecule in a mixture 4:1 of CD_2Cl_2 / CD_3NO, observing through ^{1}H-NMR experiment that the dialkylammonium ions cannot pass through the wheel due to the presence of the stoppers. However, the addition of Grubbs catalyst 2nd generation, allows the system to equilibrate to a thermodynamic minimum, resulting in the formation of the [2]rotaxane, **8a**. In an analogous fashion, the experiment was repeated with the preformed macrocycle-**7b** resulting in a similar outcome.

The examples showed in this section illustrate the synthesis of rotaxanes through clipping protocol. With synthetic methods for MIMs firmly established, a big part of the MIMs community focused on how to take advantage of the dynamic nature of the mechanical bond to make molecular machines, as we mentioned in section 1.1.[12,13] A related area of research is the synthesis of mechanically interlocked materials, where the mechanical bond imparts advantageous properties to polymers,[14] MOFs,[15] etc.

1.1.2 Polyrotaxanes

Beyond rotaxanes, a great field of research arose from the possibility to increase the number of rings present in a rotaxane structure giving place to polyrotaxanes. The boundary between rotaxanes and polyrotaxanes is sometimes not very clear. We can consider a polyrotaxane all compound with long backbone, based in whatever kind of bond (covalent, noncovalent, ionic, coordinative…) which presents rings or wheels around their main backbone structure. To simplify it, we will only focus on examples of polyrotaxanes where the backbone is constructed only by covalent bonds.

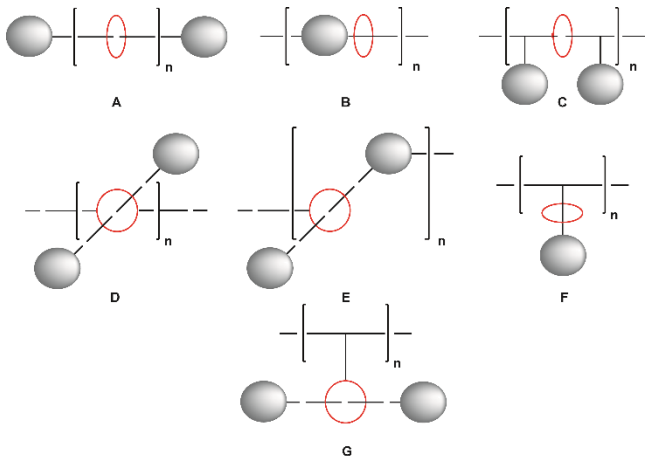

Figure 2. Schematic representation of: A-E) Main chain polyrotaxanes. F-G) Side chain polyrotaxanes.

12. H. Tian and Q.-C. Wang, *Chem. Soc. Rev.*, 2006, **35**, 361-374.
13. V. Balzani, A. Credi, F. M. Raymo and J. F. Stoddart, *Angew. Chem. Int. Ed.*, 2000, **39**, 3348-3391.
14. L. Fang, M. A. Olson, D. Benítez, E. Tkatchouk, W. A. Goddard Iii and J. F. Stoddart, *Chem. Soc. Rev.*, 2010, **39**, 17-29.
15. S. J. Loeb, *Chem. Soc. Rev.*, 2007, **36**, 226-235.

Based on how the rings and thread(s) are connected, polyrotaxanes are classified in different subgroups.[16] Depending on the position of the wheel, polyrotaxanes are divided in two types: main chain polyrotaxanes (A-E in Figure 2) where the rings form part of the main chain of the polymer, and side chain polyrotaxanes (F-G in Figure 2) where the rings are hanging to the main structure of the polymer. To illustrate the great variety of polyrotaxanes, examples of some case displayed in the Figure 2 are collected below.

To insulate molecular wires through their functionalization with macrocyclic molecules around them, obtaining polyrotaxanes, is a good strategy to avoid the formation of intermolecular excited states in luminescent materials which may lead to both reduced photoluminescence efficiency and reduced energy gap. Anderson *et al.*[17] published an example of conjugated polyrotaxanes decorated with stoppers at both ends of the chains to prevent de-threading. They synthetized insulated molecular wires based on threading conjugated macromolecules, such as poly(*p*-phenylene), poly(4,4′-diphenylene vinylene) or polyfluorene through α- or β-cyclodextrin rings, Figure 3. These mechanically interlocked derivatives are main chain polyrotaxanes of type A, according to Figure 2. The synthesis of all polyrotaxanes was carried out through polymerization by Suzuki coupling in presence of α- or β-cyclodextrin rings, using the hydrophobic effect to obtain the pseudorotaxane precursors, and stoppering as the last step.

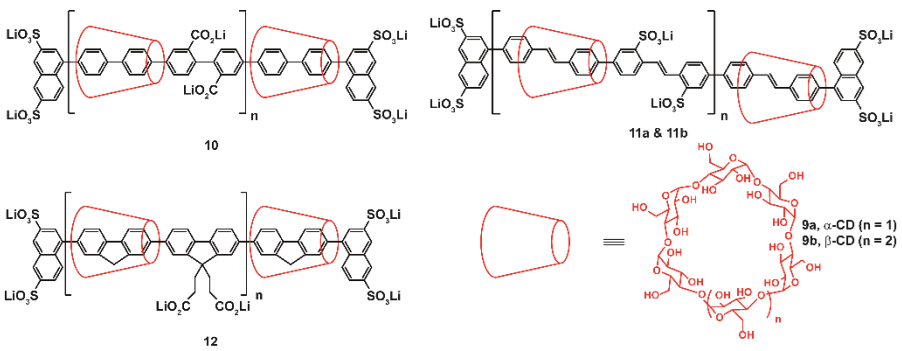

Figure 3. Chemical structures of the cyclodextrin (CD) threaded conjugated polyrotaxanes. α-CD-poly(*p*-phenylene), **10** , α and β-CD-poly(4,4′-diphenylene vinylene), **11a** and **11b**, and β-CD-polyfluorene, **12**.

16. F. Huang and H. W. Gibson, *Prog. Polym. Sci.*, 2005, **30**, 982-1018.
17. F. Cacialli, J. S. Wilson, J. J. Michels, C. Daniel, C. Silva, R. H. Friend, N. Severin, P. Samori, J. P. Rabe, M. J. O'Connell, P. N. Taylor and H. L. Anderson, *Nat. Mater.*, 2002, **1**, 160-164.

Crown ethers are not only a good supramolecular synthon for the synthesis of rotaxanes, but are also a good tool to synthetize polyrotaxanes. Gibson's group was active in the preparation of main-chain polyrotaxanes incorporating crown ethers. For example, they synthetized main chain polyrotaxanes of type B (Figure 2), through polyester[18] and polyurethane[19] polycondensation in presence of unsubstituted crown ether.

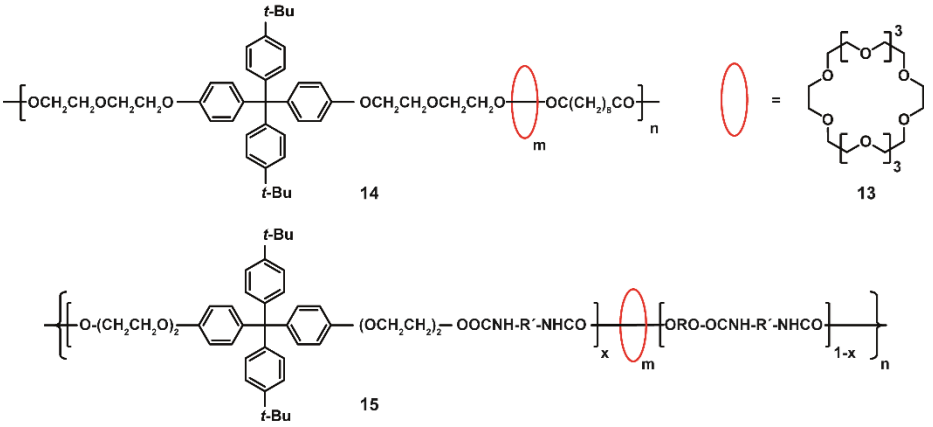

Figure 4. Top: main chain polyester derivative polyrotaxanes **14**. Bottom: main chain polyurethane derivative polyrotaxanes **15**. The wheels interlocked to the polymeric axle are 30-crown-10 ether, **13**.

The authors have achieved to synthetize polyrotaxanes structures, obtaining ratios of m/n up to 0.061 and 0.049 for polyester and polyurethane derivatives, respectively. In the case of polyurethane, the frequency with which the stoppers are present in the backbone of the polymer, and the mobility of the wheels, can be modulated by changing the monomers proportion.

In the examples showed above, the main chain polyrotaxanes grow in one dimension, exclusively. The next work,[20] carried out in the Gibson´s group, shows the possibility to obtain higher order materials from main chain polyrotaxanes, designed to produce branched or cross-linked polymers (Figure 5). They synthetized a series of co-polyurethane derivatives using different proportions of the monomers: bis(5-(hydroxymethyl)-1,3-phenylene)-32-crown-10, tetra-(ethylene glycol) and 4,4′-methylenebis(*p*-phenyl isocyanate). The authors measured the polydispersity index (PDI) of the copolymers, through gel permeation chromatography (GPC). Polyurethane derivatives with crown ethers

18. C. Gong and H. W. Gibson, *Macromolecules*, 1996, **29**, 7029-7033.
19. C. Gong, T. E. Glass and H. W. Gibson, *Macromolecules*, 1998, **31**, 308-313.
20. C. Gong and H. W. Gibson, *J. Am. Chem. Soc.*, 1997, **119**, 8585-8591.

in their structure showed much higher PDI than the polyurethanes without crown ether subunits. Since the monomer unit used to produce these polyurethane derivatives is only bi-functionalized, the increase in the PDI values is an unequivocal proof of the interpenetration of the polymers forming three-dimensional mechanical interlocked derivatives of type D, in Figure 2.

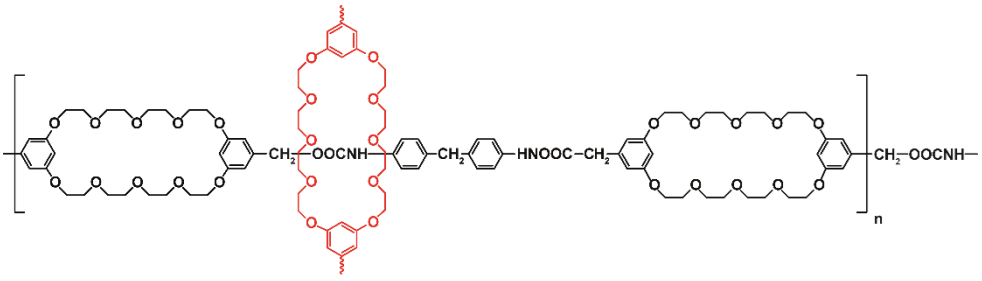

16

Figure 5. Main chain polyrotaxanes type D. Interpenetrating structure in polyurethane derivatives with crown ethers subunits **16**.

The synthesis of side chain polyrotaxanes is also a good alternative. Lee *et al.* [21] published the synthesis of side chain polymers of type F (Figure 2) starting from long methacrylate monomers, which have a polar chain decorated with a bulky end group. The polymerization of the monomer **17a** or **17b** with an excess of **13**, using AIBN as initiator, yielded side chain polyrotaxanes **19a** and **19b**, respectively, following a free-radical-polymerization mechanism. The authors reported a possible mechanism where the formation of the semi-rotaxane **18**, showed in the Scheme 4, occurs before the polymerization reaction. The ratio of crown ethers vs polymer was calculated through ^{1}H-NMR experiment, obtaining ratios m/n up to 0.018 and 0.022 for **19a** and **19b**, respectively.

21. H. W. Gibson, W. S. Bryant and S.-H. Lee, *J. Polym. Sci., Part A: Polym. Chem.*, 2001, **39**, 1978-1993.

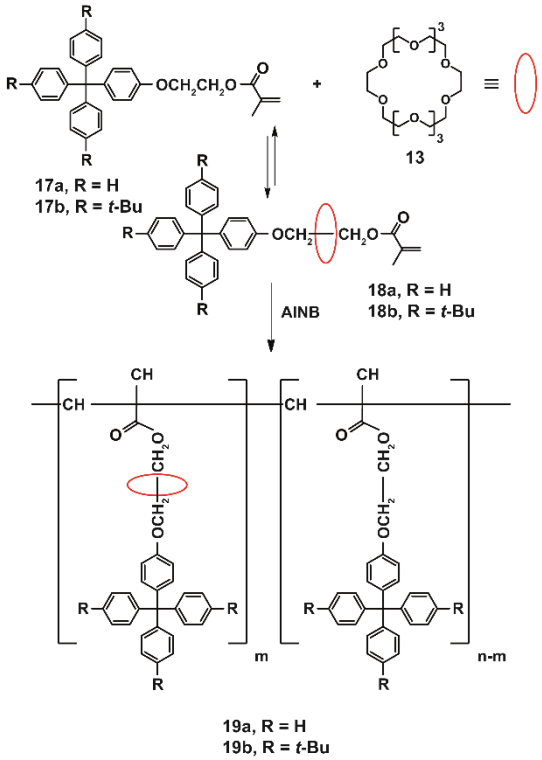

Scheme 4. Synthesis of side chain polyrotaxanes of type F through: a) threading process and b) free radical polymerization.

The last example of polyrotaxanes showed in the present thesis corresponds to side chain, type G. Woisel and coworkers[22] published a study about the versatility of the click chemistry reaction to form polypseudorotaxanes, polyrotaxanes and polycatenanes. From a synthetic point of view the procedure is simple, upon generating a polymer decorated with azide groups, pseudorotaxanes, catenanes or rotaxanes can be attached at a later stage. Woisel and co-workers synthesized the cyclophane [2]rotaxane **20** decorated with an alkyne group, by template-directed clipping methodology, using the π-π interaction between naphthalene axle and aromatic rings of cyclophane as driving force. Polymer **24** was readily synthesized from copolymerization of styrene **21** and *p*-chloromethyl styrene **22** followed by substitution of chlorine by azide group with sodium azide (Scheme 5). Then, this polymer in presence

22. M. Bria, J. Bigot, G. Cooke, J. Lyskawa, G. Rabani, V. M. Rotello and P. Woisel, *Tetrahedron*, 2009, **65**, 400-407.

of [2]rotaxane **20** and copper (I) catalyst gives the polyrotaxanes **25** through 1,3-dipolar cycloadditions, as the authors confirmed by ^{1}H-NMR experiments.

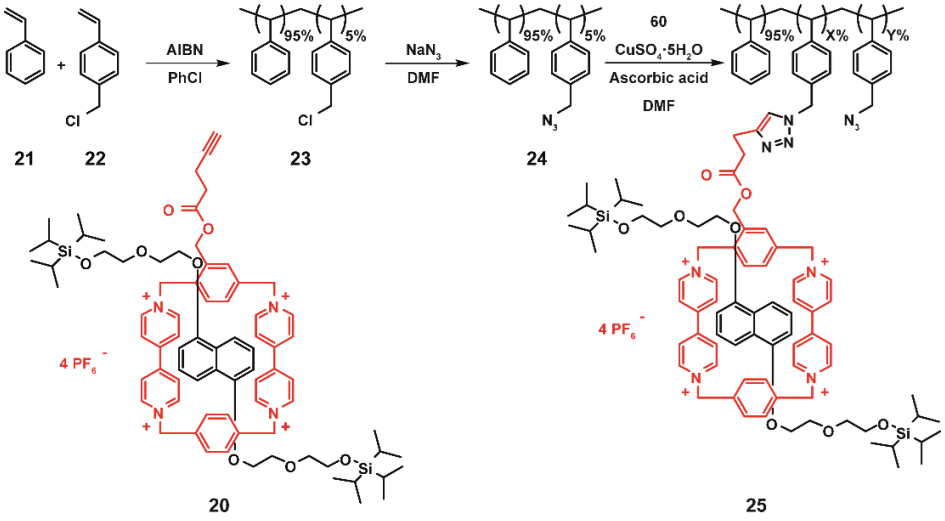

Scheme 5. Synthesis of side chain polyrotaxanes **25** of type G through 1,3-dipolar cycloaddition of preformed [2]rotaxane **20** and polymer functionalized with azide groups.

1.2 Single Walled Carbon Nanotubes (SWNTs)

Carbon nanotubes (CNTs) are an allotropic form of carbon, like diamond, graphite, or the fullerenes. Diamond is composed of four-coordinate sp^3 carbon atoms that form a three-dimensional network. In contrast, graphite has three-coordinate sp^2 carbon atoms forming two-dimensional sheets constituted by hexagonal rings. Graphite forms a three-dimensional structure due to the stacking of the two-dimensional sheets through van der Waals interactions. Fullerene C_{60}, discovered by Kroto *et al.*[23] in 1985, is a spherical cage due to the addition of pentagonal rings, which break the planarity of the hexagonal sheets of the graphitic structure. The ability to obtain C_{60} in gram scale, together the promising results in photovoltaic applications of fullerene derivatives, produced a great interest in the research community. In 1991, Ijima[24] observed the formation of nanotubules of graphite during an arc-discharge experiment, similar to the synthesis of fullerenes. These nanotubes are formed by rolled graphitic

23. H. W. Kroto, J. R. Heath, S. C. O'Brien, R. F. Curl and R. E. Smalley, *Nature*, 1985, **318**, 162-163.
24. S. Iijima, *Nature*, 1991, **354**, 56-58.

sheets, which have a concentric cylinders structure. Multi-walled carbon nanotubes (MWNTs), have a centric nanotube with ca. 1 nm diameter covered by graphitic cylindrical layers separated by ~ 3.4 Å. Single walled carbon nanotubes (SWNTs) were simultaneously discovered by Ijima[25] and Bethune,[26] in 1993. In 2004, A. K. Geim and K. S. Novoselov isolated and characterized a single layer of graphite, graphene,[27, 28] which raised great interest in the scientific community due to its outstanding electronic properties.

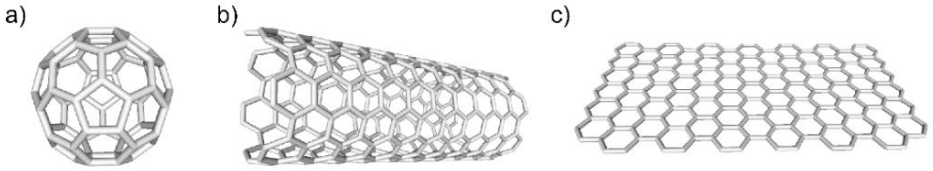

Figure 6. Chemical models of: a) Fullerene C_{60}, b) SWNT and c) Graphene sheet.

Conceptually SWNTs are the result of rolling up a graphene sheet. Depending on the angle with which the graphene sheet is rolled, there is a great variety of SWNTs with different diameters, electronic behavior and chiralities. The crystal lattice of a SWNT is defined by an n and m chiral index. Depending on the value of the chiral indices (n, m), the SWNTs are classified in three groups: zig-zag nanotubes (m = 0), armchair nanotubes (n = m) and chiral nanotubes ($n \neq m \neq 0$). SWNTs have a typical diameter of 1 – 2 nm and length of several micrometers. The large aspect ratio (typically ca. 300 – 1000) makes SWNTs a quasi-1D material, which exhibit high flexibility[29] and low mass density.[30]

25. S. Iijima and T. Ichihashi, *Nature*, 1993, **363**, 603-605.
26. D. S. Bethune, C. H. Klang, M. S. de Vries, G. Gorman, R. Savoy, J. Vázquez and R. Beyers, *Nature*, 605-607.
27. K. S. Novoselov, A. K. Geim, S. V. Morozov, D. Jiang, Y. Zhang, S. V. Dubonos, I. V. Grigorieva and A. A. Firsov, *Science*, 2004, **306**, 666.
28. A. K. Geim and K. S. Novoselov, *Nat. Mater.*, 2007, **6**, 183-191.
29. C. A. Cooper, R. J. Young and M. Halsall, *Composites Part A*, 2001, **32**, 401-411.
30. G. Guanghua, Ç. Tahir and A. G. William, III, *Nanotechnology*, 1998, **9**, 184.

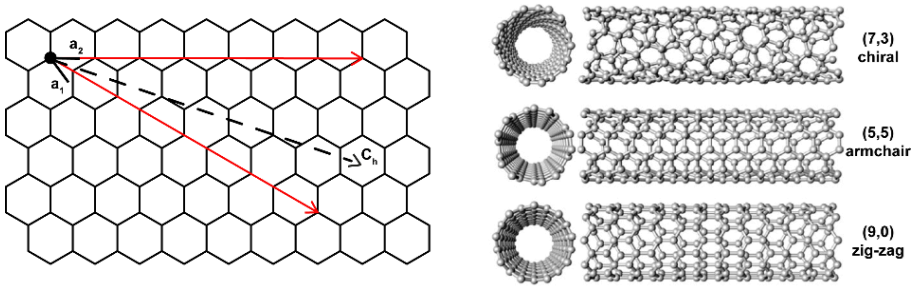

Figure 7. Left: schematic of a two-dimensional graphene sheet illustrating lattice vectors $\mathbf{a_1}$ and $\mathbf{a_2}$, and the roll-up vector $C_h = n\mathbf{a_1} + m\mathbf{a_2}$. The limiting cases of (n,0) zigzag and (n,n) armchair tubes are indicated with red arrows. Right: models of zigzag, armchair and chiral nanotubes

Because of the strength of the C–C double bond, SWNTs have great mechanical properties showing a Young's modulus up to 1.25 TPa measured in SWNT ropes.[31,32] This value is one order of magnitude higher than steel's. Moreover, the electronic properties of SWNTs are also remarkable. Depending only on their diameter and/or chilarity, SWNTs can be either metallic or semiconductors without the necessity of any doping.[33,34,35] Finally, the combination of the high aspect ratio, sharp geometry, high chemical stability and mechanical strength, make SWNTs suitable to experiment the field emission of electrons. This phenomenon consists on the emission of electrons through a solid surface of the material, when a high electric field (ca. 10^7 V cm^{-1}) with a negative electrical potential is applied.[36]

SWNTs are considered one of the most promising building blocks for future nanoelectronic technology due to the extraordinary properties showed above. Currently, they have already found application in many different fields. To illustrate it, here were enumerate some of their applications: i) as electrodes in electrochemical devices such as supercapacitors[37,38]; ii) as field emission

31. A. Krishnan, E. Dujardin, T. W. Ebbesen, P. N. Yianilos and M. M. J. Treacy, *Phys. Rev. B*, 1998, **58**, 14013-14019.
32. J.-P. Salvetat, G. A. D. Briggs, J.-M. Bonard, R. R. Bacsa, A. J. Kulik, T. Stöckli, N. A. Burnham and L. Forró, *Phys. Rev. Lett.*, 1999, **82**, 944-947.
33. J. W. Mintmire, B. I. Dunlap and C. T. White, *Phys. Rev. Lett.*, 1992, **68**, 631-634.
34. M. Ouyang, J.-L. Huang, C. L. Cheung and C. M. Lieber, *Science*, 2001, **292**, 702.
35. M. Ouyang, J.-L. Huang and C. M. Lieber, *Acc. Chem. Res.*, 2002, **35**, 1018-1025.
36. Y. Saito and S. Uemura, *Carbon*, 2000, **38**, 169-182.
37. K. H. An, W. S. Kim, Y. S. Park, J. M. Moon, D. J. Bae, S. C. Lim, Y. S. Lee and Y. H. Lee, *Adv. Funct. Mater.*, 2001, **11**, 387-392.
38. C. Niu, E. K. Sichel, R. Hoch, D. Moy and H. Tennent, *Appl. Phys. Lett.*, 1997, **70**, 1480-1482.

electron sources[39] for flat panel displays;[40,41] iii) as components in nanometer size electronic devices such as nanotube field effect transistors (NT-FETs);[42] iv) as active materials in chemical sensor applications;[43] v) as components in polymer composites;[44,45,] vi) as drug delivery[46] systems and medical nanorobots.[47]

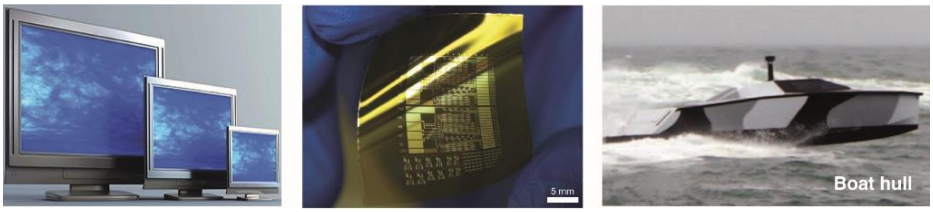

Figure 8. Left: TV screen based on carbon nanotubes OLED.[48] Middle: Photograph of a collection of SWNT transistors and circuits on a thin sheet of plastic (PI).[49] Right: CNT sheets and yarns used as lightweight data cables and electromagnetic shielding material.[50]

1.3 Chemical Functionalization of SWNTs

Carbon nanotubes present outstanding physical properties, but their synthesis leads to complex mixtures of carbon nanotubes with different diameters, chiralities and lengths, which make them less suitable for real applications. Currently, many research efforts are focused not only in the synthesis[51,52,53] of

39. W. A. de Heer, A. Châtelain and D. Ugarte, *Science*, 1995, **270**, 1179.
40. N. S. Lee, D. S. Chung, I. T. Han, J. H. Kang, Y. S. Choi, H. Y. Kim, S. H. Park, Y. W. Jin, W. K. Yi, M. J. Yun, J. E. Jung, C. J. Lee, J. H. You, S. H. Jo, C. G. Lee and J. M. Kim, *Diamond Relat. Mater.*, 2001, **10**, 265-270.
41. M. A. McCarthy, B. Liu, E. P. Donoghue, I. Kravchenko, D. Y. Kim, F. So and A. G. Rinzler, *Science*, 2011, **332**, 570.
42. S. J. Tans, A. R. M. Verschueren and C. Dekker, *Nature*, 1998, **393**, 49-52.
43. J. Kong, N. R. Franklin, C. Zhou, M. G. Chapline, S. Peng, K. Cho and H. Dai, *Science*, 2000, **287**, 622-625.
44. P. M. Ajayan, O. Stephan, C. Colliex and D. Trauth, *Science*, 1994, **265**, 1212.
45. O. Breuer and U. Sundararaj, *Polym. Compos.*, 2004, **25**, 630-645.
46. Z. Liu, X. Sun, N. Nakayama-Ratchford and H. Dai, *ACS Nano*, 2007, **1**, 50-56.
47. A. M. Popov, Y. E. Lozovik, S. Fiorito and L. Yahia, *Int J Nanomedicine*, 2007, **2**, 361-372.
48. *Patent US7473930,* Use of patterned CNT arrays for display purposes.
49. Q. Cao, H.-s. Kim, N. Pimparkar, J. P. Kulkarni, C. Wang, M. Shim, K. Roy, M. A. Alam and J. A. Rogers, *Nature*, 2008, **454**, 495-500.
50. M. F. L. De Volder, S. H. Tawfick, R. H. Baughman and A. J. Hart, *Science*, 2013, **339**, 535-539.
51. H. Dai, *Acc. Chem. Res.*, 2002, **35**, 1035-1044.
52. S. M. Bachilo, L. Balzano, J. E. Herrera, F. Pompeo, D. E. Resasco and R. B. Weisman, *J. Am. Chem. Soc.*, 2003, **125**, 11186-11187.
53. A. R. Harutyunyan, G. Chen, T. M. Paronyan, E. M. Pigos, O. A. Kuznetsov, K. Hewaparakrama, S. M. Kim, D. Zakharov, E. A. Stach and G. U. Sumanasekera, *Science*, 2009, **326**, 116.

carbon nanotubes and their purification though physical methods,[54,55,56] but also in the chemical functionalization of SWNTs covalent[57] or non-covalently[58] to purify[59] the complex mixture of them or to modulate their interesting properties. Besides the functionalization of the outer surface of the SWNTs (exohedral functionalization), the endohedral functionalization of SWNTs is an alternative that is also being extensively studied.[60,61]

1.3.1 Covalent Functionalization

The covalent modification of SWNTs involves the rupture or saturation of a C–C double bond of the scaffold of the SWNTs to form at least a new strong covalent bond between the nanotube and the molecule with which we are functionalizing it. As consequence, the products obtained have high stability, but the native properties of the pristine material change. There are two approximations to functionalize SWNTs covalently: i) amidation or esterification of carbon nanotubes previously oxidized; ii) addition reactions to the sidewalls of the SWNTs. The covalent functionalization of carbon nanotubes is a very extensive field, we have chosen to illustrate it with a few selected examples.

Amidation or esterification strategies must be carried out with pre-oxidized SWNTs. Many methods of oxidation of carbon nanotubes have been described using mixtures of H_2SO_4: HNO_3 or H_2SO_4: H_2O_2 with different proportions.[62,63] These oxidizing treatments endow SWNTs with oxygenated functional groups, a significant part of which are carboxyilic acids, which can be activated through chlorides or carbodiimide intermediates to promote the coupling with amines or alcohols. To solubilize SWNTs, Haddon and coworkers functionalized shortened SWNTs through amidation with octadecylamine to obtain the

54. R. Krupke, F. Hennrich, H. v. Löhneysen and M. M. Kappes, *Science*, 2003, **301**, 344.
55. M. S. Arnold, S. I. Stupp and M. C. Hersam, *Nano Lett.*, 2005, **5**, 713-718.
56. H. Liu, T. Tanaka, Y. Urabe and H. Kataura, *Nano Lett.*, 2013, **13**, 1996-2003.
57. S. Banerjee, T. Hemraj-Benny and S. S. Wong, *Adv. Mater.*, 2005, **17**, 17-29.
58. Y.-L. Zhao and J. F. Stoddart, *Acc. Chem. Res.*, 2009, **42**, 1161-1171.
59. X. Tu, S. Manohar, A. Jagota and M. Zheng, *Nature*, 2009, **460**, 250-253.
60. A. Hirsch, *Angew. Chem. Int. Ed.*, 2002, **41**, 1853-1859.
61. A. de Juan and E. M. Pérez, *Nanoscale*, 2013, **5**, 7141-7148.
62. Z. Chen, K. Kobashi, U. Rauwald, R. Booker, H. Fan, W.-F. Hwang and J. M. Tour, *J. Am. Chem. Soc.*, 2006, **128**, 10568-10571.
63. K. Flavin, I. Kopf, E. Del Canto, C. Navio, C. Bittencourt and S. Giordani, *J. Mater. Chem.*, 2011, **21**, 17881-17887.

derivative **26** (Scheme 6).[64] The authors obtained SWNTs derivatives soluble in most organic solvents thanks to the contribution of octadecylamine chains, which act as solubilizing groups. To produce carbon nanotubes soluble in water, the same research group decided to functionalize oxidized SWNTs with the polar poly(*m*-aminobenzene sulfonic acid) (PABS)[65] through amidation reaction. Besides solubilizing SWNTs, this approach can be used to combine the interesting properties of SWNTs with other materials. Delgado *et al*. described one of the first examples of conjugated material based on SWNTs and fullerene C_{60}, derivative **28**, coupling an aniline fullerene derivative and carboxylic SWNTS through amidation reaction.[66]

64. M. A. Hamon, J. Chen, H. Hu, Y. Chen, M. E. Itkis, A. M. Rao, P. C. Eklund and R. C. Haddon, *Adv. Mater.*, 1999, **11**, 834-840.
65. B. Zhao, H. Hu and R. C. Haddon, *Adv. Funct. Mater.*, 2004, **14**, 71-76.
66. J. L. Delgado, P. de la Cruz, A. Urbina, J. T. López Navarrete, J. Casado and F. Langa, *Carbon*, 2007, **45**, 2250-2252.

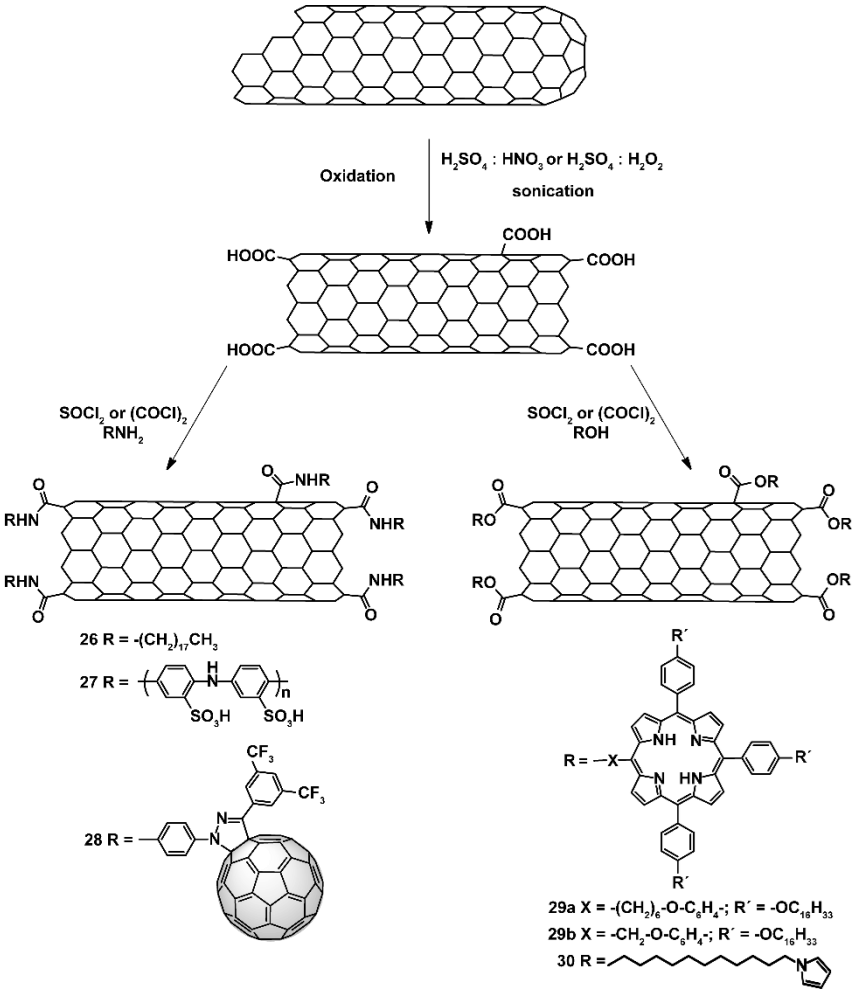

Scheme 6. Representative examples of covalent functionalization of SWNTs through amidation or esterification reaction.

Functionalization of oxidized SWNTs through esterification reaction has also been widely explored. The synthesis of SWNTs-porphyrin systems soluble in organic solvents through esterification reaction have been reported by different groups. Li and coworkers[67] reported the synthesis of compounds **29a** and **29b** (Scheme 6). They observed that the fluorescence intensity of the porphyrin units attached to the SWNTs have a strong dependence with the distance between them and the SWNTs sidewall. For shorter spacer length the fluorescence

67. H. Li, R. B. Martin, B. A. Harruff, R. A. Carino, L. F. Allard and Y. P. Sun, *Adv. Mater.*, 2004, **16**, 896-900.

intensity decreases, showing a quenching effect. The pyrrole-ester SWNTs derivative **30**, that is soluble in THF, was used to obtain carbon nanotube-polymer frameworks through electro-polymerization by Cosnier *et al.*[68]

The covalent functionalization of SWNTs through addition reactions to the sidewalls or caps of the carbon nanotube requires more reactive agents. SWNTs without significant defects nor oxygenated functional groups, present two regions with different reactivity: caps and sidewall. The closed edge of SWNTs has five membered rings, and higher curvature than the sidewall of the SWNTs. The change from sp^2 to sp^3 hybridization produced on the carbon atoms of the nanotube by the addition reaction, lead to a local geometry change from trigonal-planar to tetrahedral. This procedure is more favorable at the tips due to their higher curvature compared with the sidewall. These factors lead to a higher reactivity of the caps, comparable to fullerene. This reasoning fits when the SWNT has an ideal structure, but in reality, the reaction most probably occurs at, or close to, defect sites.[69]

Addition chemistry to SWNTs is a very wide area, Prato and coworkers[70] divided and classified it in: fluorination, addition of carbenes, addition of nitrenes, 1,3-dipolar cycloaddition, Diels-Alder cycloadditions, nucleophilic addition, free radical additions, reduction and reductive alkylation, and direct arylations.

68. S. Cosnier and M. Holzinger, *Electrochim. Acta*, 2008, **53**, 3948-3954.
69. D. Srivastava, D. W. Brenner, J. D. Schall, K. D. Ausman, M. Yu and R. S. Ruoff, *J. Phys. Chem. B*, 1999, **103**, 4330-4337.
70. P. Singh, S. Campidelli, S. Giordani, D. Bonifazi, A. Bianco and M. Prato, *Chem. Soc. Rev.*, 2009, **38**, 2214-2230.

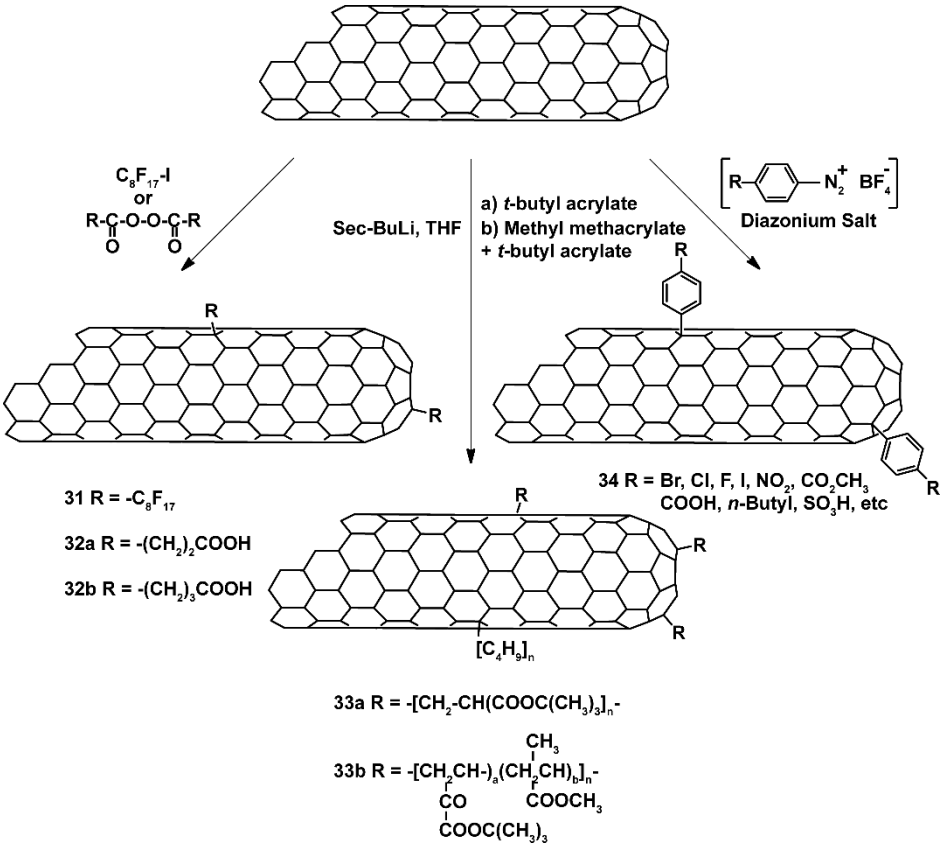

Scheme 7. Functionalization of SWNTs using radical addition (left), reduction and polymerization reaction (middle) and direct arylation (right).

Fluorination of SWNTs introduces one fluorine atom every two SWNT carbon atoms.[71] After the fluorination reaction the majority of carbon nanotubes preserve their tube-like structure at temperatures up to 400°C. Fluorinated SWNTs can be defluorinated with anhydrous hydrazine.

Free radical addition is an extended strategy of functionalization of SWNTs. The radical species can be formed from inorganic ions by photochemical or thermal reactions. Holzinger *et al.*[72] reported the reaction of SWNTs with hectadecafluorooctyl iodide to add perfluorooctyl groups (**31**). Peng *et al.*[73] used

71. E. T. Mickelson, C. B. Huffman, A. G. Rinzler, R. E. Smalley, R. H. Hauge and J. L. Margrave, *Chem. Phys. Lett.*, 1998, **296**, 188-194.
72. M. Holzinger, O. Vostrowsky, A. Hirsch, F. Hennrich, M. Kappes, R. Weiss and F. Jellen, *Angew. Chem. Int. Ed.*, 2001, **40**, 4002-4005.
73. H. Peng, L. B. Alemany, J. L. Margrave and V. N. Khabashesku, *J. Am. Chem. Soc.*, 2003, **125**, 15174-15182.

organic peroxide derivatives of succinic and glutaric acid to introduce acid groups at different distances to the nanotube surface (**32a** and **32b**) by free radical addition. These acid groups can be used to attach any amine derivative forming amide bonds at a later stage.

The reduction of carbon nanotubes to carbanionic derivatives produces suitable intermediates for different electrophilic reactions. The formation of the anionic sites on the surface of SWNTs with alkyl carbanions, followed by anionic polymerization (**33a**) or co-polymerization (**33b**) of acrylate derivatives leads to combine covalently SWNTs and polymers.[74]

The last kind of reaction, that only involves one carbon atom of the nanotube per molecule linked, is the direct arylation. This approximation was introduced in the chemistry of SWNTs by the group of Tour. It is based on diazonium salts coupling. This protocol is one of the most useful in the covalent functionalization of carbon nanotube. For example, they synthetized the family of SWNTs derivatives **34** by addition of aryl diazonium salts reduced electrochemically through the "Tour reaction".[75] The authors obtained degrees of functionalization of up to one functional group every 20 carbon atoms.

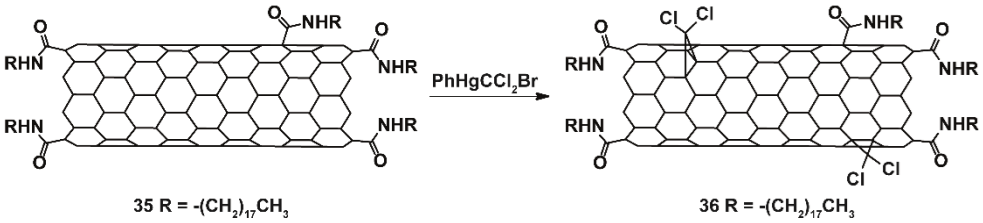

Scheme 8. Carbene addition to SWNTs previously functionalized with octadecylamine.

Addition of carbenes occurs through a cyclopropanation mechanism. In the example illustrated in the Scheme 8, functionalized SWNTs with octadecylamine **35**, through amidation reaction, were mixed with a source of dichlorocarbene (phenyl (bromodichloromethyl)-mercury) to generate the derivative **36**.[76] The authors observed by Raman and IR spectroscopies, that the reaction is reversible applying high temperature.

74. S. Chen, D. Chen and G. Wu, *Macromol. Rapid Commun.*, 2006, **27**, 882-887.
75. C. A. Dyke and J. M. Tour, *J. Phys. Chem. A*, 2004, **108**, 11151-11159.
76. H. Hu, B. Zhao, M. A. Hamon, K. Kamaras, M. E. Itkis and R. C. Haddon, *J. Am. Chem. Soc.*, 2003, **125**, 14893-14900.

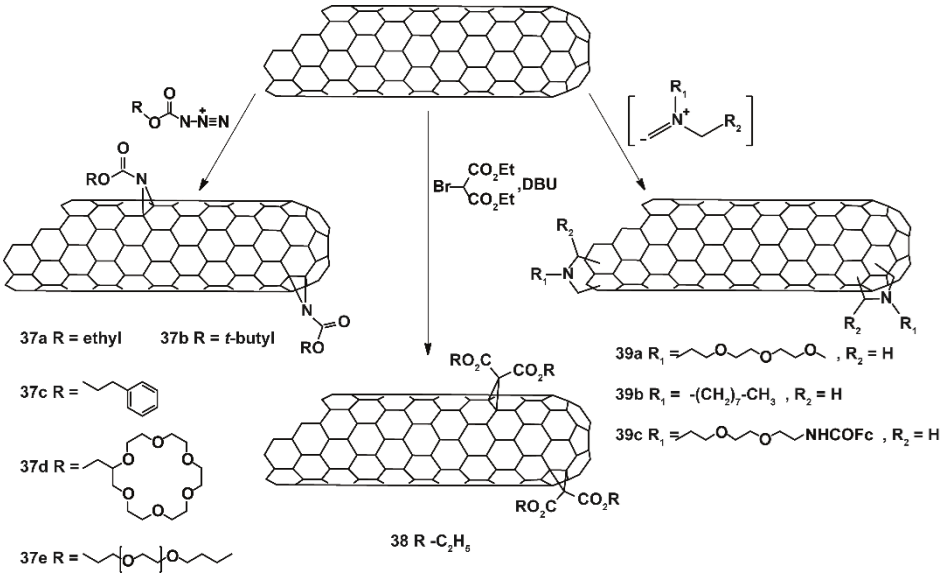

Scheme 9. Addition of nitrenes (left), nucleophile (middle) and 1,3 dipolar cycloaddition (right).

Similar to carbenes, the addition of nitrenes leads to the formation of azacyclopropanes of SWNTs. Alkyl azidoformates were used as precursors of nitrenes by thermal extrusion of nitrogen to produce alkoxycarbonylaziridino-SWNTs derivatives **37**, by Hirsch and coworkers.[77] They demonstrated that the reaction is compatible with a variety of addends independently of their size or complexity.

Nucleophilic addition of relative stable β-di-ketones to the sidewalls of carbon nanotubes was reported by Coleman *et al.*[78] They described the cyclopropanation reaction of diethyl bromo-malonate with the surface of SWNTs. To characterize the products, they tagged them through transesterification reaction with a thiol derivative and a fluorinated molecule, to attach the SWNTS derivatives to gold nanoparticles and to study them through ^{19}F-NMR, respectively.

The 1,3-dipolar cycloaddition, widely used in the chemistry of fullerenes, can be also applied to the covalent functionalization of SWNTs. This reaction offers many alternatives, such as the use of azomethine ylides generated *in situ* by

77. M. Holzinger, J. Abraham, P. Whelan, R. Graupner, L. Ley, F. Hennrich, M. Kappes and A. Hirsch, *J. Am. Chem. Soc.*, 2003, **125**, 8566-8580
78. K. S. Coleman, S. R. Bailey, S. Fogden and M. L. H. Green, *J. Am. Chem. Soc.*, 2003, **125**, 8722-8723.

thermal condensation of aldehydes and α-amino-acids,[79] from aziridines[80] or trialkylamine N-oxides,[81] etc, to functionalize SWNTs. Prato *et al.*[82] described a variety of pyrrolidine rings equipped with solubilizing chains (**39a** and **39b**) or electron donor moieties such as ferrocene (**39c**), linked to the sidewall of SWNTs.

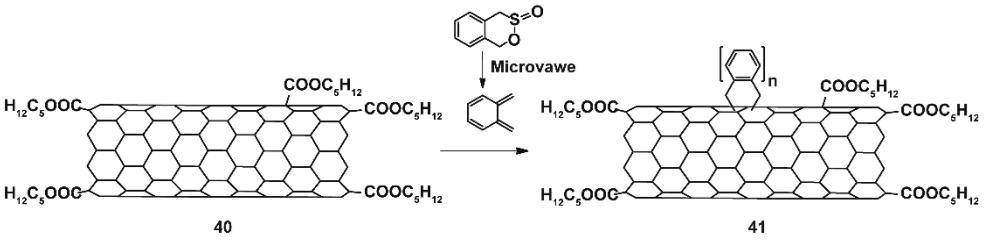

Scheme 10. Diels-Alder reaction.

Diels-Alder reactions to functionalize SWNTs have been explored by Langa and coworkers.[83] *O*-quinodimethane, which was generated *in situ* from 4,5-benzo-1,2-oxathiin-2-oxide (sultine) under microwave irradiation, reacted with oxidized and esterified SWNTs **40** to form the derivative **41**. Although the Diels-Alder reaction is applied to the chemistry of the SWNTs, due to the reversibility of the process, it is not very extended.

1.3.2 Noncovalent Functionalization

Noncovalent modification of SWNTs consist on attaching molecules, such as aromatic compounds, polymers, DNA, surfactants, etc. on the sidewalls of the carbon nanotubes, through a combination of dispersion-type forces, including mainly van der Waals and solvophobic interactions. These alternatives lead to improve the solubility and processability of carbon nanotubes, while the native structure and therefore, the properties of the SWNTs are preserved. However, although the thermodinamic stablilty of the noncovalent constructs can be tuned, their kinetic stability is usually low.

79. D. Tasis, N. Tagmatarchis, A. Bianco and M. Prato, *Chem. Rev.*, 2006, **106**, 1105-1136.
80. F. G. Brunetti, M. A. Herrero, J. d. M. Muñoz, S. Giordani, A. Díaz-Ortiz, S. Filippone, G. Ruaro, M. Meneghetti, M. Prato and E. Vázquez, *J. Am. Chem. Soc.*, 2007, **129**, 14580-14581.
81. C. Ménard-Moyon, N. Izard, E. Doris and C. Mioskowski, *J. Am. Chem. Soc*., 2006, **128**, 6552-6553.
82. D. M. Guldi, M. Marcaccio, D. Paolucci, F. Paolucci, N. Tagmatarchis, D. Tasis, E. Vázquez and M. Prato, *Angew. Chem. Int. Ed.*, 2003, **42**, 4206-4209.
83. J. L. Delgado, P. de la Cruz, F. Langa, A. Urbina, J. Casado and J. T. López Navarrete, *Chem. Commun.*, 2004, 1734-1735.

Because of their extreme aspect ratio, SWNTs experiment strong Wan der Waals interaction between them, which results in significant bundling of them, where many nanotubes are very closely aligned. In order to disaggregate this bundles of SWNTs, the use of amphiphilic molecules has been extensively studied.

The efficacy of the surfactant depends largely on the nature of the polar region. For example, sodium dodecyl sulfate (SDS) **42**, or tetraalkylammonuim bromide derivatives such as (DTAB) **43**, are charged surfactants capable to solubilize SWNTs forming stable micelles. Besides the nature of the polar group, the efficiency of the surfactant also depends on the length and shape of the hydrophobic part. The extension of the interaction increases with surface, that is, with longer and branched alkyl chains.[84] Yodh *et al.*[85] carried out a comparison between two surfactants: **42** and sodium dodecylbenzene sulfonate (SDBS) **44**, to study the influence of the presence of aromatic rings in the surfactant molecule. They observed that the phenyl ring present in **44** increases its capacity of solubilize SWNTs with respect to **41**, due to the additional π-π interaction between the hydrophobic region of the surfactant and the sidewall of the nanotube.

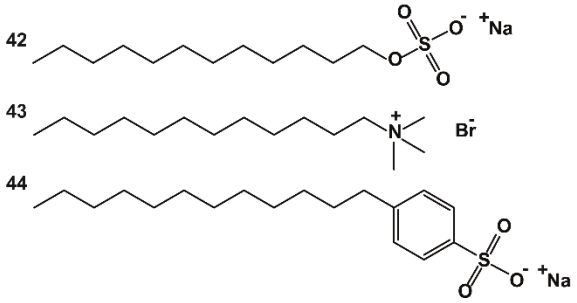

Figure 8. Amphiphilic molecules used to solubilize SWNTs. Sodium dodecyl sulfate, **42**, tetraalkylammonuim bromide, **43** and sodium dodecylbenzene sulfonate, **44**.

Large aromatic systems, such as pyrene, anthracene, porphyrins or phthalocyanins have shown interact with the sidewall of carbon nanotubes through π-π stacking. Dai *et al.*[86] discovered that *N*-succinimidyl-1-

84. W. Wenseleers, I. I. Vlasov, E. Goovaerts, E. D. Obraztsova, A. S. Lobach and A. Bouwen, *Adv. Funct. Mater.*, 2004, **14**, 1105-1112.
85. M. F. Islam, E. Rojas, D. M. Bergey, A. T. Johnson and A. G. Yodh, *Nano Lett.*, 2003, **3**, 269-273.
86. R. J. Chen, Y. Zhang, D. Wang and H. Dai, *J. Am. Chem. Soc.*, 2001, **123**, 3838-3839.

pyrenebutanoate molecule can be deposited on the sidewalls of SWNTs in organic solvents with a high degree of surface coverage, and remain attached irreversibly to the carbon nanotubes in aqueous media (Figure 9). The reactivity of the succinimidyl ester group with nucleophilic molecules leads to the further functionalization of the nanotube derivatives **45** with biological molecules, such as ferritin, streptavidin or biotinyl-3,6-dioxaoctanediamine. This strategy allows linking a wide range of molecules that could be used for sensor applications.

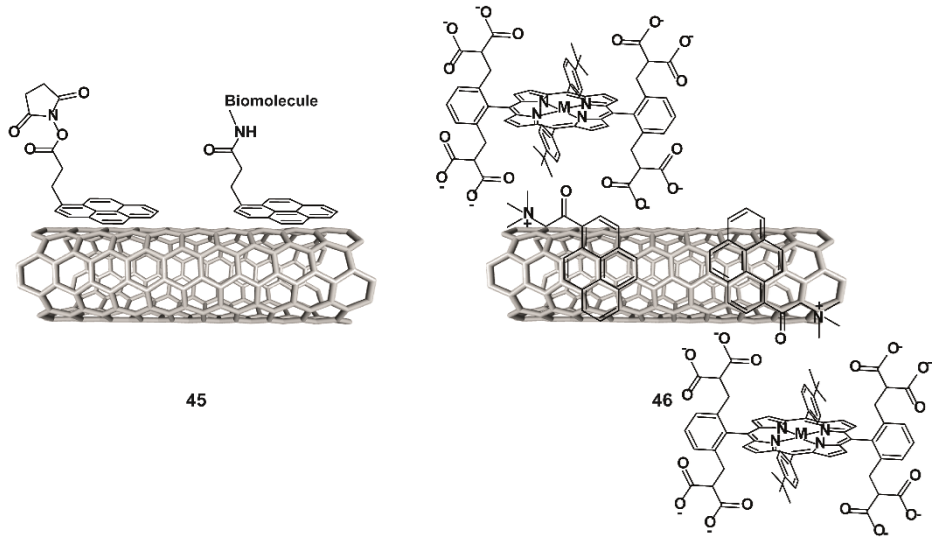

Figure 9. Left. Use of *N*-succinimidyl-1-pyrenebutanoate as anchoring for link different biomolecules, **45**. Right. Donor-acceptor nanohybrid based on SWNTs/pyrene and porphyrin molecules, **46**.

A charged pyrene derivative, 1-(trimethylammonium acetyl) pyrene was used by Prato and coworkers[87] to solubilize SWNTs in aqueous media. Then, negatively charged molecules can be attached to the positively charged surface of the SWNTs-pyrene derivative. The authors combine a negatively charged porphyrin (strong electron donor) to the SWNTs/pyrene hybrid to form **46**, a novel electron donor-acceptor nanohybrid with a microsecond-lived charge separated state upon photoirradiation.

Anthracene and their derivatives also show specific π-π stacking with the sidewalls of SWNTs. Murray and coworkers[88] observed that the absorption spectrum of anthracene derivatives **47** remains unchanged after adsorption onto

87. C. Ehli, G. M. A. Rahman, N. Jux, D. Balbinot, D. M. Guldi, F. Paolucci, M. Marcaccio, D. Paolucci, M. Melle-Franco, F. Zerbetto, S. Campidelli and M. Prato, *J. Am. Chem. Soc*., 2006, **128**, 11222-11231.
88. J. Zhang, J. K. Lee, Y. Wu and R. W. Murray, *Nano Lett.*, 2003, **3**, 403-407.

the walls of carbon nanotubes. However, their fluorescence emission is red-shifted, showing an electron charge-transfer effect from the SWNTs to the anthracene molecules. The thermodynamic stability of the supramolecular SWNTs-anthracene complexes seems high because they are not removed after several washings with organic solvent. Nevertheless, they are kinetically labile and thermodynamically less stable than pyrene derivatives, as they can be replaced with pyrene under adequate conditions.

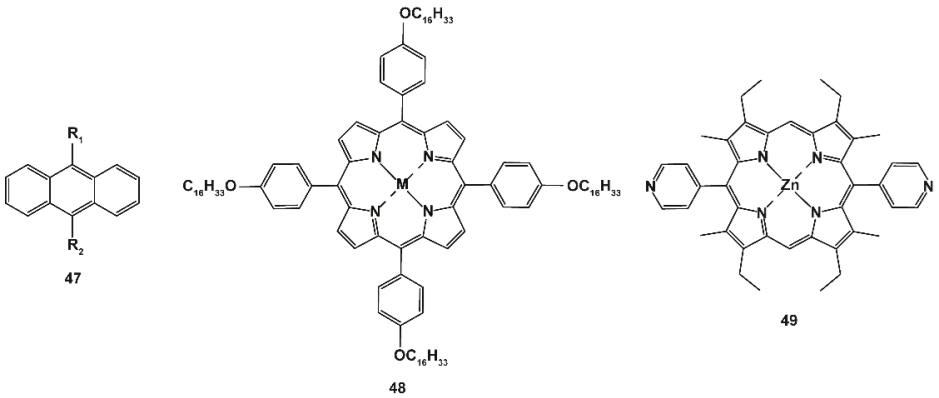

Figure 10. Anthracene and porphyrins derivatives used to functionalize SWNTs non-covalently.

Porphyrin derivatives can also interact with the surface of SWNTs effectively. A symmetric derivative of porphyrin **48**, decorated with long alkyl chains, was capable to solubilize pristine SWNTs in organic solvents, and showed some selectivity for semiconductor SWNTs.[89] Although the main reason of this selectivity is not demonstrated, the authors also observed that the metalloporphirin not allows the solubilization of SWNTs, wherein the free porphyrin is capable to extract the semiconductor SWNTs. Sttodart and coworkers designed NT-FET devices to study the electron transfer in donor-acceptor SWNTs hybrids based on noncovalently linked porphyrin **49** to SWNTs. They observed a photo-induced electron transfer from SWNTs, which act as donor, and the electron acceptor zinc porphyrin.[90] Similar heterocyclic polyaromatic molecules, such as phthalocyanine derivatives, have also been employed to functionalize SWNTs through noncovalent interactions.[91]

89. H. Li, B. Zhou, Y. Lin, L. Gu, W. Wang, K. A. S. Fernando, S. Kumar, L. F. Allard and Y.-P. Sun, *J. Am. Chem. Soc.*, 2004, **126**, 1014-1015.
90. D. S. Hecht, R. J. A. Ramírez, M. Briman, E. Artukovic, K. S. Chichak, J. F. Stoddart and G. Grüner, *Nano Lett.*, 2006, **6**, 2031-2036.
91. X. Wang, Y. Liu, W. Qiu and D. Zhu, *J. Mater. Chem.*, 2002, **12**, 1636-1639.

Martín *el al.*[92] published an example where π-extended tetrathiafulvalene (exTTF) molecules work as recognition moiety of SWNTs for their non covalent modification. In this example they used a molecular tweezer **50**, to form supramolecular derivatives of SWNTs. The molecular tweezer featuring two exTTF subunits as recognition moiety linked by an aromatic spacer which present a polar dendron based on amides and carboxylic acid to make soluble the molecular tweezer in water.

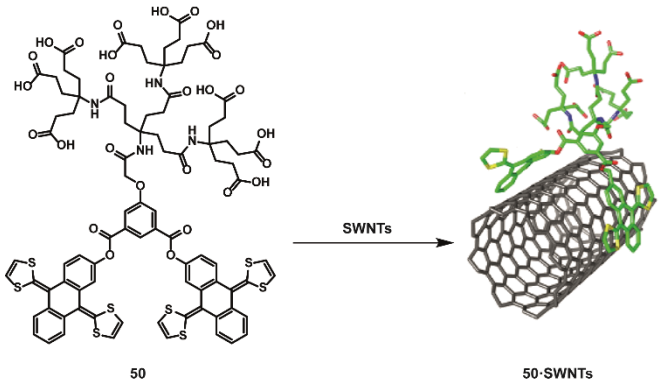

Figure 11. Molecular tweezer **50** and supramolecular complex **50·SWNTs**. Carbon atoms are shown in gray (SWNT) and green (molecular tweezer), sulfur atoms in yellow, oxygen atoms in red and nitrogen atoms in blue.

The SWNTs/exTTF tweezer hybrids were prepared by mixing 1:2 m/m of the SWNTs and molecule **50** in 0.1 M borax aqueous solution. The mixture was stirred, sonicated and centrifuged to yield the **50·SWNTs** complex. The complex obtained was thoroughly characterized by different techniques. Spectroscopic and microscopy characterization together to the changes in the physical properties suggest the presence of **50** attach to the SWNTs. HR-TEM image (Figure 12) shows the sidewalls of the SWNTs covered with organic materials.

92. C. Romero-Nieto, R. García, M. Á. Herranz, C. Ehli, M. Ruppert, A. Hirsch, D. M. Guldi and N. Martín, *J. Am. Chem. Soc.*, 2012, **134**, 9183-9192.

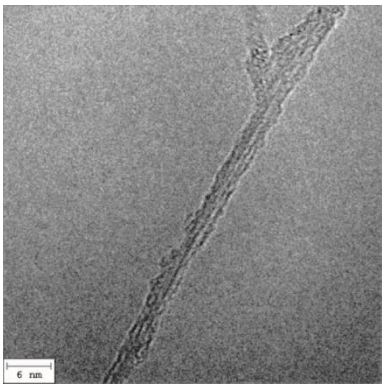

Figure 12. Representative HRTEM image of **50**·SWNT where an amorphous coating can be observed around the SWNT. Scale bar is 6 nm.

Spectroscopic analysis such as steady-state and time-resolved measurements demonstrated the electronic communication between carbon nanotube and molecule **50** in the ground and in the excited states. These experimental results together with the changes in the solubility properties of carbon nanotube show the efficacy of molecule **50** to functionalize SWNTs.

Most kinetically stable non covalent SWNTs derivatives present high stability mainly due to large supramolecular interactions, that imply K_{dis} <<< K_{ass}. This is the case for several oligomer-polymer wrapped SWNTs. Poly(9,9-dioctylfluorenyl-2,7-diyl) (PFO) **51** and their derivatives, have demonstrated the possibility not only of solubilize SWNTs, but also to separate then in function of their electronic character, solubilizing only semiconductor SWNTs.[93,94] Poly(m-phenylenevynilene) (PmPV) conjugated polymer **52** has extensively been used to functionalized SWNTs. **52** shows strong Van der Waals interaction between its conjugated backbone and the surface of carbon nanotube, as demonstrated spectroscopically by NMR[95] and confirmed by theoretical calculations[96].

93. F. Chen, B. Wang, Y. Chen and L.-J. Li, *Nano Lett.*, 2007, **7**, 3013-3017.
94. J.-Y. Hwang, A. Nish, J. Doig, S. Douven, C.-W. Chen, L.-C. Chen and R. J. Nicholas, *J. Am. Chem. Soc*., 2008, **130**, 3543-3553.
95. A. Star, J. F. Stoddart, D. Steuerman, M. Diehl, A. Boukai, E. W. Wong, X. Yang, S.-W. Chung, H. Choi and J. R. Heath, *Angew. Chem. Int. Ed.*, 2001, **40**, 1721-1725.
96. M. in het Panhuis, A. Maiti, A. B. Dalton, A. van den Noort, J. N. Coleman, B. McCarthy and W. J. Blau, *J. Phys. Chem. B*, 2003, **107**, 478-482.

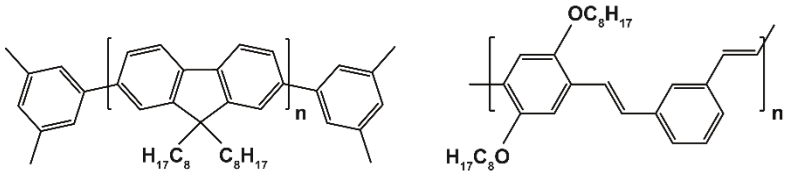

51 **52**

Figure 13. PFO, **51**, and PmPV, **52**, used to functionalize SWNTs non-covalently.

The use of oligomers of DNA (polynucleotides) for the supramolecular modification of carbon nanotubes started to be studied at the beginning of this century. DNA fragments have a hydrophilic backbone composed of sugars and phosphates and hydrophobic aromatic nucleotide bases pendants. They are rolled around the nanotube so that the aromatic pendants are in contact to the SWNTs sidewall and the polar backbone is oriented to the solvent. DNA fragments have the capacity not only to solubilize SWNTs, but also to separate them in function of their diameter and chirality. Zheng *et al.*[97] discovered that certain sequences of DNA solubilize specifically some chirality of SWNTs present in a mixture of carbon nanotubes, as showed in the UV-vis-NIR spectrum in Figure 14. The authors attributed this selectivity to differences in the electrostatic and electrodynamic interactions between the ion exchange resin and the hybrids of DNA-SWNTs.

97. M. Zheng, A. Jagota, E. D. Semke, B. A. Diner, R. S. McLean, S. R. Lustig, R. E. Richardson and N. G. Tassi, *Nat. Mater.*, 2003, **2**, 338-342.

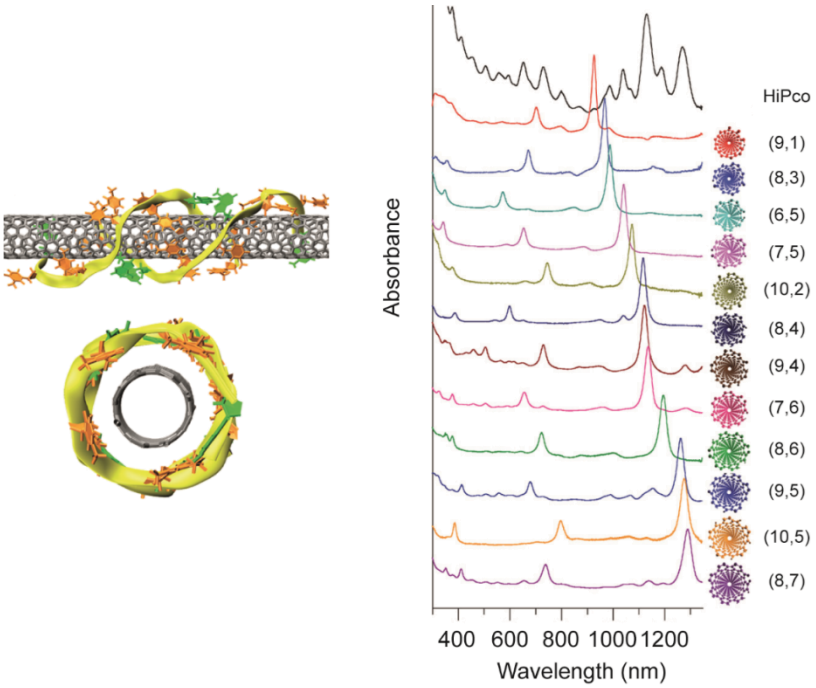

Figure 14. Left: 2 DNA sheet rolled on a (8,4) nanotube forming two hydrogen-bonded anti-parallel ATTTATTTATTT strands and that structure viewed along the tube axis. Right: UV-Vis-NIR spectrum of purified SWNTs through supramolecular complexes: (9,1) with $(TCC)_{10}$, $(TGA)_{10}$ and $(CCA)_{10}$, (8,3) with $(TTA)_4TT$, $(TTA)_3TTGTT$, and $(TTA)_5TT$, (6,5) with $(TAT)_4$, $(CGT)_3C$(7,5) $(ATT)_4$, and $(ATT)_4AT$, (10,2) with $(TATT)_2TAT$, (8,4) with $(ATTT)_3$, (9,4) with $(GTC)_2GT$, and $(CCG)_4$, (7,6) with $(GTT)_3G$, and $(TGT)_4T$, (8,6) with$(GT)_6$, $(TATT)_3T$, $(TCG)_{10}$,$(GTC)_3$,$(TCG)_2TC$,$(TCG)_4TC$, and $(GTC)_2$, (9,5) with $(TGTT)_2TGT$, (10,5) with $(TTTA)_3T$, (8,7) with $(CCG)_2CC$.

However, in a few cases, we can find examples where topology is to some extent reminiscent of that of MIMs, and might contribute to the overall stability. We will briefly describe some of those examples, as they are the closest precedents to our experimental work.

In 2003, *Kutner et al.*[98] claimed that the complexation of short SWNTs by η-cyclodextrin proceeded through threading, forming a structure similar to a pseudorotaxane (Figure 15a). Briefly, they cut the SWNTs by grinding them with β and γ–cyclodextrin. Then, the mixture was sonicated in water solution of η-cyclodextrin of 12 units of sugar obtaining the complex **53** after purification. The authors characterized the SWNTs supramolecular derivative by ^{1}H and ^{13}C – NMR experiment, checking that 12-cyclodextrins are bound to the SWNTs

98. H. Dodziuk, A. Ejchart, W. Anczewski, H. Ueda, E. Krinichnaya, G. Dolgonos and W. Kutner, *Chem. Commun.*, 2003, 986-987.

instead of free. The cyclodextrin-SWNTs complex has a high stability, but can be dissociated by heating at 300ºC.

A few years later, *Akola et al.*[99] studied the possibility to synthetize rotaxanes based on SWNTs thread from a theoretical point of view. In this work, the authors modeled two kinds of systems. The first one consists of SWNTs encapsulated by crown ethers without cross-linking between the SWNT and the macrocycle (Figure 15b). The second system is formed by SWNTs encapsulated by crown ethers analogues, where the oxygen atoms are substituted by trivalent nitrogen atoms, which are covalently linked to the SWNTs (Figure 15c). The authors concluded that cyclic macromolecules are capable to encapsulate SWNTs without modifying the electronic properties of the SWNTs. However, when the macrocycle is linked directly to the sidewall of the SWNT its electronic properties are altered. By varying the cavity size of the macrocycle, they showed it is theoretically possible to sort SWNTs according to their diameter.

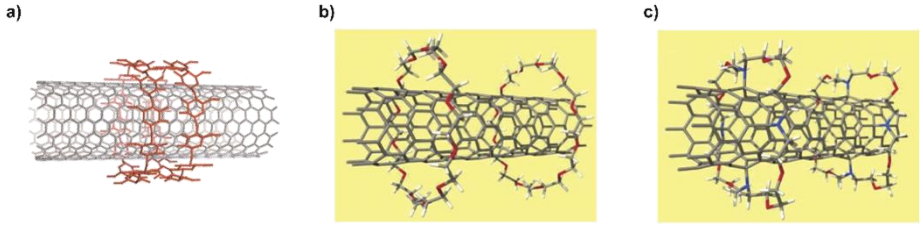

Figure 15. Molecular model of: a) two CD of 12 units in head to head arrangement around SWNT forming a pseudorotaxane **53**, b) (8,0)-SWNT@CE-12, **54** c) (8,0)-SWNT@CE-12N4, **55**.

Papadimitrakopoulos et al.[100] described the formation of an extremely stable helical pattern around SWNTs, **56**, based on Flavin mononucleotide (FMN) as repetitive unit. The amphiphilic characteristics of FMN (Figure 16), due to the presence of an aromatic region linked through an alkyne chain to a polar phosphoric group, facilitate the association of this molecule to carbon nanotubes in polar solvents because of solvophobic forces. Besides the amphiphilic behavior, FMN has two H-bond acceptor groups and one H-bond donor group that made possible the self-assembly between FMN monomers to generate the helical nanoribbon around the nanotube. They confirmed the formation of the helical pattern around SWNTs through HR-TEM, which fitted to the simulations (Figure 16). The authors have also observed through photoluminescence

99. J. Akola, K. Rytkönen and M. Manninen, *J. Phys. Chem. B*, 2006, **110**, 5186-5190.
100. S.-Y. Ju, J. Doll, I. Sharma and F. Papadimitrakopoulos, *Nat. Nanotech.*, 2008, **3**, 356-362.

emission (PLE) maps, that these kinds of superstructures show different affinity to the SWNTs depending on their chirality and diameter. Specifically, they observed that the supramolecular helical structure formed from FMN monomers show high affinity to (8,6)-SWNTs. This fact was used for the selective enrichment of the (8,6) nanotubes, using a simple surfactant replacement and subsequent salting-out precipitation.

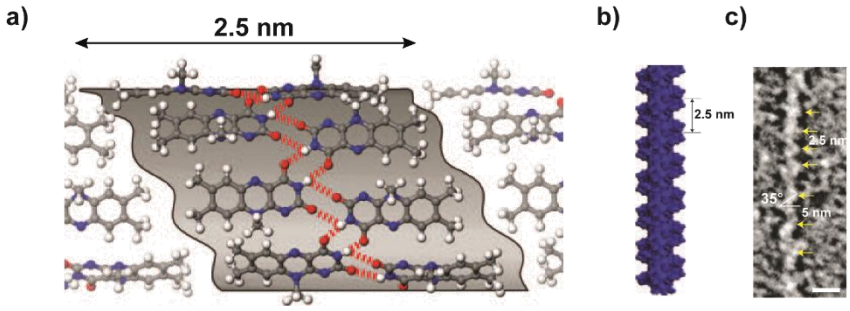

Figure 16. a) Helical wrapping motif of FMN around SWNTs (top view), b) Simulated FMN helical configurations where the *d*-ribityl phosphate moieties are collapsed in groups of two side chains, c) representative HR-TEM image of uranyl acetate stained FMN-wrapped SWNTs. Scale bars, 5 nm.

The functionalization of carbon nanotubes though polymerization of porphyrin derivatives in micelles of surfactant was published by S. Campidelli et al. in 2013. [101] In this paper, the authors were based on the micelle swelling method[102,103] to physisorb porphyrins on the nanotube sidewalls. Then, porphyrins decorated with thioacetate groups attached on the SWNTs were polymerized by the formation of disulfide bonds. They purified the derivative **58** by filtration and washing with different solvents, removing the surfactant, reagents and byproducts such as polymers of porphyrins outside the nanotubes. The authors characterized **58**, thought a combination of spectroscopic and microscopic techniques, to confirm the formation of the polymer shell around the nanotube. The addition of dithiothreitol (DTT) reduces the disulfide bonds, allowing removing the polymer shell that cover the nanotubes, as they observed through UV-visible. Accordingly, the functionalization of carbon nanotubes by polymer shell of porphyrins linked together through disulfide bonds is reversible.

101. G. Clavé, G. Delport, C. Roquelet, J.-S. Lauret, E. Deleporte, F. Vialla, B. Langlois, R. Parret, C. Voisin, P. Roussignol, B. Jousselme, A. Gloter, O. Stephan, A. Filoramo, V. Derycke and S. Campidelli, *Chem. Mater.*, 2013, **25**, 2700-2707.
102. C. Roquelet, J.-S. Lauret, V. Alain-Rizzo, C. Voisin, R. Fleurier, M. Delarue, D. Garrot, A. Loiseau, P. Roussignol, J. A. Delaire and E. Deleporte, *ChemPhysChem*, 2010, **11**, 1667-1672.
103. R. K. Wang, W.-C. Chen, D. K. Campos and K. J. Ziegler, *J. Am. Chem. Soc.*, 2008, **130**, 16330-16337.

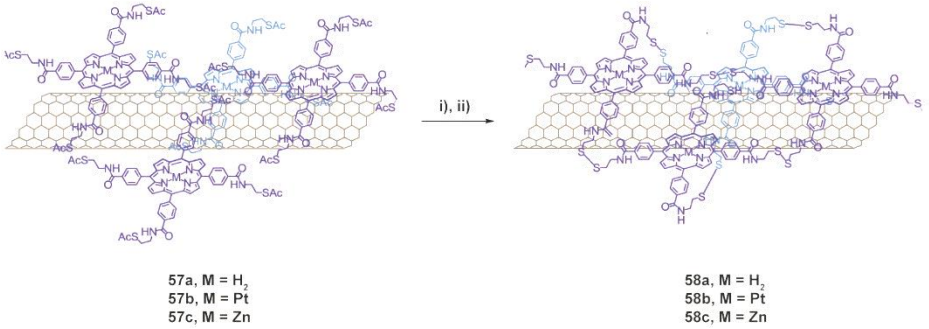

Scheme 11. Synthesis of derivatives **58a-c**. Reaction conditions: (i) hydroxylamine 50 wt % in water, Et_3N, 2 h, rt and (ii) O_2, rt, overnight.

One year later, the same group published the synthesis of porphyrin networks templated by multiwall carbon nanotubes (MWNTs) to catalyze the oxygen reduction reaction.[104] These results are based on previous work, where preformed oligomers and polymers of porphyrin were attached supramolecularly to carbon nanotubes.[105,106] In this case, the authors changed the synthetic strategy with respect to the previous work. They mixed a metalated porphyrin decorated with four terminal alkyne and MWNTs to form "in situ" concentric layers of porphyrin networks around the carbon nanotube through coupling reaction. SWNTs derivative **60** was thoroughly characterized, and its catalytic activity tested. The kinetically stable porphyrin-SWNTs hybrid improved the catalytic efficiency obtained for simple physisorbed porphyrin. In contrast with the previous work described above, the functionalization of carbon nanotubes by formation of porphyrin networks is irreversible.

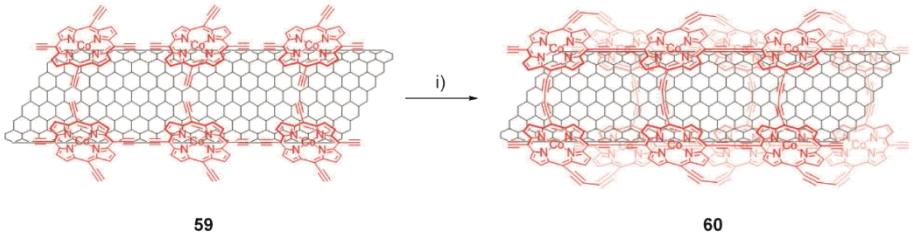

Scheme 12. Synthesis of MWNT derivative **60**. Reaction conditions: (i) CuCl, TMEDA, NMP, rt.

104. I. Hijazi, T. Bourgeteau, R. Cornut, A. Morozan, A. Filoramo, J. Leroy, V. Derycke, B. Jousselme and S. Campidelli, *J. Am. Chem. Soc*., 2014, **136**, 6348-6354.
105. F. Cheng and A. Adronov, *Chem. Eur. J.*, 2006, **12**, 5053-5059.
106. J. K. Sprafke, S. D. Stranks, J. H. Warner, R. J. Nicholas and H. L. Anderson, *Angew. Chem. Int. Ed.*, 2011, **50**, 2313-2316.

1.4 Measuring Binding Constants towards SWNTs

If we consider supramolecular chemistry in its simplest sense, as involving some kind of noncovalent binding event, we generally consider a molecule as a *host* binding another molecule as a *guest* to form a "host-guest" complex. These molecular complexes are held together by a range of noncovalent forces, all of which are fundamentally electrostatic in nature:[107] hydrogen bonding, ion pairing, π-acid to π-base interactions, metal to ligand binding, van der Waals forces, etc.

These supramolecular processes imply a balance between enthalpy (association energy) and entropy (organization penalty).[108] The binding does not only depend on the individual interaction between the binding site of the host and the guest, but also on how each interaction affects other interactions. There are different effects or inter-interactions, such as cooperativity, macrocyclic effects,[109] complementarity or host preorganization[110] that can be used to vary the equilibrium between enthalpy and entropy to favor association.

The binding constant (K_a) is defined as the equilibrium constant of the association/dissociation of the host-guest system, that is: $K_a = k_{ass}/k_{dis}$, where k_{ass} and k_{dis} are the rates of association and dissociation, respectively. For a 1:1 host guest binding equilibrium, this translates into: K_a = [HG]/[H] x [G]. Binding constants provide valuable information about the thermodynamic stability of the host-guest molecules under specific experimental conditions (concentration, solvent, temperature, etc.). For host-guest systems in solution, the determination of K_a is a routine experiment. The comparison of K_a between different supramolecular complexes is a key parameter to understand molecular recognition events. The use of supramolecular chemistry to modify SWNTs is widely employed, as we show above. However the quantification of supramolecular interactions has usually been overlooked, due to experimental difficulties.

From an experimental point of view, Jagota *et al.*[111] designed atomic force microscopy (AFM) assays to measure, through single molecule force

107. C. A. Hunter, *Angew. Chem. Int. Ed*., 2004, **43**, 5310-5324.
108. G. M. Whitesides, J. P. Mathias and C. T. Seto, *Science*, 1991, **254**, 1312.
109. R. D. Hancock, *J. Chem. Educ.*, 1992, **69**, 615.
110. D. J. Cram, *Angew. Chem. Int. Ed.*, 1986, **25**, 1039-1057.
111. S. Iliafar, J. Mittal, D. Vezenov and A. Jagota, *J. Am. Chem. Soc.*, 2014, **136**, 12947-12957.

spectroscopy (SMFS), the force of the interaction between DNA and SWNTs. The authors attached commercial single strain DNA (ssDNA) homopolymers, decorated with a thiol group on one end of the polymer, to the gold AFM probe. They prepared samples with individualized SWNTs deposited on hydrophobic methyl terminated self-assembled monolayers (SAMs). The functionalized AFM probe was approached to the surface, previously "photographed" through tapping mode with the same tip, until contact between both AFM probe and surface was observed. Then, the tip was retracted to obtain the corresponding force map (Figure 17), where both approach and retract processes were collected. From this force map, the authors obtained force histograms for peeling ssDNA homopolymers from SWNTs. After fitting the histogram to a Gaussian distribution, two clearly separated peaks were observed. The authors attributed the first peak to the separation of the homopolymer to the SAMs substrate,[112] and the second peak to the peeling of the homopolymer off the sidewall of the SWNTs.

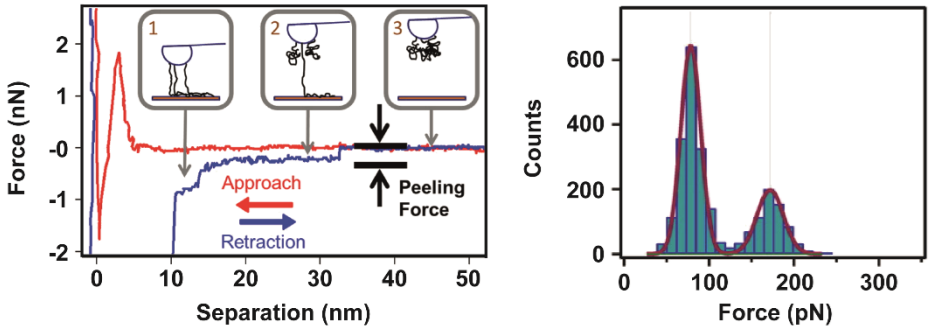

Figure 17. Left: typical force−distance curve for peeling 5′-T100 ssDNA from SWCNTs deposited on a methyl-terminated SAM on a silicon wafer. Right: force histograms for peeling of the same ssDNA homopolymers.

They measured the interaction force of different ssDNA homopolymers adsorbed on the surfaces of SWNTs, obtaining the free energy of binding. SMFS is therefore a good method to quantify the interaction of long molecules to SWNTs. However, both the complexity of the experimental set up and the limited scope of host are handicaps to the application of this methodology.

112. S. Iliafar, K. Wagner, S. Manohar, A. Jagota and D. Vezenov, *J. Phys. Chem. C*, 2012, **116**, 13896-13903.

A kinetic model to quantify chirality-specific interactions of SWNTs with hydrogels was published by Strano *et al.*[113] The authors used an amide-functionalized hydrogel (Sephacryl S200) to separate seven chiralities of semiconducting nanotubes from a HiPCO sample. Although the gel-SWNTs separation with Sephacryl S200 was published by Kataura and coworkers previously,[114] Strano managed to scale up the purification method by 15 times. Besides scaling up the process, the authors proposed a kinetic model that leads to estimate chiral-specific rate constants. They corroborated these rate constants by simulated data. However, the kinetic model estimates chiral-specific rate constants but not binding constants.

Anderson and coworkers[115] studied the noncovalent interactions of a set of porphyrins derivatives towards SWNTs. They carried out a UV/vis and fluorescence titrations to probe the kinetics and thermodynamics parameters of this kind of systems and to monitor the nanotube debundling.

Investigations *in silico* on SWNT-based supramolecular chemistry are far more abundant, and a wide variety of density functional theory (DFT) methods have been tested.[116] Dispersion-accounting DFT approaches stand as accurate yet affordable methodologies providing quantitative predictions on noncovalent interactions with chemical accuracy.

113. K. Tvrdy, R. M. Jain, R. Han, A. J. Hilmer, T. P. McNicholas and M. S. Strano, *ACS Nano*, 2013, **7**, 1779-1789.
114. H. Liu, D. Nishide, T. Tanaka and H. Kataura, *Nat. Commun.*, 2011, **2**, 309.
115. J. K. Sprafke, S. D. Stranks, J. H. Warner, R. J. Nicholas and H. L. Anderson, *Angew. Chem. Int. Ed.*, 2011, **50**, 2313-2316.
116. D. Umadevi, S. Panigrahi and G. N. Sastry, *Acc. Chem. Res.*, 2014, **47**, 2574-2581.

1.5 References

1. K. Kim, *Chem. Soc. Rev.*, 2002, **31**, 96-107.
2. J. F. Stoddart, *Chem. Soc. Rev.*, 2009, **38**, 1802-1820.
3. J. D. Crowley, S. M. Goldup, A.-L. Lee, D. A. Leigh and R. T. McBurney, *Chem. Soc. Rev.*, 2009, **38**, 1530-1541.
4. D. A. Leigh, J. K. Y. Wong, F. Dehez and F. Zerbetto, *Nature*, 2003, **424**, 174-179.
5. B. Lewandowski, G. De Bo, J. W. Ward, M. Papmeyer, S. Kuschel, M. J. Aldegunde, P. M. E. Gramlich, D. Heckmann, S. M. Goldup, D. M. D'Souza, A. E. Fernandes and D. A. Leigh, *Science*, 2013, **339**, 189-193.
6. G. Schill and H. Zollenkopf, *Justus Liebigs Ann. Chem.*, 1969, **721**, 53-74.
7. G. Schill and R. Henschel, *Justus Liebigs Ann. Chem.*, 1970, **731**, 113-119.
8. J. O. Jeppesen, J. Perkins, J. Becher and J. F. Stoddart, *Org. Lett.*, 2000, **2**, 3547-3550.
9. P. T. Glink, A. I. Oliva, J. F. Stoddart, A. J. P. White and D. J. Williams, *Angew. Chem. Int. Ed.*, 2001, **40**, 1870-1875.
10. S. J. Rowan and J. F. Stoddart, *Org. Lett.*, 1999, **1**, 1913-1916.
11. A. F. M. Kilbinger, S. J. Cantrill, A. W. Waltman, M. W. Day and R. H. Grubbs, *Angew. Chem. Int. Ed.*, 2003, **42**, 3281-3285.
12. H. Tian and Q.-C. Wang, *Chem. Soc. Rev.*, 2006, **35**, 361-374.
13. V. Balzani, A. Credi, F. M. Raymo and J. F. Stoddart, *Angew. Chem. Int. Ed.*, 2000, **39**, 3348-3391.
14. L. Fang, M. A. Olson, D. Benítez, E. Tkatchouk, W. A. Goddard Iii and J. F. Stoddart, *Chem. Soc. Rev.*, 2010, **39**, 17-29.
15. S. J. Loeb, *Chem. Soc. Rev.*, 2007, **36**, 226-235.
16. F. Huang and H. W. Gibson, *Prog. Polym. Sci.*, 2005, **30**, 982-1018.
17. F. Cacialli, J. S. Wilson, J. J. Michels, C. Daniel, C. Silva, R. H. Friend, N. Severin, P. Samori, J. P. Rabe, M. J. O'Connell, P. N. Taylor and H. L. Anderson, *Nat. Mater.*, 2002, **1**, 160-164.
18. C. Gong and H. W. Gibson, *Macromolecules*, 1996, **29**, 7029-7033.
19. C. Gong, T. E. Glass and H. W. Gibson, *Macromolecules*, 1998, **31**, 308-313.
20. C. Gong and H. W. Gibson, *J. Am. Chem. Soc.*, 1997, **119**, 8585-8591.
21. H. W. Gibson, W. S. Bryant and S.-H. Lee, *J. Polym. Sci., Part A: Polym. Chem.*, 2001, **39**, 1978-1993.
22. M. Bria, J. Bigot, G. Cooke, J. Lyskawa, G. Rabani, V. M. Rotello and P. Woisel, *Tetrahedron*, 2009, **65**, 400-407.

23. H. W. Kroto, J. R. Heath, S. C. O'Brien, R. F. Curl and R. E. Smalley, *Nature*, 1985, **318**, 162-163.
24. S. Iijima, *Nature*, 1991, **354**, 56-58.
25. S. Iijima and T. Ichihashi, *Nature*, 1993, **363**, 603-605.
26. D. S. Bethune, C. H. Klang, M. S. de Vries, G. Gorman, R. Savoy, J. Vázquez and R. Beyers, *Nature*, 1993, **363**, 605-607.
27. K. S. Novoselov, A. K. Geim, S. V. Morozov, D. Jiang, Y. Zhang, S. V. Dubonos, I. V. Grigorieva and A. A. Firsov, *Science*, 2004, **306**, 666.
28. A. K. Geim and K. S. Novoselov, *Nat. Mater.*, 2007, **6**, 183-191.
29. C. A. Cooper, R. J. Young and M. Halsall, *Composites Part A*, 2001, **32**, 401-411.
30. G. Guanghua, Ç. Tahir and A. G. William, III, *Nanotechnology*, 1998, **9**, 184.
31. A. Krishnan, E. Dujardin, T. W. Ebbesen, P. N. Yianilos and M. M. J. Treacy, *Phys. Rev. B*, 1998, **58**, 14013-14019.
32. J.-P. Salvetat, G. A. D. Briggs, J.-M. Bonard, R. R. Bacsa, A. J. Kulik, T. Stöckli, N. A. Burnham and L. Forró, *Phys. Rev. Lett.*, 1999, **82**, 944-947.
33. J. W. Mintmire, B. I. Dunlap and C. T. White, *Phys. Rev. Lett.*, 1992, **68**, 631-634.
34. M. Ouyang, J.-L. Huang, C. L. Cheung and C. M. Lieber, *Science*, 2001, **292**, 702.
35. M. Ouyang, J.-L. Huang and C. M. Lieber, *Acc. Chem. Res.*, 2002, **35**, 1018-1025.
36. Y. Saito and S. Uemura, *Carbon*, 2000, **38**, 169-182.
37. K. H. An, W. S. Kim, Y. S. Park, J. M. Moon, D. J. Bae, S. C. Lim, Y. S. Lee and Y. H. Lee, *Adv. Funct. Mater.*, 2001, **11**, 387-392.
38. C. Niu, E. K. Sichel, R. Hoch, D. Moy and H. Tennent, *Appl. Phys. Lett.*, 1997, **70**, 1480-1482.
39. W. A. de Heer, A. Châtelain and D. Ugarte, *Science*, 1995, **270**, 1179.
40. N. S. Lee, D. S. Chung, I. T. Han, J. H. Kang, Y. S. Choi, H. Y. Kim, S. H. Park, Y. W. Jin, W. K. Yi, M. J. Yun, J. E. Jung, C. J. Lee, J. H. You, S. H. Jo, C. G. Lee and J. M. Kim, *Diamond Relat. Mater.*, 2001, **10**, 265-270.
41. M. A. McCarthy, B. Liu, E. P. Donoghue, I. Kravchenko, D. Y. Kim, F. So and A. G. Rinzler, *Science*, 2011, **332**, 570.
42. S. J. Tans, A. R. M. Verschueren and C. Dekker, *Nature*, 1998, **393**, 49-52.
43. J. Kong, N. R. Franklin, C. Zhou, M. G. Chapline, S. Peng, K. Cho and H. Dai, *Science*, 2000, **287**, 622-625.
44. P. M. Ajayan, O. Stephan, C. Colliex and D. Trauth, *Science*, 1994, **265**, 1212.
45. O. Breuer and U. Sundararaj, *Polym. Compos.*, 2004, **25**, 630-645.

46. Z. Liu, X. Sun, N. Nakayama-Ratchford and H. Dai, *ACS Nano*, 2007, **1**, 50-56.
47. A. M. Popov, Y. E. Lozovik, S. Fiorito and L. Yahia, *Int J Nanomedicine*, 2007, **2**, 361-372.
48. *Patent US7473930*, Use of patterned CNT arrays for display purposes.
49. Q. Cao, H.-s. Kim, N. Pimparkar, J. P. Kulkarni, C. Wang, M. Shim, K. Roy, M. A. Alam and J. A. Rogers, *Nature*, 2008, **454**, 495-500.
50. M. F. L. De Volder, S. H. Tawfick, R. H. Baughman and A. J. Hart, *Science*, 2013, **339**, 535-539.
51. H. Dai, *Acc. Chem. Res.*, 2002, **35**, 1035-1044.
52. S. M. Bachilo, L. Balzano, J. E. Herrera, F. Pompeo, D. E. Resasco and R. B. Weisman, *J. Am. Chem. Soc.*, 2003, **125**, 11186-11187.
53. A. R. Harutyunyan, G. Chen, T. M. Paronyan, E. M. Pigos, O. A. Kuznetsov, K. Hewaparakrama, S. M. Kim, D. Zakharov, E. A. Stach and G. U. Sumanasekera, *Science*, 2009, **326**, 116.
54. R. Krupke, F. Hennrich, H. v. Löhneysen and M. M. Kappes, *Science*, 2003, **301**, 344.
55. M. S. Arnold, S. I. Stupp and M. C. Hersam, *Nano Lett.*, 2005, **5**, 713-718.
56. H. Liu, T. Tanaka, Y. Urabe and H. Kataura, *Nano Lett.*, 2013, **13**, 1996-2003.
57. S. Banerjee, T. Hemraj-Benny and S. S. Wong, *Adv. Mater.*, 2005, **17**, 17-29.
58. Y.-L. Zhao and J. F. Stoddart, *Acc. Chem. Res.*, 2009, **42**, 1161-1171.
59. X. Tu, S. Manohar, A. Jagota and M. Zheng, *Nature*, 2009, **460**, 250-253.
60. A. Hirsch, *Angew. Chem. Int. Ed.*, 2002, **41**, 1853-1859.
61. A. de Juan and E. M. Pérez, *Nanoscale*, 2013, **5**, 7141-7148.
62. Z. Chen, K. Kobashi, U. Rauwald, R. Booker, H. Fan, W.-F. Hwang and J. M. Tour, *J. Am. Chem. Soc.*, 2006, **128**, 10568-10571.
63. K. Flavin, I. Kopf, E. Del Canto, C. Navio, C. Bittencourt and S. Giordani, *J. Mater. Chem.*, 2011, **21**, 17881-17887.
64. M. A. Hamon, J. Chen, H. Hu, Y. Chen, M. E. Itkis, A. M. Rao, P. C. Eklund and R. C. Haddon, *Adv. Mater.*, 1999, **11**, 834-840.
65. B. Zhao, H. Hu and R. C. Haddon, *Adv. Funct. Mater.*, 2004, **14**, 71-76.
66. J. L. Delgado, P. de la Cruz, A. Urbina, J. T. López Navarrete, J. Casado and F. Langa, *Carbon*, 2007, **45**, 2250-2252.
67. H. Li, R. B. Martin, B. A. Harruff, R. A. Carino, L. F. Allard and Y. P. Sun, *Adv. Mater.*, 2004, **16**, 896-900.
68. S. Cosnier and M. Holzinger, *Electrochim. Acta*, 2008, **53**, 3948-3954.
69. D. Srivastava, D. W. Brenner, J. D. Schall, K. D. Ausman, M. Yu and R. S. Ruoff, *J. Phys. Chem. B*, 1999, **103**, 4330-4337.

70. P. Singh, S. Campidelli, S. Giordani, D. Bonifazi, A. Bianco and M. Prato, *Chem. Soc. Rev.*, 2009, **38**, 2214-2230.
71. E. T. Mickelson, C. B. Huffman, A. G. Rinzler, R. E. Smalley, R. H. Hauge and J. L. Margrave, *Chem. Phys. Lett.*, 1998, **296**, 188-194.
72. M. Holzinger, O. Vostrowsky, A. Hirsch, F. Hennrich, M. Kappes, R. Weiss and F. Jellen, *Angew. Chem. Int. Ed.*, 2001, **40**, 4002-4005.
73. H. Peng, L. B. Alemany, J. L. Margrave and V. N. Khabashesku, *J. Am. Chem. Soc.*, 2003, **125**, 15174-15182.
74. S. Chen, D. Chen and G. Wu, *Macromol. Rapid Commun.*, 2006, **27**, 882-887.
75. C. A. Dyke and J. M. Tour, *J. Phys. Chem. A*, 2004, **108**, 11151-11159.
76. H. Hu, B. Zhao, M. A. Hamon, K. Kamaras, M. E. Itkis and R. C. Haddon, *J. Am. Chem. Soc.*, 2003, **125**, 14893-14900.
77. M. Holzinger, J. Abraham, P. Whelan, R. Graupner, L. Ley, F. Hennrich, M. Kappes and A. Hirsch, *J. Am. Chem. Soc.*, 2003, **125**, 8566-8580.
78. K. S. Coleman, S. R. Bailey, S. Fogden and M. L. H. Green, *J. Am. Chem. Soc.*, 2003, **125**, 8722-8723.
79. D. Tasis, N. Tagmatarchis, A. Bianco and M. Prato, *Chem. Rev.*, 2006, **106**, 1105-1136.
80. F. G. Brunetti, M. A. Herrero, J. d. M. Muñoz, S. Giordani, A. Díaz-Ortiz, S. Filippone, G. Ruaro, M. Meneghetti, M. Prato and E. Vázquez, *J. Am. Chem. Soc.*, 2007, **129**, 14580-14581.
81. C. Ménard-Moyon, N. Izard, E. Doris and C. Mioskowski, *J. Am. Chem. Soc.*, 2006, **128**, 6552-6553.
82. D. M. Guldi, M. Marcaccio, D. Paolucci, F. Paolucci, N. Tagmatarchis, D. Tasis, E. Vázquez and M. Prato, *Angew. Chem. Int. Ed.*, 2003, **42**, 4206-4209.
83. J. L. Delgado, P. de la Cruz, F. Langa, A. Urbina, J. Casado and J. T. López Navarrete, *Chem. Commun.*, 2004, 1734-1735.
84. W. Wenseleers, I. I. Vlasov, E. Goovaerts, E. D. Obraztsova, A. S. Lobach and A. Bouwen, *Adv. Funct. Mater.*, 2004, **14**, 1105-1112.
85. M. F. Islam, E. Rojas, D. M. Bergey, A. T. Johnson and A. G. Yodh, *Nano Lett.*, 2003, **3**, 269-273.
86. R. J. Chen, Y. Zhang, D. Wang and H. Dai, *J. Am. Chem. Soc.*, 2001, **123**, 3838-3839.
87. C. Ehli, G. M. A. Rahman, N. Jux, D. Balbinot, D. M. Guldi, F. Paolucci, M. Marcaccio, D. Paolucci, M. Melle-Franco, F. Zerbetto, S. Campidelli and M. Prato, *J. Am. Chem. Soc.*, 2006, **128**, 11222-11231.
88. J. Zhang, J. K. Lee, Y. Wu and R. W. Murray, *Nano Lett.*, 2003, **3**, 403-407.
89. H. Li, B. Zhou, Y. Lin, L. Gu, W. Wang, K. A. S. Fernando, S. Kumar, L. F. Allard and Y.-P. Sun, *J. Am. Chem. Soc.*, 2004, **126**, 1014-1015.

90. D. S. Hecht, R. J. A. Ramírez, M. Briman, E. Artukovic, K. S. Chichak, J. F. Stoddart and G. Grüner, *Nano Lett.*, 2006, **6**, 2031-2036.
91. X. Wang, Y. Liu, W. Qiu and D. Zhu, *J. Mater. Chem.*, 2002, **12**, 1636-1639.
92. C. Romero-Nieto, R. García, M. Á. Herranz, C. Ehli, M. Ruppert, A. Hirsch, D. M. Guldi and N. Martín, *J. Am. Chem. Soc.*, 2012, **134**, 9183-9192.
93. F. Chen, B. Wang, Y. Chen and L.-J. Li, *Nano Lett.*, 2007, **7**, 3013-3017.
94. J.-Y. Hwang, A. Nish, J. Doig, S. Douven, C.-W. Chen, L.-C. Chen and R. J. Nicholas, *J. Am. Chem. Soc.*, 2008, **130**, 3543-3553.
95. A. Star, J. F. Stoddart, D. Steuerman, M. Diehl, A. Boukai, E. W. Wong, X. Yang, S.-W. Chung, H. Choi and J. R. Heath, *Angew. Chem. Int. Ed.*, 2001, **40**, 1721-1725.
96. M. in het Panhuis, A. Maiti, A. B. Dalton, A. van den Noort, J. N. Coleman, B. McCarthy and W. J. Blau, *J. Phys. Chem. B*, 2003, **107**, 478-482.
97. M. Zheng, A. Jagota, E. D. Semke, B. A. Diner, R. S. McLean, S. R. Lustig, R. E. Richardson and N. G. Tassi, *Nat. Mater.*, 2003, **2**, 338-342.
98. H. Dodziuk, A. Ejchart, W. Anczewski, H. Ueda, E. Krinichnaya, G. Dolgonos and W. Kutner, *Chem. Commun.*, 2003, 986-987.
99. J. Akola, K. Rytkönen and M. Manninen, *J. Phys. Chem. B*, 2006, **110**, 5186-5190.
100. S.-Y. Ju, J. Doll, I. Sharma and F. Papadimitrakopoulos, *Nat. Nanotech.*, 2008, **3**, 356-362.
101. G. Clavé, G. Delport, C. Roquelet, J.-S. Lauret, E. Deleporte, F. Vialla, B. Langlois, R. Parret, C. Voisin, P. Roussignol, B. Jousselme, A. Gloter, O. Stephan, A. Filoramo, V. Derycke and S. Campidelli, *Chem. Mater.*, 2013, **25**, 2700-2707.
102. C. Roquelet, J.-S. Lauret, V. Alain-Rizzo, C. Voisin, R. Fleurier, M. Delarue, D. Garrot, A. Loiseau, P. Roussignol, J. A. Delaire and E. Deleporte, *ChemPhysChem*, 2010, **11**, 1667-1672.
103. R. K. Wang, W.-C. Chen, D. K. Campos and K. J. Ziegler, *J. Am. Chem. Soc.*, 2008, **130**, 16330-16337.
104. I. Hijazi, T. Bourgeteau, R. Cornut, A. Morozan, A. Filoramo, J. Leroy, V. Derycke, B. Jousselme and S. Campidelli, *J. Am. Chem. Soc.*, 2014, **136**, 6348-6354.
105. F. Cheng and A. Adronov, *Chem. Eur. J.*, 2006, **12**, 5053-5059.
106. J. K. Sprafke, S. D. Stranks, J. H. Warner, R. J. Nicholas and H. L. Anderson, *Angew. Chem. Int. Ed.*, 2011, **50**, 2313-2316.
107. C. A. Hunter, *Angew. Chem. Int. Ed.*, 2004, **43**, 5310-5324.
108. G. M. Whitesides, J. P. Mathias and C. T. Seto, *Science*, 1991, **254**, 1312.
109. R. D. Hancock, *J. Chem. Educ.*, 1992, **69**, 615.

110. D. J. Cram, *Angew. Chem. Int. Ed.*, 1986, **25**, 1039-1057.
111. S. Iliafar, J. Mittal, D. Vezenov and A. Jagota, *J. Am. Chem. Soc.*, 2014, **136**, 12947-12957.
112. S. Iliafar, K. Wagner, S. Manohar, A. Jagota and D. Vezenov, *J. Phys. Chem. C*, 2012, **116**, 13896-13903.
113. K. Tvrdy, R. M. Jain, R. Han, A. J. Hilmer, T. P. McNicholas and M. S. Strano, *ACS Nano*, 2013, **7**, 1779-1789.
114. H. Liu, D. Nishide, T. Tanaka and H. Kataura, *Nat. Commun.*, 2011, **2**, 309.
115. J. K. Sprafke, S. D. Stranks, J. H. Warner, R. J. Nicholas and H. L. Anderson, *Angew. Chem. Int. Ed.*, 2011, **50**, 2313-2316.
116. D. Umadevi, S. Panigrahi and G. N. Sastry, *Acc. Chem. Res.*, 2014, **47**, 2574-2581.

OBJECTIVES

2. Objectives

The present thesis has four main objectives:

1. To **introduce the mechanical bond as a new tool for the chemical modification of SWNTs** obtaining Mechanically Interlocked Single Wall Carbon Nanotubes (MINTs).
2. To **optimize the MINT-forming reaction conditions** and **elucidate its mechanism** through estimation of association constants and analysis of the kinetics of the reaction.
3. To **evaluate the effect of the mechanical bond on the physical properties of SWNTs** through transient absorption spectroscopy, cyclic voltammetry and chronoamperometry.
4. To **develop a new method to quantify the interaction between organic molecules (hosts) and the sidewall of SWNTs (guest),** determining their binding constants.

CHAPTER 1

3. Mechanically Interlocked Single-Wall Carbon Nanotubes

Abstract: Extensive research has been devoted to the chemical manipulation of carbon nanotubes. The attachment of molecular fragments through covalent-bond formation produces kinetically stable products, but implies the saturation of some of the C-C double bonds of the nanotubes. Supramolecular modification maintains the structure of the SWNTs but yields labile species. Herein, we present a strategy for the synthesis of mechanically interlocked derivatives of SWNTs (MINTs). In the key rotaxane-forming step, we employed macrocycle precursors equipped with two π-extended tetrathiafulvalene SWNT recognition units and terminated with bisalkenes that were closed around the nanotubes through ring-closing metathesis (RCM). The mechanically interlocked nature of the derivatives was probed by analytical, spectroscopic, and microscopic techniques, as well as by appropriate control experiments. Individual macrocycles were observed by HR STEM to circumscribe the nanotubes.

Angew. Chem. Int. Ed., 2014, **53**, 5394-5400.

3.1 Introduction

Ever since their discovery,[1-3] carbon nanotubes have remained in the spotlight of physical and chemical research owing to their outstanding physical properties.[4,5] However, the initial excitement about their possible application in the field of organic electronics has only recently started to become a reality.[6,7] The contribution of chemistry to carbon nanotube science is focused on their

1. S. Iijima and T. Ichihashi, *Nature*, 1993, **363**, 603-605.
2. S. Iijima, *Nature*, 1991, **354**, 56-58.
3. D. S. Bethune, C. H. Klang, M. S. de Vries, G. Gorman, R. Savoy, J. Vázquez and R. Beyers, *Nature*, 1993, **363**, 605-607.
4. R. H. Baughman, A. A. Zakhidov and W. A. de Heer, *Science* 2002, **297**, 787-792.
5. K. Dirian, M. Á. Herranz, G. Katsukis, J. Malig, L. Rodríguez-Pérez, C. Romero-Nieto, V. Strauss, N. Martín and D. M. Guldi, *Chem. Sci.*, 2013, **4**, 4335-4353.
6. A. D. Franklin, M. Luisier, S.-J. Han, G. Tulevski, C. M. Breslin, L. Gignac, M. S. Lundstrom and W. Haensch, *Nano Lett.*, 2012, **12**, 758-762.
7. H. Park, A. Afzali, S.-J. Han, G. S. Tulevski, A. D. Franklin, J. Tersoff, J. B. Hannon and W. Haensch, *Nat. Nanotech.*, 2012, **7**, 787-791.

synthesis,[8-15] and their covalent[16] or noncovalent[17] modification to attain specific electronic properties. The covalent modification of single-wall nanotubes (SWNTs) provides kinetically stable products, but implies the saturation of some of the C-C double bonds of the nanotubes. The supramolecular modification of SWNTs enables conservation of the structure of the nanotubes, but in most cases the products lack kinetic stability.[18-25]

A hitherto unexplored alternative is to modify the SWNTs to form mechanically interlocked species.[26,27] Mechanically interlocked molecules (MIMs) consist of two or more separate components which are not connected by chemical (i.e. covalent) bonds. Examples of MIMs are rotaxanes, in which one or more macrocycles are trapped on a linear component (thread) by bulky substituents at its ends (stoppers) that prevent dissociation, and catenanes, in which two or more macrocycles are interlocked in the same way as links in a chain. Owing to their unique dynamic properties, MIMs have been extensively studied as candidates for the construction of synthetic molecular machinery.[28] For example, self-assembled monolayers of molecular shuttles-rotaxanes in which the macrocycle can be moved between two or more sites on the thread in

8. H. Dai, *Acc. Chem. Res.*, 2002, **35**, 1035-1044.
9. M. C. Hersam, *Nat. Nanotech.*, 2008, **3**, 387-394.
10. W. Zhou, X. Bai, E. Wang and S. Xie, *Adv. Mater.*, 2009, **21**, 4565-4583.
11. R. Jasti and C. R. Bertozzi, *Chem. Phys. Lett.*, 2010, **494**, 1-7.
12. Y. Zhang and L. Zheng, *Nanoscale*, 2010, **2**, 1919-1929.
13. H. Omachi, T. Nakayama, E. Takahashi, Y. Segawa and K. Itami, *Nat. Chem.*, 2013, **5**, 572-576.
14. H. Kimura, J. Goto, S. Yasuda, S. Sakurai, M. Yumura, D. N. Futaba and K. Hata, *ACS Nano*, 2013, **7**, 3150-3157.
15. L. T. Scott, E. A. Jackson, Q. Zhang, B. D. Steinberg, M. Bancu and B. Li, *J. Am. Chem. Soc.*, 2012, **134**, 107-110.
16. P. Singh, S. Campidelli, S. Giordani, D. Bonifazi, A. Bianco and M. Prato, *Chem. Soc. Rev.*, 2009, **38**, 2214-2230.
17. Y.-L. Zhao and J. F. Stoddart, *Acc. Chem. Res.*, 2009, **42**, 1161-1171.
18. J. Gao, M. A. Loi, E. J. F. de Carvalho and M. C. dos Santos, *ACS Nano*, 2011, **5**, 3993-3999.
19. A. Llanes-Pallas, K. Yoosaf, H. Traboulsi, J. Mohanraj, T. Seldrum, J. Dumont, A. Minoia, R. Lazzaroni, N. Armaroli and D. Bonifazi, *J. Am. Chem. Soc.*, 2011, **133**, 15412-15424.
20. S. D. Stranks, J. K. Sprafke, H. L. Anderson and R. J. Nicholas, *ACS Nano*, 2011, **5**, 2307-2315.
21. Y. Liu, Z.-L. Yu, Y.-M. Zhang, D.-S. Guo and Y.-P. Liu, *J. Am. Chem. Soc.*, 2008, **130**, 10431-10439.
22. X. Tu, S. Manohar, A. Jagota and M. Zheng, *Nature* 2009, **460**, 250-253.
23. F. D'Souza, S. K. Das, M. E. Zandler, A. S. D. Sandanayaka and O. Ito, *J. Am. Chem. Soc.*, 2011, **133**, 19922-19930.
24. H. Chaturvedi, A. N. Giordano, M.-J. Kim, F. M. MacDonnell, S. S. Subaran and J. C. Poler, *J. Phys. Chem. C*, 2009, **113**, 11254-11261.
25. G. Clavé, G. Delport, C. Roquelet, J.-S. Lauret, E. Deleporte, F. Vialla, B. Langlois, R. Parret, C. Voisin, P. Roussignol, B. Jousselme, A. Gloter, O. Stephan, A. Filoramo, V. Derycke and S. Campidelli, *Chem. Mater.*, 2013, **25**, 2700-2707.
26. J. F. Stoddart, *Chem. Soc. Rev.*, 2009, **38**, 1802-1820.
27. J.-P. Sauvage, *Chem. Commun.*, 2005, 1507-1510.
28. E. R. Kay, D. A. Leigh and F. Zerbetto, *Angew. Chem. Int. Ed.*, 2007, **46**, 72-191.

response to external stimuli-are able to produce mechanical work[29] and to store information.[30] Recently, multi-station molecular shuttles have been shown to perform sequence-specific peptide synthesis,[31] thus imitating one of the most complex pieces of naturally existing molecular machinery, the ribosome. Besides the application of MIMs to the synthesis of molecular machinery, the encapsulation of elongated molecules to form kinetically stable rotaxanes has been proven to give rise to a variety of novel properties. As a consequence, there is growing interest in the production of mechanically interlocked hybrid materials, such as polymers[32] and metal-organic frameworks.[33] The 1D structure of SWNTs opens up the possibility of utilizing them as threads in the synthesis of rotaxane-type mechanically interlocked nanotubes (MINTs).[34] To the best of our knowledge, this possibility has only been studied from a theoretical point of view.[35] Herein, we describe the synthesis of rotaxanes in which SWNTs act as threads.

3.2 Results and Discussion

Given the structural similarities between fullerenes and SWNTs, we based our design on our previous experience in the synthesis of macrocyclic receptors for fullerenes.[36,37] Macrocycles **1**-**3** (Figure 1a) feature two π-extended tetrathiafulvalene (9,10-di(1,3-dithiol-2-ylidene)-9,10-dihydroanthracene, exTTF) units, which have been previously shown to serve as a recognition motif for SWNTs.[38] The recognition units are linked together through 1,4-xylylene and C_{14}, C_{18}, or C_{20} alkenyl spacers. The macrocycles were synthesized by ring-

29. J. Berna, D. A. Leigh, M. Lubomska, S. M. Mendoza, E. M. Pérez, P. Rudolf, G. Teobaldi and F. Zerbetto, *Nat. Mater.*, 2005, **4**, 704-710.
30. J. E. Green, J. Wook Choi, A. Boukai, Y. Bunimovich, E. Johnston-Halperin, E. DeIonno, Y. Luo, B. A. Sheriff, K. Xu, Y. Shik Shin, H.-R. Tseng, J. F. Stoddart and J. R. Heath, *Nature*, 2007, **445**, 414-417.
31. B. Lewandowski, G. De Bo, J. W. Ward, M. Papmeyer, S. Kuschel, M. J. Aldegunde, P. M. E. Gramlich, D. Heckmann, S. M. Goldup, D. M. D'Souza, A. E. Fernandes and D. A. Leigh, *Science*, 2013, **339**, 189-193.
32. L. Fang, M. A. Olson, D. Benítez, E. Tkatchouk, W. A. Goddard Iii and J. F. Stoddart, *Chem. Soc. Rev.*, 2010, **39**, 17-29.
33. Q. Li, C.-H. Sue, S. Basu, A. K. Shveyd, W. Zhang, G. Barin, L. Fang, A. A. Sarjeant, J. F. Stoddart and O. M. Yaghi, *Angew. Chem. Int. Ed.*, 2010, **49**, 6751-6755.
34. A. de Juan and E. M. Pérez, *Nanoscale*, 2013, **5**, 7141-7148.
35. J. Akola, K. Rytkönen and M. Manninen, *J. Phys. Chem. B*, 2006, **110**, 5186-5190.
36. H. Isla, M. Gallego, E. M. Pérez, R. Viruela, E. Ortí and N. Martín, *J. Am. Chem. Soc.*, 2010, **132**, 1772-1773.
37. D. Canevet, M. Gallego, H. Isla, A. de Juan, E. M. Pérez and N. Martín, *J. Am. Chem. Soc.*, 2011, **133**, 3184-3190.
38. C. Romero-Nieto, R. García, M. Á. Herranz, C. Ehli, M. Ruppert, A. Hirsch, D. M. Guldi and N. Martín, *J. Am. Chem. Soc.*, 2012, **134**, 9183-9192.

closing metathesis (RCM) of the corresponding linear precursors **4**-**6** (Figure 1a). To investigate the required diameter for a SWNT to be appropriate for threading through macrocycle **1**, as a model system, we carried out an extensive theoretical search, in which the association of **1** with as many as 40 different SWNT chiralities was modeled. To that end, we chose the relatively inexpensive MMFF94 force field, which is known to provide satisfactory structural accuracy for a broad range of systems, including SWNTs. For one case, a (12,0) SWNT with **1**, we compared the force-field geometry to that obtained from a DFT calculation and found no significant difference (see Computational Details in the Experimental Details). On the basis of these calculations, we estimated that **1** was able to encapsulate SWNTs of diameters smaller than 0.91 nm with significantly positive interaction energy. Among the SWNT configurations investigated, (6,5), (7,5), (7,6), (8,4), (8,5), and (9,4) nanotubes showed the highest predicted binding energies, between 29.6 and 166.9 kJmol^{-1} (see Table S1 in the Experimental Details). The energy-minimized structure of a pseudorotaxane comprising **1** and a (7,6) SWNT is shown in Figure 1b.

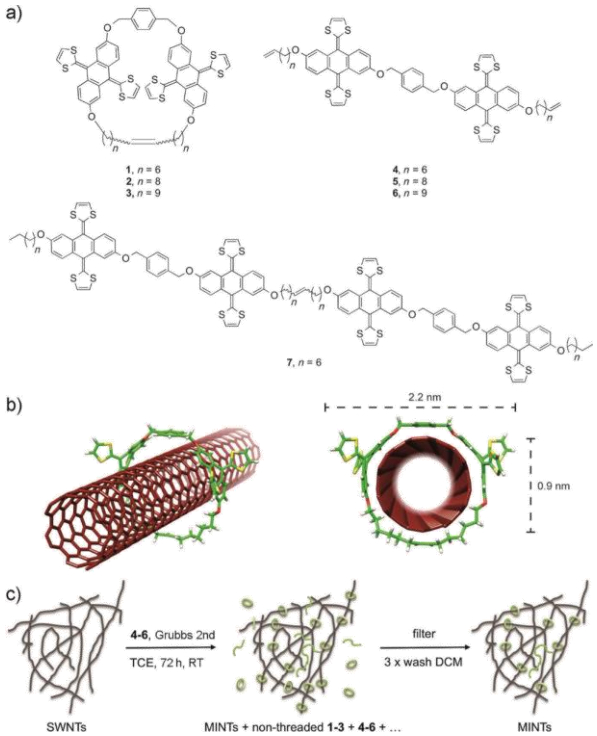

Figure 1. a) Chemical structure of macrocycles **1**-**3** and their linear precursors **4**-**6**. The structure of linear oligomer **7** is also shown. b) Energy-minimized (MMFF94) molecular model of a pseudorotaxanes comprising

1 and a (7,6) SWNT. Carbon atoms of the macrocycle are shown in green, sulfur in yellow, oxygen in red, and hydrogen in white. Carbon atoms of the SWNT are shown in dark red. The diameters of the nanotube and macrocycle **1** are also shown. c) Schematic representation of the RCM clipping reaction and purification procedure, as based on experimental data (see main text). Note that some longer oligomers/polymers might also form part of the MINT mixture.

Considering the results of the calculations, in a first attempt we utilized (7,6)-enriched SWNTs purchased from Sigma-Aldrich (0.7-1.1 nm in diameter, 90% purity after purification). The nanotubes (20 mg) were suspended in tetrachloroethane (TCE; 20 mL) through sonication and mixed with linear precursor **4** (10 mg, 0.0087 mmol) and Grubbs second-generation catalyst at room temperature for 72 h. We expected the nanotube to serve as a template for the macrocycle, which would be formed around it (Figure 1c). We relied on RCM, since the fully substituted sp^2 carbon atoms of the SWNT are unlikely to react under these conditions.[39] After this time, the suspension was filtered through a polytetrafluoroethylene membrane with a pore size of 0.2 μm, and the solid was washed profusely with CH_2Cl_2 to remove non-threaded macrocycles, catalyst, and any remaining linear precursor. Thermogravimetric analysis (TGA) of the solid thus obtained showed a weight loss of 37% at approximately 400ºC (Figure 2a). When the same reaction was carried out with plasma-purified SWNTs purchased from Cheap Tubes Inc. (0.8-1.6 nm in diameter, 99% purity), the product obtained showed a weight loss of 29% (Figure 2b), in accordance with a smaller ratio of SWNTs with diameters suitable for encapsulation with **1**. The diameter of the macrocycle also affects the degree of functionalization. For example, when the reaction was carried out with linear precursor **5** or **6** instead of **4**, under otherwise identical experimental conditions, TGA analysis showed 23 and 31% weight loss, respectively (see Figure S1 in the Experimental Details). This high loading of exTTF material suggests that, besides encapsulation by macrocycles **1**-**3**, other types of functionalization of the nanotubes, by oligomers or higher-order macrocycles formed in situ from the linear precursors, may also make a significant contribution. Functionalization by linear oligomers should be completely diameter-independent, so the dependence of the amount of exTTF material attached to the SWNTs on the size of the cavity of the macrocycle and the diameter of the nanotubes indicates that this type of functionalization plays a minor role.[†] In support of this hypothesis, HPLC

[†]The fact that larger macrocycles do not necessarily lead to a higher degree of functionalization is in agreement with our previous findings on the association of fullerenes by related macrocycles. We have shown that small changes in the structure of the receptor often lead to changes in the association constant of several orders of magnitude.

analysis of the filtrate of the clipping reaction of **4** around the plasma purified SWNTs showed macrocycle **1** and the unreacted linear precursor only, in a 64:36 **4**/**1** ratio. In comparison, analysis of an identical RCM reaction carried out in the absence of SWNTs showed a very similar HPLC trace, but with a 47:53 **4**/**1** ratio, which shows that a significant amount of **1** was retained in the SWNT material (see Figure S2 in the Experimental Details). No oligomers of **4** were detected. All these data indicate that encapsulation of the nanotubes by **1**-**3** or, to some extent, higher-order macrocycles is the major type of functionalization. Both would lead to the desired interlocked species. Nevertheless, owing to the intrinsically heterogeneous nature of the sample, the possibility of a certain degree of functionalization by oligomers/polymers cannot be fully discarded.

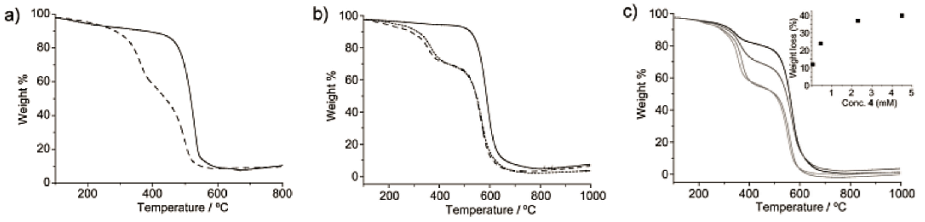

Figure 2. a) TGA analysis (air, 10ºC min^{-1}) of pristine (7,6)-enriched SWNTs (solid line) and the product formed by treatment with **4** (10 mg, 0.0087 mmol) and the Grubbs second-generation catalyst in TCE (20 mL) at room temperature for 72 h (dashed line). b) TGA analysis (air, 10ºC min^{-1}) of pristine plasma-purified SWNTs (solid line), the product formed by treatment with **4** (10 mg, 0.0087 mmol) and the Grubbs second-generation catalyst in TCE (20 mL) at room temperature for 72 h (dotted line), and the same sample after heating at reflux in TCE for 30 min and filtration (dashed line, showing the stability of the noncovalent modification). c) Variation in the degree of functionalization with the relative concentration of **4** with respect to that of the SWNTs, as shown by TGA analysis (air, 10ºC min^{-1}): 0.044 mM (black), 0.44 mM (dark gray), 2.3 mM (gray), and 4.5 mM (light gray). Inset shows the relative weight loss versus the concentration of **4**.

By varying the relative concentration of **4** with respect to SWNTs we could modulate the degree of functionalization. We performed experiments with the plasma-purified SWNTs in which the concentration of **4** was decreased by a factor of ten (0.044 mM) and increased by factors of five (2.3 mM) and ten (4.5 mM) with respect to the original experiment (0.44 mM). TGA analysis of these samples is shown in Figure 2c. The product formed with the lowest concentration of **4** showed a loss of 12% at 400ºC, whereas a weight loss of 35 or 37% was observed when the concentration of **4** was increased by a factor of five and ten, respectively. These data clearly show that the degree of functionalization does not have a linear relationship with the concentration of **4**, but instead reaches a

39. R. H. Grubbs, *Tetrahedron*, 2004, **60**, 7117-7140.

maximum at about 40%, which corresponds approximately to one macrocycle for every 140 nanotube carbon atoms (Figure 2c, inset).

This degree of functionalization was maintained even after three consecutive washes, in which the sample was re-suspended in CH_2Cl_2 (20 mL), sonicated (10 min), and filtered, thus indicating that there is little or no exchange between bound and unbound macrocycles. Even heating at reflux in tetrachloroethane (b.p. = 147ºC; 30 min), followed by a thorough rinse with CH_2Cl_2, did not lead to a significant loss of loading (Figure 2b). In fact, the only way in which the macrocycles could be removed was through calcination of the sample at 360ºC for 30 min (see Figure S3 in the Experimental Details).

We reasoned that, besides the high affinity of the macrocycles for SWNTs, this outstanding stability could originate from a high energy barrier for the de-threading process, most likely as a result of the formation of cross-points, which would act as stoppers, between the nanotubes (Figure 1c). To test this hypothesis, we carried out the clipping reaction with shorter, but otherwise identical, plasma-purified nanotubes (0.2-5 μm versus 3-30 μm), which should be less likely to form cross-points. TGA analysis of the product showed a functionalization of 20%, a significant decrease with respect to the original 29% observed for the longer tubes (see Figure S4 in the Experimental Details). Moreover, we also attempted the direct encapsulation of a suspension of the long plasma purified SWNTs (20 mg) in TCE (20 mL) by stirring with macrocycle **1** (10 mg, 0.0089 mmol) for 72 h at room temperature. The resulting product was analyzed by TGA, which showed a weight loss of only 7% (see Figure S5 in the Experimental Details); this low weight loss indicates that the threading process is indeed highly unlikely.

Since some residual functionalization was still observed, we decided to quantify the direct association of **4** with the walls of the SWNTs by mixing **4** (10 mg, 0.0087 mmol) and SWNTs (20 mg) in TCE (20 mL) in the absence of the RCM catalyst. Similarly to the previous experiment, we observed a weight loss of around 6% by TGA (see Figure S6 in the Experimental Details). This value suggests that both products are the result of the adsorption of either **1** or **4** on the sidewalls of the SWNTs. An increase in the number of exTTF units to four, with linear dimer **7**, led to a slight increase in the amount of material attached to the SWNTs (9% weight loss in TGA at the same temperature; see Figure S7 in the

Experimental Details), thus providing further evidence that functionalization by oligomers plays a minor role only.

To characterize our MINT samples, we carried out solid-state cross-polarization magic-angle spinning (CP MAS) ^{13}C NMR spectroscopy, UV/Vis/NIR spectroscopy, photoluminescence excitation intensity mapping (PLE), and Raman spectroscopy, all of which were in agreement with the noncovalent functionalization of the SWNTs with **1**. The CP MAS ^{13}C NMR spectrum of the mechanically interlocked sample of the plasma-purified nanotubes, $MINT_{pp}$-**1**, showed signals in the δ = 150-100, 80-60, and 40-20 ppm regions, which were assigned to the sp^2-hybridized nanotube carbon atoms plus the aromatic atoms of **1**, the alkene moieties, and the alkyl spacers of **1**, respectively. For comparison, the CP MAS ^{13}C NMR spectrum of **1** was also recorded and showed much better defined signals in similar areas of the spectrum. The relative integrals of the aromatic/alkene/alkyl regions in **1** are approximately 2.6:0.2:1.0, whereas in $MINT_{pp}$-**1** they are 4.7:0.2:1.0, thus showing that the nanotube carbon atoms are cross-polarized via the hydrogen atoms of the macrocycle. In contrast, neither the pristine nanotubes nor the products of the control experiments without the Grubbs catalyst or with the preformed macrocycle **1** showed any signals (Figure 3a). The UV/Vis/NIR spectra of pristine (7,6)-enriched SWNTs and the corresponding $MINT_{(7,6)}$-**1** sample are shown in Figure 3b. The absorption spectra of the SWNTs shows features in the M_{11}, S_{22}, and S_{11} regions of the spectra, with the absorption of the (7,6) nanotube clearly distinguishable at λ = 650 and 1120 nm.[40] Upon derivatization, these bands are significantly shifted bathochromically, to λ = 660 and 1150 nm, respectively. Most other absorption bands in the S_{11} and S_{22} regions of the spectra are also shifted to a similar extent.

40. S. M. Bachilo, M. S. Strano, C. Kittrell, R. H. Hauge, R. E. Smalley and R. B. Weisman, *Science* 2002, **298**, 2361-2366.

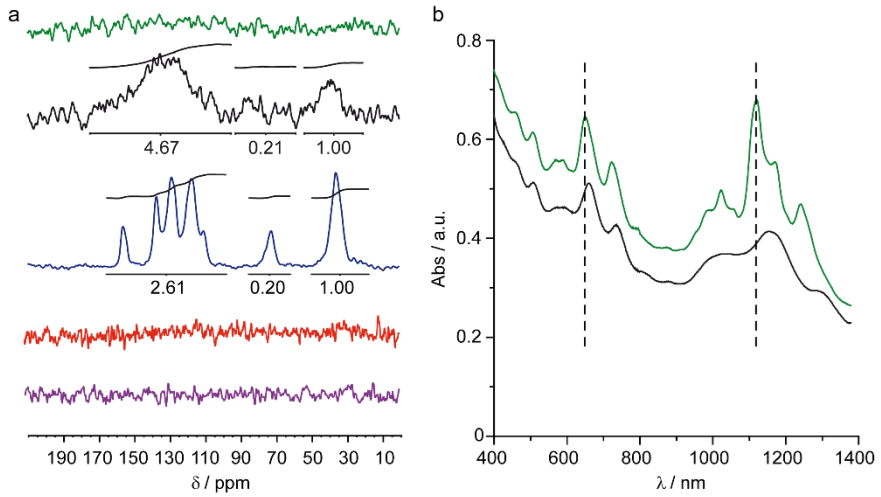

Figure 3. a) CP MAS ^{13}C NMR spectra of (from top to bottom): pristine plasma-purified SWNTs, MINT$_{pp}$-**1**, macrocycle **1**, SWNTs after treatment with **4**, and SWNTs after treatment with **1**. b) UV/Vis/NIR spectra (D_2O, 1 % sodium dodecyl sulfate (SDS), 298 K) of pristine (7,6)-enriched SWNTs (top, green) and MINT$_{(7,6)}$-**1** (bottom, black). The absorption features of the (7,6) nanotube are marked with a vertical dashed line.

In the PLE experiments (Figure 4), SWNTs of configurations (6,5), (7,5), (7,6), (8,4), and (9,4) were detected in the (7,6)-enriched sample, all of which should present significant positive interactions with **1** according to our calculations. Upon the formation of MINT$_{(7,6)}$-**1**, their luminescence is significantly quenched and red-shifted, as could be expected. For example, in the case of the (7,6) tubes, as compared to a sample of pristine SWNTs of the same optical density, the excitation is shifted from 644 to 648 nm, and the emission is shifted from 1142 to 1152 nm and quenched to approximately half the intensity.

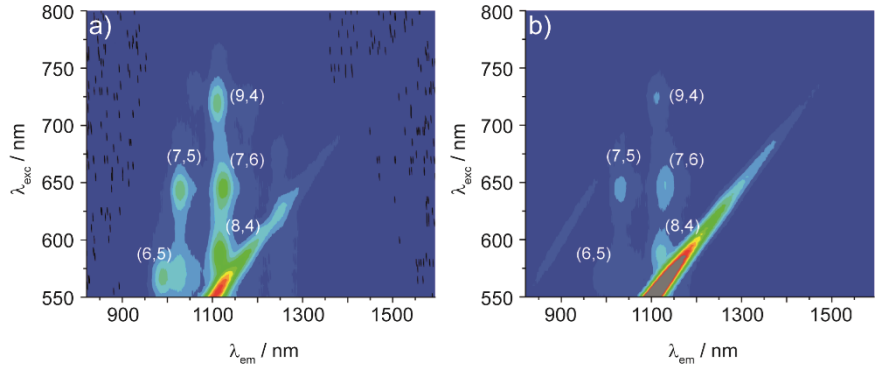

Figure 4. PLE intensity maps (D_2O, 1% SDS, 298 K) of a) pristine (7,6)-enriched SWNTs and b) MINT$_{(7,6)}$-**1**. Intensities range from 0 to 1650 counts. Rayleigh scattering has not been filtered.

The Raman spectra of as-purchased plasma-purified SWNTs and MINT$_{pp}$-**1** are compared in Figure 5 a-c (λ_{exc} = 785 nm). The two spectra are very similar, thus proving that the structure of the nanotubes is preserved upon modification, with no increase in the relative intensity of the D band. Meanwhile, the G band is shifted from 1576 cm^{-1} in the pristine SWNT to 1577 cm^{-1} in MINT$_{pp}$-**1** (Figure 5b). This small shift is in agreement with previous findings for the noncovalent modification of SWNTs with exTTF-based tweezers[38] and implies that there is no significant charge transfer from the electron-donor exTTF moiety to the SWNTs in the ground state. The change in the radial breathing modes (RBM) are also small. The signals at lower wave numbers (150-200 cm^{-1}), which correspond to SWNTs too large to be encapsulated by **1**, are unaltered, whereas those appearing between 250 and 300 cm^{-1} (SWNT diameter: 1-0.8 nm) are shifted to higher frequencies, for example, from 259 to 260 cm^{-1}. The shifts in the spectra of the (7,6)-enriched sample upon functionalization are very similar (Figure 5d-f). The G band is shifted from 1585 to 1587 cm^{-1}, whereas the RBM of the (7,6) SWNT is shifted from 259 to 260 cm^{-1}. The modifications with green laser excitation follow the same trends (see Figure S8 in the Experimental Details). All these data are consistent with the modification of the nanotubes to form MINT-**1**.

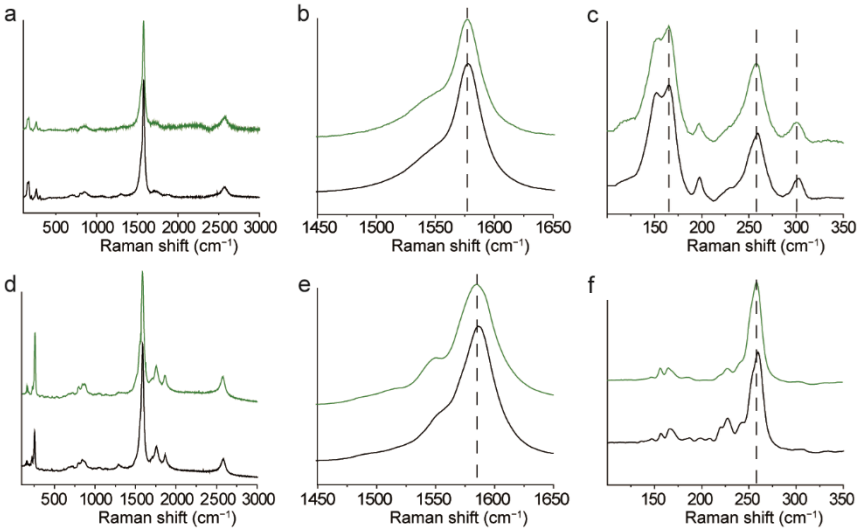

Figure 5. a) Raman spectra (λ_{exc} = 785 nm) of plasma-purified SWNTs (top, green) and the corresponding MINT$_{pp}$-**1** (bottom, black); b) magnification of the G zone; c) magnification of the RBM zone (dashed vertical lines have been added as a guide to the eye). d) Raman spectra of (7,6)-enriched SWNTs (top, green) and the corresponding MINT$_{(7,6)}$-**1** (bottom, black); e) magnification of the G zone; f) magnification of the RBM zone. All spectra are the average of three different measurements.

The investigation of a sample of $MINT_{(7,6)}$-**1** under atomic force microscopy (AFM, dynamic mode) was also in agreement with the formation of the rotaxane-type species. Figure 6a shows a topographic image of a single SWNT with a height of approximately 1 nm, on which three separate elevations of approximately 2.5 nm are observed. The dimensions and the regularity of these elevations are perfectly consistent with the formation of **1** around a SWNT (Figure 1b). If either **1** or unreacted **4** were simply adsorbed on top of the SWNT, the vertical dimension would be significantly smaller (ca. 1.6 nm; see Figure S9 in the Experimental Details). The phase image (Figure 6b) shows that there is higher energy diffusion at the protuberances, thus indicating that they are not nanotube inhomogeneities. In contrast, AFM images of the pristine SWNTs do not show protuberances of regular height nor differences in the phase channel (see Figure S10 in the Experimental Details).

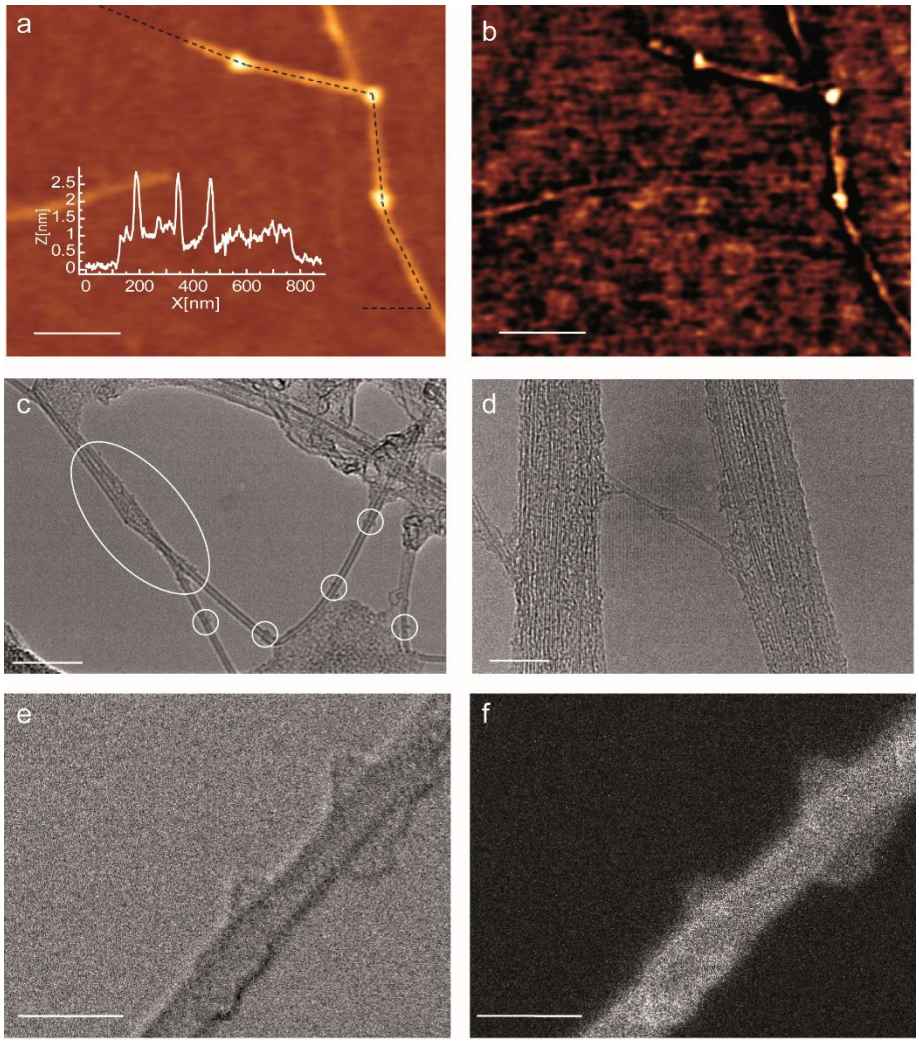

Figure 6. a) AFM topographic image of a spin-cast suspension of MINT$_{(7,6)}$-**1** in TCE. The inset shows the profile along the dashed black line. b) Phase image of the area shown in (a). c) TEM image of nanotubes (showing a densely covered surface) and several individual macrocycles in the MINT$_{pp}$-**1** sample. d) TEM image of an individual SWNT in the MINT$_{(7,6)}$-**1** sample; the image shows an object of appropriate dimensions to be **1**. e) HR STEM bright-field image of a single SWNT surrounded by two macrocycles in the MINT$_{(7,6)}$-**1** sample. f) HR STEM dark-field image of the same nanotube. Scale bars are 100 nm for (a,b), 20 nm for (c), 10 nm for (d), and 2 nm for (e,f). Figure 6c and d are showed enlarged in the Experimental Details.

Finally, transmission electron microscopy (TEM) provided conclusive support for the formation of MINTs. Pioneering studies by Nakamura and co-workers have offered extensive evidence of the observation of a variety of small

organic molecules under TEM in the vicinity of carbon nanotubes.[41] An image of MINT$_{pp}$-**1** obtained under a JEOL-JEM 2100F microscope (2.5 Å resolution), like the microscope utilized by Nakamura and co-workers in their seminal study,[42] is shown in Figure 6c. Most of the individual SWNTs show densely covered walls (Figure 6c, white ellipse), in agreement with the high degree of functionalization determined by TGA, but we were pleased to observe that in numerous cases distinct circular objects could be detected around the nanotubes, in several different areas of the sample (Figure 6c, white circles). The diameter of the nanotubes (ca. 1.4 nm) and of the macrocyclic components (ca. 4 nm) suggests that these circular objects are the result of a bimolecular macrocyclization of **4**. Figure 6d shows a TEM image of the MINT$_{(7,6)}$-**1** sample, in which an isolated SWNT of diameter 0.8 nm surrounded by an object of an appropriate size to be **1** (ca. 2.2 nm) can be seen. To perform a more precise characterization, we also employed an aberration-corrected microscope. The microscope was operated at 80 kV to prevent damage to the nanotubes and macrocycles. Under these working conditions, in scanning transmission electron (STEM) mode, a spatial resolution of 1.1 Å is guaranteed. Figure 6e,f shows the bright-field and dark-field high-resolution (HR) STEM images, recorded simultaneously, of the MINT$_{(7,6)}$-**1** sample. In the bright-field image, a single SWNT of 0.8 nm in diameter and functionalized with two separate macrocycles can be observed. The macrocycles are again commensurate with **1** in terms of their size (ca. 2.2 nm). The dark-field image shows a similar contrast for the macrocycles and the SWNT, in accordance with their composition. Energy-dispersive X-ray spectroscopy (EDX) of the MINT-**1** samples confirmed the presence of a significant amount of sulfur (ca. 1%), in good agreement with the TGA data (see Figure S11 in the Experimental Details).

3.3 Conclusions

In conclusion, we have introduced the mechanical bond as a new tool for the chemical manipulation of SWNTs. Our synthetic approach is based on a clipping strategy in which the macrocycles are formed around the SWNTs by RCM. Once in place, the macrocycles remained attached to the nanotubes even after reflux

41. E. Nakamura, *Angew. Chem. Int. Ed.*, 2013, **52**, 236-252.
42. M. Koshino, T. Tanaka, N. Solin, K. Suenaga, H. Isobe and E. Nakamura, *Science*, 2007, **316**, 853-853.

in TCE for 30 min, and could only be removed by calcination at 360ºC. Raman spectroscopy showed that the changes to the electron-phonon structure of the SWNTs upon formation of the mechanically interlocked species are small, and comparable to those observed after typical noncovalent modification. PLE maps suggest that a charge-transfer process occurs from the donor exTTF unit to the nanotubes upon photoexcitation. We now intend to extend this strategy to other types of macrocycles and to investigate the properties of the MINTs exhaustively.

3.4 Experimental Details

3.4.1 Synthesis and characterization

General. All solvents were dried according to standard procedures. Reagents were used as purchased. All air-sensitive reactions were carried out under argon atmosphere. Flash chromatography was performed using silica gel (Merck, Kieselgel 60, 230-240 mesh, or Scharlau 60, 230-240 mesh). Analytical thin layer chromatographies (TLC) were performed using aluminium-coated Merck Kieselgel 60 F254 plates. NMR spectra were recorded on a BrukerAvance 300 (^{1}H: 300 MHz; ^{13}C: 75 MHz), a BrukerAvance 500 (^{1}H: 500 MHz; ^{13}C: 125 MHz) spectrometers at 298 K, unless otherwise stated, using partially deuterated solvents as internal standards. Coupling constants (J) are denoted in Hz and chemical shifts (δ) in ppm. Multiplicities are denoted as follows: s = singlet, d = doublet, t = triplet, m = multiplet, b = broad. Electrospray ionization mass spectrometry (ESI-MS) and Matrix-assisted Laser desorption ionization (coupled to a Time-Of-Flight analyzer) experiments (MALDI-TOF) were recorded on a HP1100MSD spectrometer and a Bruker REFLEX spectrometer, respectively. Thermogravimetric analyses (TGA) were performed using a TA Instruments TGAQ500 with a ramp of 10 °C/min under air from 100 to 1000 °C. The ^{13}C CP-MAS-NMR spectra were obtained with a Bruker AV 400 WB spectrometer. UV-vis-NIR spectrums were performed using a Shimadzu UV-VIS-NIR Spectrophotometer UV-3600. Photoluminescence excitation intensity maps (PLE) were obtained with NanoLog 4 HORIBA. Raman spectra were acquired with a RenishawinVia confocal Raman microscopy instrument, equipped with 532, and 785 nm lasers. Transmission electron microscopy (TEM) images were obtained with JEOL-JEM 2100F (2.5 Å resolution) instrument.

Scanning Transmission Electron (STEM) mode images were obtained with JEOL-JEM ARM200cF.

Synthesis of molecular receptors **4**, **5**, **6** and macrocycles **1**, **2**, **3**.

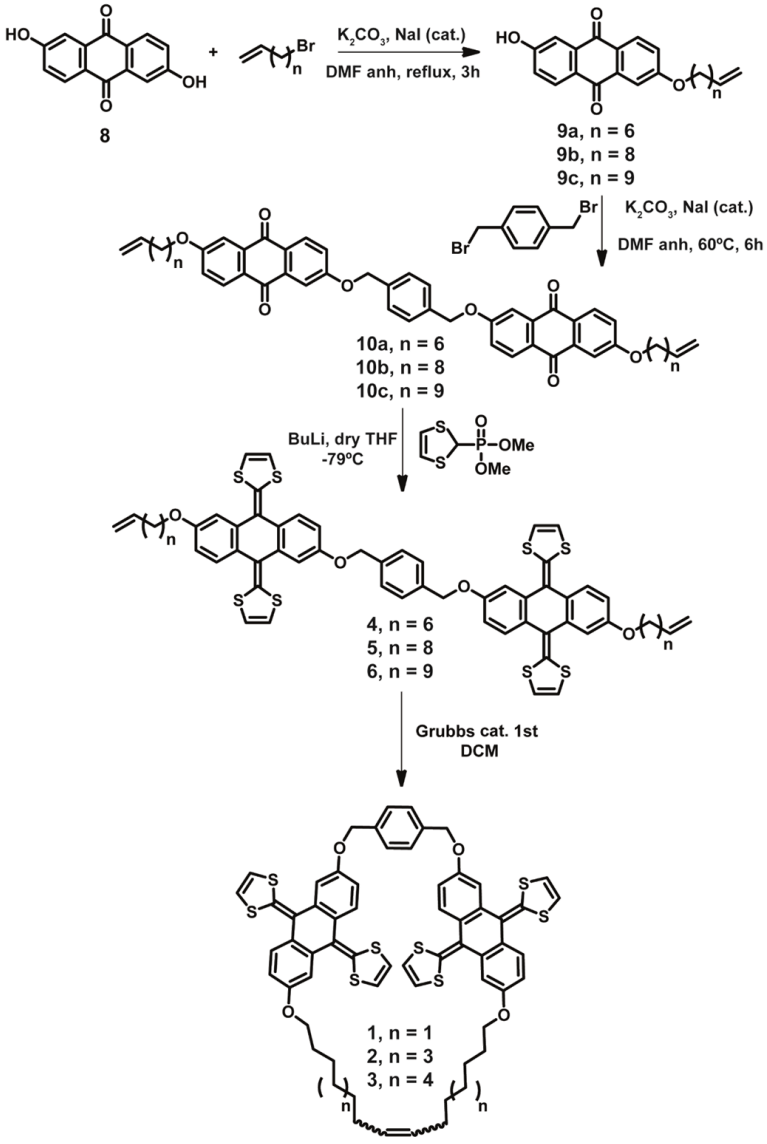

General procedure to synthetize compounds 9a-c. Anthraflavic acid 94% (1.0 g, 4.16 mmol) was dispersed with sonication in dry DMF (180 mL). Then, dry K_2CO_3 (0.57 g,4.16 mmol), the corresponding α-bromo-ω-alkene (4.16 mmol) and a catalytic amount of NaI were added and the mixture refluxed for three hours. The crude reaction was poured into ice-cold 1 M hydrochloric acid (1 L), and filtrated. The solid was redissolved in CH_2Cl_2 and washed with water (2 x 150 mL). The organic fraction was dried over $MgSO_4$, the solvent evaporated, and the corresponding residue subjected to column chromatography (CH_2Cl_2 to CH_2Cl_2:CH_3OH 2%) affording the pure product as a light yellow solid (**9a**, y = 31%; **9b**, y = 25%; **9c**, y = 28%).

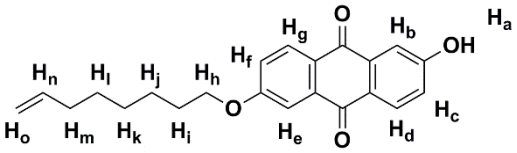

Compound **9a** (31% yield). ^{1}H NMR (d_6-DMSO, 300 MHz) δ 11.03 (s, 1H, H_a), 8.09 (d, *J* = 8.7 Hz, 1H, H_g), 8.06 (d, *J* = 8.7 Hz, 1H, H_d), 7.54 (d, *J* = 2.6 Hz, 1H, H_e), 7.48 (d, *J* = 2.7 Hz, 1H, H_b), 7.37 (dd, *J* = 8.7 Hz, *J* = 2.7 Hz, 1H, H_f), 7.20 (dd, *J* = 8.6 Hz, *J* = 2.6 Hz, 1H, H_c), 5.79 (ddt, *J* = 17.0 Hz, *J'* = 10.2 Hz, *J''* = 6.6 Hz, 1H, H_n), 5.04-4.90 (m, 2H, H_o), 4.16 (t, *J* = 6.5 Hz, 2H, H_h), 2.03 (m, 2H, H_m), 1.76 (m, 2H, H_i), 1.49-1.30 (m, 6H, H_{j+k+l}). ^{13}C NMR (d_6-DMSO, 75 MHz) δ 182.22, 181.85, 164.29, 164.09, 139.62, 136.22, 136.15, 130.67, 130.22, 127.15, 126.02, 121.90, 121.19, 115.55, 113.08, 111.42, 69.21, 33.98, 29.25, 29.07, 26.07. MS *m/z*: calculated for $C_{22}H_{21}O_4$ [M-H$^+$] 349.1 found ESI (neg.) 349.0.

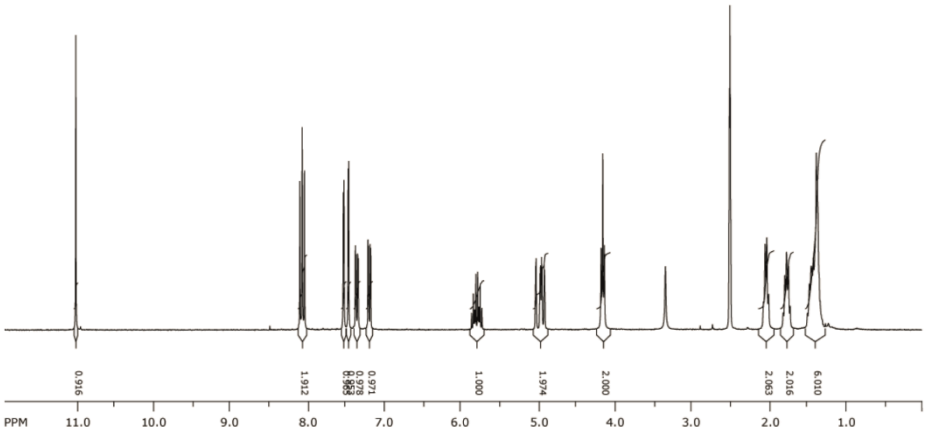
0.916
1.912
0.971
1.000
1.974
2.000
2.063
2.016
6.010
PPM
11.0
10.0
9.0
8.0
7.0
6.0
5.0
4.0
3.0
2.0
1.0

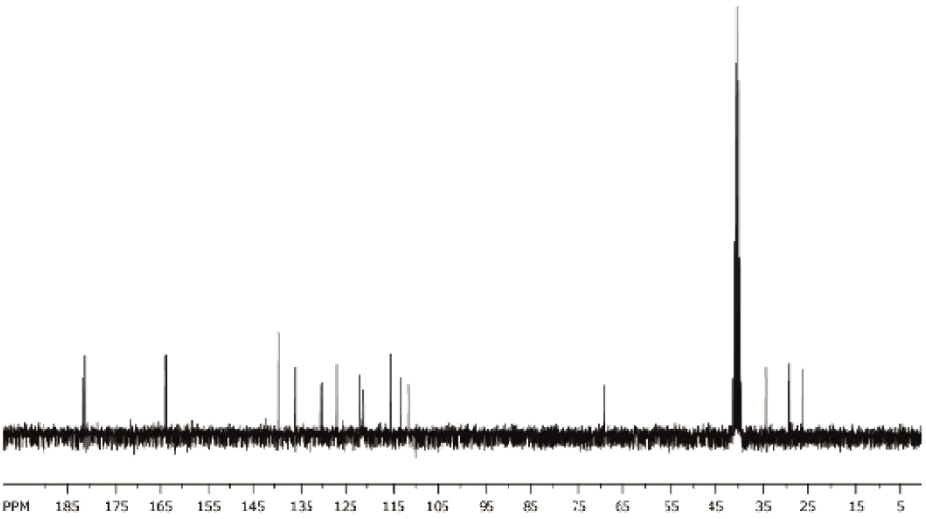
PPM
185
175
165
155
145
135
125
115
105
95
85
75
65
55
45
35
25
15
5

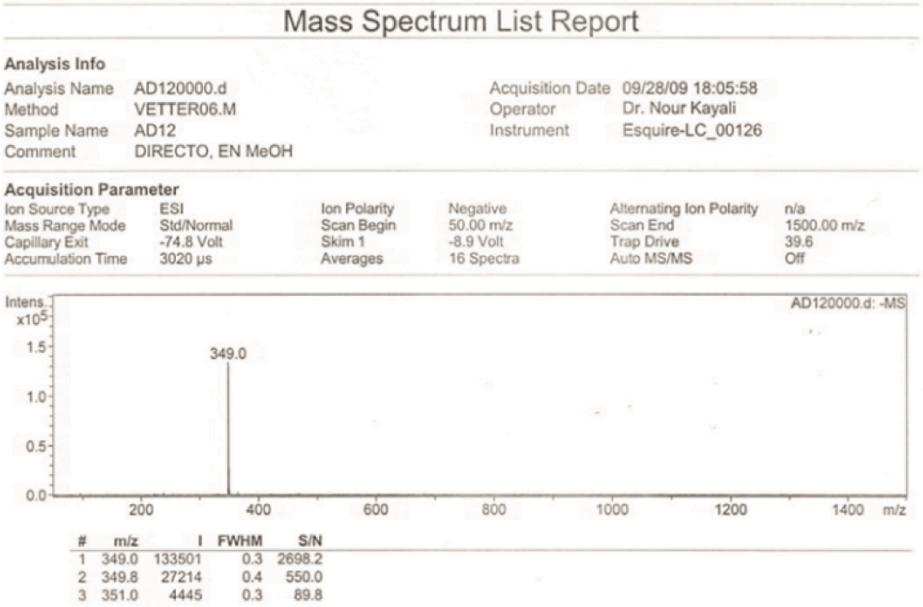

Mass Spectrum List Report

Analysis Info

Analysis Name	AD120000.d	Acquisition Date	09/28/09 18:05:58
Method	VETTER06.M	Operator	Dr. Nour Kayali
Sample Name	AD12	Instrument	Esquire-LC_00126
Comment	DIRECTO, EN MeOH		

Acquisition Parameter

Ion Source Type	ESI	Ion Polarity	Negative	Alternating Ion Polarity	n/a
Mass Range Mode	Std/Normal	Scan Begin	50.00 m/z	Scan End	1500.00 m/z
Capillary Exit	-74.8 Volt	Skim 1	-8.9 Volt	Trap Drive	39.6
Accumulation Time	3020 µs	Averages	16 Spectra	Auto MS/MS	Off

#	m/z	I	FWHM	S/N
1	349.0	133501	0.3	2698.2
2	349.8	27214	0.4	550.0
3	351.0	4445	0.3	89.8

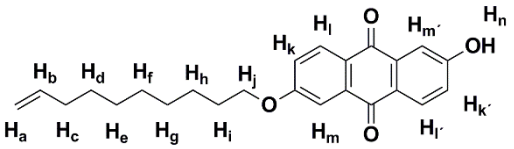

Compound **9b** (25% yield).^{1}H NMR (300 MHz, $CDCl_3$) δ 8.20 (dd, *J* = 8.6, 2.5 Hz, 2H, $H_{l+l'}$), 7.95 (s, 1H, H_n), 7.71 (d, *J* = 2.6 Hz, 1H, H_m), 7.69 (d, *J* = 2.6 Hz, 1H, $H_{m'}$), 7.20 (dd, *J* = 8.7, 2.4 Hz, 2H, $H_{k+k'}$), 5.91 – 5.71 (m, 1H, H_b), 5.05 – 4.87 (m, 2H, H_a), 4.13 (t, *J* = 6.5 Hz, 2H, H_j), 2.10 – 2.00 (m, 2H, H_c), 1.90 – 1.77 (m, 2H, H_i), 1.60 – 1.20 (m, 10H, $H_{d+e+f+g+h}$).^{13}C NMR (75 MHz, $CDCl_3$) δ 182.45, 182.35, 164.19, 162.20, 139.27, 136.12, 136.04, 130.30, 129.72, 127.11, 126.92, 121.06, 120.99, 114.30, 113.16, 110.73, 68.93, 33.90, 31.05, 29.50, 29.40, 29.16, 29.03.MS m/z: calculated for $C_{24}H_{26}O_4$ $[M+H]^+$379.18 found FAB 379.2.

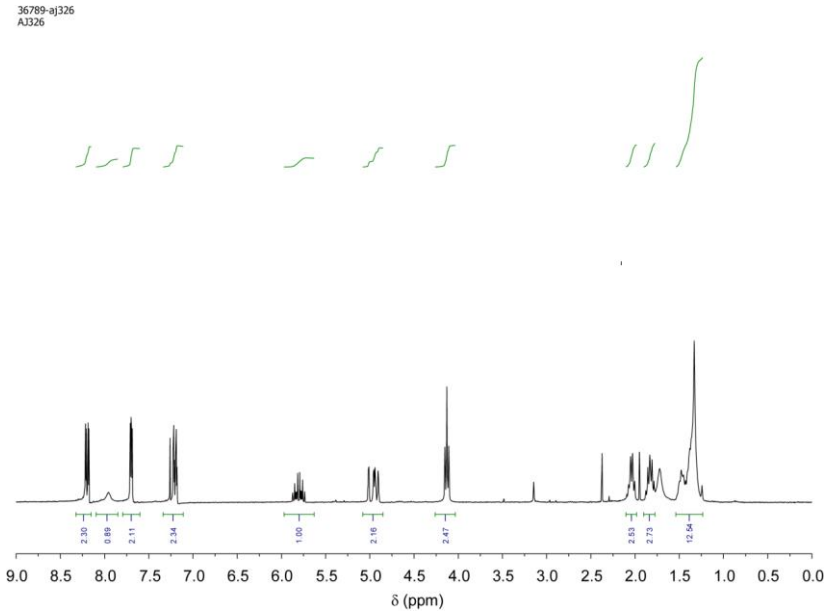
36789-aj326
AJ326
2.30
0.89
2.11
2.34
1.00
2.16
2.47
2.53
2.73
12.64
9.0 8.5 8.0 7.5 7.0 6.5 6.0 5.5 5.0 4.5 4.0 3.5 3.0 2.5 2.0 1.5 1.0 0.5 0.0
δ (ppm)

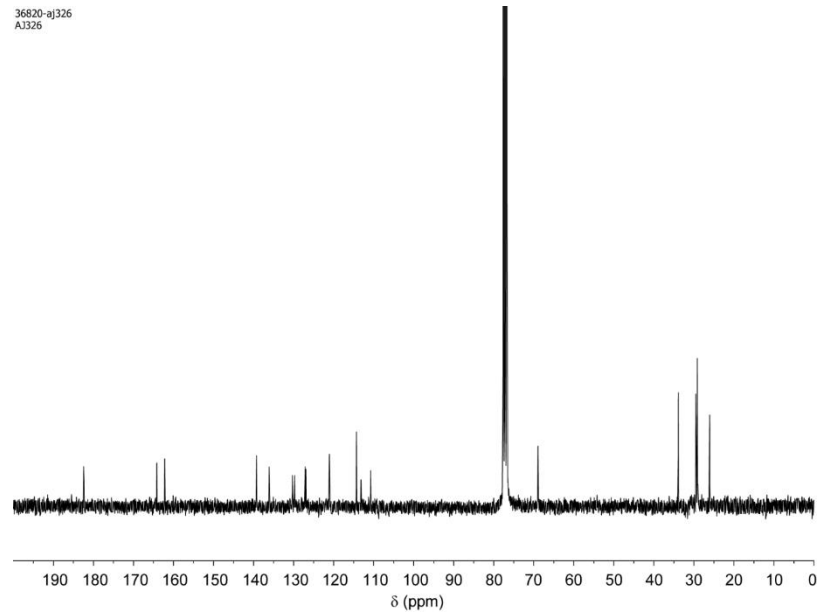
36820-aj326
AJ326
190 180 170 160 150 140 130 120 110 100 90 80 70 60 50 40 30 20 10 0
δ (ppm)

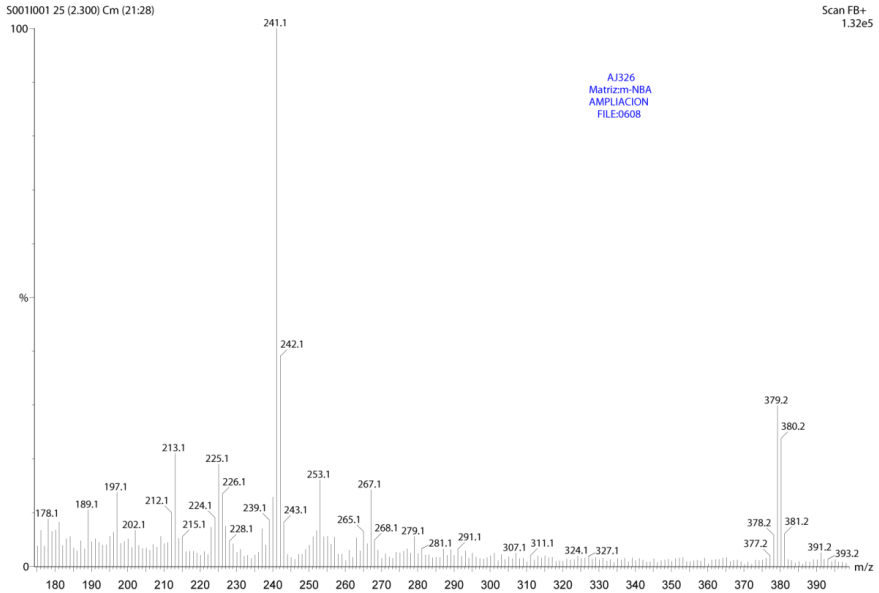

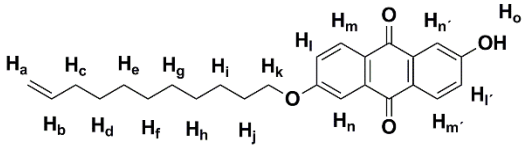

Compound **9c** (28% yield). ^{1}H NMR (300 MHz, $CDCl_3$) δ 8.25 (d, *J* = 8.6 Hz, 1H, H_m), 8.22 (d, *J* = 8.6 Hz, 1H, $H_{m'}$), 7.82 (d, *J* = 2.6 Hz, 1H, H_n), 7.72 (d, *J* = 2.6 Hz, 1H, $H_{n'}$), 7.23 (dd, *J* = 8.6, 2.6 Hz, 2H, $H_{l+l'}$), 6.73 (s, 1H, H_o), 5.83 (ddt, *J* = 16.9, 10.2, 6.7 Hz, 1H, H_b), 5.06 – 4.87 (m, 2H, H_a), 4.15 (t, *J* = 6.5 Hz, 2H, H_k), 2.10 – 1.99 (m, 2H, H_c), 1.92 – 1.76 (m, 2H, H_j), 1.56 – 1.21 (m, 12H, $H_{d+e+f+g+h+i}$). ^{13}C NMR (75 MHz, $CDCl_3$) δ 182.71, 182.29, 164.44, 161.48, 139.35, 136.07, 130.48, 129.87, 127.38, 126.95, 121.14, 114.29, 113.27, 110.91, 69.03, 33.95, 29.64, 29.56, 29.46, 29.26, 29.17, 29.08, 26.09. MS m/z: calculated for $C_{25}H_{28}O_4$ $[M+H]^+$ 393.20 found FAB 393.2.

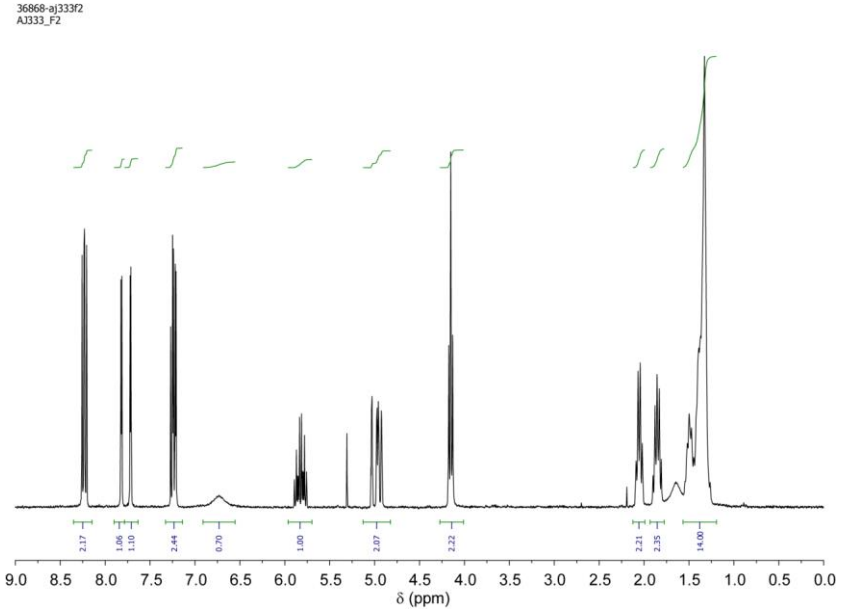
36868-aj333f2
AJ333_F2
2.17
1.06
1.10
2.44
0.70
1.00
2.07
2.22
2.21
2.35
14.00
9.0 8.5 8.0 7.5 7.0 6.5 6.0 5.5 5.0 4.5 4.0 3.5 3.0 2.5 2.0 1.5 1.0 0.5 0.0
δ (ppm)

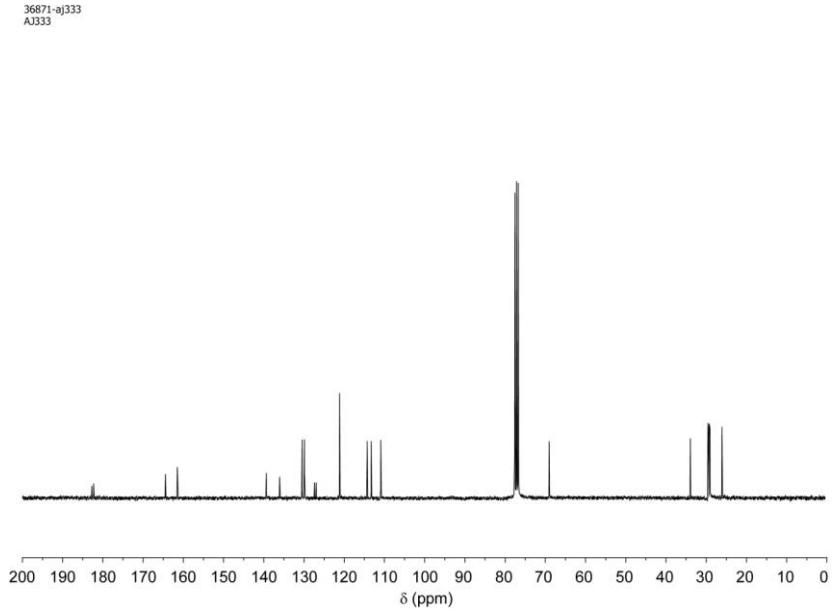
36871-aj333
AJ333
200 190 180 170 160 150 140 130 120 110 100 90 80 70 60 50 40 30 20 10 0
δ (ppm)

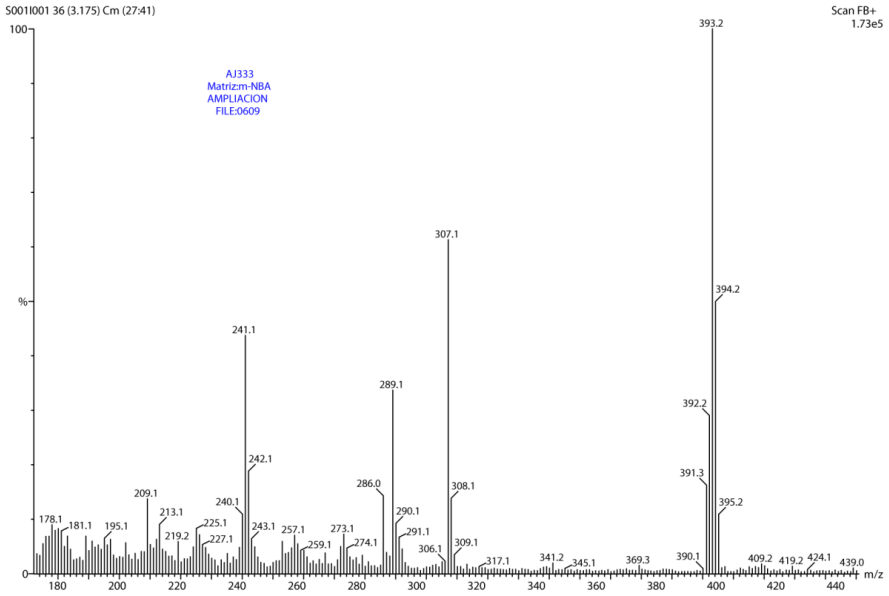

General procedure to synthetize compounds 10a-c. Dry K_2CO_3 (1.23 g, 8.91 mmol), α,α'-dibromoxylene (1.17 g, 4.0 mmol) and a catalytic amount of sodium iodide were added to a solution of monoalkylated anthraflavic acid **1** (10.0 mmol, 2.5 eq.) in dry DMF (20-25 mL). The solution was heated to 60 ºC for 4-6 h, and the resulting suspension was filtrated. The corresponding solid was successively washed with methanol (30 mL) and diethyl ether (30 mL) to remove unreacted starting materials affording pure compounds without further purification (**10a**, y = 79%; **10b**, y = 86%; **10c**, y = 66%).

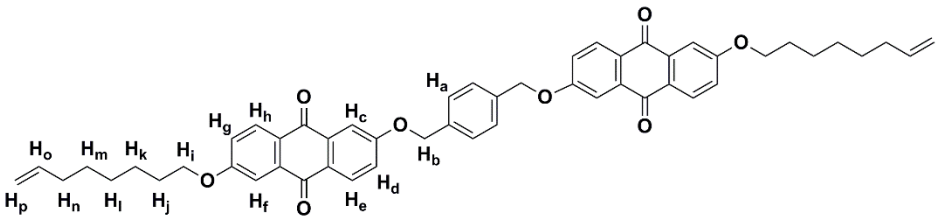

Compound **10a** (79% yield). ^{1}H NMR ($C_2D_2Cl_4$, 500 MHz, 353 K) δ 8.26 (bd, *J* = 7.8 Hz, 2H, H_e), 8.24 (bd, *J* = 8.6 Hz, 2H, H_h), 7.84 (bs, 2H, H_c), 7.74 (bs, 2H, H_f), 7.55 (bs, 4H, H_a), 7.35 (bd, *J* = 7.8 Hz, 2H, H_d), 7.26 (bd, *J* = 8.6 Hz, 2H, H_g), 5.87 (m, 2H, H_o), 5.31 (m, 4H, H_b), 5.05 (m, 4H, H_p), 4.19 (bt, 4H, H_i), 2.12 (m, 4H, H_n), 1.89 (m, 4H, H_j), 1.50 (m, 12H, H_{k+l+m}). ^{13}C NMR

($C_2D_2Cl_4$, 125 MHz, 353 K) δ 182.05, 181.91, 164.25, 163.61, 138.91, 136.22, 136.11, 135.65, 129.75, 128.87, 128.16, 127.75, 121.10, 120.90, 120.42, 114.39, 111.56, 111.24, 70.44, 69.06, 33.52, 29.04, 28.80, 28.74, 25.80. MS *m/z*: calculated for $C_{52}H_{51}O_8$ $[M+H^+]$ 803.36 found MALDI-TOF 803.34; calculated for $C_{52}H_{50}O_8Na$ $[M+Na^+]$ 824.34 found MALDI-TOF 824.35.

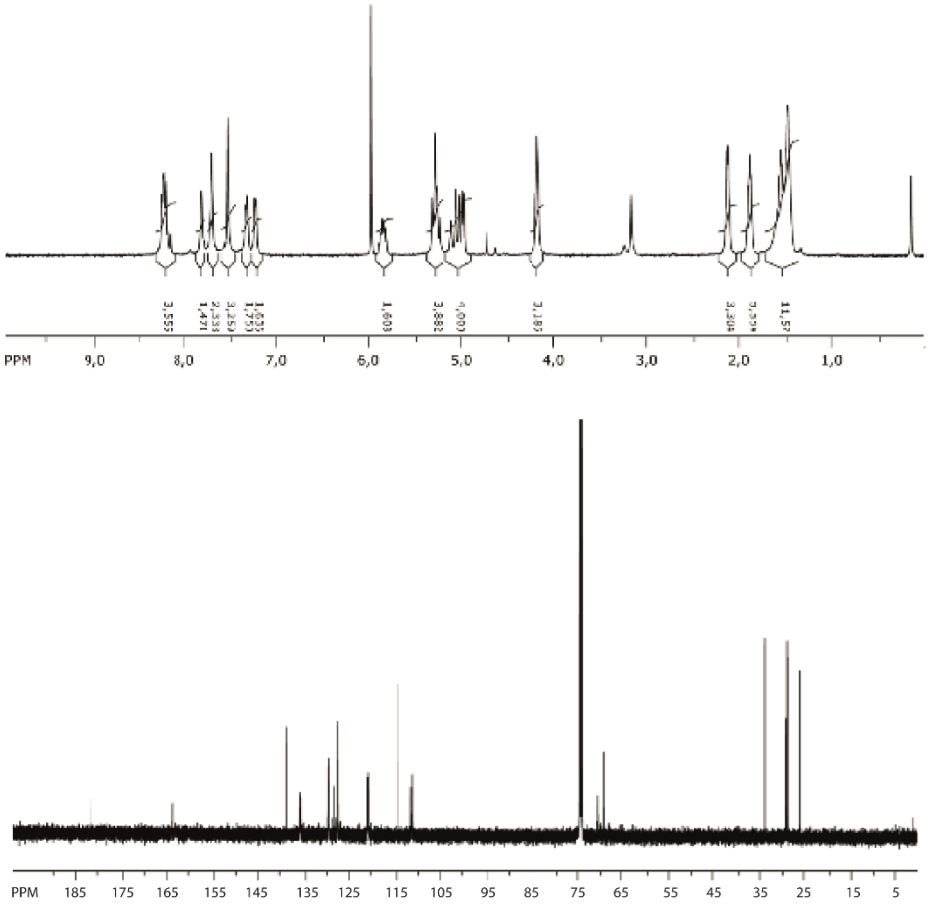

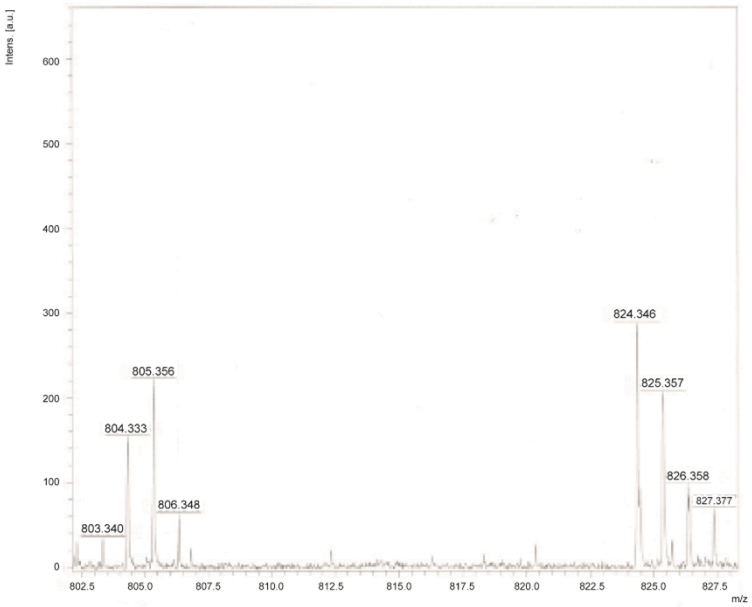

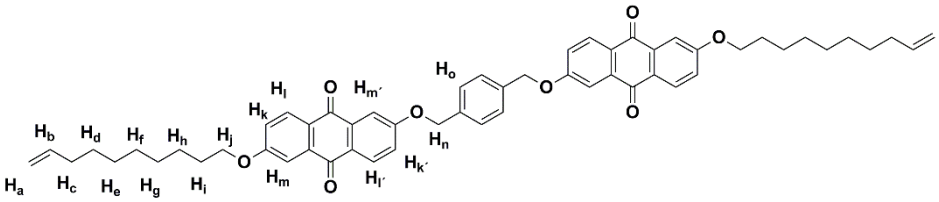

Compound **10b** (86% yield). ^{1}H NMR (500 MHz, $C_2D_2Cl_4$, 373 k) δ 8.24 (d, *J* = 8.6 Hz, 2H, H_l), 8.21 (d, *J* = 8.6 Hz, 2H, $H_{l'}$), 7.82 (d, *J* = 2.7 Hz, 2H, H_m), 7.72 (d, *J* = 2.6 Hz, 2H, $H_{m'}$), 7.51 (s, 4H, H_o), 7.32 (dd, *J* = 8.6, 2.7 Hz, 2H, H_k), 7.23 (dd, *J* = 8.6, 2.6 Hz, 2H, $H_{k'}$), 5.89 – 5.75 (m, 2H, H_a), 5.28 (s, 4H, H_n), 5.05 – 4.91 (m, 4H, H_b), 4.17 (t, *J* = 6.6 Hz, 4H, H_j), 2.10 – 2.04 (m, 4H, H_c), 1.92 – 1.82 (m, 4H, H_i), 1.57 – 1.46 (m, 4H, H_h), 1.47 – 1.32 (m, 16H, $H_{d+e+f+g}$).

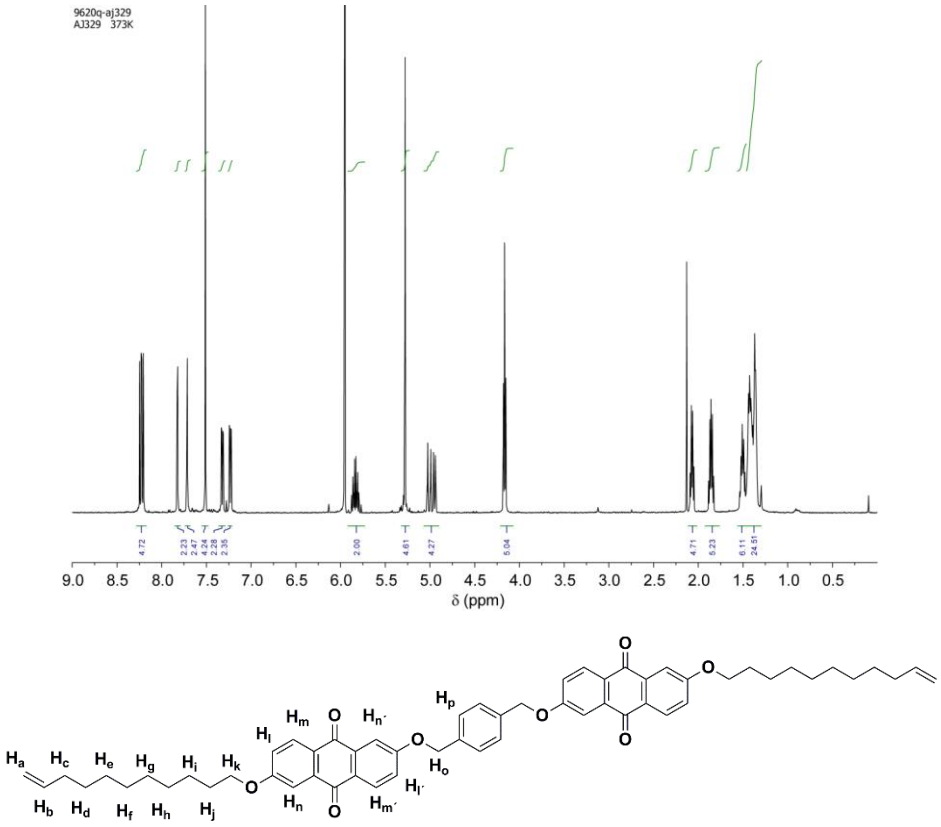

Compound **10c** (66% yield). ^{1}H NMR (500 MHz, $C_2D_2Cl_4$) δ 8.24 (d, *J* = 8.6 Hz, 2H, H_m), 8.21 (d, *J* = 8.6 Hz, 2H, $H_{m'}$), 7.82 (d, *J* = 2.7 Hz, 2H, H_n), 7.72 (d, *J* = 2.6 Hz, 2H, $H_{n'}$), 7.51 (s, 4H, H_p), 7.32 (dd, *J* = 8.6, 2.7 Hz, 2H, H_l), 7.23 (dd, *J* = 8.6, 2.6 Hz, 2H, $H_{l'}$), 5.90 – 5.74 (m, 2H, H_a), 5.28 (s, 4H, H_o), 5.05 – 4.90 (m, 4H, H_b), 4.17 (t, *J* = 6.6 Hz, 4H, H_k), 2.11 – 2.02 (m, 4H, H_c), 1.91 – 1.80 (m, 4H, H_j), 1.58 – 1.46 (m, 4H, H_i), 1.46 – 1.27 (m, 20H, $H_{d+e+f+g+h}$).

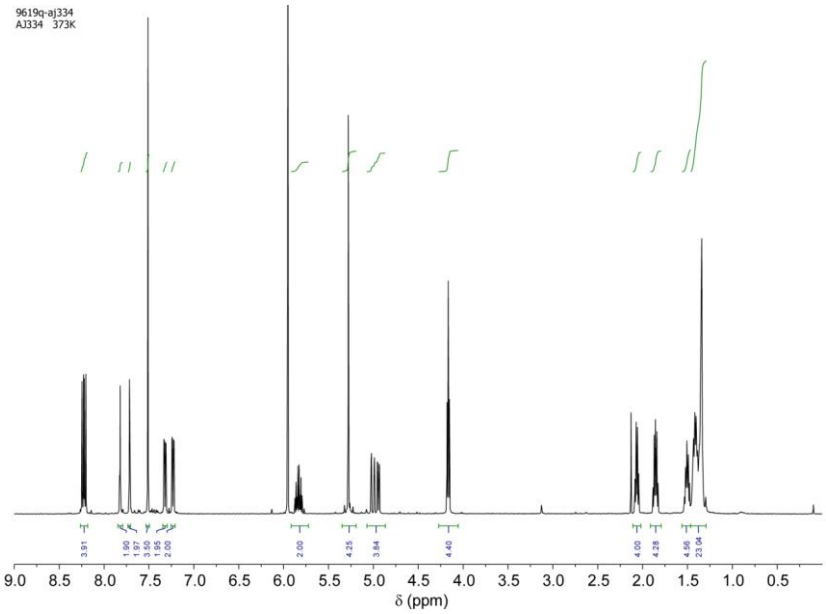

General procedure to synthetize compounds 4-6. A solution of dimethyl 1,3-dithiol-2-ylphosphonate 1.372 mg (6.48 mmol) in 20 mL of dry THF was cooled to -78 ºC, and butyllithium 1.6 M in hexanes (4.25 mL, 6.8 mmol) was added. The solution was left to stir at -78 ºC for 30 min, with appearance of a precipitate. In the meantime, a suspension of anthraquinone precursor (0.54 mmol) in dry THF (20 mL) was sonicated for *ca.* 30 min. The resulting suspension was added to the phosphorous ylide suspension, and the cooling bath immediately removed. The mixture was allowed to warm to room temperature and left to stir for 2 h. The resulting solution was quenched with methanol, with precipitation of a yellow solid. The solid was filtrated, redissolved in CH_2Cl_2, and subjected to column chromatography (CH_2Cl_2:Hexane 2:1 to 3:1) to obtain the pure product as a bright yellow solid (**4**, y = 31%; **5**, y = 29%; **6**, y = 27%).

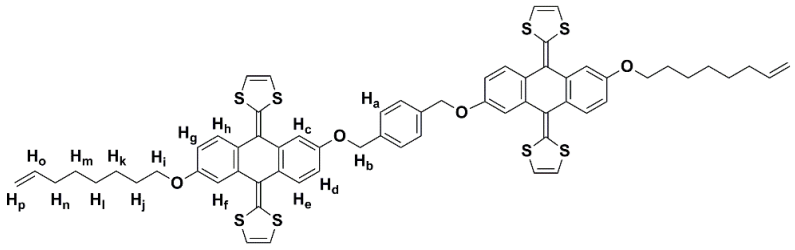

Compound **4** (31% yield). ^{1}H NMR ($CDCl_3$, 500 MHz) δ 7.60 (d, *J* = 8.4 Hz, 2H, H_e), 7.56 (bd, *J* = 9.3 Hz, 2H, H_h), 7.50 (s, 4H, H_a), 7.24 (bs, 2H, H_c), 7.20 (bs, 2H, H_f), 6.91 (bd, *J* = 8.4 Hz, 2H, H_d), 6.81 (bm, 2H, H_g), 6.24 (m, 8H, $H_{dithiole}$), 5.85 (m, 2H, H_o), 5.17 (m, 4H, H_b), 5.00 (m, 4H, H_p), 4.03 (bt, 4H, H_i), 2.10 (m, 4H, H_n), 1.83 (m, 4H, H_j), 1.46 (m, 12H, H_{k+l+m}). ^{13}C NMR ($CDCl_3$, 125 MHz) δ 157.53, 156.99, 139.47, 137.46, 137.33, 137.20, 134.38, 134.19, 129.14, 128.66, 128.14, 126.53, 126.44, 122.48, 122.23, 117.54, 117.45, 114.70, 112.46, 111.64, 111.36, 70.30, 68.60, 34.14, 30.11, 29.65, 29.30, 29.26, 29.34. MS *m/z*: calculated for $C_{64}H_{58}O_4S_8$ [M^+] 1146.21 found MALDI-TOF 1146.20.

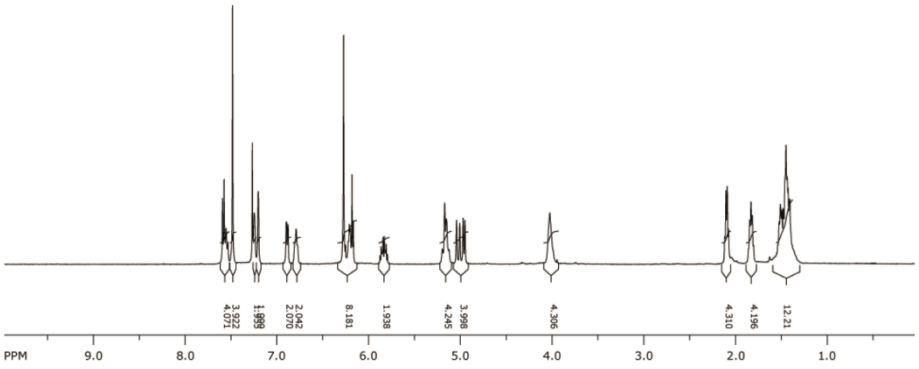

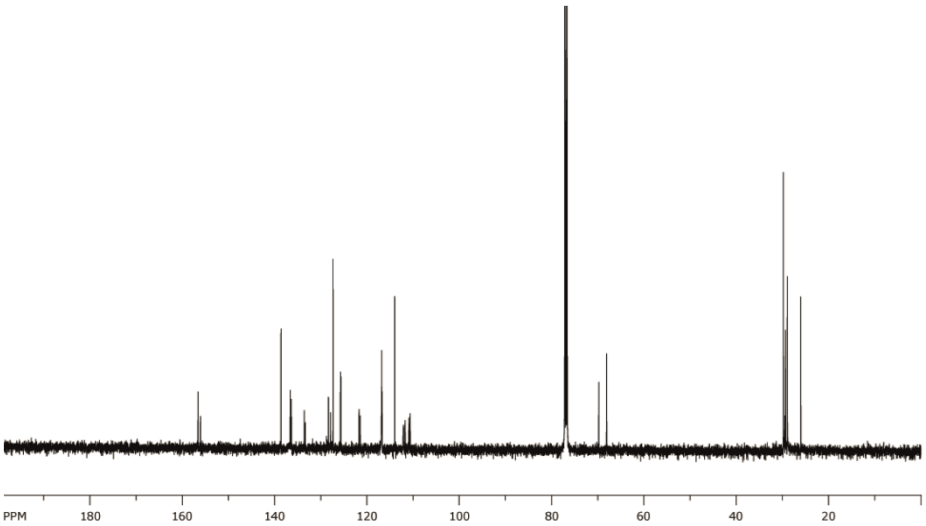
PPM
180
160
140
120
100
80
60
40
20

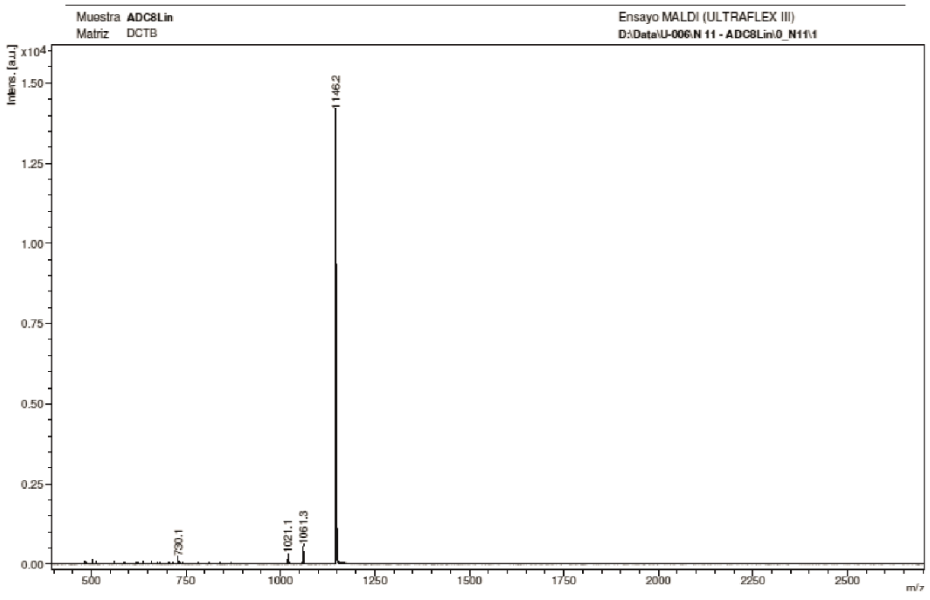
Muestra ADC8Lin
Matriz DCTB
Ensayo MALDI (ULTRAFLEX III)
D:\Data\U-006\N 11 - ADC8Lin\0_N11\1
Intens. [a.u.]
x10⁴
1.50
1.25
1.00
0.75
0.50
0.25
0.00
1146.2
790.1
1021.1
1061.3
500
750
1000
1250
1500
1750
2000
2250
2500
m/z

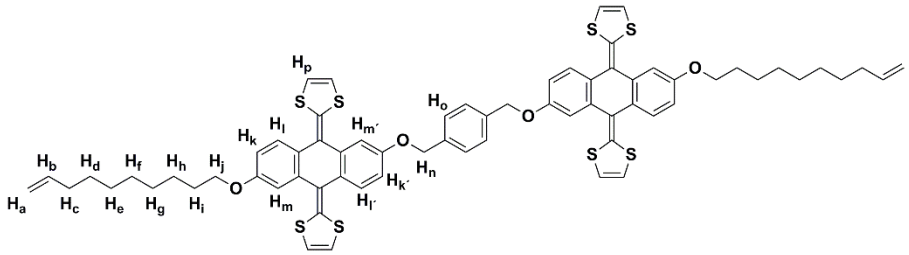

Compound **5** (29% yield). ^{1}H NMR (300 MHz, $CDCl_3$) δ 7.65 – 7.53 (m, 4H, $H_{l+l'}$), 7.50 (s, 4H, H_o), 7.26 (bd, *J* = 2.4 Hz, 2H, H_m), 7.22 (d, *J* = 2.4 Hz, 2H, $H_{m'}$),6.91 (dd, *J* = 8.6, 2.6 Hz, 2H, H_k), 6.81 (bd, *J* = 8.4 Hz, 2H, $H_{k'}$), 6.33 – 6.17 (m, 8H, H_p), 5.84 (m, 2H, H_b), 5.08 (m, 4H, H_n), 5.22 – 4.91 (m, 4H, H_a), 4.02 (t, *J* = 6.5 Hz, 4H, H_j), 2.12 – 2.02 (m, 4H, H_c), 1.88 – 1-77 (m,4H, H_i), 1.54 – 1.27 (m, 20H, $H_{d+e+f+g+h}$). ^{13}C NMR (126 MHz, $CDCl_3$) δ 157.16, 156.60, 139.23, 137.07, 136.94, 136.82, 133.96, 133.76, 128.76, 128.26, 127.75, 126.13, 126.05, 122.11, 121.85, 117.15, 117.06, 114.17, 112.49, 112.08, 111.21, 110.97, 69.92, 68.26, 33.83, 29.45, 29.39, 29.31, 29.11, 28.95, 26.08. MS m/z: calculated for $C_{68}H_{66}O_4S_8$ $[M]^+$ 1202.27 found MALDI-TOF 1202.3.

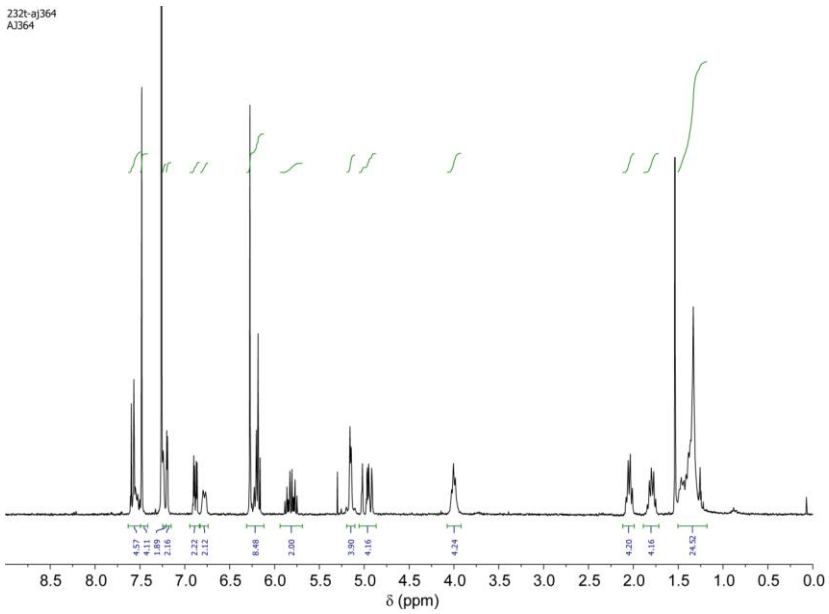

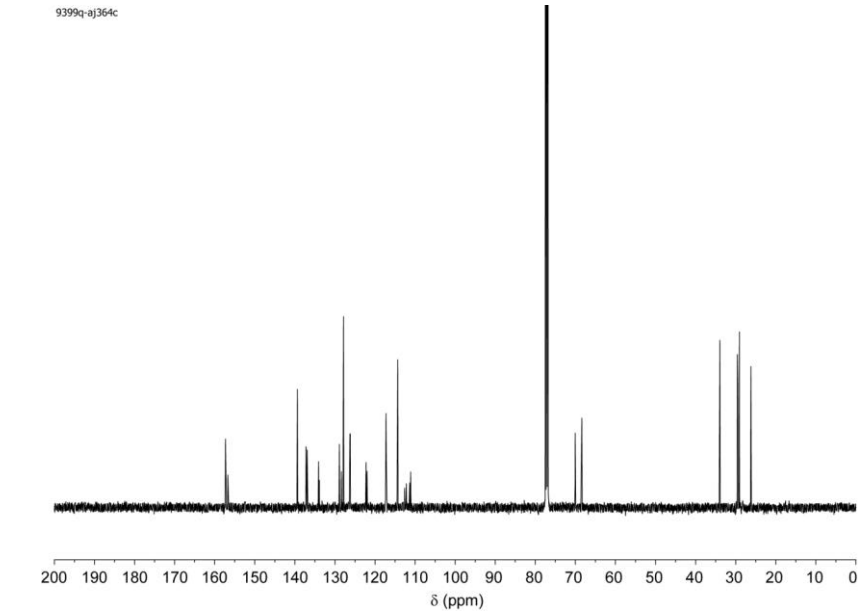
9399q-aj364c
200 190 180 170 160 150 140 130 120 110 100 90 80 70 60 50 40 30 20 10 0
δ (ppm)

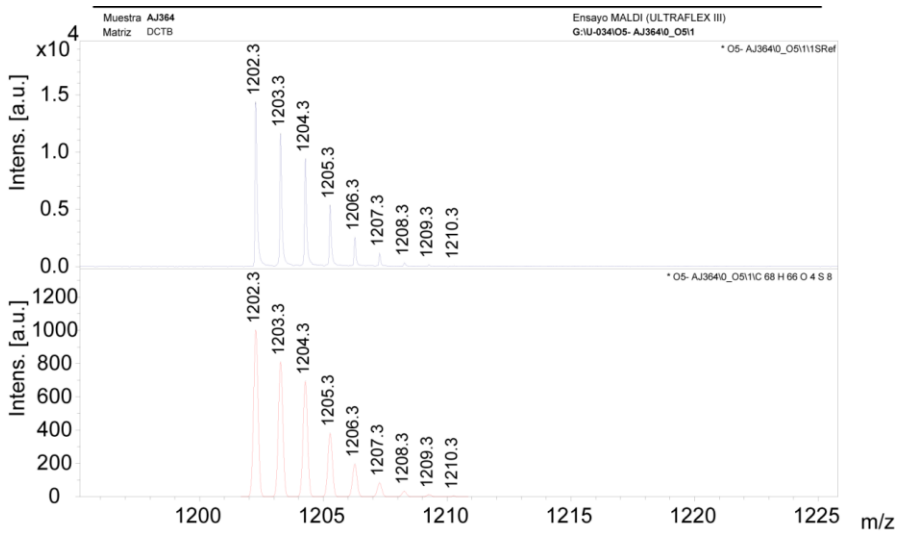
Muestra AJ364
Matriz DCTB
Ensayo MALDI (ULTRAFLEX III)
G:\U-034\O5- AJ364\0_O5\1
* O5- AJ364\0_O5\1\1SRef
x10^4
Intens. [a.u.]
1.5
1.0
0.5
0.0
1202.3
1203.3
1204.3
1205.3
1206.3
1207.3
1208.3
1209.3
1210.3
* O5- AJ364\0_O5\1\C 68 H 66 O 4 S 8
1200
1000
800
600
400
200
0
1200 1205 1210 1215 1220 1225
m/z

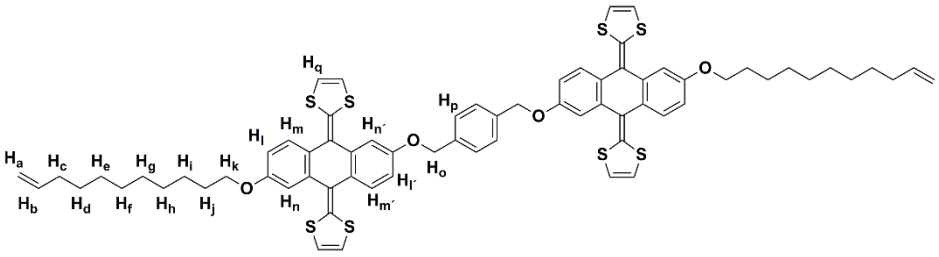

Compound **6** (27% yield). ^{1}H NMR (300 MHz, $CDCl_3$) δ 7.58 (m, 4H, H_{m+m}), 7.50 (s, 4H, H_p), 7.25 (bd, *J* = 2.5 Hz, 2H, H_n), 7.22 (d, *J* = 2.5 Hz, 2H, $H_{n'}$), 6.91 (dd, *J* = 8.6, 2.6 Hz, 2H, H_l), 6.81 (bd, *J* = 8.6 Hz, 2H, $H_{l'}$), 6.33 – 6.16 (m, 8H, H_q), 5.84 (m, 2H, H_b), 5.18 (m, 4H, H_o), 5.05 – 4.90 (m, 4H, H_a), 4.03 (t, *J* = 6.1 Hz, 4H, H_k), 2.11 – 2.02 (m, 4H, H_c), 1.90 – 1.74 (m, 4H, H_j), 1.54 – 1.25 (m, 24H, $H_{d+e+f+g+h+i}$). ^{13}C NMR (126 MHz, $CDCl_3$) δ 157.16, 156.60, 139.26, 137.07, 136.94, 136.81, 133.94, 133.75, 128.76, 128.25, 127.75, 126.13, 126.04, 122.12, 121.86, 117.15, 117.06, 114.14, 112.48, 112.08, 111.23, 110.96, 69.92, 68.27, 33.84, 29.56, 29.46, 29.43, 29.31, 29.16, 28.96, 26.09. MS m/z: calculated for $C_{70}H_{70}O_4S_8$ $[M]^+$ 1230.30 found MALDI-TOF 1230.3.

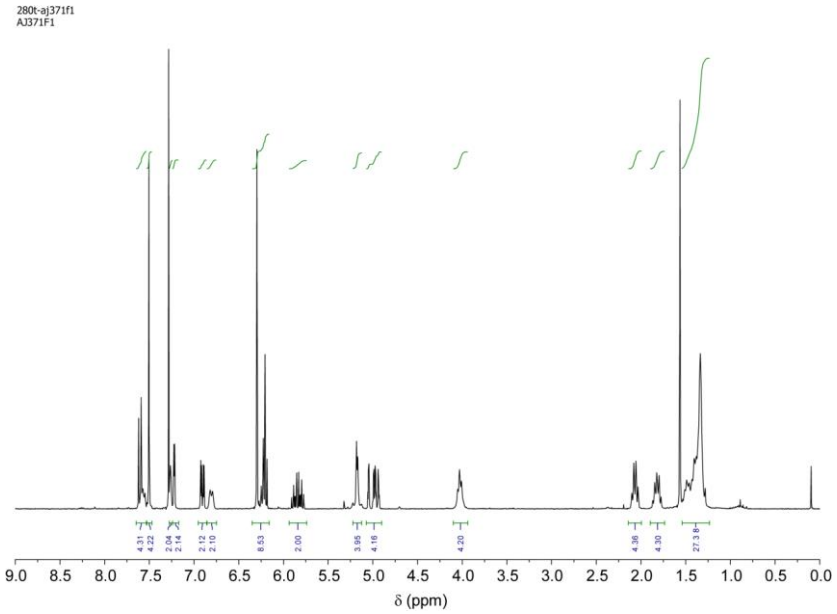

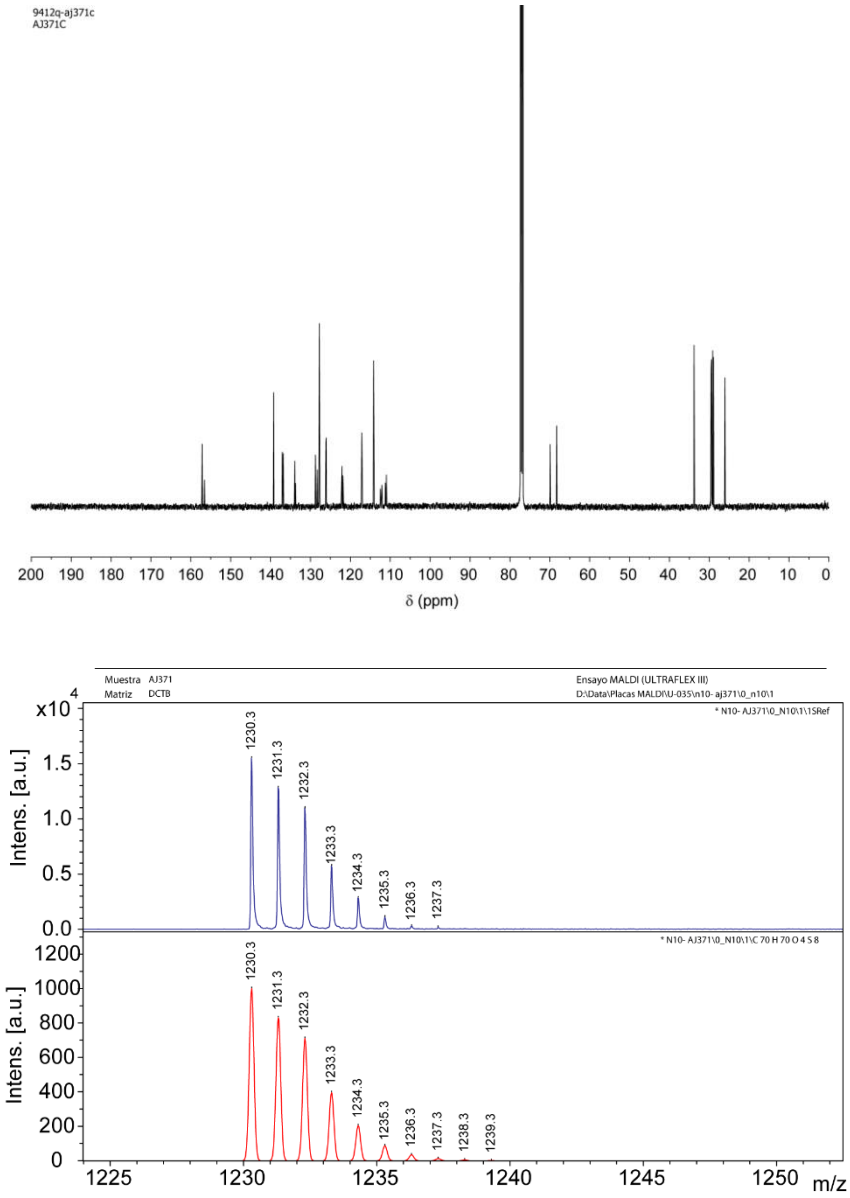

General procedure to synthetize 1-3. A 10^{-4} M solution of bis(exTTF) **4-6** was prepared in dichloromethane and was degassed by nitrogen bubbling during 30 minutes. Then, a catalytic amount of Grubbs catalyst 1st generation was introduced and the mixture was stirred for three hours at room temperature. The mixture was filtered on celite and concentrated in vacuo. The desired macrocycles were finally isolated by silica gel chromatography (eluent:

CH_2Cl_2/Hexane: 2/1 to 3/1) obtaining a yellow solid (**1**, y = 25%; **2**, y = 17%; **3**, y = 20%). The products show complicated ^1H NMR, consistent with an asymmetric molecule in several conformations in slow chemical exchange at NMR timescale (see *J. Am. Chem. Soc.* **2010**, *132*, 1772-1773). Their identity and purity was unambiguously established by ^1H NMR and MS.

Compound **1** (25% yield). ^1H NMR ($CDCl_3$, 300 MHz, 298 K) δ 7.78 – 7.69 (m, 0.75H), 7.60 – 7.36 (m, 6.25H), 7.15 – 7.08 (m, 1H), 7.04 – 7.71 (m, 6H), 6.47 – 6.13 (5H), 5.78 – 5.70 (m, 1H), 5.51 – 5.03 (m, 8H), 4.32 – 3.40 (m, 6H), 2.39 – 1.93 (m, 6H), 1.88 – 1.65 (m, 6H), 1.55 – 1.37 (m, 8H) ppm. MS m/z: calculated for $C_{62}H_{54}O_4S_8$ [M+] 1118.17878 found HR-ESI 1118.17500.

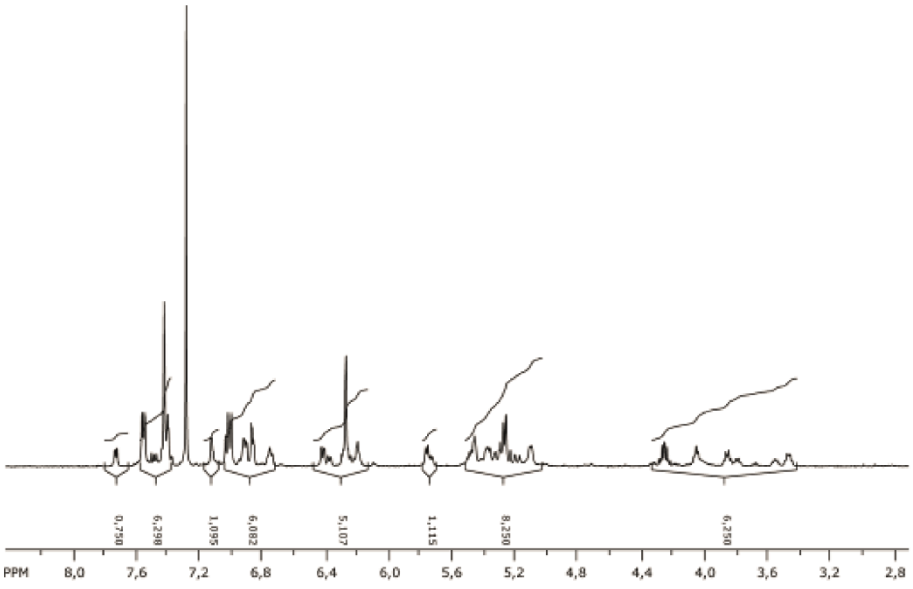

Mass Spectrum List Report

Analysis Info

Analysis Name	MGC8MAC_000002.d	Acquisition Date	01/12/2010 19:29:23
Method	ESI_pos	Operator	
Sample Name	MGC8MAC directo,EN DCM+MeOH	Instrument	apex-Ultra

Acquisition Parameter

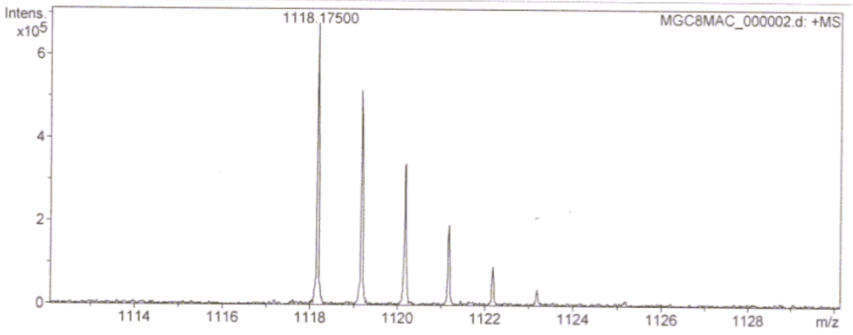

Compound **2** (17% yield**)**. ^{1}H NMR (500 MHz, CDCl3) δ 7.66 – 7.48 (m, 4H), 7.44 (s, 4H), 7.28 – 6.48 (m, 8H), 6.38 – 4.91 (m, 14H), 4.09 – 3.54 (m, 4H), 2.17 – 1.93 (m, 4H), 1.88 – 1.68 (m, 4H), 1.54 – 1.12 (m, 20H).MS m/z: calculated for $C_{66}H_{62}O_4S_8$ $[M]^+$1174.24 found MALDI-TOF 1174.2.

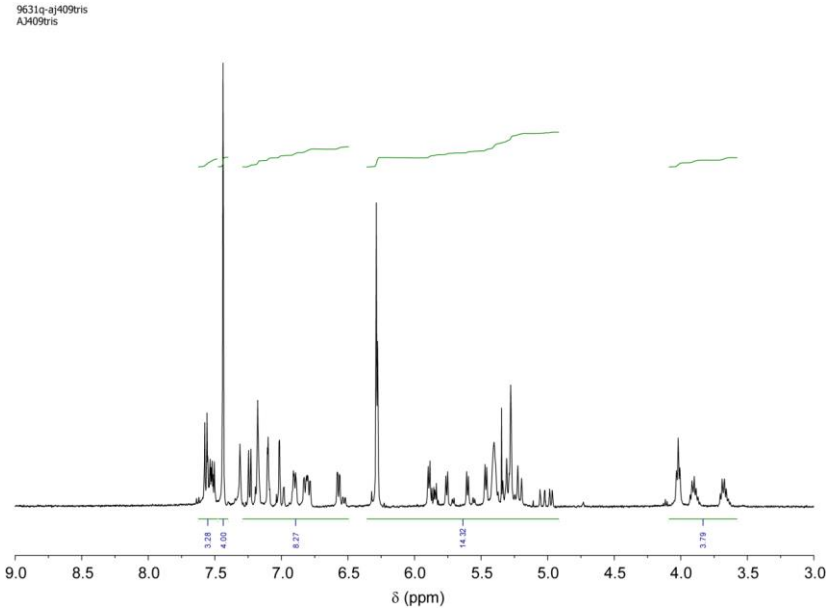

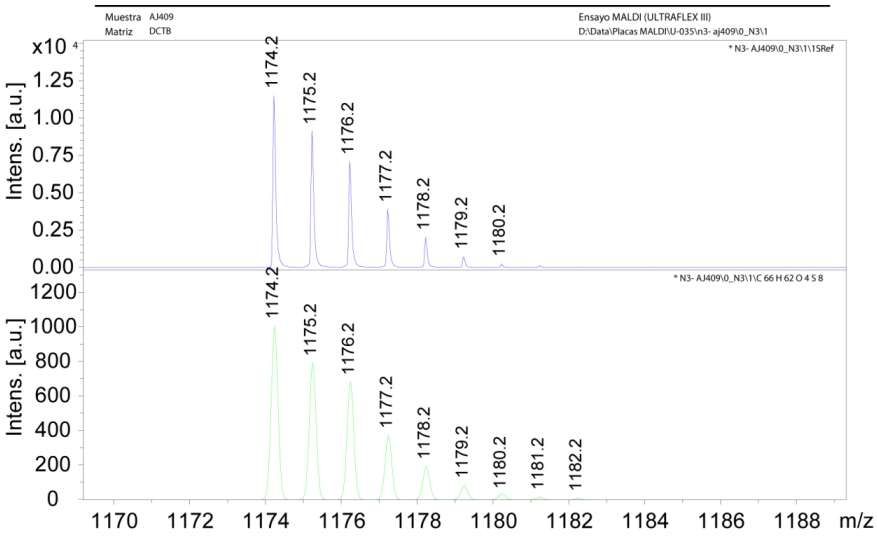

Compound **3** (20% yield).^{1}H NMR (500 MHz, $CDCl_3$) δ 7.68 – 7.48 (m, 4H), 7.44 (s, 4H), 7.27 – 6.52 (m, 8H), 6.38 – 4.94 (m, 14H), 4.12 – 3.63 (m, 4H), 2.15 – 1.90 (m, 4H), 1.88 – 1.68 (m, 4H), 1.70 – 1.04 (m, 24H).MS m/z: calculated for $C_{68}H_{66}O_4S_8$ $[M]^+$ 1202.27 found MALDI-TOF 1202.3.

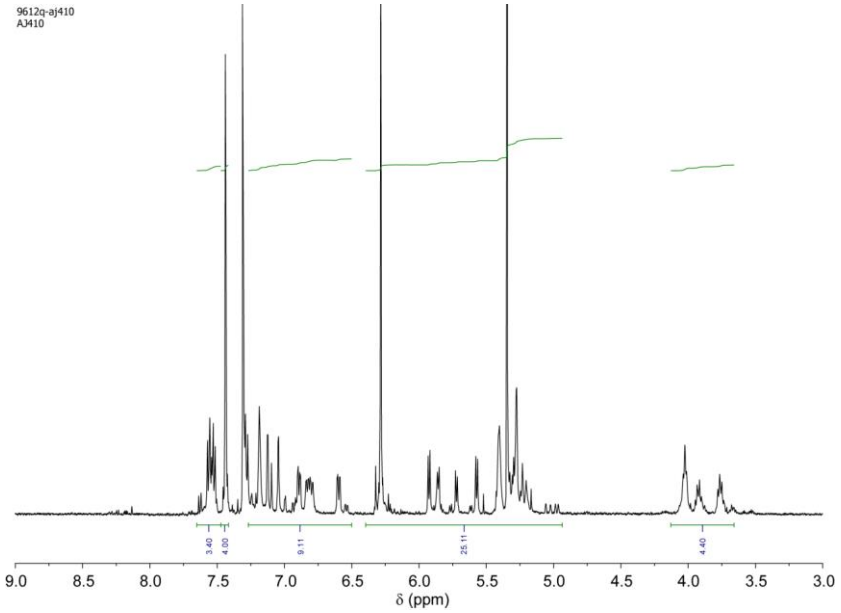

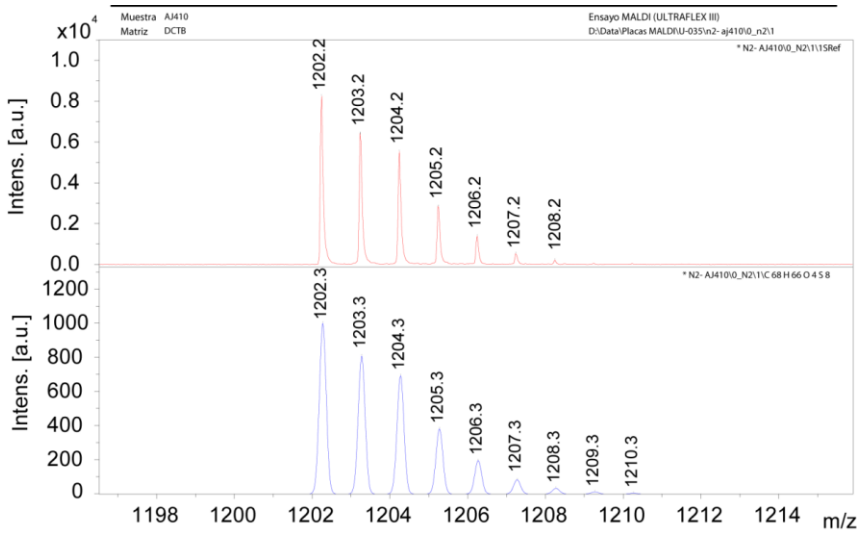

Synthesis of dimer of **1**.

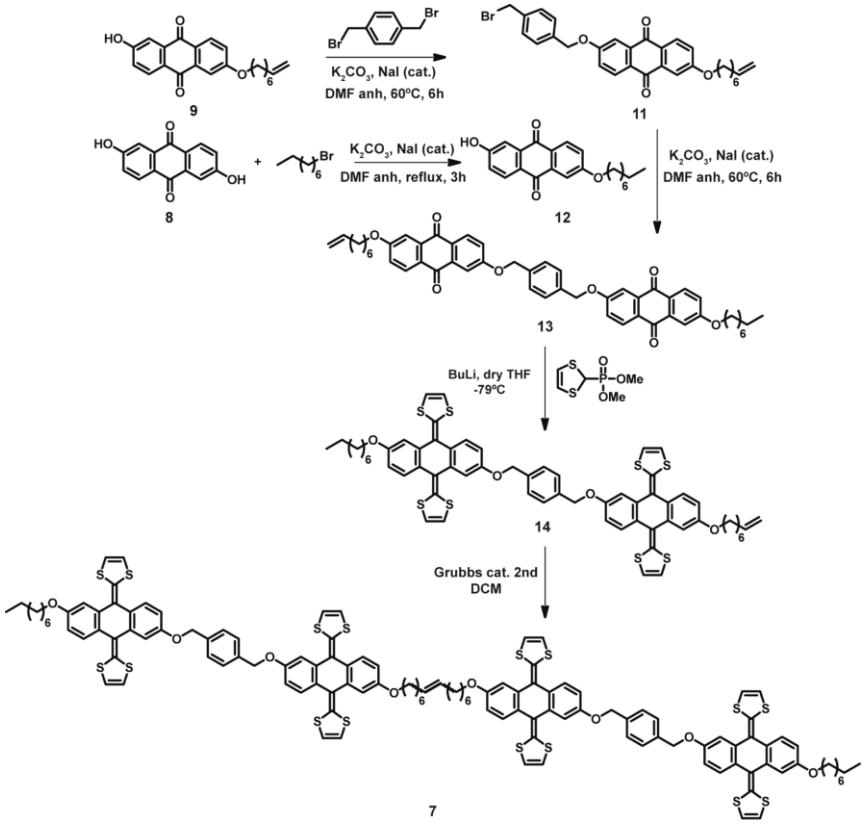

Synthesis of compound **11**. Compound **9** (0.4 g, 1.14 mmol, 1 equiv.) was dissolved in dry DMF (12 mL) under Ar and K_2CO_3 (0.15 g, 1.14 mmol, 1 equiv.) and a catalytic amount of NaI (cat.) were added. Later, α,α – dibrome-*p*-xylene (0.66 g, 2.53 mmol, 2.2 equiv.) was added and the resulting mixture stirred at 60ºC for 6 hours. The mixture was poured in cold HCl 1N and the solid was removed by filtration and re-dissolved in DCM, then washed with water. The organic phase was dried over $MgSO_4$ and solvent was removed under vacuum. The crude product was purified by column chromatography (silica gel, Hexane/CH_2Cl_2 1/1). The compound **11** (0.12 g, 20 % yield) was characterized by ^1H, ^{13}C-NMR and MALDI-TOF.

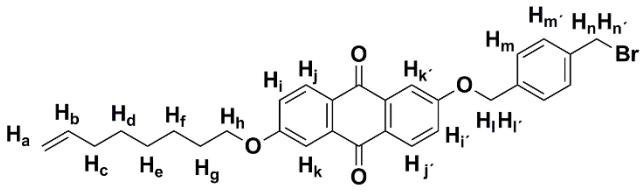

Compound **11** (20% yield).^1H NMR (300 MHz, $CDCl_3$) δ 8.04 (d, *J* = 8.6 Hz, 1H, H_j), 8.02 (d, *J* = 8.6 Hz, 1H, $H_{j'}$) 7.59 (d, *J* = 2.6 Hz, 1H, H_k), 7.50 (d, *J* = 2.6 Hz, 1H, $H_{k'}$), 7.26 – 7.18 (m, 4H, $H_{m+m'}$), 7.09 (dd, *J* = 8.6, 2.7 Hz, 1H, H_i), 7.02 (dd, *J* = 8.7, 2.6 Hz, 1H, $H_{i'}$), 5.64 (ddt, *J* = 16.9, 10.1, 6.7 Hz, 1H, H_b), 5.04 (s, 1H, H_n), 5.01 (s, 1H, $H_{n'}$), 4.89 – 4.73 (m, 2H, H_a), 4.32 (s, 1H, H_l), 4.28 (s, 1H, $H_{l'}$), 3.95 (t, *J* = 6.5 Hz, 2H, H_h), 1.94 – 1.84 (m, 2H, H_c), 1.73 – 1.60 (m, 2H, H_g), 1.40 – 1.18 (m, 6H, H_{d+e+f}). ^{13}C NMR (75 MHz, $CDCl_3$) δ 182.30, 182.16, 164.17, 163.43, 139.04, 138.11, 136.17, 135.99, 135.88, 129.86, 129.80, 129.56, 128.08, 127.57, 127.04, 121.26, 121.08, 114.51, 111.00, 110.69, 70.17, 68.89, 33.81, 33.06, 29.10, 28.91, 25.94. MS m/z: calculated for $C_{30}H_{29}BrO_4 \cdot Na$ $[M+Na]^+$ 555.1 found MALDI-TOF 555.2.

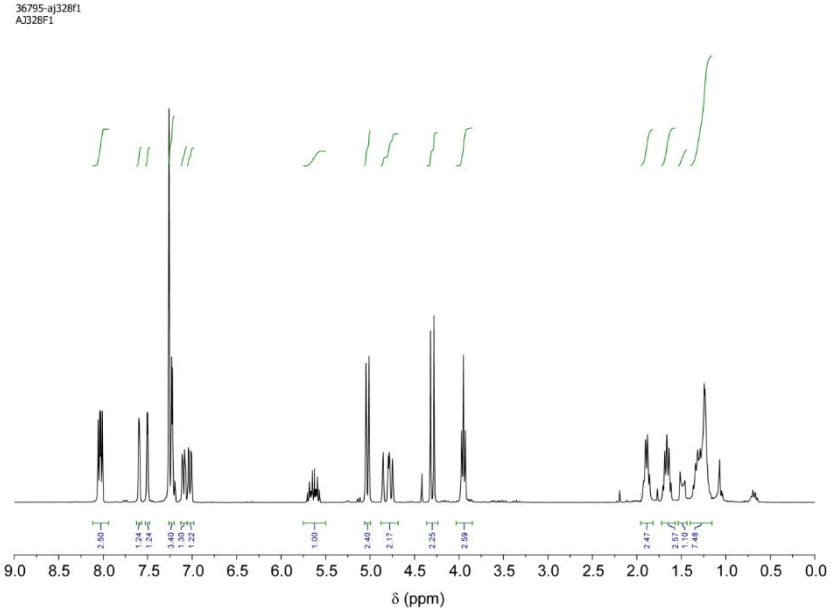
36795-aj328f1
AJ328F1
2.60
1.24
1.24
3.40
1.00
1.22
1.00
2.40
2.17
2.25
2.69
2.47
2.57
1.00
7.48
9.0 8.5 8.0 7.5 7.0 6.5 6.0 5.5 5.0 4.5 4.0 3.5 3.0 2.5 2.0 1.5 1.0 0.5 0.0
δ (ppm)

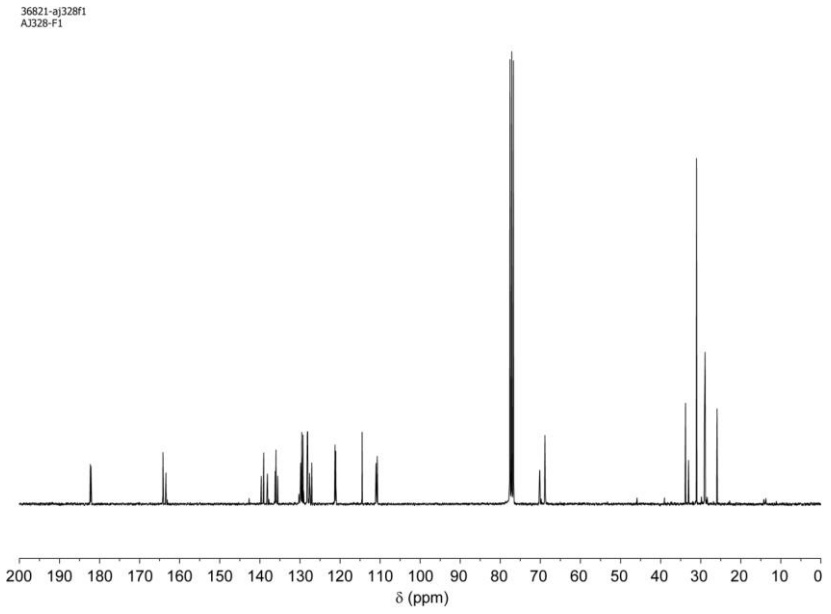
36821-aj328f1
AJ328-F1
200 190 180 170 160 150 140 130 120 110 100 90 80 70 60 50 40 30 20 10 0
δ (ppm)

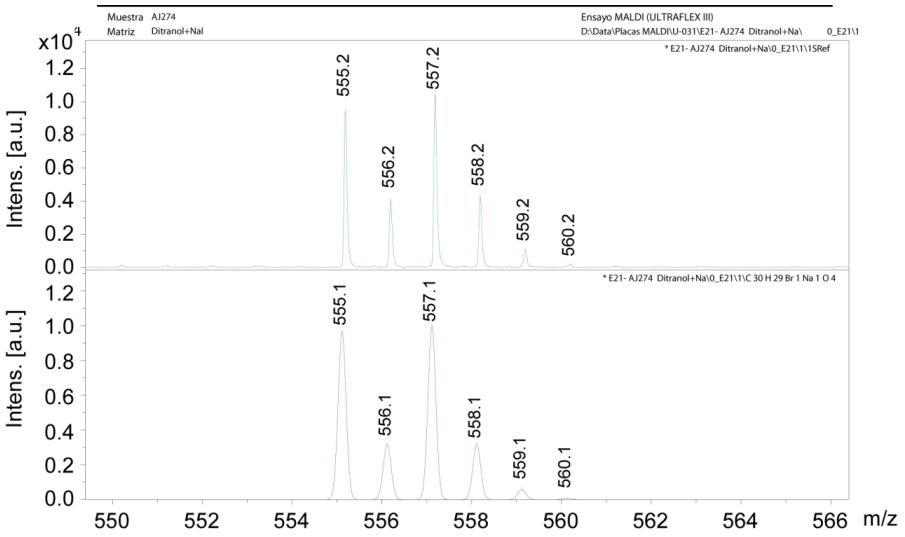

Synthesis of compound **12**. Anthraflavic acid 94% (0.2 g, 0.8 mmol) was dispersed with sonication in dry DMF (30 mL). Then, dry K_2CO_3 (0.11 g, 0.8 mmol), 1-bromooctane (0.153 g, 0.8 mmol) and a catalytic amount of NaI were added and the mixture refluxed for three hours. The crude reaction was poured into ice-cold 1 M hydrochloric acid (1 L), and filtrated. The solid was redissolved in CH_2Cl_2 and washed with water (2 x 50 mL). The organic fraction was dried over $MgSO_4$, the solvent evaporated, and the corresponding residue subjected to column chromatography (CH_2Cl_2 to CH_2Cl_2:CH_3OH 2%) affording the pure product as a light yellow solid (y = 29%).

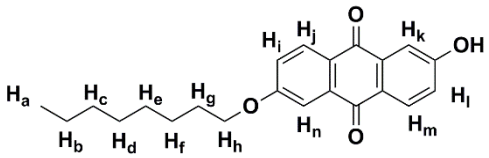

Compound **12** (29% yield). ^{1}H NMR (300 MHz, $CDCl_3$) δ 8.22 (d, *J* = 8.0 Hz, 1H, H_j), δ 8.19 (d, *J* = 8.0 Hz, 1H, H_m) 7.84 (d, *J* = 2.4 Hz, 1H, H_n), 7.69 (d, *J* = 2.5 Hz, 1H, H_k), 7.25 – 7.17 (m, 2H, H_{i+l}), 4.13 (t, *J* = 6.5 Hz, 2H, H_h), 1.91 – 1.77 (m, 2H, H_g), 1.56 – 1.42 (m, 2H, H_f), 1.30 (m, 8H, $H_{b+c+d+e}$), 0.89 (t, *J* = 6.7 Hz, 3H, H_a). ^{13}C NMR (75 MHz, $CDCl_3$) δ 182.91, 182.30, 164.48, 161.81, 136.10, 136.02, 130.49, 129.87, 127.21, 126.89, 121.25, 121.11, 113.34, 110.94,

77.58, 77.16, 76.74, 69.05, 31.95, 29.46, 29.37, 29.18, 26.10, 22.81, 14.25. MS *m/z*: calculated for $C_{22}H_{24}O_4[M^+]$ 352.17 found MALDI-TOF 352.16.

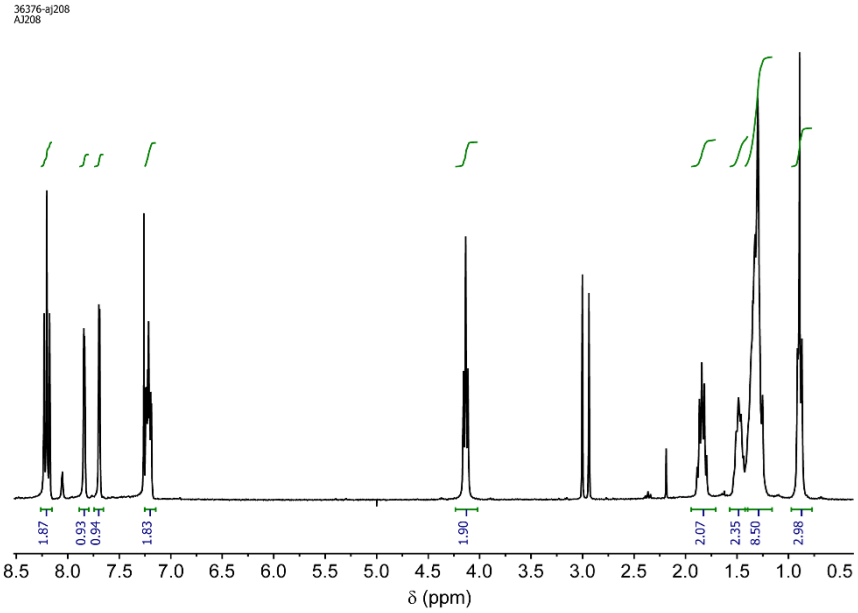

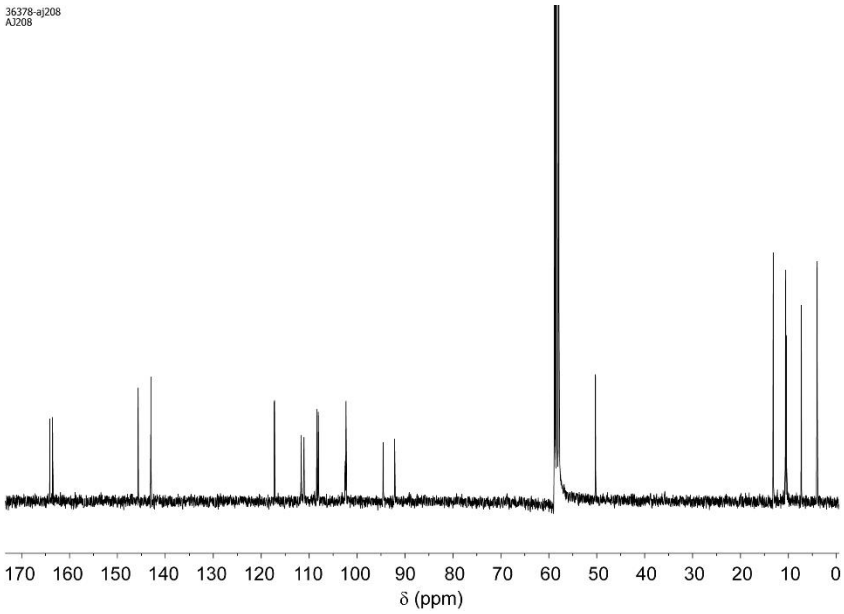

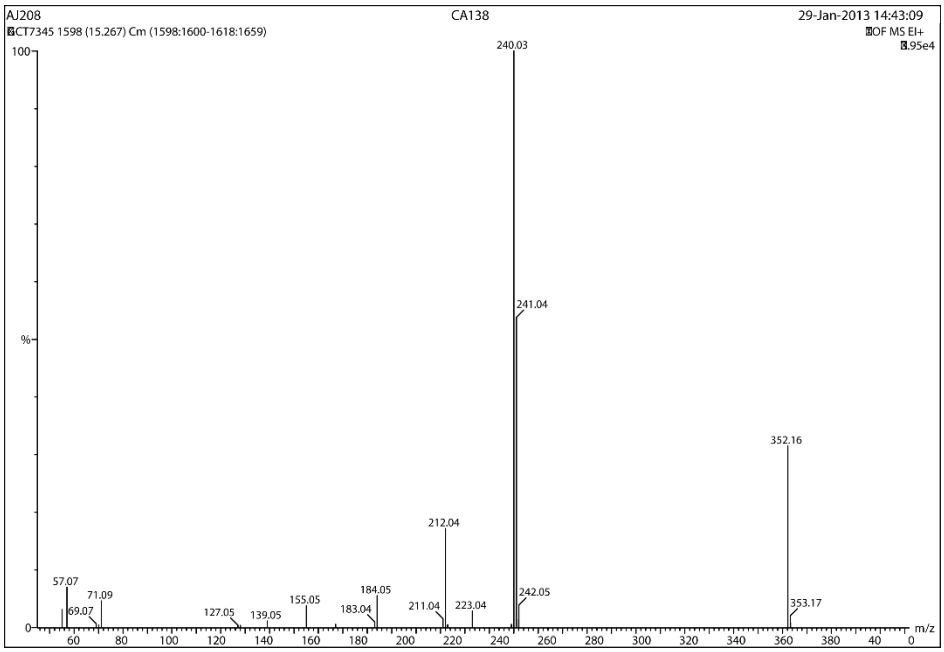

Synthesis of compound **13**. Compound **12** (0.11 g, 0.3 mmol, 1.5 equiv.) was dissolved in dry DMF (5 mL) under Ar and K_2CO_3 (0.04 g, 0.3 mmol,1.5 equiv.) and NaI (cat.) were added. Later, compound **11** (0.11 g, 0.2 mmol, 1 equiv.) was added and the resulting mixture stirred at 60ºC for 6 hours. The mixture of reaction was poured in cold HCl 1N and filtered. The solid was washed with cold MeOH. The yellow solid (0.137 g, 83% yield) was characterized by ^{1}H-NMR and MALDI-TOF.

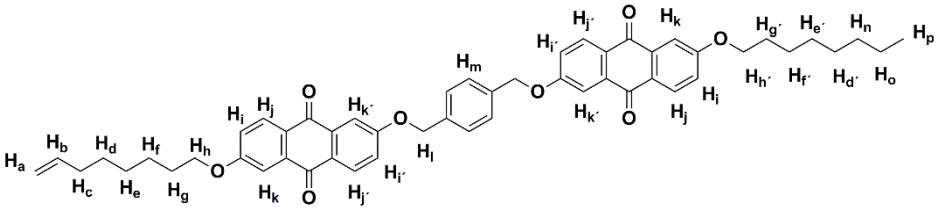

Compound **13** (83% yield).^{1}H NMR (500 MHz, $C_2D_2Cl_4$, 373K) δ 8.28 (d, *J* = 8.6 Hz, 2H, H_j), 8.26 (d, *J* = 8.6 Hz, 2H, $H_{j'}$), 7.87 (d, *J* = 2.6 Hz, 2H, H_k), 7.76 (d, *J* = 2.6 Hz, 2H, $H_{k'}$), 7.56 (s, 4H, H_m), 7.37 (dd, *J* = 8.6, 2.6 Hz, 2H, H_i), 7.28 (dd, *J* = 8.6, 2.6 Hz, 2H, $H_{i'}$), 5.96 – 5.77 (m, 1H, H_b), 5.33 (s, 4H, H_l), 5.05 (m, 2H, H_a), 4.21 (t, *J* = 6.5 Hz, 4H, $H_{h+h'}$), 2.12 – 2.06 (m, 2H, H_c), 1.95 – 1.85 (m, 4H, $H_{g+g'}$), 1.62 – 1.29 (m, 16H, $H_{d+d'+e+e'+f+f'+n+o}$), 0.96 (t, *J* = 7.0 Hz, 3H, H_p).

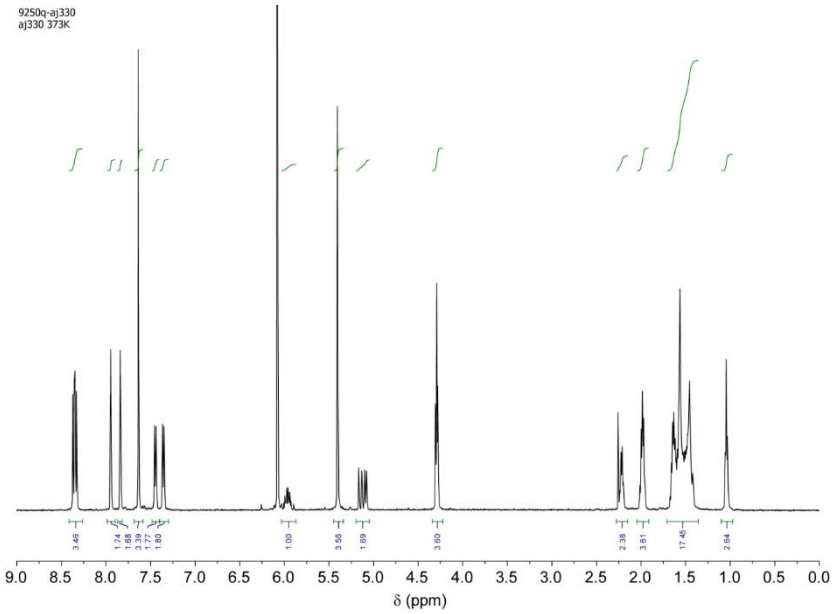

Synthesis of compound **14**. A solution of dimethyl 1,3-dithiol-2-ylphosphonate (0.35g, 1.6 mmol, 12 equiv.) in 12 mL of dry THF was cooled to –78 ºC, and butyllithium1.6 M in hexanes (1.0 mL, 1.6 mmol, 12 equiv.) was added. The solution was left to stir at -78 ºC for 30 min, with appearance of a precipitate. In the meantime, a suspension of compound **13** (0.1 g, 0.13 mmol, 1 equiv.) in dry THF (9 mL) was sonicated for 30 min. The resulting suspension was added to the suspension, and the cooling bath immediately removed. The mixture was allowed to warm to room temperature and left to stir for 30 minutes. The resulting solution was quenched with methanol. Crude was purified by column chromatography (DCM: Hexane 2:1 to 3:1) to obtain the pure product (0.045 g, 30% yield). Yellow solid was characterized by ^{1}H, ^{13}C-NMR and MALDI-TOF.

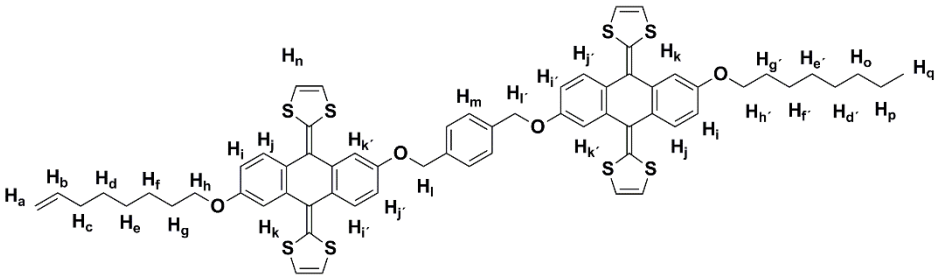

Compound **14** (30% yield). ^{1}H NMR (300 MHz, $CDCl_3$) δ 7.59 (d, *J* = 8.6 Hz, 2H, H_j), 7.54 (bd, *J* = 8.6Hz, 2H, H_j´) 7.48 (s, 4H, H_m), 7.24 (bd, *J* = 2.4 Hz, 2H, H_k), 7.20 (d, *J* = 2.4 Hz, 2H, $H_{k'}$), 6.88 (dd, *J* = 8.6, 2.5 Hz, 2H, H_i), 6.78 (bd, *J* = 8.7 Hz, 2H, $H_{i'}$), 6.31 – 6.14 (m, 8H, H_n), 5.82 (ddt, *J* = 16.9, 10.2, 6.7 Hz, 1H, H_b), 5.16 (s, 2H, H_l), 5.14 (s, 2H, $H_{l'}$) 5.06 – 4.90 (m, 2H, H_a), 4.01 (t, *J* = 6.2 Hz, 4H, $H_{h+h'}$), 2.12 – 2.01 (m, 2H, H_c), 1.88 – 1.73 (m, 4H, $H_{g+g'}$), 1.61 – 1.17 (m, 16H, $H_{d+d'+e+e'+f+f'+o+p}$), 0.87 (t, *J* =, 6.0 Hz, 3H, H_q).^{13}C NMR (75 MHz, $CDCl_3$) δ 157.31, 157.28, 156.74, 139.20, 137.21, 137.08, 136.95, 134.07, 133.88, 128.90, 128.39, 127.87, 126.26, 126.18, 122.26, 121.99, 117.29, 117.19, 114.43, 112.60, 112.56, 112.20, 111.36, 111.11, 70.06, 68.43, 68.35, 33.88, 32.08, 31.99, 30.48, 29.85, 29.54, 29.46, 29.41, 29.04, 29.01, 26.24, 26.08, 22.83, 14.27. MS m/z: calculated for $C_{64}H_{60}O_4S_8$ $[M]^+$ 1148.23 found MALDI-TOF 1148.2.

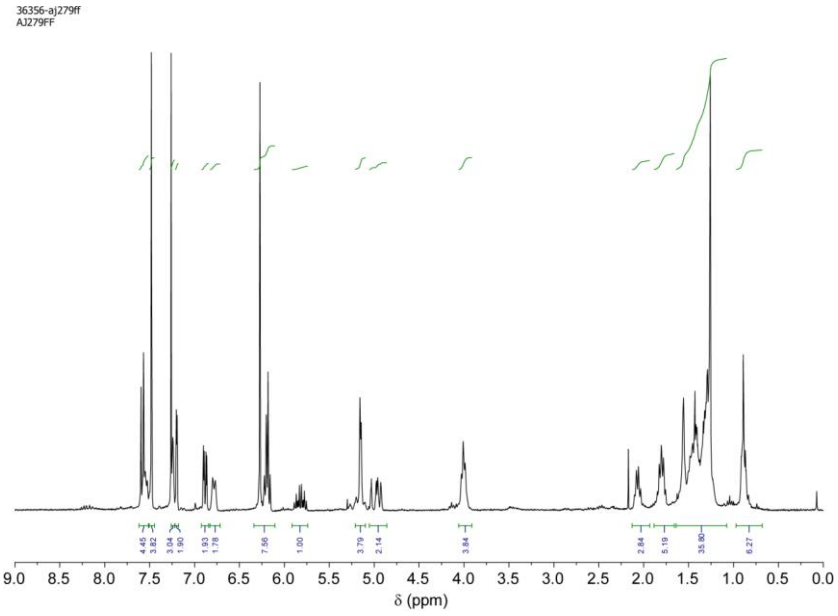

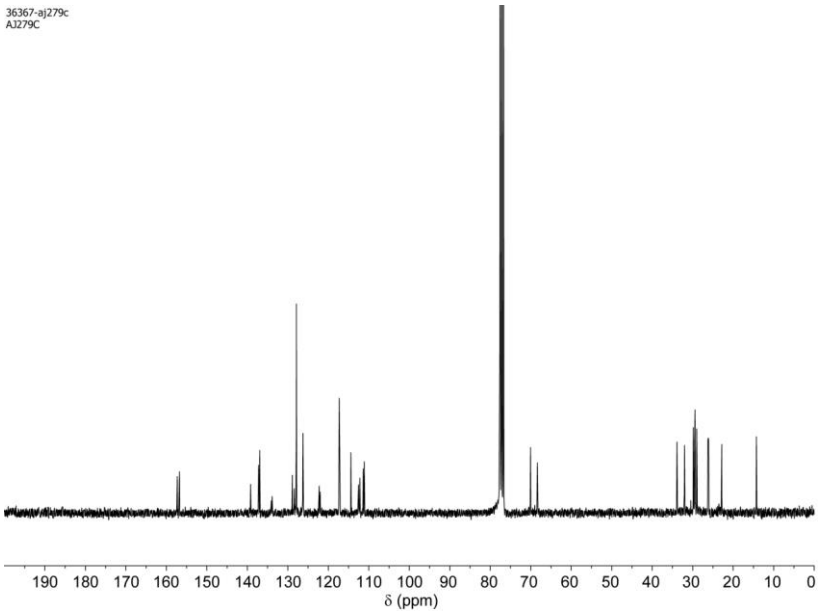

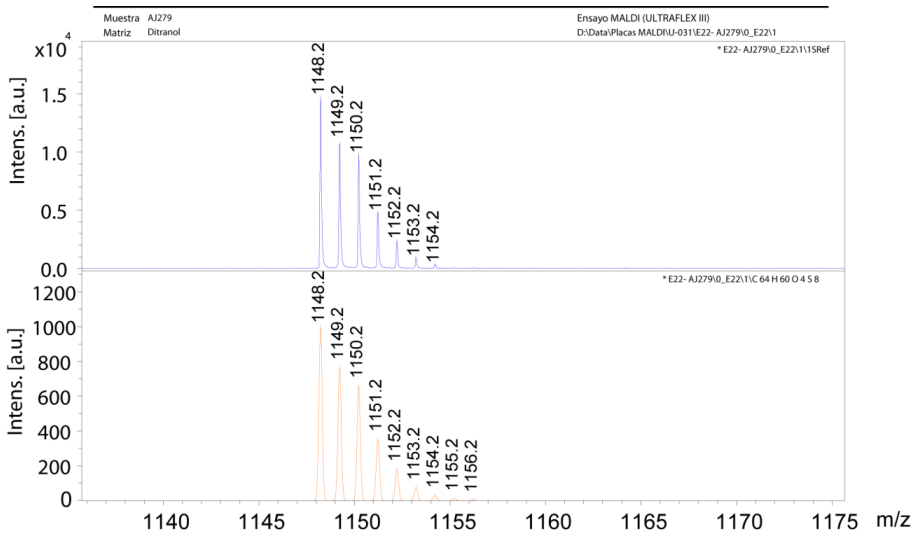

Synthesis of compound **7**. Compound **14** (13 mg, 0.01 mmol) was dissolved in 1.5 mL of DCM and was degassed by nitrogen bubbling during 2 minutes. Then, Grubbs catalyst, 2nd generation (1 mg, 0.01 mmol) was added. The solution was heated at reflux overnight. The mixture was filtered on celite and concentrated in vacuo. The crude was purified by silica gel chromatography

(eluent: DCM/Hexane: 1/3 to 3/1). The product (9 mg, 30 % yield) was characterized by ^{1}H, ^{13}C-NMR and MALDI TOF.

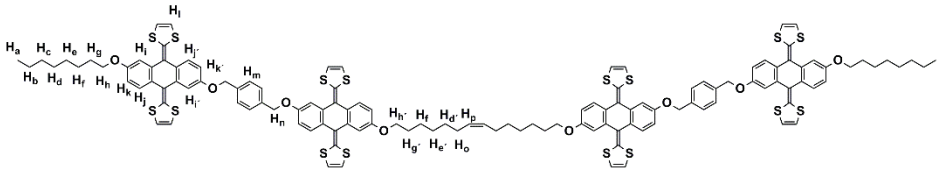

Compound **7** (30% yield). ^{1}H NMR (500 MHz, $CDCl_3$) δ 7.66 – 7.54 (m, 8H, $H_{j+j'}$), 7.51 (s, 8H, H_m), 7.27 (s, 4H, H_i), 7.25 – 7.20 (m, 4H, $H_{i'}$), 6.94 – 6.88(m, 4H, H_k), 6.85 – 6.78 (m, 4H, $H_{k'}$), 6.35 – 6.16 (m, 16H, H_l), 5.48 – 5.40 (m, 2H, H_p), 5.25 – 5.12 (m, 8H, H_n), 4.04 (s, 8H, $H_{h+h'}$), 2.12 – 2.00 (m, 4H, H_o), 1.89 – 1.78 (m, 8H, $H_{g+g'}$), 1.61 (s, 8H, $H_{f+f'}$), 1.57 – 1.47 (m, 8H, H_b), 1.45 - 130 (m, 16H, H_{c+d+e}), 0.98 – 0.84 (m, 6H, H_a).^{13}C NMR (126 MHz, $CDCl_3$) δ 157.17, 156.59, 137.06, 136.93, 136.81, 133.96, 130.40, 129.91, 128.75, 128.24, 127.73, 126.13, 126.04, 122.11, 122.08, 121.85, 117.14, 117.05, 112.46, 112.03, 111.23, 110.98, 69.91, 68.29, 68.21, 32.49, 31.86, 29.72, 29.51, 29.41, 29.32, 29.28, 28.83, 26.10, 25.96, 25.91, 22.69, 14.13.MS m/z: calculated for $C_{126}H_{116}O_8S_{16}$ $[M+H]^+$2270.42 found MALDI-TOF 2270.3.

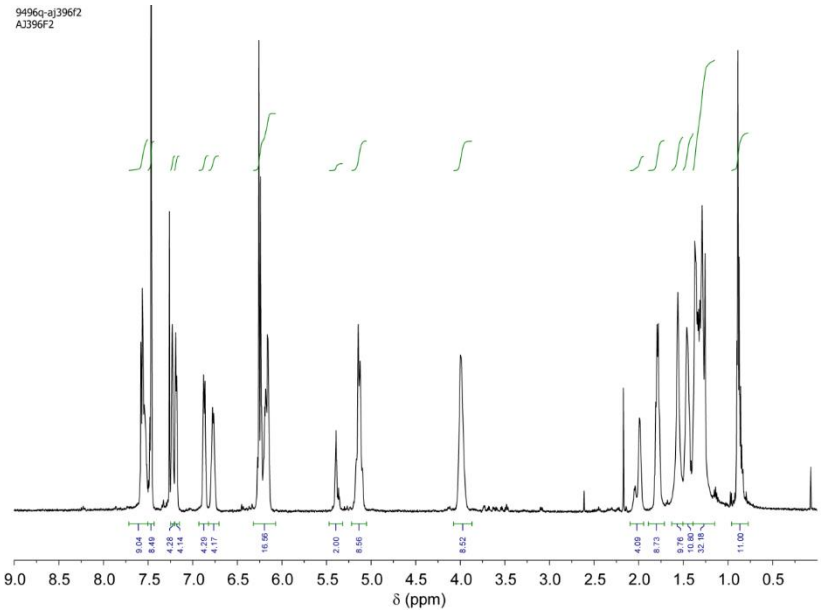

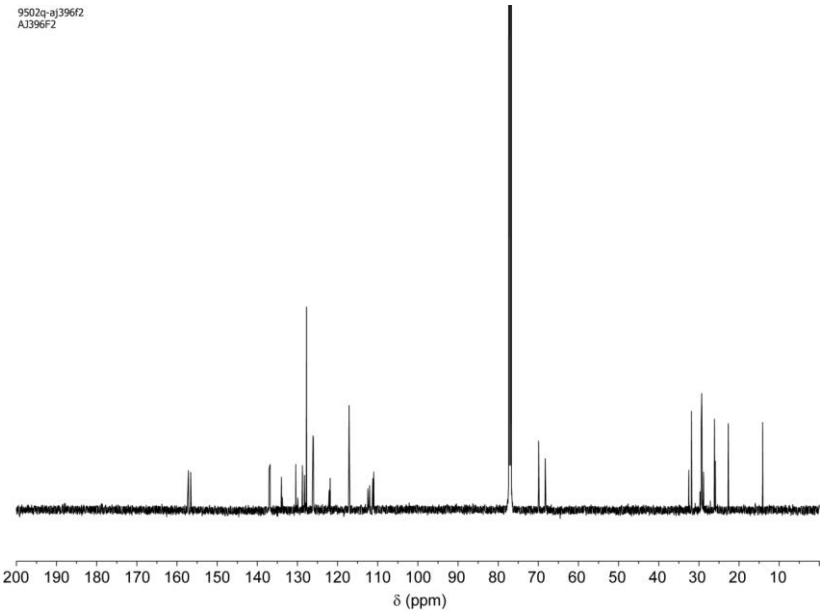
9502q-aj396f2
AJ396F2
200 190 180 170 160 150 140 130 120 110 100 90 80 70 60 50 40 30 20 10
δ (ppm)

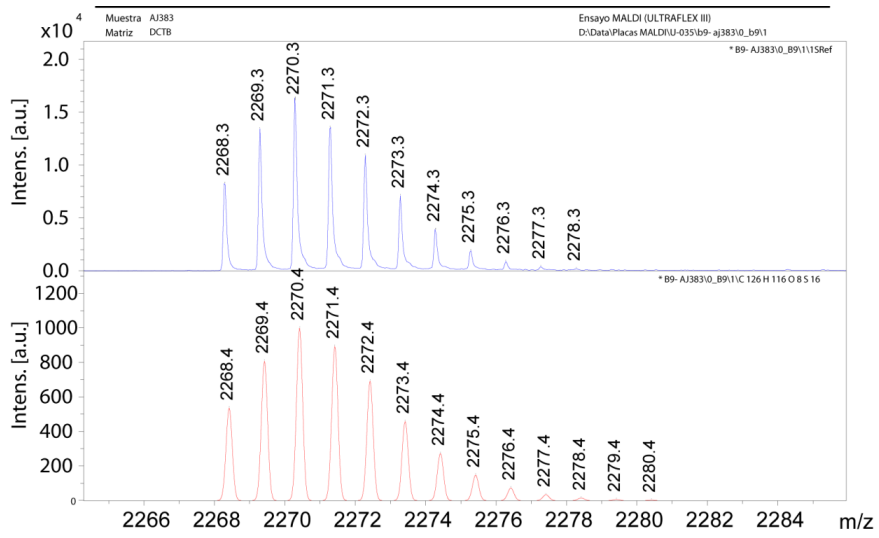
Muestra AJ383
Matriz DCTB
Ensayo MALDI (ULTRAFLEX III)
D:\Data\Placas MALDI\U-035\b9- aj383\0_b9\1
* B9- AJ383\0_B9\1\1SRef
x10 4
Intens. [a.u.]
2268.3
2269.3
2270.3
2271.3
2272.3
2273.3
2274.3
2275.3
2276.3
2277.3
2278.3
* B9- AJ383\0_B9\1\C 126 H 116 O 8 S 16
2268.4
2269.4
2270.4
2271.4
2272.4
2273.4
2274.4
2275.4
2276.4
2277.4
2278.4
2279.4
2280.4
2266 2268 2270 2272 2274 2276 2278 2280 2282 2284
m/z

General procedure for SWNTs functionalization

The (7,6)-enriched SWNTs purchased from Sigma Aldrich Co were purified previously. 50 mg of (7,6)-enriched SWNTs were suspended in 34 mL of 35% HCl, and sonicated for 10 min. The mixture was poured in 100 mL of miliQ water and filtered through a polycarbonate membrane of 0.2 μm pore size. The solid was washed with water to neutral pH and then dried in an oven at 350^0C for 30 min.

Pristine plasma-purified SWNTs were used without previous purification.

The nanotubes (20 mg) were suspended in 20 mL of tetrachloroethane (TCE) through sonication (10 min.) and mixed with linear precursors **4**-**6** (0.0087 mmol), and Grubb's 2nd generation catalyst at room temperature for 72 hours. After this time, the suspension was filtered through a PTFE membrane of 0.2 μm pore size, and the solid washed profusely with dichloromethane (DCM). The solid was re-suspended in 20 mL of DCM through sonication for 10 min. and filtered through a PTFE membrane of 0.2 μm pore size again. This washing procedure was repeated three times.

General procedure for SWNTs functionalization (varying the relative concentration of 4 with respect to SWNTs)

The nanotubes (1 mg/mL) were suspended in TCE through sonication (10 min.) and mixed with linear precursor **4** (0.044 mM, 2.3 mM or 4.5 mM), and Grubb's 2nd generation catalyst at room temperature for 72 hours. After this time, the suspension was filtered through a PTFE membrane of 0.2 μm pore size, and the solid washed profusely with DCM. The solid was re-suspended in 20 mL of DCM through sonication for 10 min. and filtered through a PTFE membrane of 0.2 μm pore size again. This washing procedure was repeated three times.

General procedure for SWNTs functionalization (control experiments).

The nanotubes (20 mg) were suspended in 20 mL of TCE through sonication (10 min.) and mixed with either linear precursor **4** or macrocycle **1** (10 mg, 0.0087 mmol) at room temperature for 72 hours. After this time, the suspension was filtered through a PTFE membrane of 0.2 μm pore size, and the solid washed profusely with DCM. The solid was re-suspended in 20 mL of DCM through sonication for 10 min. and filtered through a PTFE membrane of 0.2 μm pore size again. This washing procedure was repeated three times.

General procedure for de-threading functionalized SWNTs.

The functionalized nanotubes (2 mg) were suspended in 5 mL of TCE by sonication for 5 min. and then heated to reflux (bp = 146^{0}C) for 30 min. The suspension was filtered through a PTFE membrane of 0.2 µm pore size, and the solid washed profusely with DCM. No de-threading was observed by TGA (Figure 2b, main text).

The functionalized nanotubes (1 mg) were heated at 360^{0}C in an oven for 30 min. A complete de-functionalization of the nanotubes was observed by TGA (Figure S3).

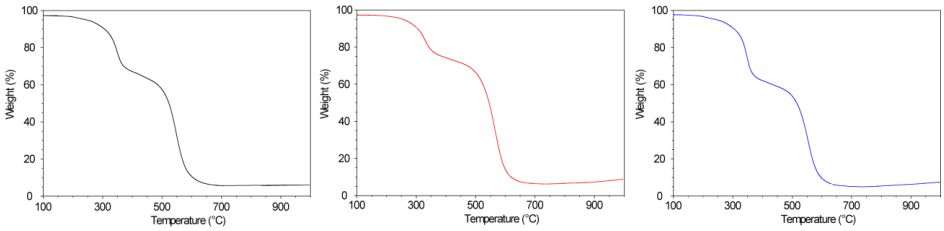

Figure S1. TGA analysis (air, 10 ºC min^{-1}) of: plasma-purified SWNTs treatment with **4** (0.44mM) and Grubb's 2nd generation catalyst in TCE at room temperature for 72 hours (black) and under identical reaction conditions with linear precursors **5** (red) and **6** (blue).

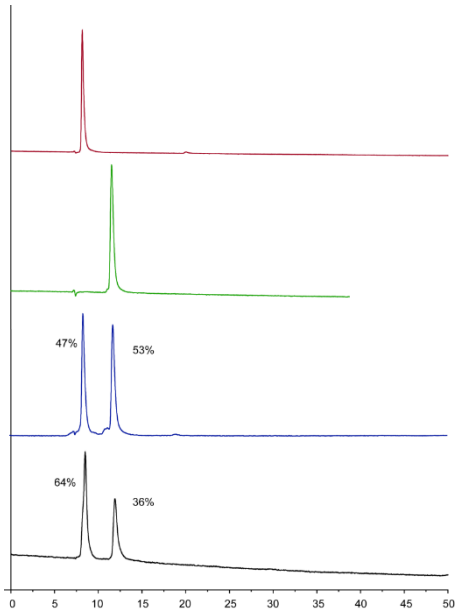

Figure S2. HPLC analysis of: compound **4** (red), compound **1** (green), crude of RCM of compound **4** (blue) and of the filtrate of the clipping reaction of **4** around the plasma-purified SWNTs (black).

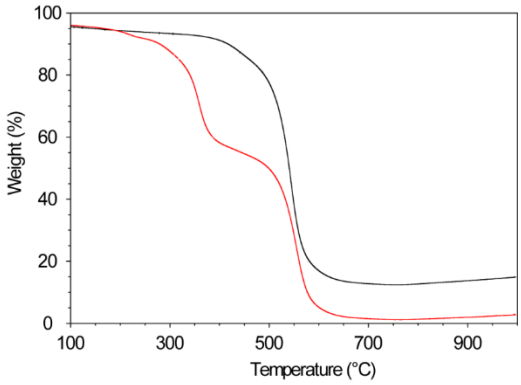

Figure S3. TGA analysis (air, 10 ºC min^{-1}) of: as purchased SWNTs treatment with **4** (2.3 mM) and Grubb's 2nd generation catalyst in TCE at room temperature for 72 hours (red) and after calcination of the sample at 360 ºC for 30 min (black).

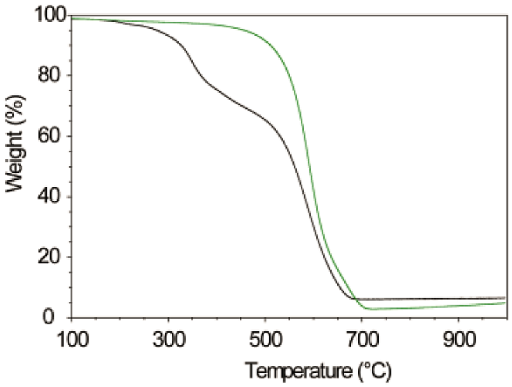

Figure S4. TGA analysis (air, 10 ºC min^{-1}) of: as purchased short (0.2-5 µm) plasma-purified SWNTs (green), and after treatment with **4** (10 mg, 0.0087 mmol) in TCE (20 mL) and Grubb's 2nd generation catalyst at room temperature for 72 hours (black).

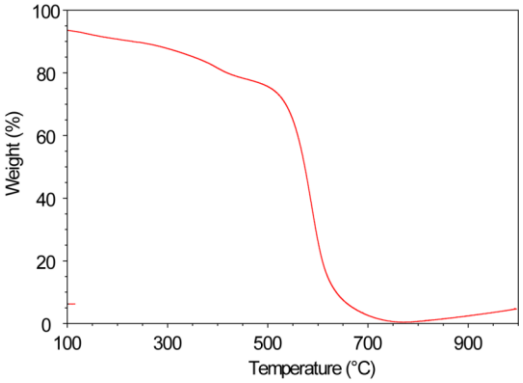

Figure S5. TGA analysis (air, 10 ºC min^{-1}) of: as purchased SWNTs after treatment with **1** (10 mg, 0.0089 mmol) in TCE (20 mL) at room temperature for 72 hours (red).

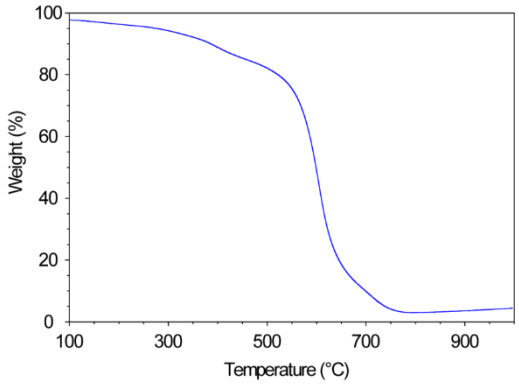

Figure S6. TGA analysis (air, 10 ºC / min) of: as purchased SWNTs after treatment with **4** (10 mg, 0.0087 mmol) in TCE (20 mL) at room temperature for 72 hours (blue).

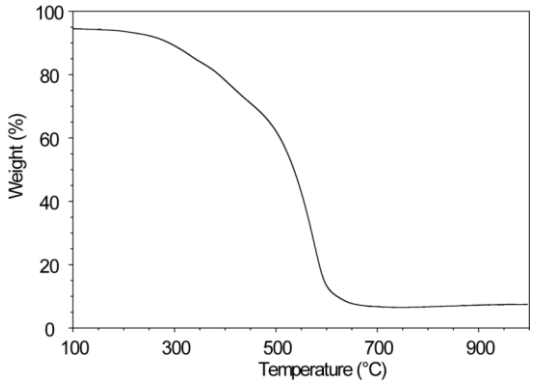

Figure S7.TGA analysis (air, 10 ºC min^{-1}) of: as purchased SWNTs after treatment with **7** (2.1 mg, 0.0008mmol) in TCE (20 mL) at room temperature for 72 hours (black).

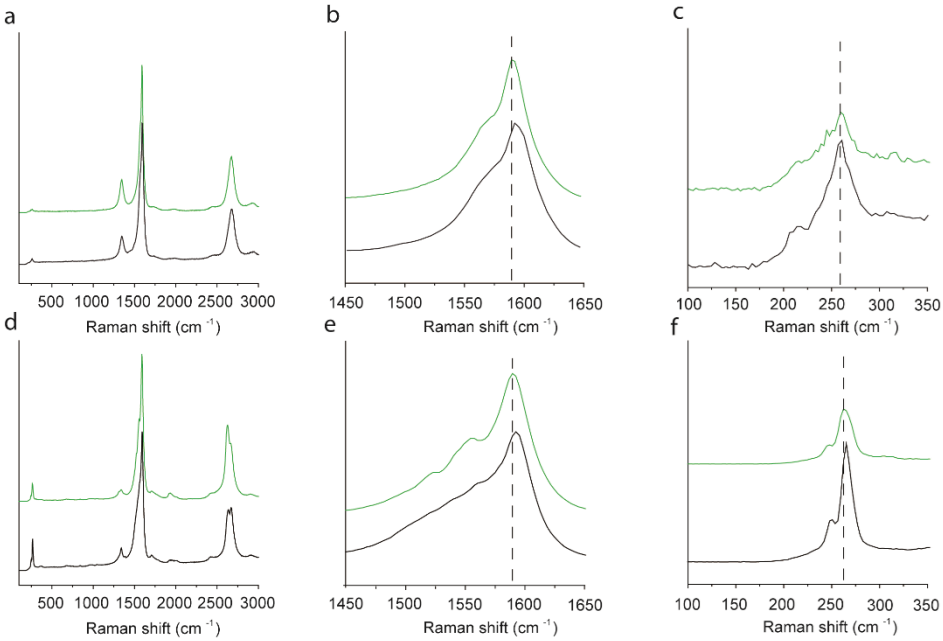

Figure S8. a) Raman spectra of plasma-purified SWNTs (green) and the corresponding $MINT_{pp}$-**1** (black); b) zoom in on the G zone; c) zoom in on the RBM zone. d) Raman spectra of (7,6)-enriched SWNTs (green) and the corresponding $MINT_{(7,6)}$-**1** (black); e) zoom in on the G zone; f) zoom in on the RBM zone. All spectra are the average of three different measurements (λ_{exc} = 532 nm). Dashed vertical lines have been added as a guide to the eye.

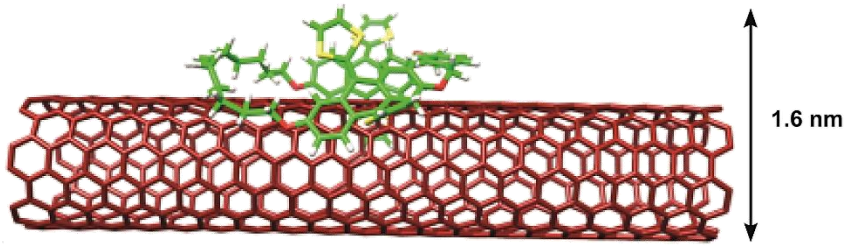

Figure S9. Energy-minimized (MMFF94) model of macrocycle **4** adsorbed on top of a (7,6) SWNT. The vertical dimension is shown.

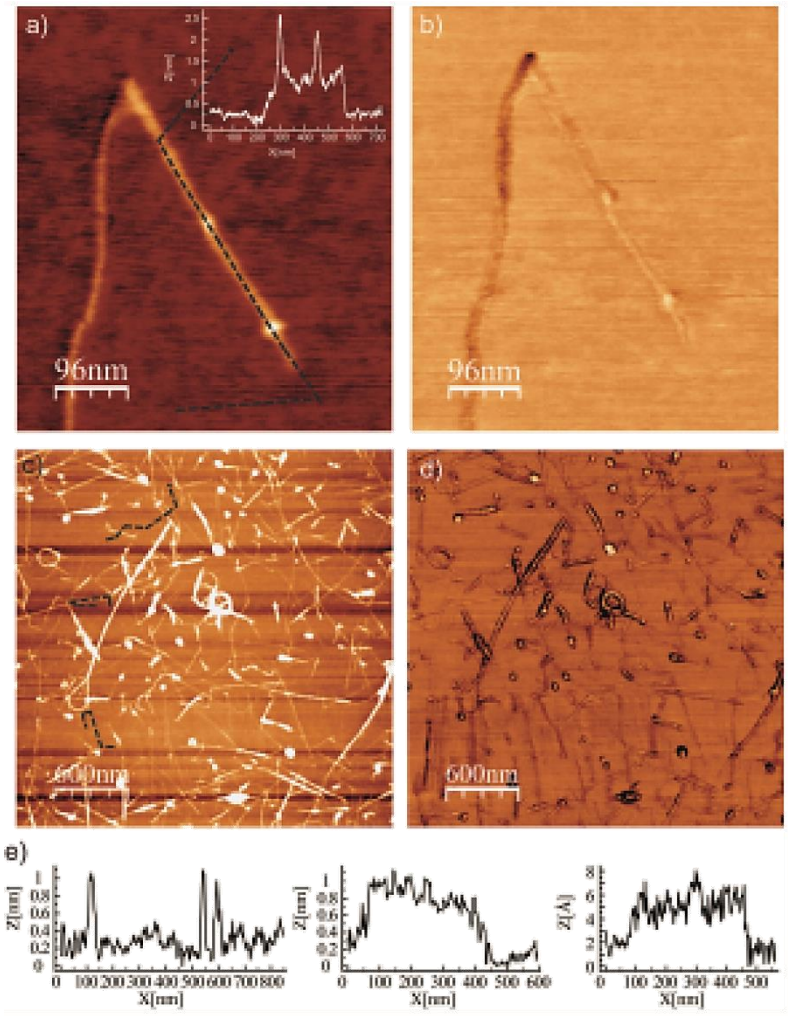

Figure S10. a) Topography AFM image of a spin-casted suspension of MINT$_{(7,6)}$-**1** in TCE (inset shows the profile along the black dotted line) and b) phase contrast image. c) Topography AFM image of a spin- casted suspension of pristine (7,6) SWNTs in TCE and d) corresponding phase contrast image. e) profiles along the black dotted lines in the topography image c), shown from top to bottom. The first profile shows that there are abundant individualized SWNTs, and the second and third prove that the irregularities found along their axes are small. The phase image does not show any significant differences on top of the SWNTs.

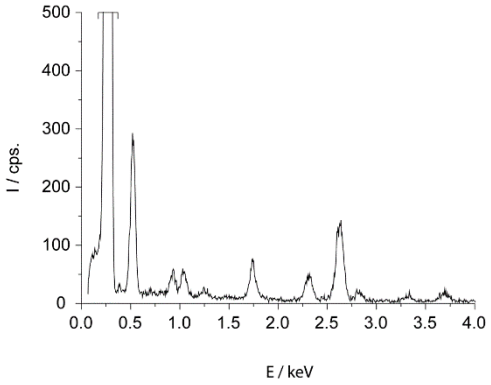

Figure S11. Energy Dispersion X-ray (EDS Oxford Inca detector) spectroscopy of $MINT_{pp}$-**1**, taken with a spot of 30 nm diameter, in an area of high nanotube density, sulfur peak can be found at 2.3 eV.

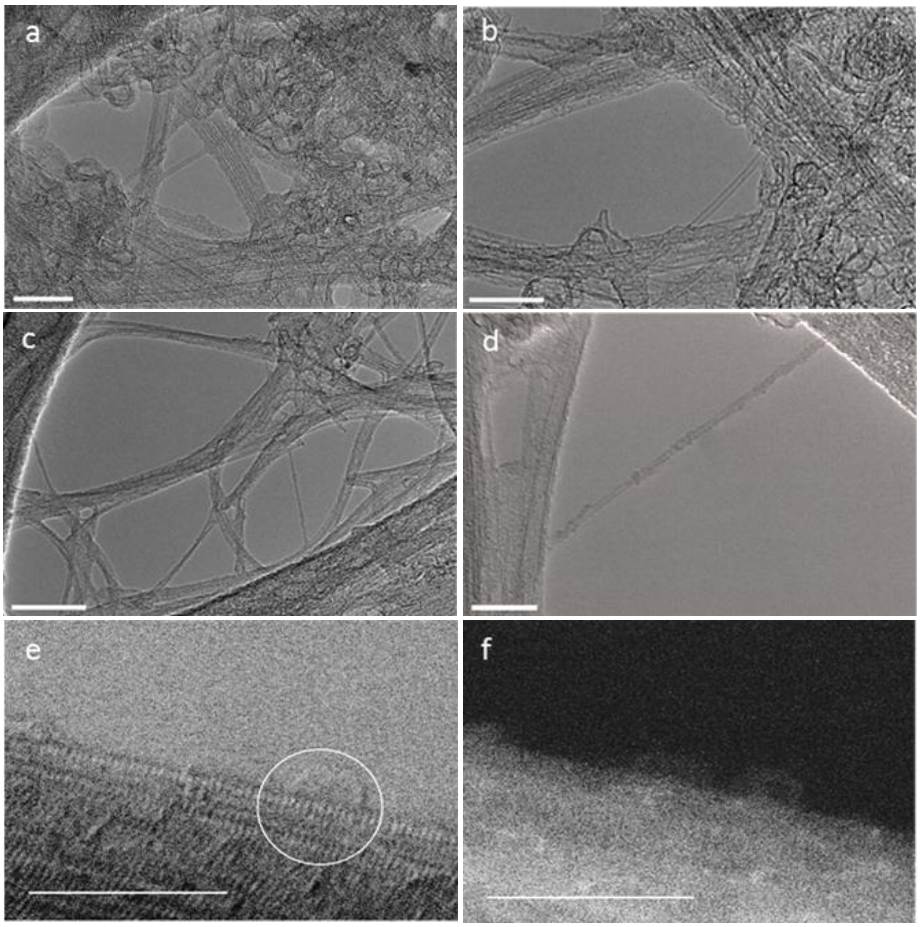

Figure S12. a) and b) TEM images of pristine plasma-purified SWNTs showing two different areas with high density of bundles. c and d) TEM images of $MINT_{pp}$-**1** showing isolated SWNTs and the presence of

macrocycles around them. e) HR-STEM bright-field image of a bundle of SWNTs, note that the uppermost tube is surrounded by up to four macrocycles, two of which are circled in white. f) HR-STEM dark-field image of the same bundle of nanotubes. Note that the cavity of the macrocycles circled in white in c) is clearly distinguishable. Scale bars are 20 nm for a-d) and 5 nm for e) and f).

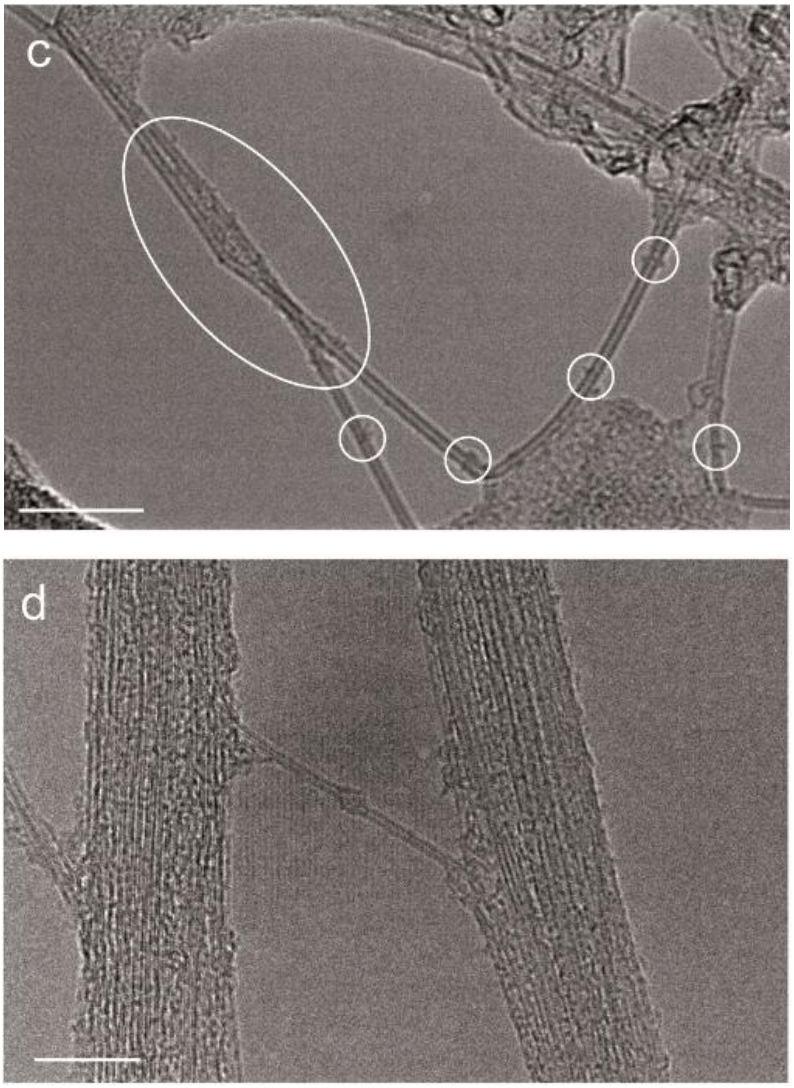

Enlarged Figure 6. c) TEM image of nanotubes (showing a densely covered surface) and several individual macrocycles in the $MINT_{pp}$-**1** sample. d) TEM image of an individual SWNT in the $MINT_{(7,6)}$-**1** sample; the image shows an object of appropriate dimensions to be **1**.

3.4.2 Computational details

Our calculations have considered a set of SWNTs associated to macrocycle **1**. All systems have been prepared with TubeGen[‡] and Avogadro.[43] Their geometries have been optimized with a MMFF94[44] force-field, known to provide a satisfactory structural accuracy for a broad range of systems, including SWNTs. For one case, a (12,0) SWNT with **1**, we have compared the force-field geometry to that obtained from a Gaussian09[45] DFT calculation (geometry shown in figure S13), without noticing any significant difference.

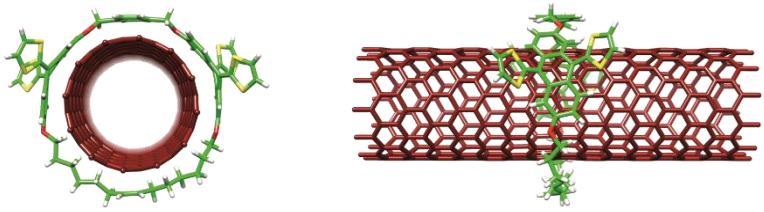

Figure S13. Energy-minimized (DFT) structure of a pseudorotaxane comprising a (12, 0) SWNT and **1**.

The diameter (in nanometers) of an ideal nanotube is related to its (n,m) chirality parameters through the following formula :

$$d = \frac{a}{\pi}\sqrt{n^2 + nm + m^2}$$

with a=0.246 nm for carbon. Using the 0.953 nm diameter of the (8,6) SWNT as a reference, we have explored the geometrical configurations of macrocycle **1** around a set of SWNTs presenting similar diameters. For each case, we have evaluated the binding of the cycle to the SWNT.

[‡] See http://turin.nss.udel.edu/research/tubegenonline.html for details.

43. M. D. Hanwell, D. E. Curtis, D. C. Lonie, T. Vandermeersch, E. Zurek and G. R. Hutchison, *J. Cheminformatics*, 2012, **4**, 17.
44. T. A. Halgren, *J. Comput. Chem.*, 1996, **17**, 616-641.
45. M. J. Frisch, G. W. Trucks, H. B. Schlegel, G. E. Scuseria, M. A. Robb, J. R. Cheeseman, G. Scalmani, V. Barone, B. Mennucci, G. A. Petersson, H. Nakatsuji, M. Caricato, H. P. H. X. Li, A. F. Izmaylov, J. Bloino, G. Zheng, J. L. Sonnenberg, M. Hada, M. Ehara, K. Toyota, R. Fukuda, J. Hasegawa, M. Ishida, T. Nakajima, Y. Honda, O. Kitao, H. Nakai, T. Vreven, J. A. Montgomery, J. E. P. Jr., F. Ogliaro, M. Bearpark, J. J. Heyd, E. Brothers, K. N. Kudin, V. N. Staroverov, R. Kobayashi, J. Normand, K. Raghavachari, A. Rendell, J. C. Burant, S. S. Iyengar, J. Tomasi, M. Cossi, N. Rega, J. M. Millam, M. Klene, J. E. Knox, J. B. Cross, V. Bakken, C. Adamo, J. Jaramillo, R. Gomperts, R. E. Stratmann, O. Yazyev, A. J. Austin, R. Cammi, C. Pomelli, J. W. Ochterski, R. L. Martin, K. Morokuma, V. G. Zakrzewski, G. A. Voth, P. Salvador, J. J. Dannenberg, S. Dapprich, A. D. Daniels, Ö. Farkas, J. B. Foresman, J. V. Ortiz, J. Cioslowski and G. D. J. Fox, *Gaussian 09*, Revision B.01, Gaussian Inc., Wallingford CT., 2009

In all systems under examination the atom displacements within the SWNTs have remained very small (≈ 0.02 Å) during the geometry optimizations, suggesting that the binding between the cycle and the SWNTs is of van der Waals type. This has been confirmed both by the cycle not sliding along the tubes whatever its initial position was and by the evaluation of the corresponding binding energies. In all cases, the alkyl chain is the only part of the cycle that has undergone a significant deformation. Table S1 shows that the cycle can wrap 27 SWNT chiralities and its alkyl chain can withstand a diameter expansion of at least 0.75 Å, allowing its formation within all mixes of SWNTs containing the chiralities listed in the table. The value range spanned by the binding energies confirms that van der Waals interactions are dominant between the cycle and the SWNTs.

Chirality	**Diameter (nm)**	**E_b (kJ mol^{-1})**
(06,05)	0.747	-166.88
(07,05)	0.818	-115.45
(08,04)	0.829	-101.04
(07,06)	0.882	-43.42
(08,05)	0.889	-29.59
(09,04)	0.903	-16.08
(11,01)	0.903	-9.48
(10,03)	0.923	15.52
(12,00)	0.94	37.03
(08,06)	0.953	48.16
(07,07)	0.949	53.77
(11,02)	0.949	55.35
(09,05)	0.962	78.24
(10,04)	0.978	100.09
(12,01)	0.981	101.18
(11,03)	1	137.95
(08,07)	1.018	159.59
(13,00)	1.018	165.29
(09,06)	1.024	171.04
(12,02)	1.027	178.37
(14,00)	1.096	282.07
(15,00)	1.175	412.32
(16,00)	1.253	551.92
(17,00)	1.331	715.26
(18,00)	1.409	899.49
(19,00)	1.488	10505.9

(20,00)	1.566	N/D

Table S1. Exploration of SWNT chiralities compatible with the *p*-xylmac14 cycle. For each case, the CNT diameter and cycle/CNT binding energy are provided. Negative energies correspond to globally attractive interactions.

3.5 References

1. S. Iijima and T. Ichihashi, *Nature*, 1993, **363**, 603-605.
2. S. Iijima, *Nature*, 1991, **354**, 56-58.
3. D. S. Bethune, C. H. Klang, M. S. de Vries, G. Gorman, R. Savoy, J. Vázquez and R. Beyers, *Nature*, 1993, **363**, 605-607.
4. R. H. Baughman, A. A. Zakhidov and W. A. de Heer, *Science* 2002, **297**, 787-792.
5. K. Dirian, M. A. Herranz, G. Katsukis, J. Malig, L. Rodríguez-Pérez, C. Romero-Nieto, V. Strauss, N. Martín and D. M. Guldi, *Chem. Sci.*, 2013, **4**, 4335-4353.
6. A. D. Franklin, M. Luisier, S.-J. Han, G. Tulevski, C. M. Breslin, L. Gignac, M. S. Lundstrom and W. Haensch, *Nano Lett.*, 2012, **12**, 758-762.
7. H. Park, A. Afzali, S.-J. Han, G. S. Tulevski, A. D. Franklin, J. Tersoff, J. B. Hannon and W. Haensch, *Nat. Nanotech.*, 2012, **7**, 787-791.
8. H. Dai, *Acc. Chem. Res.*, 2002, **35**, 1035-1044.
9. M. C. Hersam, *Nat. Nanotech.*, 2008, **3**, 387-394.
10. W. Zhou, X. Bai, E. Wang and S. Xie, *Adv. Mater.*, 2009, **21**, 4565-4583.
11. R. Jasti and C. R. Bertozzi, *Chem. Phys. Lett.*, 2010, **494**, 1-7.
12. Y. Zhang and L. Zheng, *Nanoscale*, 2010, **2**, 1919-1929.
13. H. Omachi, T. Nakayama, E. Takahashi, Y. Segawa and K. Itami, *Nat. Chem.*, 2013, **5**, 572-576.
14. H. Kimura, J. Goto, S. Yasuda, S. Sakurai, M. Yumura, D. N. Futaba and K. Hata, *ACS Nano*, 2013, **7**, 3150-3157.
15. L. T. Scott, E. A. Jackson, Q. Zhang, B. D. Steinberg, M. Bancu and B. Li, *J. Am. Chem. Soc.*, 2012, **134**, 107-110.
16. P. Singh, S. Campidelli, S. Giordani, D. Bonifazi, A. Bianco and M. Prato, *Chem. Soc. Rev.*, 2009, **38**, 2214-2230.
17. Y.-L. Zhao and J. F. Stoddart, *Acc. Chem. Res.*, 2009, **42**, 1161-1171.
18. J. Gao, M. A. Loi, E. J. F. de Carvalho and M. C. dos Santos, *ACS Nano*, 2011, **5**, 3993-3999.

19. A. Llanes-Pallas, K. Yoosaf, H. Traboulsi, J. Mohanraj, T. Seldrum, J. Dumont, A. Minoia, R. Lazzaroni, N. Armaroli and D. Bonifazi, *J. Am. Chem. Soc.*, 2011, **133**, 15412-15424.
20. S. D. Stranks, J. K. Sprafke, H. L. Anderson and R. J. Nicholas, *ACS Nano*, 2011, **5**, 2307-2315.
21. Y. Liu, Z.-L. Yu, Y.-M. Zhang, D.-S. Guo and Y.-P. Liu, *J. Am. Chem. Soc.*, 2008, **130**, 10431-10439.
22. X. Tu, S. Manohar, A. Jagota and M. Zheng, *Nature* 2009, **460**, 250-253.
23. F. D'Souza, S. K. Das, M. E. Zandler, A. S. D. Sandanayaka and O. Ito, *J. Am. Chem. Soc.*, 2011, **133**, 19922-19930.
24. H. Chaturvedi, A. N. Giordano, M.-J. Kim, F. M. MacDonnell, S. S. Subaran and J. C. Poler, *J. Phys. Chem. C*, 2009, **113**, 11254-11261.
25. G. Clavé, G. Delport, C. Roquelet, J.-S. Lauret, E. Deleporte, F. Vialla, B. Langlois, R. Parret, C. Voisin, P. Roussignol, B. Jousselme, A. Gloter, O. Stephan, A. Filoramo, V. Derycke and S. Campidelli, *Chem. Mater.*, 2013, **25**, 2700-2707.
26. J. F. Stoddart, *Chem. Soc. Rev.*, 2009, **38**, 1802-1820.
27. J.-P. Sauvage, *Chem. Commun.*, 2005, 1507-1510.
28. E. R. Kay, D. A. Leigh and F. Zerbetto, *Angew. Chem. Int. Ed.*, 2007, **46**, 72-191.
29. J. Berna, D. A. Leigh, M. Lubomska, S. M. Mendoza, E. M. Pérez, P. Rudolf, G. Teobaldi and F. Zerbetto, *Nat. Mater.*, 2005, **4**, 704-710.
30. J. E. Green, J. Wook Choi, A. Boukai, Y. Bunimovich, E. Johnston-Halperin, E. DeIonno, Y. Luo, B. A. Sheriff, K. Xu, Y. Shik Shin, H.-R. Tseng, J. F. Stoddart and J. R. Heath, *Nature*, 2007, **445**, 414-417.
31. B. Lewandowski, G. De Bo, J. W. Ward, M. Papmeyer, S. Kuschel, M. J. Aldegunde, P. M. E. Gramlich, D. Heckmann, S. M. Goldup, D. M. D'Souza, A. E. Fernandes and D. A. Leigh, *Science*, 2013, **339**, 189-193.
32. L. Fang, M. A. Olson, D. Benítez, E. Tkatchouk, W. A. Goddard Iii and J. F. Stoddart, *Chem. Soc. Rev.*, 2010, **39**, 17-29.
33. Q. Li, C.-H. Sue, S. Basu, A. K. Shveyd, W. Zhang, G. Barin, L. Fang, A. A. Sarjeant, J. F. Stoddart and O. M. Yaghi, *Angew. Chem. Int. Ed.*, 2010, **49**, 6751-6755.
34. A. de Juan and E. M. Pérez, *Nanoscale*, 2013, **5**, 7141-7148.
35. J. Akola, K. Rytkönen and M. Manninen, *J. Phys. Chem. B*, 2006, **110**, 5186-5190.
36. H. Isla, M. Gallego, E. M. Pérez, R. Viruela, E. Ortí and N. Martín, *J. Am. Chem. Soc.*, 2010, **132**, 1772-1773.
37. D. Canevet, M. Gallego, H. Isla, A. de Juan, E. M. Pérez and N. Martín, *J. Am. Chem. Soc.*, 2011, **133**, 3184-3190.

38. C. Romero-Nieto, R. García, M. Á. Herranz, C. Ehli, M. Ruppert, A. Hirsch, D. M. Guldi and N. Martín, *J. Am. Chem. Soc.*, 2012, **134**, 9183-9192.
39. R. H. Grubbs, *Tetrahedron*, 2004, **60**, 7117-7140.
40. S. M. Bachilo, M. S. Strano, C. Kittrell, R. H. Hauge, R. E. Smalley and R. B. Weisman, *Science* 2002, **298**, 2361-2366.
41. E. Nakamura, *Angew. Chem. Int. Ed.*, 2013, **52**, 236-252.
42. M. Koshino, T. Tanaka, N. Solin, K. Suenaga, H. Isobe and E. Nakamura, *Science*, 2007, **316**, 853-853.
43. M. D. Hanwell, D. E. Curtis, D. C. Lonie, T. Vandermeersch, E. Zurek and G. R. Hutchison, *J. Cheminformatics*, 2012, **4**, 17.
44. T. A. Halgren, *J. Comput. Chem.*, 1996, **17**, 616-641.
45. M. J. Frisch, G. W. Trucks, H. B. Schlegel, G. E. Scuseria, M. A. Robb, J. R. Cheeseman, G. Scalmani, V. Barone, B. Mennucci, G. A. Petersson, H. Nakatsuji, M. Caricato, H. P. H. X. Li, A. F. Izmaylov, J. Bloino, G. Zheng, J. L. Sonnenberg, M. Hada, M. Ehara, K. Toyota, R. Fukuda, J. Hasegawa, M. Ishida, T. Nakajima, Y. Honda, O. Kitao, H. Nakai, T. Vreven, J. A. Montgomery, J. E. P. Jr., F. Ogliaro, M. Bearpark, J. J. Heyd, E. Brothers, K. N. Kudin, V. N. Staroverov, R. Kobayashi, J. Normand, K. Raghavachari, A. Rendell, J. C. Burant, S. S. Iyengar, J. Tomasi, M. Cossi, N. Rega, J. M. Millam, M. Klene, J. E. Knox, J. B. Cross, V. Bakken, C. Adamo, J. Jaramillo, R. Gomperts, R. E. Stratmann, O. Yazyev, A. J. Austin, R. Cammi, C. Pomelli, J. W. Ochterski, R. L. Martin, K. Morokuma, V. G. Zakrzewski, G. A. Voth, P. Salvador, J. J. Dannenberg, S. Dapprich, A. D. Daniels, Ö. Farkas, J. B. Foresman, J. V. Ortiz, J. Cioslowski and G. D. J. Fox, *Gaussian 09*, Gaussian Inc., Wallingford CT., 2009

CHAPTER 2

4. Optimization and Insights into the Mechanism of Formation of Mechanically Interlocked Derivatives of Single-Walled Carbon Nanotubes

*The mechanical bond provides a stable yet dynamic link between the submolecular components of mechanically interlocked molecules, such as rotaxanes and catenanes. We introduced the mechanical bond as a new tool for the chemical modification of single-walled carbon nanotubes (SWNTs), producing the first mechanically interlocked derivatives of nanotubes (MINTs). To do so, we used U-shaped molecules featuring two units of a SWNT-recognition unit, which were cyclized around the SWNT by means of ring-closing metathesis (RCM). Here we report optimized conditions for the synthesis of MINTs obtained by systematic investigation of the effect of the concentration of the U-shaped molecule **1**, reaction time, and catalyst concentration. Analysis of the data also provides insights into the mechanism of formation of MINTs. In particular, the effect of the concentration of **1** supports the formation of a **1**·SWNT complex. The kinetic data follow a pseudo-first-order behavior that validates the RCM as the rate-determining step. An excess of RCM catalyst leads to the formation of supramolecularly adsorbed linear oligomers of **1**.*

ChemPlusChem, 2015, **80**, 1153-1157.

4.1 Introduction

The functionalization of single-walled carbon nanotubes (SWNTs)[1-4] can be aimed at either the attachment of molecules of interest to the nanotubes or the saturation of some of their $C(sp^2)$ - $C(sp^2)$ bonds. In the first case, the connection between the SWNT and the addend can be either covalent or supramolecular, depending on the final aim of the functionalized SWNT. Examples of both abound in the literature.[5,6] For suspension or purification purposes, supramolecular interactions are more suitable due to their reversibility.[7]

1. C. N. R. Rao, B. C. Satishkumar, A. Govindaraj and M. Nath, *ChemPhysChem*, 2001, **2**, 78-105.
2. H. Dai, *Acc. Chem. Res.*, 2002, **35**, 1035-1044.
3. A. Hirsch, *Angew. Chem., Int. Ed.*, 2002, **41**, 1853-1859.
4. D. Tasis, N. Tagmatarchis, A. Bianco and M. Prato, *Chem. Rev.*, 2006, **106**, 1105-1136.
5. P. Singh, S. Campidelli, S. Giordani, D. Bonifazi, A. Bianco and M. Prato, *Chem. Soc. Rev.*, 2009, **38**, 2214-2230.
6. Y.-L. Zhao and J. F. Stoddart, *Acc. Chem. Res.*, 2009, **42**, 1161-1171.
7. E. M. Pérez and N. Martín, *Org. Biomol. Chem.*, 2012, **10**, 3577-3583.

Prominent examples have shown that SWNTs can be associated with exquisite chiral selectivity by specifically designed DNA oligomers[8] or by small-molecule hosts,[9-11] allowing for their purification. If the aim is to glue together the SWNT and the addend, both covalent and noncovalent chemistry are valid options. On the other hand, if the chemist's objective is to tune the properties of the SWNTs through the (selective) modification of its structure, covalent chemistry is usually the choice. In that way, chemists have managed to react metallic SWNTs selectively to obtain purely semiconducting samples.[12] On an apparently unrelated note, rotaxanes are mechanically interlocked molecules (MIMs) in which one or more macrocycles encapsulate a linear component (thread), which is modified by bulky substituents (stoppers), so that the macrocycles can only be de-threaded by breaking a covalent bond.[13] The mechanical bond provides rotaxanes with unique dynamic properties that have been exploited in the synthesis of molecular machinery.[14-16] Most examples of rotaxanes reported to date comprise small-molecule organic components, but there is a growing interest in mechanically interlocked materials, such as polyrotaxanes,[17-20] rotaxanated metal organic frameworks,[21-23] and organic-inorganic rotaxane hybrids.[24-26]

---

8. X. Tu, S. Manohar, A. Jagota and M. Zheng, *Nature* 2009, **460**, 250-253.
9. G. Liu, F. Wang, S. Chaunchaiyakul, Y. Saito, A. K. Bauri, T. Kimura, Y. Kuwahara and N. Komatsu, *J. Am. Chem. Soc.*, 2013, **135**, 4805-4814.
10. K. Akazaki, F. Toshimitsu, H. Ozawa, T. Fujigaya and N. Nakashima, *J. Am. Chem. Soc.*, 2012, **134**, 12700-12707.
11. H. Ozawa, T. Fujigaya, Y. Niidome, N. Hotta, M. Fujiki and N. Nakashima, *J. Am. Chem. Soc.*, 2011, **133**, 2651-2657.
12. M. Kanungo, H. Lu, G. G. Malliaras and G. B. Blanchet, *Science*, 2009, **323**, 234-237.
13. J. F. Stoddart, *Chem. Soc. Rev.*, 2009, **38**, 1802-1820.
14. E. R. Kay, D. A. Leigh and F. Zerbetto, *Angew. Chem. Int. Ed.*, 2007, **46**, 72-191.
15. B. Lewandowski, G. De Bo, J. W. Ward, M. Papmeyer, S. Kuschel, M. J. Aldegunde, P. M. E. Gramlich, D. Heckmann, S. M. Goldup, D. M. D'Souza, A. E. Fernandes and D. A. Leigh, *Science*, 2013, **339**, 189-193.
16. G. De Bo, S. Kuschel, D. A. Leigh, B. Lewandowski, M. Papmeyer and J. W. Ward, *J. Am. Chem. Soc.*, 2014, **136**, 5811-5814.
17. J. P. Coelho, G. González-Rubio, A. Delices, J. O. Barcina, C. Salgado, D. Ávila, O. Peña-Rodríguez, G. Tardajos and A. Guerrero-Martínez, *Angew. Chem. Int. Ed.*, 2014, **53**, 12751-12755.
18. S. Yu, Y. Zhang, X. Wang, X. Zhen, Z. Zhang, W. Wu and X. Jiang, *Angew. Chem. Int. Ed.*, 2013, **52**, 7272-7277.
19. J.-H. Seo, S. Kakinoki, Y. Inoue, T. Yamaoka, K. Ishihara and N. Yui, *J. Am. Chem. Soc.*, 2013, **135**, 5513-5516.
20. C. A. Scarff, J. R. Snelling, M. M. Knust, C. L. Wilkins and J. H. Scrivens, *J. Am. Chem. Soc.*, 2012, **134**, 9193-9198.
21. K. Zhu, V. N. Vukotic, C. A. O'Keefe, R. W. Schurko and S. J. Loeb, *J. Am. Chem. Soc.*, 2014, **136**, 7403-7409.
22. I.-H. Park, R. Medishetty, J.-Y. Kim, S. S. Lee and J. J. Vittal, *Angew. Chem. Int. Ed.*, 2014, **53**, 5591-5595.
23. V. N. Vukotic, K. J. Harris, K. Zhu, R. W. Schurko and S. J. Loeb, *Nat. Chem.*, 2012, **4**, 456-460.
24. A. Cecconello, C.-H. Lu, J. Elbaz and I. Willner, *Nano Lett.*, 2013, **13**, 6275-6280.

We have recently introduced the mechanical bond as a new tool for the chemical derivatization of carbon nanotubes, bringing together the fields of SWNT chemistry and MIMs.[27] In particular, we synthesized rotaxane-like mechanically interlocked derivatives of SWNTs (MINTs).[28] To do so, we relied on a clipping strategy in which U-shaped molecules featuring two SWNT-recognition units associate with the nanotubes supramolecularly, templating the cyclization around the SWNTs via ring-closing metathesis (RCM), as depicted schematically in Figure 1a. In our first example, we utilized a π-extended derivative of tetrathiafulvalene as a SWNT-recognition motif (exTTF, Figure 1b), and we have later proven that pyrene is also a valid templating agent.[29] Here, we report the systematic investigation of the effect of concentration of the U-shaped molecule, reaction time, and catalyst concentration on the MINT forming reaction.

4.2 Results and Discussion

Based on our previous results, we have chosen the U-shaped molecule **1**, the corresponding macrocycle **2** (Figure 1b), and plasma-purified SWNTs (0.8-1.6 nm in diameter, 99% purity) as a model system. In our original experimental conditions for the synthesis of MINTs we used tetrachloroethane (TCE) as the solvent, in which 1 mg mL^{-1} of SWNTs was suspended by bath sonication (10 min, 40 kHz) and mixed with U-shaped **1** (0.44 mM) and Grubbs' 2nd generation catalyst (ca. 1 equiv. with respect to **1**). This mixture was stirred at room temperature for 72 h, and filtered through a 0.2 μm pore polytetrafluoroethylene membrane, and the solid was washed thoroughly with CH_2Cl_2. To fully remove any non-interlocked macrocycles, remaining U-shaped **1**, or catalyst, the solid was then resuspended in CH_2Cl_2, sonicated (10 min, 40 kHz), and filtered. This washing procedure was repeated three times, and then the nanotube material was dried and subjected to thermogravimetric analysis (TGA) to quantify the degree of functionalization. The loss in weight observed as a function of temperature is

25. B. Ballesteros, T. B. Faust, C.-F. Lee, D. A. Leigh, C. A. Muryn, R. G. Pritchard, D. Schultz, S. J. Teat, G. A. Timco and R. E. P. Winpenny, *J. Am. Chem. Soc.*, 2010, **132**, 15435-15444.
26. C.-F. Lee, D. A. Leigh, R. G. Pritchard, D. Schultz, S. J. Teat, G. A. Timco and R. E. P. Winpenny, *Nature* 2009, **458**, 314-318.
27. A. de Juan and E. M. Pérez, *Nanoscale*, 2013, **5**, 7141-7148.
28. A. de Juan, Y. Pouillon, L. Ruiz-González, A. Torres-Pardo, S. Casado, N. Martín, Á. Rubio and E. M. Pérez, *Angew. Chem., Int. Ed.*, 2014, **53**, 5394-5400.
29. A. López-Moreno and E. M. Pérez, *Chem. Commun.*, 2015, **51**, 5421-5424.

a direct indication of the degree of functionalization. Under these conditions, a loading of 29% exTTF material was observed. A very thorough collection of control experiments, Raman, UV/Vis-NIR, PLE, NMR, HR-TEM, and AFM analyses proved beyond reasonable doubt the interlocked nature of the MINT-**2** product.[28]

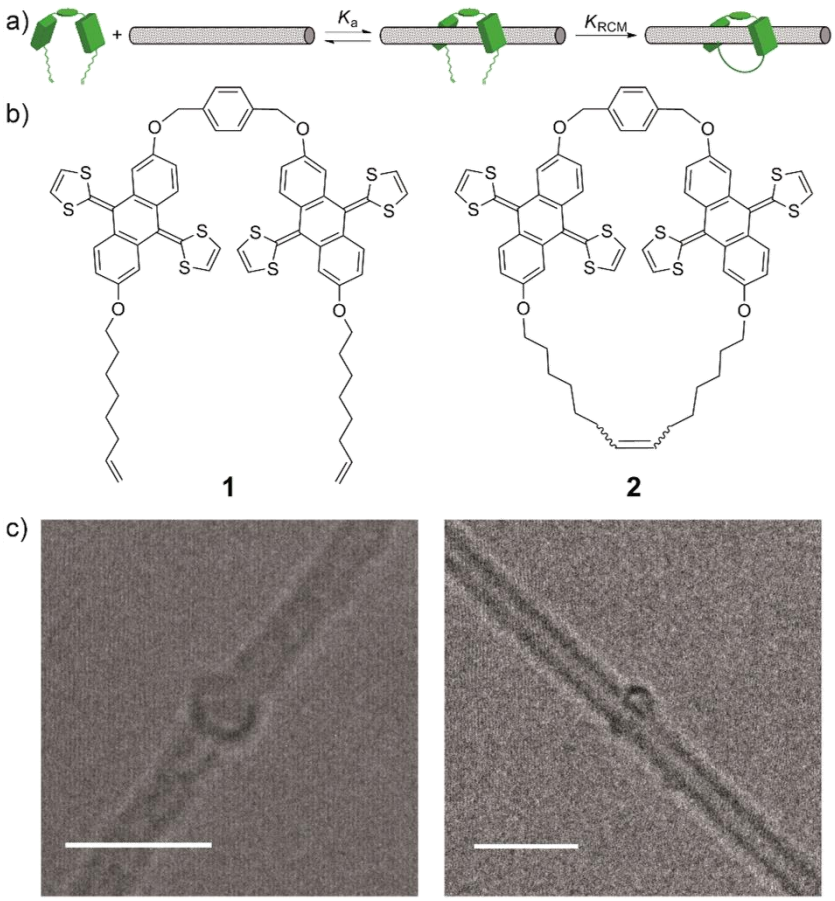

Figure 1. a) Representation of the clipping strategy for the synthesis of MINTs (stoppers not depicted, see main text). b) Chemical structures of **1** and **2**. c) HR-TEM images of MINT-**2**; scale bars are 5 nm.

For the present study, we have relied on TGA to quantify the degree of functionalization and Raman spectroscopy as a quick and reliable method for spectroscopic characterization. All the samples showed Raman spectra in conformity with MINTs, that is, no significant increase in the ID/IG ratio and small shifts of the G band; the results are summarized in Table S1 in the Experimental Details. For some selected samples, we have also carried out HR-

TEM imaging. Two representative micrographs are shown in Figure 1c. From left to right, they show nanotubes of diameter 1.2 and 0.9 nm, surrounded by a unit of **2**, which in both cases shows a diameter of about 2.5 nm, in perfect agreement with the size predicted by molecular mechanics calculations. Note that in the first case the macrocycle fits significantly tighter around the SWNT.

We started by investigating the effect of the relative concentration of U-shaped **1**. In particular, we employed **1** at concentrations of 0, 0.044, 0.44, 2.3, and 4.5 mM, at a constant loading of 1 mg mL^{-1} of SWNTs and with 0.5 molar equivalents of catalyst. We reproduced the reaction and purification procedure described above; subsequent TGA analysis afforded the results shown in Figure 2. Upon increasing the concentration of **1**, the degree of functionalization increases but reaches a plateau at around 35%. From a purely synthetic point of view, we estimate that concentrations of U-shaped **1** above 1 mM are optimal.

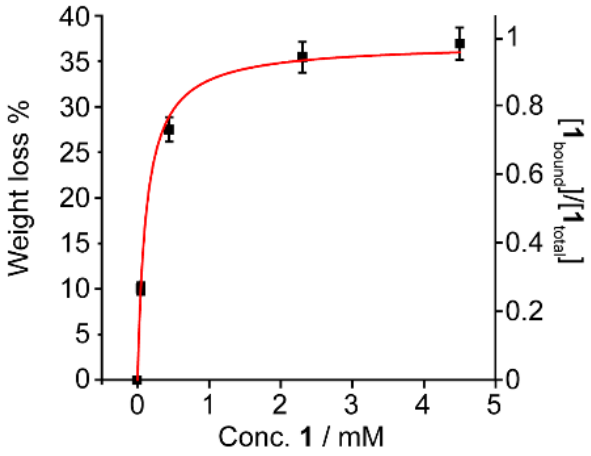

Figure 2. Degree of functionalization with increasing concentration of U-shaped **1** (catalyst and solvent adsorption subtracted), and its fit to calculate the approximate binding constant between **1** and SWNTs (see main text for details). Data are the average of three separate experiments; error bars show the standard deviation.

Note that the trend in Figure 2 is clearly reminiscent of the typical square hyperbolic shape of a 1:1 binding isotherm. A major obstacle in the study of the supramolecular chemistry of nanomaterials such as SWNTs is that there is no method to determine binding constants. This is usually explained by the impossibility of determining the molar concentration of SWNTs in solution. However, it is well known that association constants can be calculated from the concentration of free host species only. This method is not usually applied to

traditional host-guest systems since the total concentration of host and guest are known quantities and the calculation of the concentration of free species is problematic.[30] In our case, each TGA data point is directly related to the concentration of associated **1** in the **1**+SWNT binding equilibrium, which is fixed by the RCM as a MINT-**2** product (see Figure 1a). Assuming that maximum functionalization is equivalent to saturation of the binding equilibrium, when $[\mathbf{1}]_{bound}/[\mathbf{1}]_{total} = 1$, we could fit our data to a 1:1 binding isotherm as a function of the concentration of $[\mathbf{1}]_{free}$ only, which can be extracted from the TGA data. In particular, we used Equation (1)[30] and obtained K_a = (8.2 ± 0.7) x 10^3 M^{-1}, with r^2 = 0.998.

$$\frac{[\mathbf{1}]_{bound}}{[\mathbf{1}]_{total}} = \frac{k_a[\mathbf{1}]_{free}}{1+k_a[\mathbf{1}]_{free}} \quad (1)$$

Despite the good mathematical fit, the physical meaning of this apparent binding constant should not be overinterpreted, as in our case the data are not extracted under thermodynamic equilibrium conditions. For instance, the binding constant should be slightly overestimated, as the association equilibrium is displaced by the RCM. However, we consider it is a valid indication that the MINT-forming reaction proceeds through a **1**·SWNT complex, as anticipated. Numerically speaking, the value is in good agreement with that found for the closest system for which an accurate association constant has been determined, composed of structurally related bis-exTTF tweezers and C_{60}, which show K_a = 10^3-10^4 M^{-1} in various solvents at room temperature.[31-33]

Next, we evaluated the progress of the reaction with time. To do so, we set up MINT-forming reactions with a concentration of **1** of 0.44 mM, 1 mg mL^{-1} of SWNTs and 0.2 mg mL^{-1} of Grubbs' 2nd generation catalyst, and extracted aliquots at 3, 6, 24, 48, 72, 168, and 240 h, which were purified as described above, and then subjected to TGA. Figure 3a shows that the degree of functionalization increases rapidly during the first 24 h and reaches a plateau at 24 ± 2 % after 48 h. Longer reaction times do not seem to produce a significant increase in functionalization.

30. P. Thordarson, *Chem. Soc. Rev.*, 2011, **40**, 1305-1323.
31. S. S. Gayathri, M. Wielopolski, E. M. Pérez, G. Fernández, L. Sánchez, R. Viruela, E. Ortí, D. M. Guldi and N. Martín, *Angew. Chem. Int. Ed.*, 2009, **48**, 815-819.
32. E. M. Pérez, A. L. Capodilupo, G. Fernández, L. Sánchez, P. M. Viruela, R. Viruela, E. Ortí, M. Bietti and N. Martín, *Chem. Commun.*, 2008, 4567-4569.
33. E. M. Pérez, L. Sánchez, G. Fernández and N. Martín, *J. Am. Chem. Soc.*, 2006, **128**, 7172-7173.

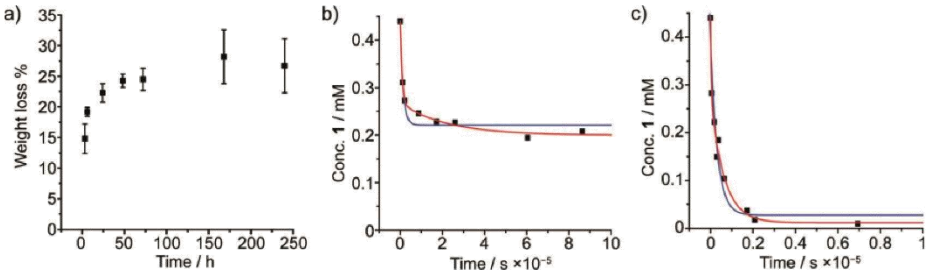

Figure 3. a) Degree of functionalization with increasing reaction time ([**1**] = 0.44 mM, 1 mg mL^{-1} of SWNTs, and 0.2 mg mL^{-1} (0.5 equivalent) of Grubbs' 2nd generation catalyst. b) Kinetic data for the formation of MINT$_{pp}$-**1**, and its fit to a monoexponential (blue) and biexponential (red) decay. c) Kinetic data for the formation of **1**, and its fit to a monoexponential (blue) and biexponential (red) decay.

An important concern during the synthesis of MINTs was the fact that bis-alkenes such as **1** can either cyclize via RCM or poly/oligomerize through acyclic diene metathesis polymerization (ADMP). Despite the reversibility of RCM reactions, they typically proceed with pseudo-first-order kinetics,[34] while ADMPs are second-order in diene concentration.[35] Analysis of the kinetics of formation of MINTs with respect to the concentration of **1** should therefore provide valuable information with regards to the degree of participation of oligomers/polymers in the final MINT product. In order to analyze the MINT-forming reaction kinetics, we calculated the decrease of concentration of **1** from our TGA data. As shown in Figure 3b, the conversion of **1** to MINT-**2** reaches only about 50 %. The remaining material is accounted for by unreacted **1**, non-interlocked **2**, and linear oligomers formed in situ, which are all washed away during the purification steps. In contrast, the RCM of **1** to form **2** in the absence of SWNTs, but under otherwise identical experimental conditions, reaches nearly 100 % conversion, and proceeds approximately ten times faster (Figure 3c). For a first approximation, we fitted the kinetic data to a mono-exponential decay using Equation (2).

$$[\mathbf{1}] = A + Be^{-k_1 t} \quad (2)$$

Here A should approach 0 and B should approach $[\mathbf{1}]_0$ if the reactions were first order and the reaction proceeded to completion. Indeed, this is the case for the macrocyclization of **1** to form **2** ($r^2 = 0.932$), where A is over fourteen times smaller than B, and B is 84 % of $[\mathbf{1}]_0$. In contrast, for the MINT-forming reaction

34. E. L. Dias, S. T. Nguyen and R. H. Grubbs, *J. Am. Chem. Soc.*, 1997, **119**, 3887-3897.
35. K. B. Wagener, K. Brzezinska, J. D. Anderson, T. R. Younkin, K. Steppe and W. DeBoer, *Macromolecules*, 1997, **30**, 7363-7369.

(r^2 = 0.946), A = B = 2.2 x 10^{-4} m, reflecting the low conversion. With regards to the associated rate constants the formation of MINT-**2** shows a k_1 value one order of magnitude smaller for than that found for **2**, reflecting the decreased probability of a productive RCM taking place (Table 1).

Table 1. Kinetic parameters for the formation of MINT-**2** and **2** as obtained from the fits shown in Figure 3b and c, according to the equations in the main text.

Product	**A [M]**	**B [M]**	**C [M]**	k_1 **[s^{-1}]**	k_2 **[s^{-1}]**	**r^2**
1	$2.7x10^{-5}$	$3.7x10^{-4}$	-	$3.1x10^{-4}$	-	0.932
$MINT_{pp}$-**1**	$2.2x10^{-4}$	$2.2x10^{-4}$	-	$7.4x10^{-5}$	-	0.946
1	$1.1x10^{-5}$	$2.7x10^{-4}$	$1.6x10^{-4}$	$1.6x10^{-4}$	$3.1x10^{-3}$	0.981
$MINT_{pp}$-**1**	$2.0x10^{-4}$	$6.8x10^{-5}$	$1.7x10^{-4}$	$4.4x10^{-6}$	$1.2x10^{-5}$	0.990

As previously reported for RCM,[34] the kinetic data for both reactions fits even better to a biexponential decay according to Equation (3).

$$[\mathbf{1}] = A + Be^{-k_1 t} + Ce^{-k_2 t} \quad (3)$$

A detailed molecular interpretation of the kinetic parameters of that model was not originally described by Grubbs' and coworkers, and is beyond our grasp particularly for such a complicated heterogeneous system. However, some general trends in comparison with the mono-exponential decay are worth underlining. For both the formation of MINT-**2** (r^2 = 0.990) and **2** (r^2 = 0.981), A remains nearly constant, as expected, since it is an indication of the "unproductive" concentration of **1** and is therefore directly related to the conversion. As for the remaining factors, C and k_2 are one order of magnitude larger than B and k_1 for both reactions, which indicates that, although the mathematical fit is significantly improved, the pseudo-first order model provides a valid approximation. In contrast, our experimental data are incompatible with the second-order model required by ADMP (see Figure S1 in the Experimental Details).[35] Therefore, the kinetic data are perfectly consistent with the reaction mechanism for the formation of MINTs depicted in Figure 1a, and discard a significant participation of oligomers/polymers in the MINT-forming reaction.

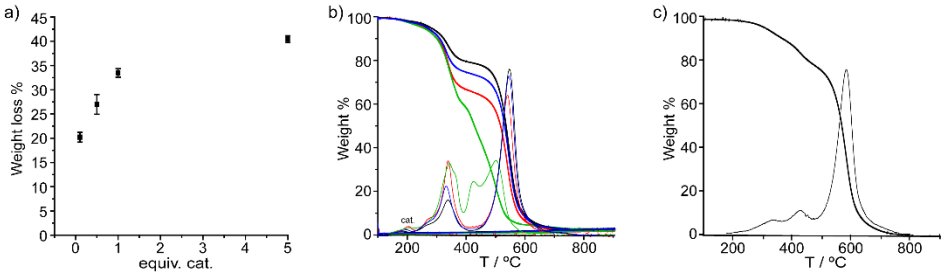

Figure 4. a) Degree of functionalization with increasing relative concentration of catalyst. Data are the average of three separate experiments; error bars show the standard deviation. b) TGA (air, 10ºC min^{-1}) for the reactions run with 0.1 (black), 0.5 (blue), 1 (red), and 5 (green) equivalents of catalyst; the weight vs. temperature derivatives are depicted in the same colors but with thinner lines. c) TGA (air, 10ºC min^{-1}) for the adsorption of a dimer of **1** onto SWNTs, the weight vs. temperature derivative is depicted with a thinner line.

Finally, we also investigated influence of the catalyst concentration using a concentration of **1** of 0.44 mM, 1 mg mL^{-1} of SWNTs, and 0.1, 0.5, 1, and 5 equivalents of Grubbs' 2nd generation catalyst with respect to **1**. All reactions were run for 72 h. The results are summarized in Figure 4. As expected, the degree of functionalization increases with the relative catalyst concentration, reaching up to 40% with 5 equiv. However, the TGA in this last case (green in Figure 4b) shows a distinctively different shape. An additional shoulder and new peak at 423ºC can be observed in its derivative. We tentatively assigned them to supramolecularly attached oligomers of **1**, formed in situ under the RCM reaction conditions. To test this hypothesis, we synthesized a linear dimer of **1**, adsorbed it onto the SWNTs in TCE (see Figure S2 in the Experimental Details), and analyzed the product by TGA. The results are shown in Figure 4c. As expected, the derivative of the TGA shows two peaks for the adsorbate, a smaller one around 325ºC and a larger one at 425ºC, in very good agreement with the new peaks observed in Figure 4b. This control experiment not only confirms the identity of the by-products formed when 5 equiv. of catalyst is used, but also underscores the relative purity of the other MINT samples.

4.3 Conclusion

In summary, the data presented here provide optimized conditions for the synthesis of MINTs. In particular, we have shown that a concentration of **1** greater than or equal to 1 mM, reaction times of at least 48 h, and relative catalyst concentration of less than 1 equiv. with respect to **1** are the ideal conditions to maximize the functionalization of MINTs without forming significant amounts

of oligomeric byproducts. Analysis of the bulk reaction data helped us shed light on the inner workings of our clipping strategy to form MINTs through RCM. Specifically, from the degree of functionalization as a function of the concentration of **1**, we infer that the MINT-forming reaction proceeds via a **1**·SWNT complex, with affinity in the millimolar range. Analysis of conversion-time data provided valuable information with regards to the mechanism of formation of MINTs. In particular, we have proven that the macrocyclization of **1** in the presence of SWNTs to form MINT-**2**, or in their absence to form **2**, follow the typical trends of RCM, but with significantly different kinetic parameters. By following a pseudo-first-order approximation, analysis of our data support a mechanism in which the cyclization of **1** in the MINT-forming reaction is the rate-determining step. Finally, we have observed that an excess of catalyst (>1 equivalent with respect to **1**) leads to the formation of undesired by-products, which were identified as supramolecularly associated oligomers of **1**. Their footprint on the TGA will help identify similar impurities in future syntheses of MINTs.

4.4 Experimental Details

Computational details

Calculations performed to obtain kinetic data for the formation of **2** and MINT-**2** (Origin file):

- Column C(2) (M) represents the concentration of **2** or MINT-**2** in M. Conversion data was divided by the molecular weight of **2** (Mw = 1148 g/mol).
- Column P represent the extent of the reaction, calculated as column C(2) (M) divided by the initial concentration of **1** in M.
- Column C(1) (M) represents the concentration of **1** in M. C(1) is calculated applying: $P = 1 - C(1)/C(1)0$, where C(1)0 is the initial concentration of **1** in M.

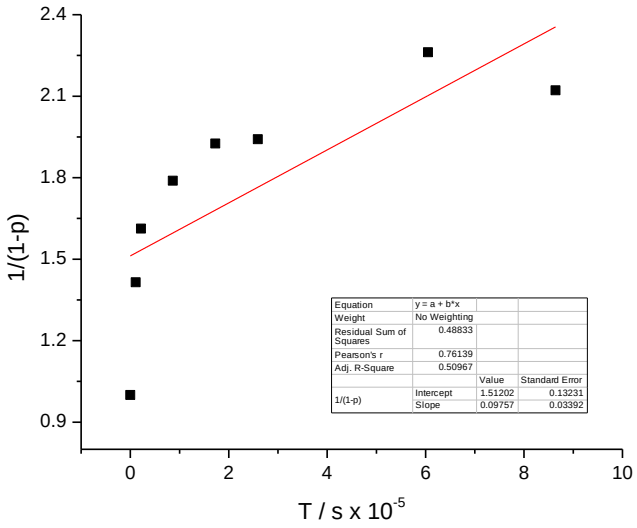

Figure S1. Second-order kinetic plot for the formation of MINT-**2**.

Synthetic details

Compounds **1**, **2**, dimer of **1**, and MINTs derivatives were synthetized following the procedures showed in the Experimental Details of Chapter 1.

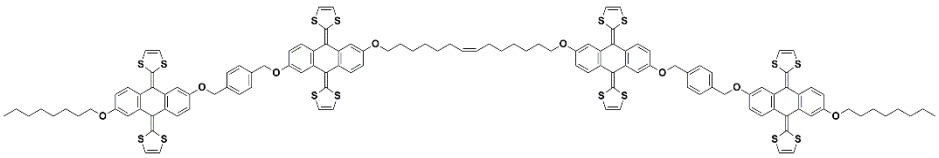

Figure S2. Structure of the linear dimer of **1** mentioned in the main text. To adsorb it onto SWNTs, plasma purified SWNTs (1 mg/mL) were suspended through sonication (10 min, 40 KHz) in TCE, linear dimer of **1** was added and the mixture stirred for 72 hours. Then, the mixture was filtered through PTFE membrane 0.2 µm of pore and washed several times with DCM. The solid obtained was characterized by TGA, shown in the main text.

Characterization

General. Thermogravimetric analyses (TGA) were performed using a TA Instruments TGAQ500 with a ramp of 10 °C/min under air from 100 to 1000 °C. Raman spectra were acquired with a Renishaw inVia confocal Raman microscopy instrument, equipped with 532, 633 and 785 nm lasers. Transmission electron microscopy (TEM) images were obtained with JEOL-JEM 2100F (2.5 Å resolution).

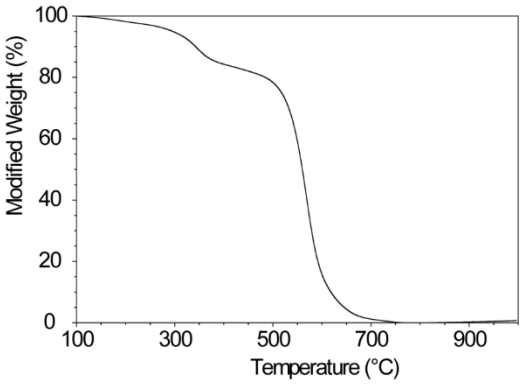

Figure S3. TGA analysis (air, 10ºC min^{-1}) of plasma-purified SWNTs treatment with **4** (0.044 mM) and Grubb's 2nd generation catalyst (0.5 equivalents) in TCE at room temperature for 72 hours.

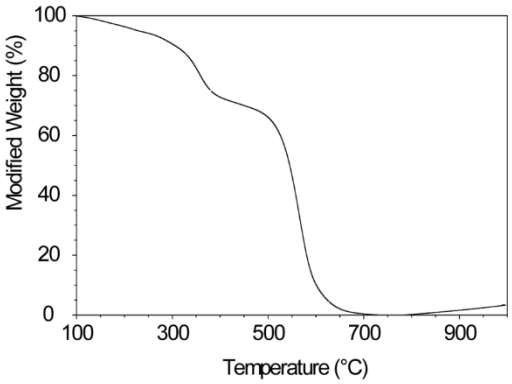

Figure S4. TGA analysis (air, 10ºC min^{-1}) of plasma-purified SWNTs treatment with **4** (0.44 mM) and Grubb's 2nd generation catalyst (0.5 equivalents) in TCE at room temperature for 72 hours.

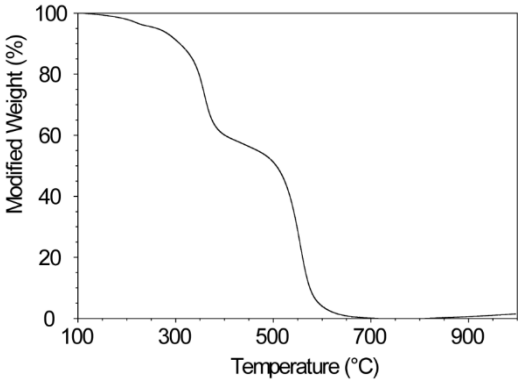

Figure S5. TGA analysis (air, 10ºC min^{-1}) of plasma-purified SWNTs treatment with **4** (2.3 mM) and Grubb's 2nd generation catalyst (0.5 equivalents) in TCE at room temperature for 72 hours.

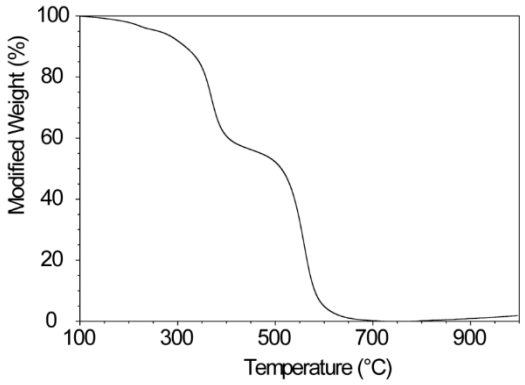

Figure S6. TGA analysis (air, 10ºC min^{-1}) of plasma-purified SWNTs treatment with **4** (4.5 mM) and Grubb's 2nd generation catalyst (0.5 equivalents) in TCE at room temperature for 72 hours.

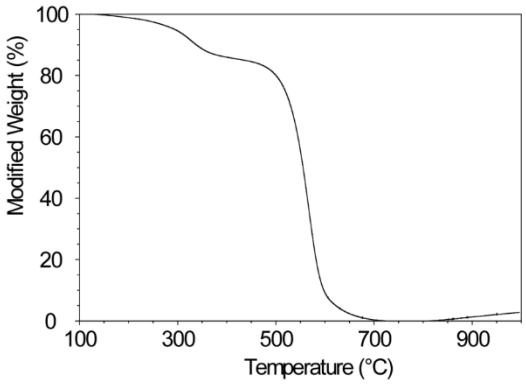

Figure S7. TGA analysis (air, 10ºC min^{-1}) of plasma-purified SWNTs treatment with **4** (0.44 mM) and Grubb's 2nd generation catalyst (0.5 equivalents) in TCE at room temperature for 3 hours.

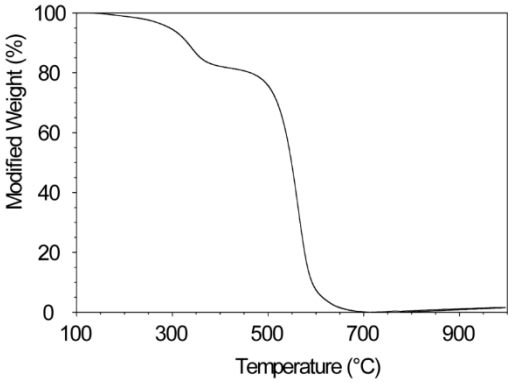

Figure S8. TGA analysis (air, 10ºC min^{-1}) of plasma-purified SWNTs treatment with **4** (0.44 mM) and Grubb's 2nd generation catalyst (0.5 equivalents) in TCE at room temperature for 6 hours.

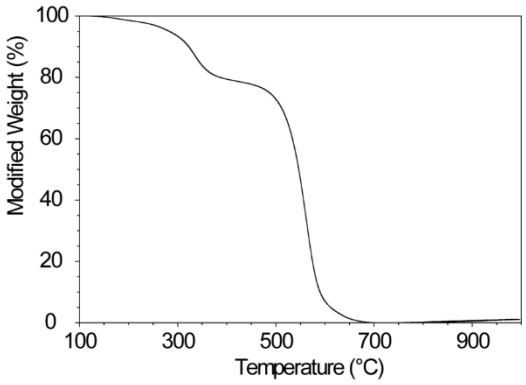

Figure S9. TGA analysis (air, 10ºC min^{-1}) of plasma-purified SWNTs treatment with **4** (0.44 mM) and Grubb's 2nd generation catalyst (0.5 equivalents) in TCE at room temperature for 24 hours.

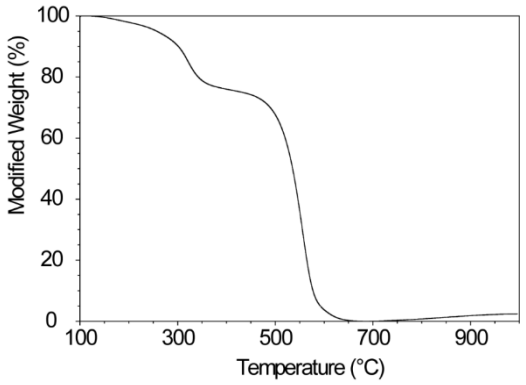

Figure S10. TGA analysis (air, 10ºC min^{-1}) of plasma-purified SWNTs treatment with **4** (0.44 mM) and Grubb's 2nd generation catalyst (0.5 equivalents) in TCE at room temperature for 48 hours.

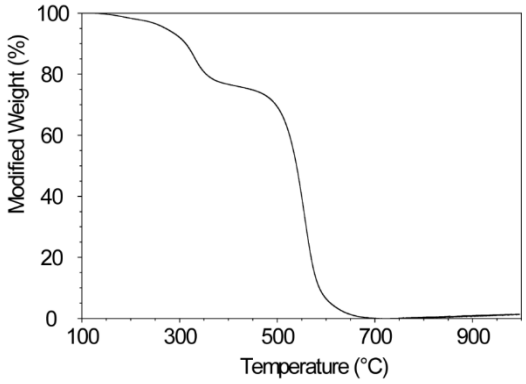

Figure S11. TGA analysis (air, 10ºC min^{-1}) of plasma-purified SWNTs treatment with **4** (0.44 mM) and Grubb's 2nd generation catalyst (0.5 equivalents) in TCE at room temperature for 72 hours.

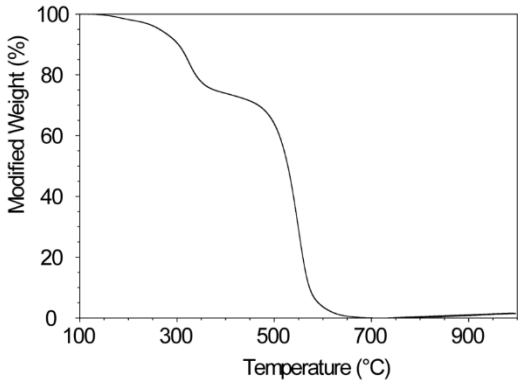

Figure S12. TGA analysis (air, 10ºC min^{-1}) of plasma-purified SWNTs treatment with **4** (0.44 mM) and Grubb's 2nd generation catalyst (0.5 equivalents) in TCE at room temperature for 168 hours.

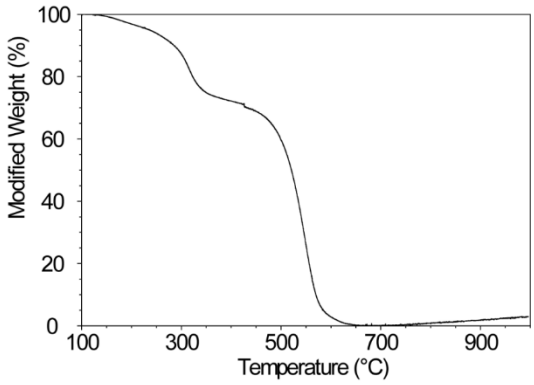

Figure S13. TGA analysis (air, 10ºC min^{-1}) of plasma-purified SWNTs treatment with **4** (0.44 mM) and Grubb's 2nd generation catalyst (0.5 equivalents) in TCE at room temperature for 240 hours.

Table S1. Selective Raman data for the samples mentioned in the main text.

Raman data		**λ = 785 nm**		**λ = 633 nm**		**λ = 532 nm**	
		I_D/I_G	G_{max}	I_D/I_G	G_{max}	I_D/I_G	G_{max}
Pristine NTs		0.18	1582	0.16	1572	0.05	1568
U-shape concentration (mM)	0.044	0.16	1581	0.14	1580	0.03	1569
	0.44	0.14	1584	0.14	1586	0.04	1570
	2.3	0.16	1583	0.08	1571	0.04	1570
	4.5	0.13	1579	0.12	1576	0.04	1570
Reaction time (h)	3	0.15	1582	0.18	1584	0.06	1570
	6	0.16	1580	0.13	1584	0.03	1568
	24	0.17	1581	0.16	1582	0.04	1569
	48	0.16	1584	0.10	1573	0.04	1570
	72	0.14	1580	0.14	1580	0.05	1570

	168	0.09	1572	0.16	1586	0.05	1570
	240	0.12	1576	0.15	1584	0.04	1570
Catalyst concentration (mM)	0.044	0.14	1582	0.14	1582	0.06	1570
	0.22	0.14	1584	0.14	1586	0.04	1570
	0.44	0.15	1581	0.13	1582	0.05	1569
	2.3	0.18	1582	0.06	1570	0.06	1570

4.5 References

1. C. N. R. Rao, B. C. Satishkumar, A. Govindaraj and M. Nath, *ChemPhysChem*, 2001, **2**, 78-105.
2. H. Dai, *Acc. Chem. Res.*, 2002, **35**, 1035-1044.
3. A. Hirsch, *Angew. Chem., Int. Ed.*, 2002, **41**, 1853-1859.
4. D. Tasis, N. Tagmatarchis, A. Bianco and M. Prato, *Chem. Rev.*, 2006, **106**, 1105-1136.
5. P. Singh, S. Campidelli, S. Giordani, D. Bonifazi, A. Bianco and M. Prato, *Chem. Soc. Rev.*, 2009, **38**, 2214-2230.
6. Y.-L. Zhao and J. F. Stoddart, *Acc. Chem. Res.*, 2009, **42**, 1161-1171.
7. E. M. Pérez and N. Martín, *Org. Biomol. Chem.*, 2012, **10**, 3577-3583.
8. X. Tu, S. Manohar, A. Jagota and M. Zheng, *Nature* 2009, **460**, 250-253.
9. G. Liu, F. Wang, S. Chaunchaiyakul, Y. Saito, A. K. Bauri, T. Kimura, Y. Kuwahara and N. Komatsu, *J. Am. Chem. Soc.*, 2013, **135**, 4805-4814.
10. K. Akazaki, F. Toshimitsu, H. Ozawa, T. Fujigaya and N. Nakashima, *J. Am. Chem. Soc.*, 2012, **134**, 12700-12707.
11. H. Ozawa, T. Fujigaya, Y. Niidome, N. Hotta, M. Fujiki and N. Nakashima, *J. Am. Chem. Soc.*, 2011, **133**, 2651-2657.
12. M. Kanungo, H. Lu, G. G. Malliaras and G. B. Blanchet, *Science*, 2009, **323**, 234-237.
13. J. F. Stoddart, *Chem. Soc. Rev.*, 2009, **38**, 1802-1820.
14. E. R. Kay, D. A. Leigh and F. Zerbetto, *Angew. Chem. Int. Ed.*, 2007, **46**, 72-191.
15. B. Lewandowski, G. De Bo, J. W. Ward, M. Papmeyer, S. Kuschel, M. J. Aldegunde, P. M. E. Gramlich, D. Heckmann, S. M. Goldup, D. M. D'Souza, A. E. Fernandes and D. A. Leigh, *Science*, 2013, **339**, 189-193.
16. G. De Bo, S. Kuschel, D. A. Leigh, B. Lewandowski, M. Papmeyer and J. W. Ward, *J. Am. Chem. Soc.*, 2014, **136**, 5811-5814.

17. J. P. Coelho, G. González-Rubio, A. Delices, J. O. Barcina, C. Salgado, D. Ávila, O. Peña-Rodríguez, G. Tardajos and A. Guerrero-Martínez, *Angew. Chem. Int. Ed.*, 2014, **53**, 12751-12755.
18. S. Yu, Y. Zhang, X. Wang, X. Zhen, Z. Zhang, W. Wu and X. Jiang, *Angew. Chem. Int. Ed.*, 2013, **52**, 7272-7277.
19. J.-H. Seo, S. Kakinoki, Y. Inoue, T. Yamaoka, K. Ishihara and N. Yui, *J. Am. Chem. Soc.*, 2013, **135**, 5513-5516.
20. C. A. Scarff, J. R. Snelling, M. M. Knust, C. L. Wilkins and J. H. Scrivens, *J. Am. Chem. Soc.*, 2012, **134**, 9193-9198.
21. K. Zhu, V. N. Vukotic, C. A. O'Keefe, R. W. Schurko and S. J. Loeb, *J. Am. Chem. Soc.*, 2014, **136**, 7403-7409.
22. I.-H. Park, R. Medishetty, J.-Y. Kim, S. S. Lee and J. J. Vittal, *Angew. Chem. Int. Ed.*, 2014, **53**, 5591-5595.
23. V. N. Vukotic, K. J. Harris, K. Zhu, R. W. Schurko and S. J. Loeb, *Nat. Chem.*, 2012, **4**, 456-460.
24. A. Cecconello, C.-H. Lu, J. Elbaz and I. Willner, *Nano Lett.*, 2013, **13**, 6275-6280.
25. B. Ballesteros, T. B. Faust, C.-F. Lee, D. A. Leigh, C. A. Muryn, R. G. Pritchard, D. Schultz, S. J. Teat, G. A. Timco and R. E. P. Winpenny, *J. Am. Chem. Soc.*, 2010, **132**, 15435-15444.
26. C.-F. Lee, D. A. Leigh, R. G. Pritchard, D. Schultz, S. J. Teat, G. A. Timco and R. E. P. Winpenny, *Nature* 2009, **458**, 314-318.
27. A. de Juan and E. M. Pérez, *Nanoscale*, 2013, **5**, 7141-7148.
28. A. de Juan, Y. Pouillon, L. Ruiz-González, A. Torres-Pardo, S. Casado, N. Martín, Á. Rubio and E. M. Pérez, *Angew. Chem., Int. Ed.*, 2014, **53**, 5394-5400.
29. A. López-Moreno and E. M. Pérez, *Chem. Commun.*, 2015, **51**, 5421-5424.
30. P. Thordarson, *Chem. Soc. Rev.*, 2011, **40**, 1305-1323.
31. S. S. Gayathri, M. Wielopolski, E. M. Pérez, G. Fernández, L. Sánchez, R. Viruela, E. Ortí, D. M. Guldi and N. Martín, *Angew. Chem. Int. Ed.*, 2009, **48**, 815-819.
32. E. M. Pérez, A. L. Capodilupo, G. Fernández, L. Sánchez, P. M. Viruela, R. Viruela, E. Ortí, M. Bietti and N. Martín, *Chem. Commun.*, 2008, 4567-4569.
33. E. M. Pérez, L. Sánchez, G. Fernández and N. Martín, *J. Am. Chem. Soc.*, 2006, **128**, 7172-7173.
34. E. L. Dias, S. T. Nguyen and R. H. Grubbs, *J. Am. Chem. Soc.*, 1997, **119**, 3887-3897.
35. K. B. Wagener, K. Brzezinska, J. D. Anderson, T. R. Younkin, K. Steppe and W. DeBoer, *Macromolecules*, 1997, **30**, 7363-7369.

CHAPTER 3

5. The Mechanical Bond on Carbon Nanotubes: Diameter-Selective Functionalization and Effects on Physical Properties

We describe the functionalization of SWNTs enriched in (6,5) chirality with electron donating macrocycles to yield rotaxane-type mechanically interlocked carbon nanotubes (MINTs). Investigations by means of electron microscopy and control experiments corroborated the interlocked nature of the MINTs. A comprehensive characterization of the MINTs through UV-vis-NIR, Raman, fluorescence, transient absorption spectroscopy, cyclic voltammetry, and chronoamperometry was carried out. Analyses of the spectroscopic data reveal that the MINT-forming reaction proceeds with diameter selectivity, favoring functionalization of (6,5) SWNTs rather than larger (7,6) SWNTs. In the ground state, we found a lack of significant charge-transfer interactions between the electron donor exTTF and the SWNTs. Upon photoexcitation, efficient charge-transfer between the electron donating exTTF macrocycles and SWNTs was demonstrated. As a complement, we established significantly different charge-transfer rate constants and diffusion coefficients for MINTs and the supramolecular models, which confirms the fundamentally different type of interactions between exTTF and SWNTs in the presence or absence of the mechanical bond. Molecular mechanics and DFT calculations support the experimental findings.

Nanoscale, 2016, **8**, 9254-9264.

5.1 Introduction

Mechanically interlocked molecules (MIMs) feature submolecular components linked together as a consequence of their topology,[1] in the absence of covalent bonds between them. The different constituents of MIMs cannot be detached from one another without breaking a covalent bond.[2] Compared to supramolecular constructs, the fingerprint of the mechanical bond is therefore the absence of equilibrium between associated and dissociated components. In other words, the rate of dissociation in MIMs is 0, so that they can be looked at

1. G. A. Breault, C. A. Hunter and P. C. Mayers, *Tetrahedron*, 1999, **55**, 5265-5293.
2. J. F. Stoddart, *Chem. Soc. Rev.*, 2009, **38**, 1802-1820.

as supramolecular associates where the binding constant between their components is infinite.[3]

Rotaxanes are a leading example of MIMs, wherein one or more macrocycles are threaded around a linear component (thread) from which they cannot be detached due to the presence of bulky substituents (stoppers) at both ends of the thread.[2] The possibility of moving the macrocycle(s) along the thread in a controlled fashion has attracted a great deal of attention towards rotaxanes as components in artificial molecular machinery.[4-9] Besides their extraordinary dynamic properties, the mechanical bond between macrocycle and thread in rotaxanes often results in a significant influence on their respective properties.[10] For instance, the macrocycle can serve as a non-covalently attached protecting group for the thread,[11-16] or modulate its photophysical properties.[17-21] These observations have motivated the search for mechanically interlocked materials

3. A. de Juan and E. M. Pérez, *Nanoscale*, 2013, **5**, 7141-7148.
4. E. R. Kay, D. A. Leigh and F. Zerbetto, *Angew. Chem. Int. Ed.*, 2007, **46**, 72-191.
5. J. Berná, G. Bottari, D. A. Leigh and E. M. Pérez, *Pure Appl. Chem.*, 2007, **79**, 39-54.
6. C. Cheng, P. R. McGonigal, S. T. Schneebeli, H. Li, N. A. Vermeulen, C. Ke and J. F. Stoddart, *Nat. Nanotech.*, 2015, **10**, 547-553.
7. B. Lewandowski, G. De Bo, J. W. Ward, M. Papmeyer, S. Kuschel, M. J. Aldegunde, P. M. E. Gramlich, D. Heckmann, S. M. Goldup, D. M. D'Souza, A. E. Fernandes and D. A. Leigh, *Science*, 2013, **339**, 189-193.
8. H. Tian and Q.-C. Wang, *Chem. Soc. Rev.*, 2006, **35**, 361-374.
9. K. Zhu, C. A. O'Keefe, V. N. Vukotic, R. W. Schurko and S. J. Loeb, *Nat. Chem.*, 2015, **7**, 514-519.
10. E. A. Neal and S. M. Goldup, *Chem. Commun.*, 2014, **50**, 5128-5142.
11. R. Barat, T. Legigan, I. Tranoy-Opalinski, B. Renoux, E. Peraudeau, J. Clarhaut, P. Poinot, A. E. Fernandes, V. Aucagne, D. A. Leigh and S. Papot, *Chem. Sci.*, 2015, **6**, 2608-2613.
12. M. Franz, J. A. Januszewski, D. Wendinger, C. Neiss, L. D. Movsisyan, F. Hampel, H. L. Anderson, A. Görling and R. R. Tykwinski, *Angew. Chem. Int. Ed.*, 2015, **54**, 6645-6649.
13. L. D. Movsisyan, D. V. Kondratuk, M. Franz, A. L. Thompson, R. R. Tykwinski and H. L. Anderson, *Org. Lett.*, 2012, **14**, 3424-3426.
14. J. Winn, A. Pinczewska and S. M. Goldup, *J. Am. Chem. Soc.*, 2013, **135**, 13318-13321.
15. A. Fernandes, A. Viterisi, F. Coutrot, S. Potok, D. A. Leigh, V. Aucagne and S. Papot, *Angew. Chem. Int. Ed.*, 2009, **48**, 6443-6447.
16. J. M. Baumes, J. J. Gassensmith, J. Giblin, J.-J. Lee, A. G. White, W. J. Culligan, W. M. Leevy, M. Kuno and B. D. Smith, *Nat. Chem.*, 2010, **2**, 1025-1030.
17. E. M. Pérez, D. T. F. Dryden, D. A. Leigh, G. Teobaldi and F. Zerbetto, *J. Am. Chem. Soc.*, 2004, **126**, 12210-12211.
18. F. Cacialli, J. S. Wilson, J. J. Michels, C. Daniel, C. Silva, R. H. Friend, N. Severin, P. Samori, J. P. Rabe, M. J. O'Connell, P. N. Taylor and H. L. Anderson, *Nat. Mater.*, 2002, **1**, 160-164.
19. Q.-C. Wang, D.-H. Qu, J. Ren, K. Chen and H. Tian, *Angew. Chem. Int. Ed.*, 2004, **43**, 2661-2665.
20. A. Mateo-Alonso, C. Ehli, D. M. Guldi and M. Prato, *Org. Lett.*, 2013, **15**, 84-87.
21. A. Mateo-Alonso, C. Ehli, D. M. Guldi and M. Prato, *J. Am. Chem. Soc.*, 2008, **130**, 14938-14939.

beyond small-molecules, including metal organic frameworks,[22-28] and polymers.[29-37]

One of the main reasons carbon nanotubes continue to attract ever-increasing attention[38-44] is their potential application in the field of organic electronics.[45-49] Any such applications will require a precise modulation of the electronic

22. V. N. Vukotic, C. A. O'Keefe, K. Zhu, K. J. Harris, C. To, R. W. Schurko and S. J. Loeb, *J. Am. Chem. Soc.*, 2015, **137**, 9643-9651.
23. K. Zhu, V. N. Vukotic, C. A. O'Keefe, R. W. Schurko and S. J. Loeb, *J. Am. Chem. Soc.*, 2014, **136**, 7403-7409.
24. V. N. Vukotic, K. J. Harris, K. Zhu, R. W. Schurko and S. J. Loeb, *Nat. Chem.*, 2012, **4**, 456-460.
25. P. R. McGonigal, P. Deria, I. Hod, P. Z. Moghadam, A.-J. Avestro, N. E. Horwitz, I. C. Gibbs-Hall, A. K. Blackburn, D. Chen, Y. Y. Botros, M. R. Wasielewski, R. Q. Snurr, J. T. Hupp, O. K. Farha and J. F. Stoddart, *Proc. Natl. Acad. Sci. U.S.A.*, 2015, **112**, 11161-11168.
26. A. Coskun, M. Hmadeh, G. Barin, F. Gándara, Q. Li, E. Choi, N. L. Strutt, D. B. Cordes, A. M. Z. Slawin, J. F. Stoddart, J.-P. Sauvage and O. M. Yaghi, *Angew. Chem. Int. Ed.*, 2012, **51**, 2160-2163.
27. Q. Li, W. Zhang, O. S. Miljanic, C. B. Knobler, J. F. Stoddart and O. M. Yaghi, *Chem. Commun.*, 2010, **46**, 380-382.
28. Q. Li, C.-H. Sue, S. Basu, A. K. Shveyd, W. Zhang, G. Barin, L. Fang, A. A. Sarjeant, J. F. Stoddart and O. M. Yaghi, *Angew. Chem. Int. Ed.*, 2010, **49**, 6751-6755.
29. X.-Q. Wang, W. Wang, G.-Q. Yin, Y.-X. Wang, C.-W. Zhang, J.-M. Shi, Y. Yu and H.-B. Yang, *Chem. Commun.*, 2015, **51**, 16813-16816.
30. J. Wang and X. Zhang, *ACS Nano*, 2015, **9**, 11389-11397.
31. E. M. Peck, W. Liu, G. T. Spence, S. K. Shaw, A. P. Davis, H. Destecroix and B. D. Smith, *J. Am. Chem. Soc.*, 2015, **137**, 8668-8671.
32. C. Hu, Y. Lan, K. R. West and O. A. Scherman, *Adv. Mater.*, 2015, **27**, 7957-7962.
33. A. Goujon, G. Du, E. Moulin, G. Fuks, M. Maaloum, E. Buhler and N. Giuseppone, *Angew. Chem. Int. Ed.*, 2016, **55**, 703-707.
34. A. Tamura and N. Yui, *Chem. Commun.*, 2014, **50**, 13433-13446.
35. H. W. Gibson, H. Wang, Z. Niu, C. Slebodnick, L. N. Zhakharov and A. L. Rheingold, *Macromolecules*, 2012, **45**, 1270-1280.
36. Z. Niu, F. Huang and H. W. Gibson, *J. Am. Chem. Soc.*, 2011, **133**, 2836-2839.
37. M. Lee, R. B. Moore and H. W. Gibson, *Macromolecules*, 2011, **44**, 5987-5993.
38. H. Dai, *Acc. Chem. Res.*, 2002, **35**, 1035-1044.
39. A. Jorio, G. Dresselhaus and M. S. Dresselhaus, in *Carbon Nanotubes: Advanced Topics in the Synthesis, Structure, Properties and Applications*, Top. Appl. Phys., 2008, vol. 111.
40. Z. Liu, S. Tabakman, K. Welsher and H. Dai, *Nano Res.*, 2009, **2**, 85-120.
41. N. Saito, Y. Usui, K. Aoki, N. Narita, M. Shimizu, K. Hara, N. Ogiwara, K. Nakamura, N. Ishigaki, H. Kato, S. Taruta and M. Endo, *Chem. Soc. Rev.*, 2009, **38**, 1897-1903.
42. J. M. Schnorr and T. M. Swager, *Chem. Mater.*, 2011, **23**, 646-657.
43. S. Park, M. Vosguerichian and Z. Bao, *Nanoscale*, 2013, **5**, 1727-1752.
44. D. Jariwala, V. K. Sangwan, L. J. Lauhon, T. J. Marks and M. C. Hersam, *Chem. Soc. Rev.*, 2013, **42**, 2824-2860.
45. H. Park, A. Afzali, S.-J. Han, G. S. Tulevski, A. D. Franklin, J. Tersoff, J. B. Hannon and W. Haensch, *Nat. Nanotech.*, 2012, **7**, 787-791.
46. A. D. Franklin, M. Luisier, S.-J. Han, G. Tulevski, C. M. Breslin, L. Gignac, M. S. Lundstrom and W. Haensch, *Nano Lett.*, 2012, **12**, 758-762.
47. C. Wang, D. Hwang, Z. Yu, K. Takei, J. Park, T. Chen, B. Ma and A. Javey, *Nat. Mater.*, 2013, **12**, 899-904.
48. Q. Cao, S.-j. Han, G. S. Tulevski, Y. Zhu, D. D. Lu and W. Haensch, *Nat. Nanotech.*, 2013, **8**, 180-186.
49. M. M. Shulaker, G. Hills, N. Patil, H. Wei, H.-Y. Chen, H. S. P. Wong and S. Mitra, *Nature*, 2013, **501**, 526-530.

properties of the nanotubes. To that end, several strategies for the covalent[50-54] or supramolecular[55-58] chemical modification of single wall carbon nanotubes (SWNT) have been developed. The main factor governing SWNT electronic properties is their chirality, but strategies for the noncovalent functionalization of SWNTs in a chirality selective-fashion are scarce.[59-63]

We have recently introduced the mechanical bond as a new tool for the chemical modification of SWNTs. In particular, we described the synthesis of rotaxane-type derivatives of SWNTs – the first example of mechanically interlocked SWNTs (MINTs).[64-66] With synthetic routes towards MINTs established, we decided to investigate the consequences of the mechanical bond on the properties of both SWNT and macrocycle(s).

Here, we report that the MINT-forming reaction proceeds in a chirality-selective fashion, favoring functionalization of smaller diameter SWNTs. Moreover, the mechanical bond shows distinctive effects on the electronic properties of macrocycles and nanotubes in MINTs. Our conclusions are based on the complete photophysical and electrochemical characterization of MINTs in comparison with pristine nanotubes, and whenever possible, the corresponding supramolecular model compounds. The experimental results are backed up by calculations at the molecular mechanics and DFT levels.

---

50. P. Singh, S. Campidelli, S. Giordani, D. Bonifazi, A. Bianco and M. Prato, *Chem. Soc. Rev.*, 2009, **38**, 2214-2230.
51. M. Kanungo, H. Lu, G. G. Malliaras and G. B. Blanchet, *Science*, 2009, **323**, 234-237.
52. J. Zhao, Y. Gao, J. Lin, Z. Chen and Z. Cui, *J. Mater. Chem.*, 2012, **22**, 2051-2056.
53. J. L. Delgado, P. de la Cruz, F. Langa, A. Urbina, J. Casado and J. T. López Navarrete, *Chem. Commun.*, 2004, 1734-1735.
54. R. Martín, F. J. Céspedes-Guirao, M. de Miguel, F. Fernández-Lázaro, H. García and Á. Sastre-Santos, *Chem. Sci.*, 2012, **3**, 470-475.
55. Y.-L. Zhao and J. F. Stoddart, *Acc. Chem. Res.*, 2009, **42**, 1161-1171.
56. A. Wurl, S. Goossen, D. Canevet, M. Sallé, E. M. Pérez, N. Martín and C. Klinke, *J. Phys. Chem. C*, 2012, **116**, 20062-20066.
57. S. D. Stranks, J. K. Sprafke, H. L. Anderson and R. J. Nicholas, *ACS Nano*, 2011, **5**, 2307-2315.
58. A. de Juan, A. López-Moreno, J. Calbo, E. Ortí and E. M. Pérez, *Chem. Sci.*, 2015, **6**, 7008-7014.
59. E. M. Pérez and N. Martín, *Org. Biomol. Chem.*, 2012, **10**, 3577-3583.
60. A. F. M. M. Rahman, F. Wang, K. Matsuda, T. Kimura and N. Komatsu, *Chem. Sci.*, 2011, **2**, 862-867.
61. G. Liu, F. Wang, S. Chaunchaiyakul, Y. Saito, A. K. Bauri, T. Kimura, Y. Kuwahara and N. Komatsu, *J. Am. Chem. Soc.*, 2013, **135**, 4805-4814.
62. G. Liu, Y. Saito, D. Nishio-Hamane, A. K. Bauri, E. Flahaut, T. Kimura and N. Komatsu, *J. Mater. Chem. A*, 2014, **2**, 19067-19074.
63. F. Vialla, G. Delport, Y. Chassagneux, P. Roussignol, J. S. Lauret and C. Voisin, *Nanoscale*, 2016, **8**, 2326-2332.
64. A. López-Moreno and E. M. Pérez, *Chem. Commun.*, 2015, **51**, 5421-5424.
65. A. de Juan, M. Mar Bernal and E. M. Pérez, *ChemPlusChem*, 2015, **80**, 1153-1157.
66. A. de Juan, Y. Pouillon, L. Ruiz-González, A. Torres-Pardo, S. Casado, N. Martín, Á. Rubio and E. M. Pérez, *Angew. Chem., Int. Ed.*, 2014, **53**, 5394-5400.

5.2 Results and Discussion

For all measurements, we have used CoMoCat (6,5) enriched SWNTs. The synthesis of MINTs was carried out with the U-shaped molecule **1**, depicted in Figure 1, which features two units of a π-extended tetrathiafulvalene (exTTF) as recognition motif towards SWNTs.[67,68] The experimental procedures for synthesis and purification have been described previously for other types of SWNTs.[66] Very briefly, we exploited the positive exTTF-SWNT interaction[67] to template the ring closing metathesis (RCM) of **1** around the nanotubes, to form MINTs (Figure 1). Unreacted **1**, non-threaded **2**, linear oligomers of **1**, formed in situ under the RCM reaction conditions, catalyst, etc. were removed by extensive washing with dichloromethane. The MINT$_{(6,5)}$-**2** samples used in these experiments showed a macrocycle loading of 32% by themogravimetric analysis. The extreme aspect ratio of the nanotubes guarantees the formation of cross-points between them, which act as stoppers and prevent de-threading of **2** in MINTs, even under reflux in tetrachloroethane (see the Experimental Details).[66]

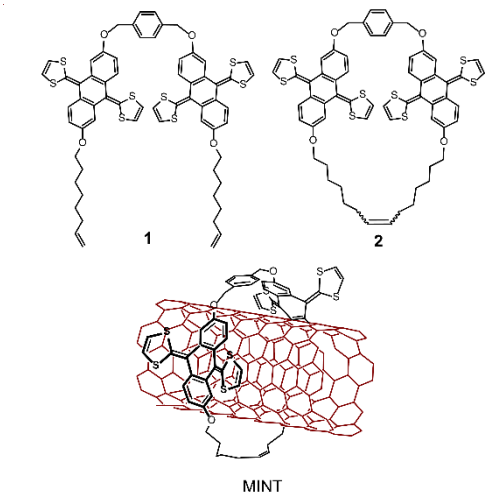

Figure 1. Structure of U-shape **1**, macrocycle **2** and schematic representation of the structure of MINTs.

Firstly, we characterized our samples by transmission electron microscopy (TEM). To that end, the samples were dispersed in methanol by using

67. C. Romero-Nieto, R. García, M. Á. Herranz, C. Ehli, M. Ruppert, A. Hirsch, D. M. Guldi and N. Martín, *J. Am. Chem. Soc.*, 2012, **134**, 9183-9192.
68. E. M. Pérez, B. M. Illescas, M. Á. Herranz and N. Martín, *New J. Chem.*, 2009, **33**, 228-234.

ultrasonication for 10 min. The sample dispersions were then applied onto Lacey-carbon grids by the suction method. Throughout the scanned areas, large bundles of SWNTs, on one hand, and individualized SWNTs wrapped with objects of appropriate size and shape to be identified as macrocycle **2**, on the other hand, were noted. Representative images are shown in Figure 2, where several individual macrocycles are highlighted with white arrows. The micrographs are therefore in perfect agreement with the formation of MINT$_{(6,5)}$-**2**. In contrast, pristine (6,5)-SWNTs show clean walls under TEM (see in the Experimental Details). To complement the TEM microscopy characterization, we used atomic force microscopy (AFM). The samples were suspended in tetrachloroethane (TCE) by sonication for 1 hour and the suspension was spin coated over mica. Figure 2d shows a representative image of an individual SWNT that presents two objects with suitable height (ca. 2 nm, see calculations below) to be macrocycles around (and not on top of) the nanotube. As expected, AFM images of pristine (6,5)-SWNTs did not show any protuberances of this kind.

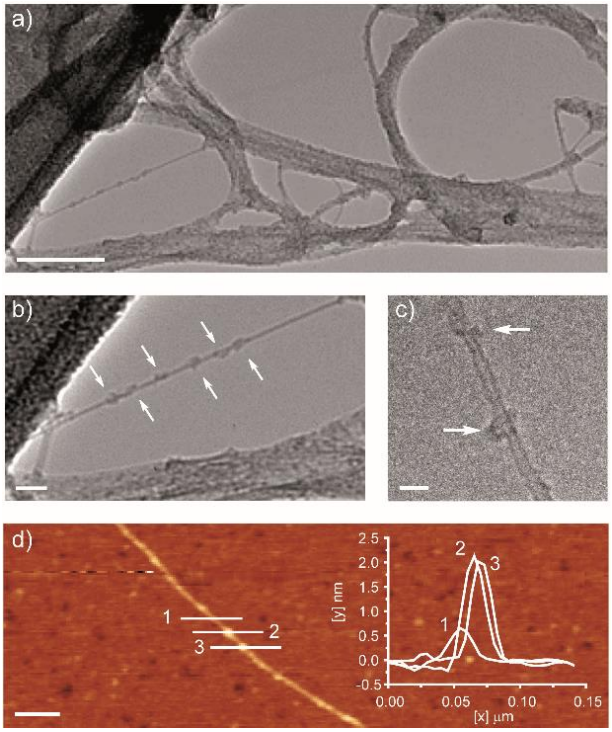

Figure 2. (a-c). Transmission electron micrographs (80 kV) of freestanding MINT$_{(6,5)}$-**2** applied on a Lacey carbon/Cu film. (d) AFM image of MINT$_{(6,5)}$-**2** sample deposited on mica substrate, showing a single SWNT

with two macrocycles and height profiles across the nanotube (1) and the macrocycles (2 and 3). Scale bars are 50 nm for (a), 10 nm for (b), 2 nm for (c), and 100 nm for (d).

To investigate the influence of the mechanically bound macrocycle **2** on the electronic structure of SWNTs, we performed a series of comparative spectroscopic assays with $MINT_{(6,5)}$-**2** and pristine (6,5)-SWNTs, including steady state absorption and emission spectroscopy, Raman spectroscopy, and femtosecond transient absorption spectroscopy. To this end, complementary spectroscopic studies were conducted with the nanotube and MINT samples suspended in D_2O with the help of sodium dodecyl benzenesulfonate (SDBS) as a surfactant. Additionally, we performed experiments with sodium dodecyl sulfate (SDS), which corroborate our SDBS findings and are presented in the Experimental Details.

Steady state absorption spectra give rise to typical absorption features of S_{22} transitions in the visible and S_{11} transitions in the near-infrared region of the spectrum (Figure 3). For instance, prominent absorptions for (6,5)-SWNTs at 569 and 979 nm together with less-intense absorptions of (7,6)-SWNTs, at 647 and 1138 nm, are detected for the pristine nanotube sample. Although TEM micrographs corroborate the high degree of functionalization for $MINT_{(6,5)}$-**2**, the typical absorption of the exTTF chromophore is not noticeable, as we have previously observed.[64,66] The $MINT_{(6,5)}$-**2** spectrum failed to exhibit major changes as far as absorption maxima are concerned. Nevertheless, a slight broadening as well as an overall intensity decrease of the absorption features for $MINT_{(6,5)}$-**2** point to weak electronic interactions between the exTTF macrocycles and SWNTs in the ground state. Baseline correction and subsequent normalization of the absorption spectra of the nanotubes and $MINT_{(6,5)}$-**2** shed light onto intensity variations in the ratio between peaks of different SWNT chiralities. Upon normalizing the absorption relative to the 1138 nm intensity (Figure 3) the (6,5)-SWNT related absorption peak appears significantly weaker in $MINT_{(6,5)}$-**2** than in the pristine nanotubes. These observations point to a noticeable effect of the nanotube chirality on the electronic interactions in the MINT sample.

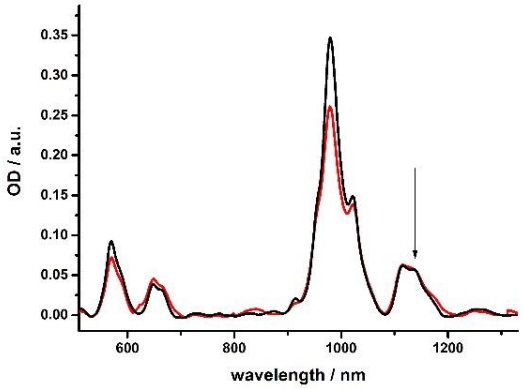

Figure 3. Absorption spectra of (6,5)-enriched SWNTs (black) and MINT$_{(6,5)}$-**2** (red) in D_2O/SDBS (1 wt%) at room temperature – the spectra have been base-line corrected and normalized to the 1138 nm absorption.

In addition to absorption, fluorescence of the different samples was probed. Selective excitation with various wavelengths in a range between 530-800 nm leads to characteristic fluorescence features of (6,5), (8,4), (8,3), (7,5), and (7,6) SWNTs in the near-infrared region. Even at first glance, the 3D fluorescence maps of SWNTs and MINT$_{(6,5)}$-**2** reveal striking differences (Figure 4). In particular, appreciable fluorescence intensity variations are noted between the pristine and mechanically interlocked samples. The aforementioned is accompanied by a macrocycle-induced red shift of the fluorescence maxima from 986, 1121, 965, 1029 and 1130 nm in SWNTs to 991, 1127, 968, 1033 and 1133 nm in MINT$_{(6,5)}$-**2**. The individual emission spectra, shown in the Experimental Details, clearly demonstrate the selective fluorescence quenching of smaller diameter SWNTs such as (6,5), (8,3), and (7,5), when compared to the slightly larger (8,4) and (7,6), in line with our observations in absorption. Given the similar electronic nature of these chiralities, this selective quenching most likely stems from a higher degree of functionalization with macrocycle **2**.

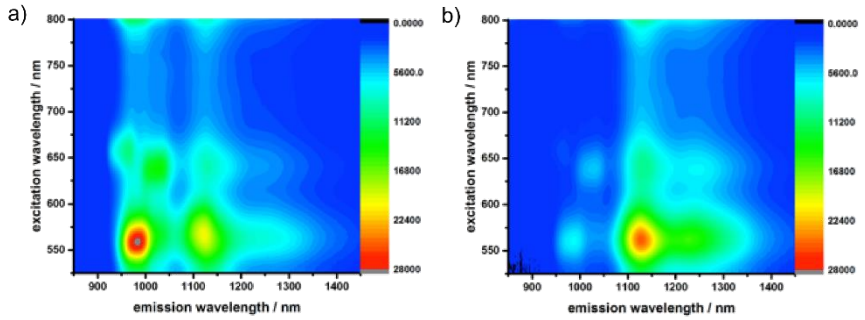

Figure 4. 3D NIR fluorescence spectra of (a) (6,5)-enriched SWNTs and (b) $MINT_{(6,5)}$-**2** in D_2O/SDBS (1 wt%) measured with an OD of 0.35 at 570 nm.

We also recorded Raman spectra of SWNTs and $MINT_{(6,5)}$-**2** with λ_{exc} = 532, 785 and 1064 nm. The results are shown in Figure 5. The left panels of the figure show a comparison of the G-band of (6,5)-enriched SWNTs (black) and $MINT_{(6,5)}$-**2** (red), which reveals quantitatively small up-shifts for all three excitation wavelengths, namely from 1573 to 1575, 1577 to 1582 and 1590 to 1591 cm^{-1}, respectively. This observation points to weak charge-transfer interactions between electron donating exTTF and SWNT in the ground state, and is in accordance with our previous observations.[66]

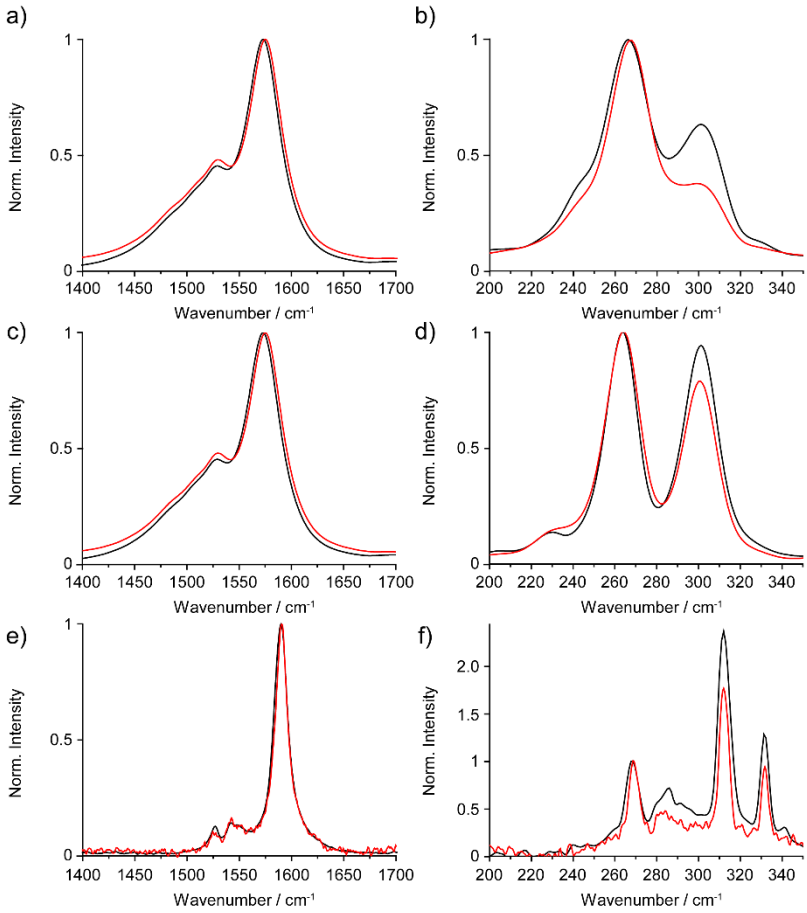

Figure 5. Raman spectra (λ_{exc} = 532, 785 and 1064 nm from top to bottom) of SWNTs (black) and MINT$_{(6,5)}$-**2** (red). Left: Comparison of the G-band. Right: Comparison of the RBMs.

The size selectivity was investigated by careful analysis of the low frequency radial breathing mode (RBM) bands (Figure 5, right panels). For the on-resonance spectra, two RBMs were detected at 265 and 301 cm^{-1}, corresponding to (7,6) and (6,5)-SWNTs. When the Raman spectra are recorded with 1064 nm excitation, three main RBM features, at 268, 311, and 331 cm^{-1} originating from (7,6), (6,5), and (6,4)-SWNTs, respectively, were detected. When the spectra were normalized with respect to the (7,6)-RBM intensity, a noticeable decrease in the intensity of the RBMs corresponding to (6,5) and (6,4) SWNTs was observed in MINT$_{(6,5)}$-**2** (red) when compared to pristine nanotubes with all three excitation wavelengths. Although the Raman-based evidence is less compelling, the relative intensity decrease of the RBM features assigned to the smaller

nanotubes is in line with the observations described for absorption and emission data. In summary, MINT-forming reaction favours functionalization of the smaller SWNTs diameter, in good agreement with theoretical predictions – *vide infra*.

To investigate the impact of the mechanically bound **2** on the excited state dynamics of SWNTs, we performed femtosecond transient absorption spectroscopic measurements. A set of transient absorption spectra of MINT$_{(6,5)}$-**2** with time delays from 0 to 125 ps are shown in Figure 6. The spectra are dominated by the instantaneously occurring ground state bleaching of the S_{11} transitions in the near infrared and the S_{22} transitions in the visible. The minima are located at 570, 648, 983, and 1121 nm. Features, which are assigned to excited state absorption, are found at 483, 531, 610, 711, 1072 and >1200 nm. In reference measurements with (6,5)-enriched SWNTs these features appear marginally blue-shifted. Considering the coverage in MINT$_{(6,5)}$-**2** in comparison to noncovalent SWNT hybrids, in which SWNTs are densely covered with exTTF, small shifts are likely to evolve.[67-70]

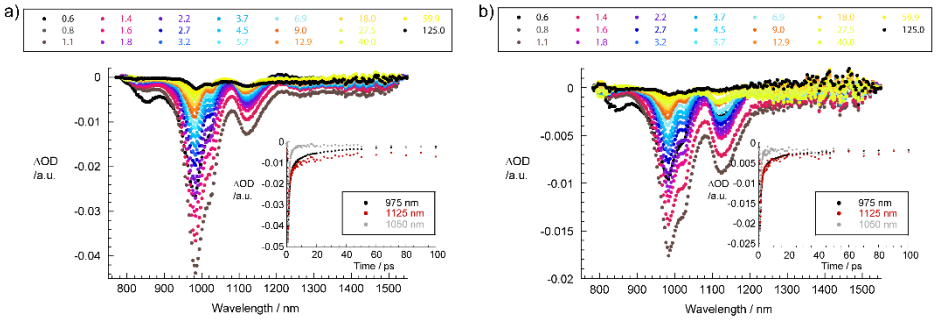

Figure 6. Differential absorption spectra obtained upon femtosecond pump probe experiments (λ_{exc} = 387 nm) of (a) (6,5)-enriched SWNTs and (b) MINT$_{(6,5)}$-**2** in SDBS/D_2O (1 wt%) with several time delays between 0.6 and 125 ps at room temperature.

More important are the differences in the temporal analyses of the excited state decays in MINT$_{(6,5)}$-**2** compared to the unfunctionalized SWNTs. For example, fitting the kinetic decay of the ground state bleaching of (6,5)-enriched SWNTs in SDBS, which give rise to the stronger fluorescence quenching, at 1000 nm yields three lifetimes of 230, 8, and 1 ps. The two shorter components

69. C. Romero-Nieto, R. García, M. Á. Herranz, L. Rodríguez-Pérez, M. Sánchez-Navarro, J. Rojo, N. Martín and D. M. Guldi, *Angew. Chem. Int. Ed.*, 2013, **52**, 10216-10220.
70. V. Strau, A. Gallego, G. d. l. Torre, T. W. Chamberlain, A. N. Khlobystov, T. Torres and D. M. Guldi, *Faraday Discuss.*, 2014, **172**, 61-79.

are attributed to inter-band or inter-tube charge carrier recombination, while the longer component is characteristic for the radiative exciton recombination. Notably, the lifetimes for MINT$_{(6,5)}$-**2** are drastically shortened compared to the values obtained in the SWNT reference, namely 80, 6, and 1 ps. In the insets of Figure 6, representative time profiles taken at different wavelengths for MINT$_{(6,5)}$-**2** and pristine nanotubes are compared. Please note that features of the one electron oxidized exTTF appear as a rather broad positive absorption at ~680 nm.[67,71] In MINT$_{(6,5)}$-**2**, this wavelength range is, however, dominated by ground state bleaching of SWNT related S_{22} transitions. A weak positive signal at 700 nm is discernable and taken as evidence for the exTTF oxidation (see the Experimental Details). In terms of SWNT reduction, we turn to the 1200 to 1600 nm range, where the broad and positive absorption is in line with spectroelectrochemical reduction of SWNTs. Based on this spectroscopic comparison we postulate that photoexcitation of MINT$_{(6,5)}$-**2** is followed by charge separation – 6 ps – affording a metastable charge separated state. Charge recombination – 80 ps – leads to the population of the ground state.

Turning to the weakly quenched fluorescent MINT$_{(7,6)}$-**2** fit at 1130 nm the kinetics are 270, 8, and 1 ps in comparison to 350, 12, and 1 ps obtained in the reference measurements with unfunctionalized SWNTs in SDBS. Thus, relative to the shortening of the lifetimes observed with the smaller (6,5)-SWNTs, the impact on the larger (7,6)-SWNTs is less pronounced.

A fair comparison of the photophysical properties of the supramolecular complexes SWNT + **2** vs. MINT$_{(6,5)}$-**2** was prevented by the insolubility of macrocycle **2** in aqueous solutions. However, this observation further confirms the mechanical link between the nanotubes and **2** in MINT$_{(6,5)}$-**2**, which allows for the solubilization of the non-polar **2** in water. Such radical changes in solubility are one of the earliest and most frequent observations in the chemistry of MIMs, and are one of the fingerprints of the mechanical bond.[72]

To investigate the influence of the mechanical link on the redox properties of macrocycle **2**, we studied the electrochemical behavior of solutions/suspensions containing **1**, **2**, and MINT$_{(6,5)}$-**2**, as well as mixtures of **1** or **2** with (6,5)-SWNT

71. S. S. Gayathri, M. Wielopolski, E. M. Pérez, G. Fernández, L. Sánchez, R. Viruela, E. Ortí, D. M. Guldi and N. Martín, *Angew. Chem. Int. Ed.*, 2009, **48**, 815-819.
72. A. G. Johnston, D. A. Leigh, A. Murphy, J. P. Smart and M. D. Deegan, *J. Am. Chem. Soc.*, 1996, **118**, 10662-10663.

with identical loading of exTTF material. In particular, we used 0.34 mg mL^{-1} of $MINT_{(6,5)}$-**2** suspended in 0.1 M TBAP/DMF (TBAP = tetrabutylammonium perchlorate). In this case, the use of an organic solvent allows for comparison of the mechanically interlocked sample with the relevant supramolecular associates. In particular, we utilized SWNT + **1** and SWNT + **2** mixtures composed of 0.34 mg mL^{-1} of SWNT and 0.16 mg mL^{-1} of either **1** or **2**, which were also suspended in 0.1 M TBAP/DMF. As references, U-shape and macrocycle measurements, 0.16 mg mL^{-1} of either **1** or **2** were dissolved in 0.1 M TBAP/DMF. As shown in Figure 7, in all cases cyclic voltammograms show a reversible redox couple at around 0.26 V, which is ascribed to the two-electron oxidation/reduction of exTTF.[73,74]

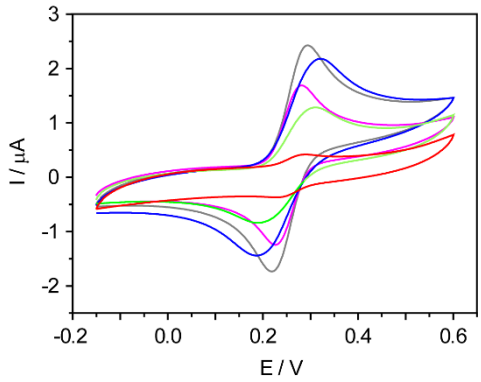

Figure 7. Cyclic voltammetry (room temperature, 10 mV s^{-1}, 0.1 M TBAP in DMF, glassy carbon as working electrode, Pt wire as counter electrode, specific calomel electrode 1 M LiCl for organic media as reference electrode) of 0.1 mg mL^{-1} **1** (gray), and **2** (pink); 0.16 mg mL^{-1} **1** + 0.34 mg mL^{-1} (6,5)-SWNT(blue); 0.16 mg mL^{-1} **2** + 0.34 mg mL^{-1} (6,5)-SWNT (green) and 0.34 mg mL^{-1} $MINT_{(6,5)}$-**2** (red).

Table 1 shows the anodic (E_a) and cathodic (E_c) peak potentials, the formal potential ($E^{0\prime}$), as well as their separation ($\Delta E_p = E_c - E_a$) taken from cyclic voltammograms as shown in Figure 7. The first observation is that the formal potential remains basically invariable for all samples, which supports the lack of significant charge-transfer from exTTF to the SWNTs in the ground state, as observed in the absorption and Raman assays – *vide supra*. The exTTF oxidation/reduction becomes more irreversible for **2** relative to **1**. Upon mixing with SWNTs this tendency holds, but the peak separation is reduced for both species, which indicates a better electron transfer and a more reversible process thanks to the interactions with SWNTs. This effect is much stronger in $MINT_{(6,5)}$-

73. S.-G. Liu, I. Pérez, N. Martín and L. Echegoyen, *J. Org. Chem.*, 2000, **65**, 9092-9102.
74. M. R. Bryce and A. J. Moore, *Synth. Met.*, 1988, **27**, 557-561.

2, indicating that there is a distinctive and more intimate interaction between the macrocycle and the nanotubes in the mechanically interlocked sample when compared to the **2** + SWNT supramolecular construct.

Table 1. Anodic, cathodic, formal and peak potential separation extracted from the voltammograms of Figure 7.

Sample	E_a / mV	E_c / mV	$E^{o\prime}$ / mV	ΔE_p / mV
1	291	221	256	70
2	315	195	255	120
1 + SWNTs	279	28	254	51
2 + SWNTs	303	198	251	105
$MINT_{(6,5)}$-**2**	282	238	260	44

Moreover, different current intensities are observed for the different solutions/suspensions. The current intensities observed in the presence of the supramolecular models, **1** + SWNT and **2** + SWNT, are lower than those for **1** and **2** in the absence of the nanotubes. Considering that the concentrations of **1** and **2** were the same for all four samples (0.16 mg mL^{-1}), the current intensity is proportional to the square root of diffusion coefficient of each species. Thus, the lower diffusion coefficients of the mixtures with SWNTs, compared to that of pure **1** and **2**, suggests that there is a partial adsorption of the latter on the nanotube surface. In accordance with the observations on the peak potentials, the decrease in current intensity is more evident in the case of $MINT_{(6,5)}$-**2**, again pointing to stronger interactions between the (6,5)-SWNTs and the macrocycles.

To study the consequences of this different interaction between SWNTs and the electroactive exTTFs in more detail, we have deposited equivalent amounts of the suspensions and solutions described above onto GC electrodes by drop casting. After drying in the dark – to avoid the photodecomposition of the electroactive molecule – under ambient conditions, the resulting modified electrodes were transferred to an electrochemical cell containing clean electrolyte (0.1 M TBAP in DMF) and cyclic voltammograms at different scan rates were recorded. Figure 8a-c shows the results of these experiments. In all

cases, the voltammograms show the typical shape of a surface-confined redox couple with small, although not zero, ΔE_p. They also show chemically reversible but electrochemically quasi-reversible charge-transfer kinetics for the exTTF/exTTF^{2+} couple (+0.2 V vs. SCE), as indicated by their voltammetric wave-shape and changes in oxidative and reductive peak potentials (ΔE_p) as a function of sweep rate. The linear dependence of the anodic and cathodic peak currents (see the Experimental Details) with the potential sweep rate also confirms that the redox couple is confined to the electrode surface.[75]

We performed Laviron analysis from the cyclic voltammetry of the three configurations shown in Figure 8a-c to assess how the presence of the mechanical bond in MINT$_{(6,5)}$-**2** affects the electron-transfer rates as compared to **1** or **2** when they are supramolecularly attached to the carbon nanotubes. The results are summarized in Figure 8d-f.

In all cases, the peak potentials (E_p) in the anodic and cathodic scans converge to the values of the formal potential $E^{0\prime}$ at low scan rates (ν), whereas larger peak separations are observed at higher scan rates. The symmetry and the similar slopes in the linear parts of each plot for the anodic and cathodic branches suggest a transfer coefficient α of around 0.5. Analyses of the scan rate dependence yield significantly different charge-transfer rate constants for the MINT sample (21.4 s^{-1}) and the supramolecular models (26.1 s^{-1} for both **1** + (6,5)-SWNT and **2** + (6,5)-SWNT). Such differences confirm the fundamentally different type of interaction between the electroactive molecule and the carbon nanotube in the presence or absence of the mechanical bond, as they demonstrate a better disposition of the electroactive exTTF fragment to interact with the electrode surface in the case of the supramolecular models.

75. R. H. Wopschall and I. Shain, *Anal. Chem.*, 1967, **39**, 1514-1527.

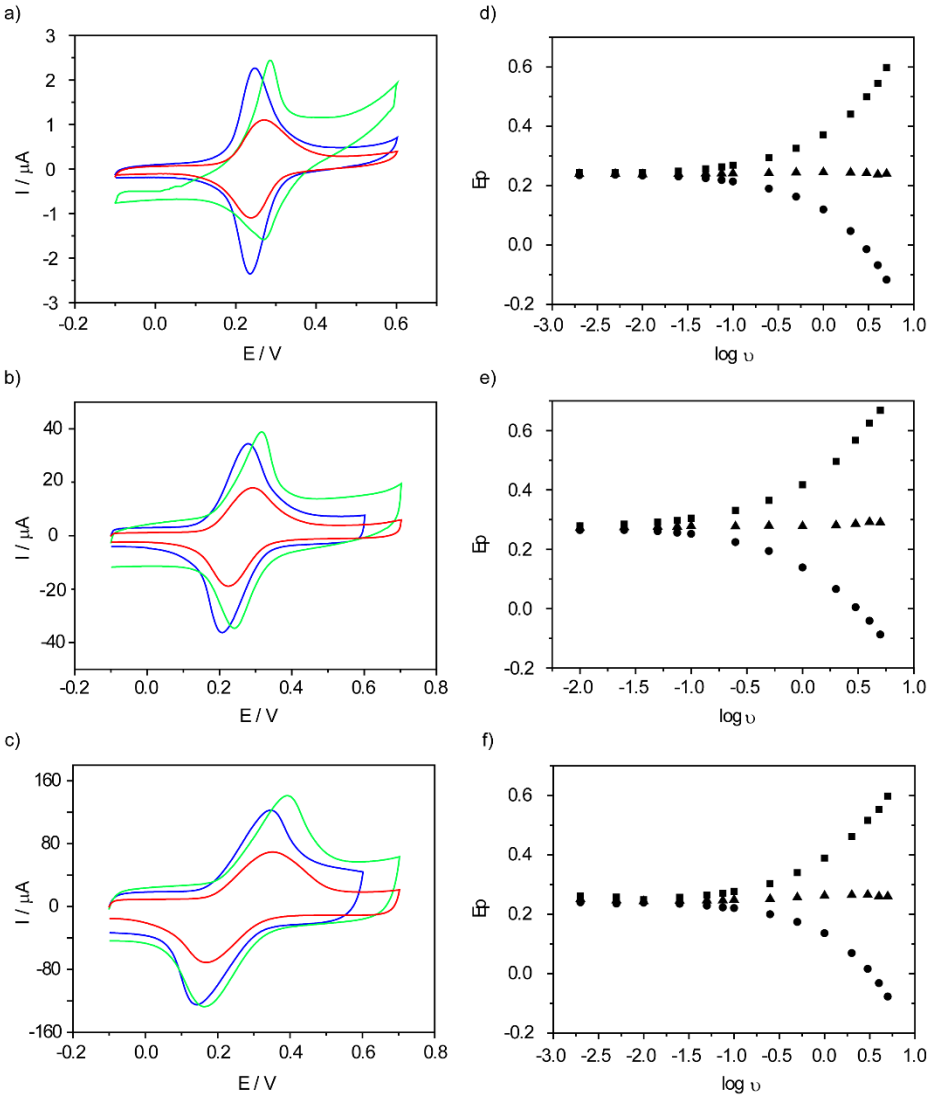

Figure 8. Drop casting modified electrode with **1** + (6,5)-SWNT (blue), **2** + (6,5)-SWNT (green) and MINTs (red), electrochemical behavior in DMF/0.1 M TBAP at (a) 10 mV s^{-1}, (b) 100 mV s^{-1} and (c) 500 mV s^{-1}. Laviron plots of (d) **1** + (6,5)-SWNT; (e) **2** + (6,5)-SWNT and (f) $MINT_{(6,5)}$-**2**; peak potentials at different scan rates (0.005 to 5 V s^{-1}) on GC electrodes. (■) E_{an}-oxidation peak potential, (●) E_{ca}-reduction peak potential and (▲) (E_{an} + E_{ca})/2 formal potential.

Finally, we have performed chronoamperometric measurements to quantify the diffusion coefficients of **1**, **2**, **1** + SWNT, **2** + SWNT, and MINTs, using a rotating ring-disc electrode (RRDE). Diffusion coefficients are a direct measurement of the size of the electroactive entity and, thus, any significant differences in the diffusion coefficient of **1** or **2** directly relate to their interaction

with the SWNTs. Figure 9 shows the linear fits from chronoamperometric experiments at glassy carbon RRDE. We started recording the current intensity when the potential at the disc is competitive with the oxidation of exTTF. At this moment, exTTF is oxidized at both the disk and the ring. Consequently, the current intensity collected at the ring decreases, due to competitive processes. The time at which the current decreases (transit-time) is a function of the rotating rate, as explained in the Experimental Details.[76,77] As the rotating rate (ω) increases, the oxidized species needs less time at the disc to arrive to the ring. In turn, fewer of the species to be oxidized reaches the ring electrode and the current intensity decreases.

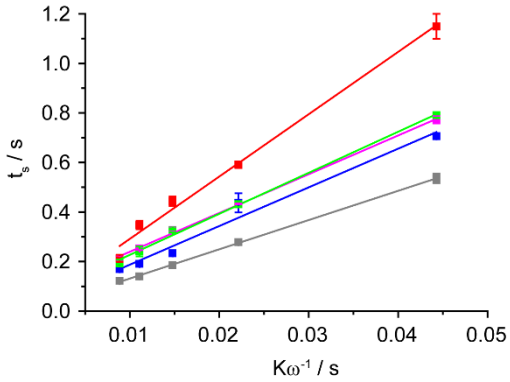

Figure 9. Transit time (t_s) vs. $K\omega^{-1}$ plot enabling diffusion coefficient determination of **1** (gray), **2** (pink), **1** + (6,5)-SWNT (blue), **2** + (6,5)-SWNT (green) and $MINT_{(6,5)}$-**2** (red).

In the absence of SWNTs, **1** and **2** show diffusion coefficients of 5.73 and 2.38 x 10^{-6} cm^2 s^{-1}, respectively. As expected, **1** shows a significantly larger diffusion coefficient, due to its quasi 1-D geometry in its extended configuration. Macrocycle **2**, on the other hand, is approximately disk-shaped. In the presence of SWNTs, the diffusion coefficient of **1** decreases significantly to 2.29 x 10^{-6} cm^2 s^{-1} as a consequence of its interaction with the carbon nanotubes. The tendency with **2** is the same, but quantitatively speaking the decrease is much smaller for **2** + SWNTs, for which a diffusion coefficient of 2.01 x 10^{-6} cm^2 s^{-1} was measured. Notably, the calculated diffusion coefficient is the average value of the diffusion coefficients of the electroactive species present in solution. A larger concentration of species bound to the carbon nanotube would lead to a

76. M. Chatenet, M. B. Molina-Concha, N. El-Kissi, G. Parrour and J. P. Diard, *Electrochim. Acta*, 2009, **54**, 4426-4435.
77. S. Bruckenstein and G. A. Feldman, *J. Electroanal. Chem.*, 1965, **9**, 395-399.

more pronounced decrease in the diffusion coefficients. Therefore, the experimental values reflect a more efficient interaction of **1** with SWNTs compared to **2**. Finally, $MINT_{(6,5)}$-**2** show a diffusion coefficient of 5.8×10^{-7} $cm^2\ s^{-1}$, that is, a decrease of nearly one order of magnitude with respect to **1** and **2**. Such a pronounced decrease in the diffusion coefficient is yet one more proof of fundamentally irreversible interactions between the macrocycle and the carbon nanotube in MINTs. As macrocycles and SWNTs are mechanically interlocked in MINTs, no dissociation takes place, so the diffusion coefficient of the electroactive species approaches that of the larger nanotubes.

We have also modelled the MINTs at the Molecular Mechanics (MM) and Quantum Mechanical (QM) levels. For MM, we have used the MMFF94 force field to identify the SWNTs compatible with each macrocycle and facilitate the preparation of the experiments. Although we were mostly interested in a qualitative description of the bonding, we remained attentive to the limitations of this force field and only considered its results with an error bar of 10 kcal mol^{-1}, which is almost twice as much as its standard deviation with respect to ab initio calculations.[78] In this simplified description, if the diameter of the SWNT is smaller than the cavity of the macrocycle, its wall will have a small attractive effect on the molecule. The equilibrium geometries show that the thinner the SWNT are the more the macrocycle tends to fold around it – as much as permitted by its own internal structure – and the more the alkyl chain spreads over the surface of the SWNT, establishing positive dispersion interactions. In this case, the closing of the ring around SWNTs is favored by a template effect, and the absolute limit corresponds to the smallest existing diameter of around 0.4 nm. However, if the SWNT diameter is larger than the cavity of the macrocycle, the closing of the ring will only occur within the flexibility limits of the alkyl chain. In turn, the interactions between the SWNT and the macrocycle become repulsive. To obtain the upper diameter limit, we optimized the geometry of the closed macrocycle around SWNTs of increasing diameters until their interaction energy reaches half the opposite of a C–H bond, namely 40 kcal mol^{-1}. This is meant to remain well below the limit of what would become covalent bonding between SWNTs and the macrocycle. Furthermore, we take this as the limit at which we cannot apply the force field anymore. Using these criteria, we define a favourable region for the formation of MINTs and allow for

78. T. A. Halgren and R. B. Nachbar, *J. Comput. Chem.*, 1996, **17**, 587-615.

the automatic screening of a broad range of SWNTs. The results for **2** are summarised in Figure 10 (full dataset and details can be found in the Experimental Details). All SWNT chiralities presented in the sample are indeed found in the favourable diameter and energy ranges for the formation of the MINTs. In agreement with the absorption and Raman data, we observe that the smaller (6,5) SWNTs show significantly more favourable interaction energy than the larger (7,6), in particular, we have calculated -40 kcal mol^{-1} and -10 kcal mol^{-1}, respectively.

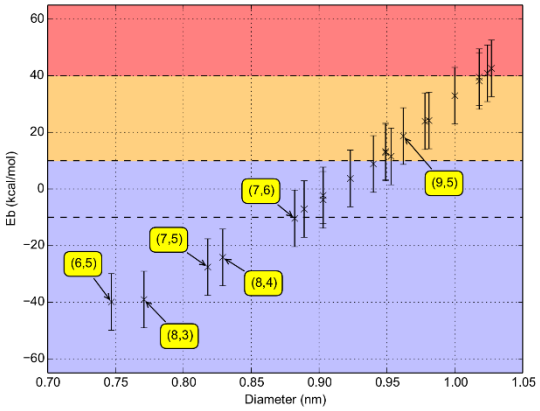

Figure 10. Interaction energies of a series of SWNTs with macrocycle **2** (negative = attractive). Error bars of 10 kcal mol^{-1} have been represented for each combination. Blue: most favorable formation energy range. Orange: unfavorable formation energy range. Red: limit of the model. The SWNT chiralities observed experimentally have been labelled, as well as the largest diameter in the favourable area. The complete dataset is available in the Experimental Details.

At the QM level, we have used Density Functional Theory (DFT) with a 6-31(d) Gaussian basis set and the PBE exchange – correlation functional, as implemented in the Gaussian 09 software package,[79] to model the charge transfer between **2** and (6,5)-SWNT. The results have been further processed with the

79. M. J. Frisch, G. W. Trucks, H. B. Schlegel, G. E. Scuseria, M. A. Robb, J. R. Cheeseman, G. Scalmani, V. Barone, B. Mennucci, G. A. Petersson, H. Nakatsuji, M. Caricato, H. P. H. X. Li, A. F. Izmaylov, J. Bloino, G. Zheng, J. L. Sonnenberg, M. Hada, M. Ehara, K. Toyota, R. Fukuda, J. Hasegawa, M. Ishida, T. Nakajima, Y. Honda, O. Kitao, H. Nakai, T. Vreven, J. A. Montgomery, J. E. P. Jr., F. Ogliaro, M. Bearpark, J. J. Heyd, E. Brothers, K. N. Kudin, V. N. Staroverov, R. Kobayashi, J. Normand, K. Raghavachari, A. Rendell, J. C. Burant, S. S. Iyengar, J. Tomasi, M. Cossi, N. Rega, J. M. Millam, M. Klene, J. E. Knox, J. B. Cross, V. Bakken, C. Adamo, J. Jaramillo, R. Gomperts, R. E. Stratmann, O. Yazyev, A. J. Austin, R. Cammi, C. Pomelli, J. W. Ochterski, R. L. Martin, K. Morokuma, V. G. Zakrzewski, G. A. Voth, P. Salvador, J. J. Dannenberg, S. Dapprich, A. D. Daniels, Ö. Farkas, J. B. Foresman, J. V. Ortiz, J. Cioslowski and G. D. J. Fox, *Gaussian 09 (Revision B.01), Gaussian Inc., Wallingford CT., 2009*

VESTA software package.[80] Both molecules remain neutral, in agreement with the small charge-transfer interactions observed spectroscopically, with a very small overlap between a few hydrogen atoms of the alkyl chain of **2** and the SWNT. As shown in Figure 11a, the density overlap between the two components occurs at levels below 0.014 a.u. The weakness of their bonding is further confirmed by the contour plot in Figure 11b for low densities, where the contour slopes are extremely steep. The interaction of **2** with the SWNT is therefore based on dispersion interactions only, which opens up the intriguing possibility of **2** moving freely along the SWNT.[81]

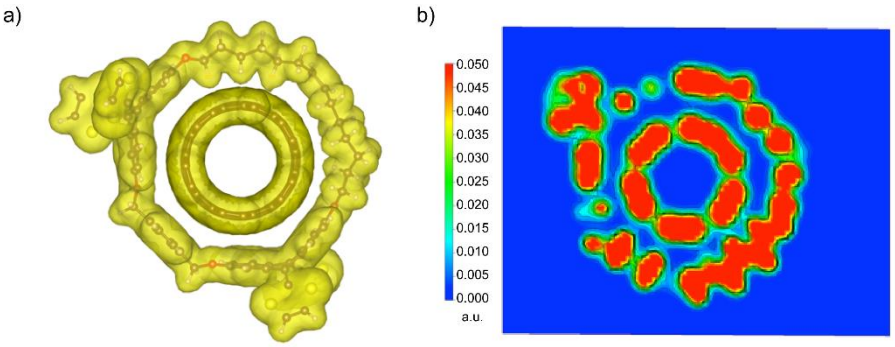

Figure 11. (a) Isosurface plot of the electronic density at 0.014 a.u., corresponding to the level where the intermolecular density bridges the SWNT and the macrocycle. (b) Contour plot of the density from 0 (blue) to 0.05 a.u. (red) within the plane defined by the maximum intermolecular density.

5.3 Conclusion

This is the first report in which ample evidence for the influence of the mechanical bond on the properties of SWNTs is provided. Our results demonstrate that the formation of MINTs goes hand in hand with distinct effects on the carbon nanotubes, clearly different from what is found in non-interlocked supramolecular references.

In particular, we have described the synthesis and comprehensive characterization of MINTs based on (6,5)-enriched SWNTs and macrocycle **2**. TEM microscopy is consistent with the formation of rotaxane-type species. Raman, UV-vis-NIR absorption and vis-NIR steady state fluorescence indicate

80. K. Momma and F. Izumi, *J. Appl. Crystallogr.*, 2011, **44**, 1272-1276.
81. S. Freddi, L. D'Alfonso, M. Collini, M. Caccia, L. Sironi, G. Tallarida, S. Caprioli and G. Chirico, *J. Phys. Chem. C*, 2009, **113**, 2722-2730.

that the MINT-forming reaction is diameter-selective, which, together with the remarkable kinetic stability of MINTs,[3,64-66] suggests that mechanical interlocking could be a valuable strategy for the purification of complex mixtures of SWNTs. In the ground state, there is no significant charge-transfer between the electron donating exTTF and the SWNTs. However, in the excited state, transient absorption spectroscopy prompt to the efficient charge-transfer between the exTTF macrocycles as electron donors and SWNTs as electron acceptors.

The significantly different charge-transfer rate constants for MINTs and the supramolecular models confirm the different type of interactions between the exTTF and SWNT in the presence or absence of the mechanical bond. In addition, significant differences in the diffusion coefficients reflect irreversible interactions between the macrocycle and SWNT in MINTs.

From the multi-level theoretical description, we are able to preselect the best SWNT candidates for MINT functionalization and check the absence of covalent bonding between SWNTs and the macrocycles. The screening at the MM level can also be automated to accelerate the matching of SWNT macrocycle pairs. As an add-on, the MM description is able to quickly provide relevant information about the overall flexibility of the macrocycles and has been used to eliminate precursors, which would be too rigid to close around SWNTs, before trying their synthesis experimentally.

5.4 Experimental details

5.4.1 Synthesis

General. All solvents were dried according to standard procedures. Reagents were used as purchased. All air-sensitive reactions were carried out under argon atmosphere. Flash chromatography was performed using silica gel (Merck, Kieselgel 60, 230-240 mesh, or Scharlau 60, 230-240 mesh). Analytical thin layer chromatographies (TLC) were performed using aluminium-coated Merck Kieselgel 60 F254 plates. NMR spectra were recorded on a Bruker Avance 400 (^{1}H: 400 MHz; ^{13}C: 100 MHz), spectrometers at 298 K, unless otherwise stated, using partially deuterated solvents as internal standards. Coupling constants (J) are denoted in Hz and chemical shifts (δ) in ppm. Multiplicities are denoted as

follows: s = singlet, d = doublet, t = triplet, m = multiplet, b = broad. Electrospray ionization mass spectrometry (ESI-MS) and Matrix-assisted Laser desorption ionization (coupled to a Time-Of-Flight analyzer) experiments (MALDI-TOF) were recorded on a HP1100MSD spectrometer and a Bruker REFLEX spectrometer, respectively. Thermogravimetric analyses (TGA) were performed using a TA Instruments TGAQ500 with a ramp of 10 °C/min under air from 100 to 1000 °C.

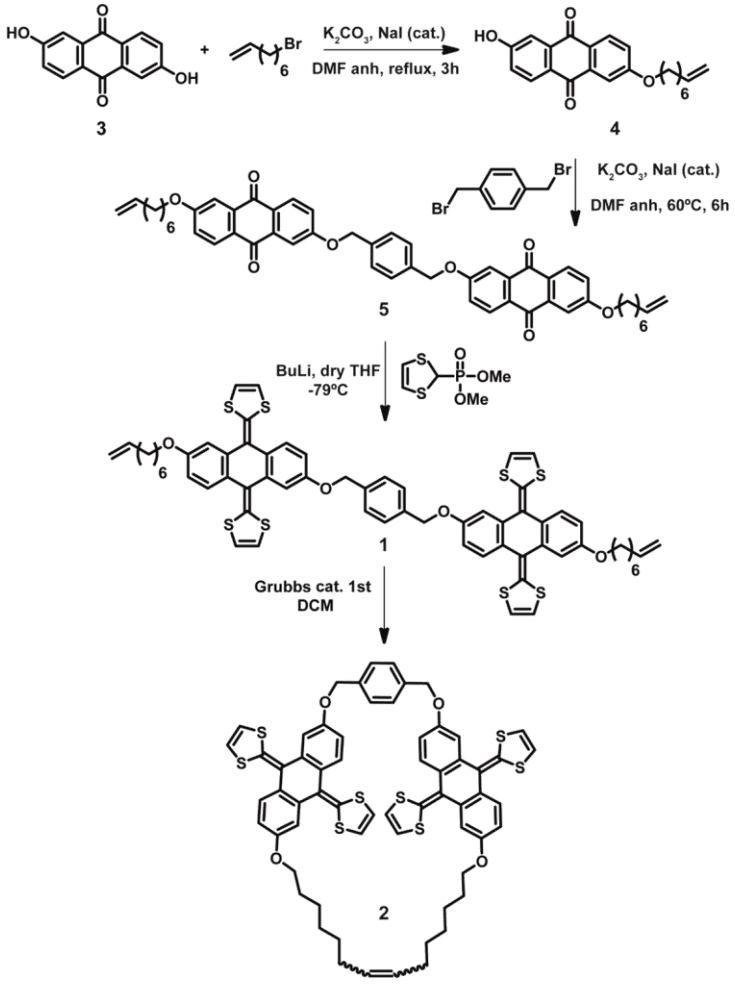

Figure S1. Synthetic scheme towards **1** and **2**.

Compounds **1** and **2** were synthetized following the Figure S1 as described the Experimental Details of Chapter 1. The spectroscopic properties of the target molecules and intermediates match with the description carried out in that work.

General procedure for SWNTs purification.

50 mg of (6,5)- enriched SWNTs were suspended in 34 mL of 35% HCl, and sonicated for 10 min. The mixture was poured in 100 mL of miliQ water and filtered through a polycarbonate membrane of 0.2 µm pore size. The solid was washed with water until neutral pH, with diethyl-ether to remove water and then dried in an oven at 350^0C for 30 min.

General procedure for MINTs synthesis.

20 mg of purified (6,5)-enriched SWNTs were suspended in 20 mL of tetrachloroethane (TCE) through sonication (10 min.) and mixed with linear precursor **1** (10 mg, 0.0087 mmol, 1 equiv.). The mixture was bubbled with N_2 flow for 30 min and Grubb's 2^{nd} generation catalyst (7.4 mg, 0.0087 mmol, 1 equiv.) was added at room temperature and stirred for 72 hours. After this time, the suspension was filtered through a PTFE membrane of 0.2 µm pore size, and the solid washed profusely with dichloromethane (DCM). The solid was re-suspended in 20 mL of DCM through sonication for 10 min. and filtered through a PTFE membrane of 0.2 µm pore size again. This washing procedure was repeated three times. The degree of functionalization, 32% load in organic material was determined by thermogravimetric analysis (TGA, Figure S2).

General procedure for control experiments.

10 mg of purified (6,5)- enriched SWNTs were suspended in 10 mL of TCE through sonication bath (10 min.) and mixed with compound **1** or **2** (5 mg, 0.0043 mmol) at room temperature for 72 hours. After this time, the suspension was filtered through a PTFE membrane of 0.2 µm pore size, and the solid washed profusely with DCM. The solid was re-suspended in 20 mL of DCM through sonication for 10 min. and filtered through a PTFE membrane of 0.2 µm pore size again. This washing procedure was repeated three times. The Figure S3 shows a little bit amount of organic material (around 9% in weight loss) link to the nanotubes. Also, the temperature at organic material burn is different.

Stability test for MINTs.

4 mg of MINTs were suspended in 10 mL of TCE by sonication for 10 min. and then heated to reflux (bp = 146^0C) for 30 min. The suspension was filtered through a PTFE membrane of 0.2 µm pore size, and the solid washed profusely with DCM. No de-threading was observed by TGA (Figure S2). The

macrocycles can be removed by heating under air. 2 mg of MINTs were heated at 370ºC for 30 min in an oven. All organic material was removed (Figure S4).

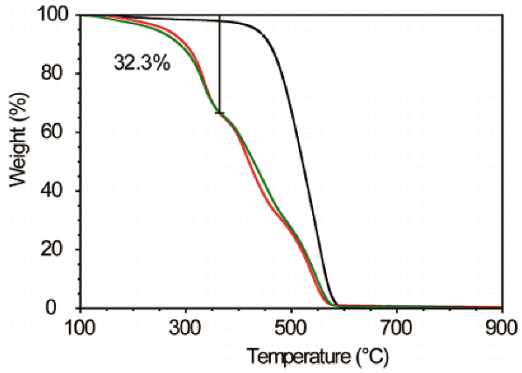

Figure S2. Thermogravimetric analysis in air (10ºC min^{-1}) of (6,5)-enriched SWNTs (black), $MINT_{(6,5)}$-**2** (red) and $MINT_{(6,5)}$-**2** after reflux in TCE (green).

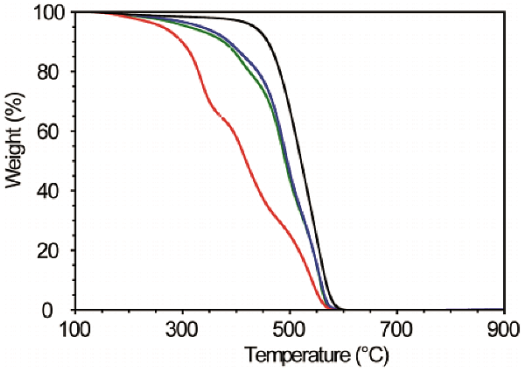

Figure S3. Thermogravimetric analysis in air (10ºC min^{-1}) of (6,5)-enriched SWNTs (black), $MINT_{(6,5)}$-**2** (red), control experiments (6,5)-enriched SWNTs + **1** (green) and (6,5)-enriched SWNTs + **2** (blue).

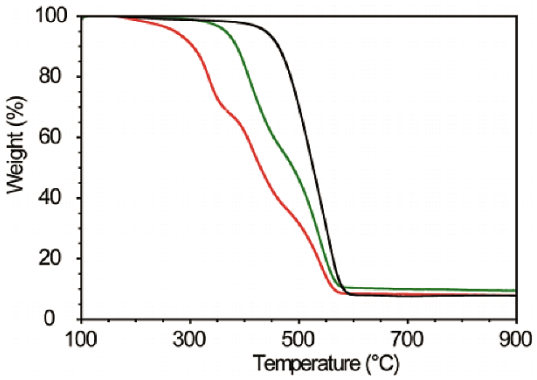

Figure S4. Thermogravimetric analysis in air (10ºC min^{-1}) of (6,5)-enriched SWNTs (black), $MINT_{(6,5)}$-**2** (red) and MINTs after heat at 370ºC for 30 min (green).

5.4.2 Microscopic Characterization.

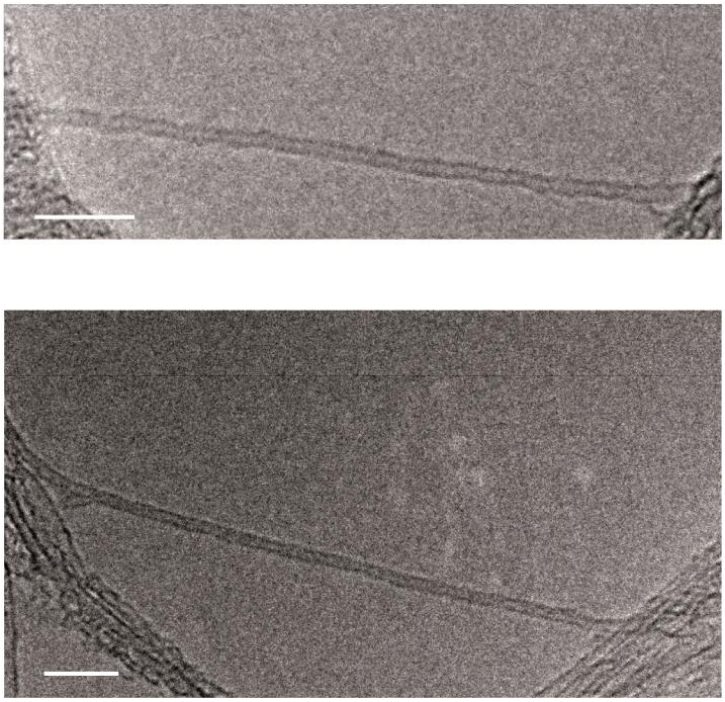

Figure S5. Transmission electron microscopy photograph of pristine (6,5)-enriched SWNTs. Scale bars are 5 nm.

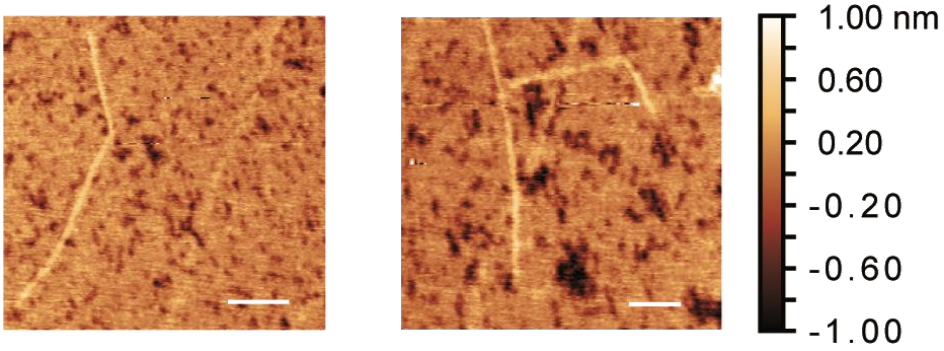

Figure S6. AFM topographic images of pristine (6,5)-enriched SWNTs. Scale bars are 100 nm.

5.4.3 Electronic Characterization.

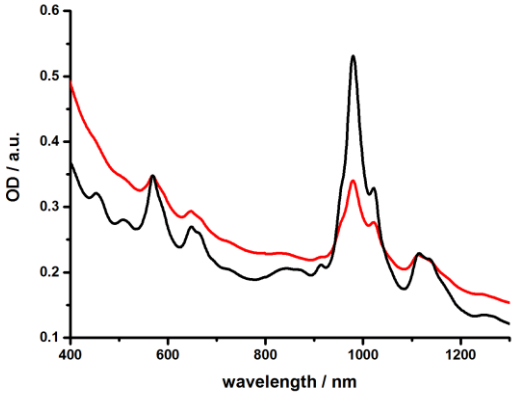

Figure S7. As-obtained absorption spectra of (6,5)-enriched-SWNTs (black) and MINT$_{(6,5)}$-**2** (red) in D_2O/SDBS (1 wt%) at room temperature.

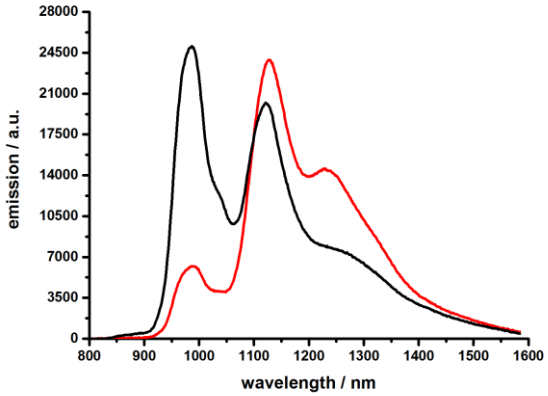

Figure S8. Fluorescence spectra of (6,5)-enriched – SWNTs (black) and MINT$_{(6,5)}$-**2** (red) in D_2O/SDBS (1wt%) at excitation wavelengths of 570 nm.

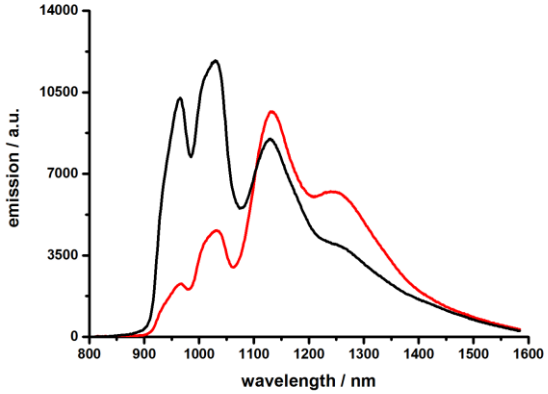

Figure S9. Fluorescence spectra of (6,5)-enriched – SWNTs (black) and $MINT_{(6,5)}$-**2** (red) in D_2O/SDBS (1wt%) at excitation wavelengths of 650 nm.

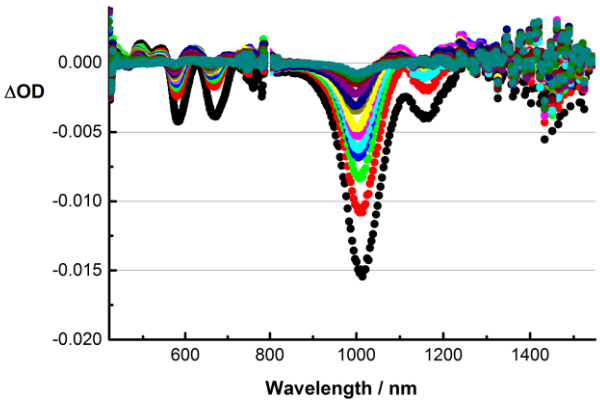

Figure S10. Differential absorption spectra obtained upon femtosecond pump probe experiments (λ_{exc} = 387 nm) of (6,5) SWNTs in SDS/D_2O (1wt%) with several time delays between 0.5 and 500 ps at room temperature.

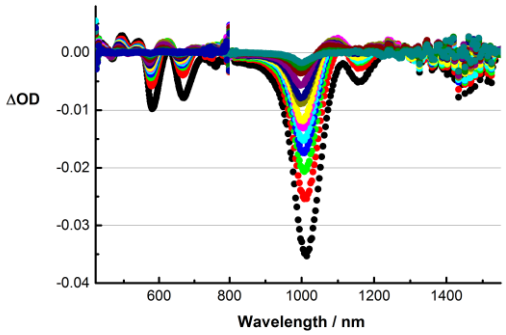

Figure S11. Differential absorption spectra obtained upon femtosecond pump probe experiments (λ_{exc} = 387 nm) of MINT$_{(6,5)}$-**2** in SDS/D_2O (1wt%) with several time delays between 0.5 and 500 ps at room temperature.

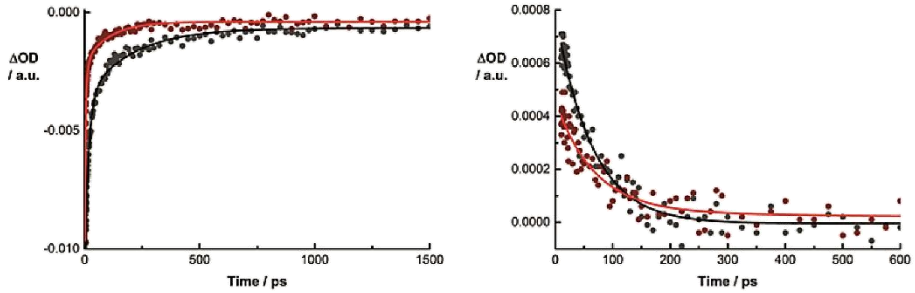

Figure S12. Left part – Time absorption profiles of SWNTs (black) and MINT$_{(6,5)}$-**2** (red) SDS/D_2O (1wt%) at 1000 nm monitoring the excited state decay. Right part – Time absorption profiles of SWNTs (black) and MINT$_{(6,5)}$-**2** (red) at 700 nm monitoring the excited state decay.

5.4.4 Electrochemical Characterization.

Materials. N,N- Dimethylformamide (99.8%) (DMF), Tetrabutylammonium perchlorate (TBAP) specific for electrochemical measures were purchase from Sigma-Aldrich.

Electrochemical studies were carried out with a potentiostat Autolab PGSTAT128N (EcoChemie, NL) using the software package GPES 4.9 (General Purpose Elec. Experiments). All measurements were performed in a homemade single compartment three electrodes electrochemical cell. Glassy Carbon (GC) electrodes (0.07 cm^2 Ø with an electrochemical area of 0.1 cm^2) from CH Instruments were used as working electrodes and Pt wire as counter

electrode. Specific calomel electrode, 1M LiCl for organic media from Radiometer Analytical was used as reference electrode.

Rotating disk-ring electrode (RRDE) measurements were carried out using a bipotentiostat CHI900B (CH Instruments) and a Glassy Carbon disk/platinum ring RRDE electrode from PINE. A modulated speed rotator from PINE Instruments was used and measures were carried out in a commercial electrochemical cell adapted to rotating disc electrodes.

Preparation of samples for measurements.

For solution electrochemical experiments and coefficient diffusion measures 0.34 mg/ml of MINTs were suspended in 0.1M TBAP/DMF. At purified (6,5)-enriched-SWNTs + compound **1** or **2** measurements 0.34 mg/ml of non-modified SWNT were suspended at 0.16 mg compound **1** or **2** /ml 0.1M TBAP/DMF solution. At compound **1** or **2** measurements 0.16 mg/ml were dissolve in 0.1M TBAP/DMF. For solution electrochemical experiments we use 5 ml of these suspensions for carried the measures. In the case of coefficient diffusion measures we use 15 ml of each suspensions.

For drop casting deposition experiments we prepared the same solution proportions and the same solvent DMF but without using TBAP. 5 μL of these suspensions were deposited onto Glassy Carbon disc electrode and dried at ambient conditions. We measures the different electrodes immersed in 5 ml 0.1M TBAP/DMF.

Cyclic voltammetry (CV) measures: In the CV electrochemical measures we have scan the potential between -0.2 to 0.6 V at different scan rates.

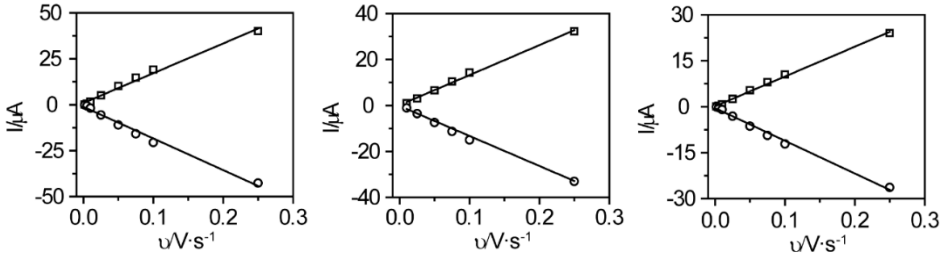

Figure S13. Oxidation (○) and reduction (□) peak current intensity *vs.* potential scan rate of (6,5)-enriched-SWNTs + **1**, (6,5)-enriched-SWNTs **+ 2**, and $MINT_{(6,5)}$-**2**; on GC electrodes from left to right.

In the case of drop casting electrodes, we have carried out an intensive scan rate study in order to obtain the necessary data to performed a Laviron's plot

(peak potential (E_p) vs. log scan rate (ν)), from the linear region we can determine the heterogeneous electron transfer rate constant K_{ET}, which is a kinetic constant of the electrochemical process, and the transfer coefficient α, which is a measure of the symmetry of the energy barrier of the redox reaction. Ideally, α = 0.5 for all overpotentials, however in many cases α deviates from 0.5. Therefore, determination of α is crucial to finding k_{ET}.

Laviron's equation:

$$E_p = E^0 + \frac{RT}{\alpha nF} - \frac{RT}{\alpha nF} \ln \nu$$

Where α is the cathodic electron transfer coefficient, n is the number of electrons, T is the temperature (293 K here), R the gas constant (8.314 $JK^{-1}mol^{-1}$) and F the Faraday constant (96,485 C mol^{-1}).

Diffusion coefficient determination

The diffusion coefficient (D) was determined by the method reported by Chatenet et al. basic on the transit-time technique on platinum-glassy carbon rotating ring-disk electrodes (RRDEs). A potential step of +0.4 V was first applied to the ring from the open-circuit potential to a potential at which the electroactive species is consumed at the ring–solution interface. After the ring current had reached its steady-state value (which was attained within a few seconds), the same potential step is applied to the disk for 2 seconds. The induced lack of electroactive species created at the disk reaches the ring after a so-called transit time, t_s [s], related to the electrode rotational speed, ω [rpm], the diffusion coefficient of the electroactive species, D [cm^2/s], K [s/rpm] constant, and the solution kinematic viscosity, ν [cm^2/s], according to the equation:

$$t_s = [K (\nu/D)^{1/3}]/\omega$$

K only depends on the electrode dimensions, and for an ideal RRDE, with an absolutely concentric ring and disk electrodes and a perfectly smooth surface, K [s/rpm] is given by the equation:

$$K = 43.1 \times [\log(r_{\text{inner ring}}/\, r_{\text{outer disk}})]^{2/3}$$

From this equation a value of 4.428 for the RRDE used ($r_{\text{outer disk}}$ = 4.6 mm, $r_{\text{inner ring}}$ = 5.0 mm) was calculated. Since the experiments were carried out in DMF, the value of kinematic viscosity was 0.00912 (cm^2/s).

5.4.5 Calculation

Table S1. Interaction energies of a series of SWNTs with macrocycle **2**.

Chirality	Diameter (nm)	SWNT[a]	2[a]	SWNT+2[a]	Eb[a]	Eb[b]	Atoms	SWNT units	Exp.
(06,05)	0.747	22187.8	1257.98	23278.9	-166.88	-39.88	492	1	1
(07,05)	0.818	25371.9	1393.75	26650.2	-115.45	-27.59	564	1	1
(07,06)	0.882	28621.9	1623.22	30201.7	-43.42	-10.38	636	1	1
(07,07)	0.949	17715.3	2004.53	19773.6	53.77	12.85	408	10	0
(08,03)	0.771	23386.1	2385.71	25608.4	-163.41	-39.05	516	1	1
(08,04)	0.829	25732.5	1431.74	27063.2	-101.04	-24.14	576	4	1
(08,05)	0.889	20375.7	1680.19	22026.3	-29.59	-7.07	472	2	0
(08,06)	0.953	18072.3	2274.04	20394.5	48.16	11.51	424	1	0
(08,07)	1.018	35958.6	2536.91	38655.1	159.59	38.13	804	1	0
(09,04)	0.903	29614.1	1721.28	31319.3	-16.08	-3.84	660	1	0
(09,05)	0.962	32656.3	2077.26	34811.8	78.24	18.7	732	1	1
(09,06)	1.024	25378.9	2581.46	28131.4	171.04	40.87	584	2	0
(10,03)	0.923	30784.5	1829.08	32629.1	15.52	3.71	684	1	0
(10,04)	0.978	18374.7	2215.21	20690	100.09	23.92	440	3	0
(11,01)	0.903	29928.6	1721.48	31640.6	-9.48	-2.27	660	1	0
(11,02)	0.949	22214.1	2005.85	24275.3	55.35	13.23	520	2	0
(11,03)	1	34933.4	2352.45	37423.8	137.95	32.96	780	1	0
(12,00)	0.94	19663.2	1982.17	21682.4	37.03	8.85	512	8	0
(12,01)	0.981	34022.4	2186.92	36310.5	101.18	24.18	756	1	0
(12,02)	1.027	19477.1	2569.93	22225.4	178.37	42.62	472	1	0
(13,00)	1.018	15686	2513.31	18364.6	165.29	39.5	440	6	0
(14,00)	1.096	13878.5	3297.63	17458.2	282.07	67.4	408	5	0
(15,00)	1.175	14586.9	4287.28	19286.5	412.32	98.52	428	5	0
(16,00)	1.253	15310.6	5444.58	21307.1	551.92	131.88	448	5	0
(17,00)	1.331	16046.9	6804.44	23566.6	715.26	170.91	468	5	0
(18,00)	1.409	13984.1	8361.71	23245.3	899.49	214.93	488	5	0
(19,00)	1.488	13712.9	13383.7	37602.5	10505.9	2510.37	508	5	0
(20,00)	1.566	14435.3	Breaks	Breaks	N/D	N/D	528	5	0

[a] Energy in kJ mol^{-1}.

[b] Energy in kcal mol^{-1}.

6.5 References

1. G. A. Breault, C. A. Hunter and P. C. Mayers, *Tetrahedron*, 1999, **55**, 5265-5293.
2. J. F. Stoddart, *Chem. Soc. Rev.*, 2009, **38**, 1802-1820.
3. A. de Juan and E. M. Pérez, *Nanoscale*, 2013, **5**, 7141-7148.
4. E. R. Kay, D. A. Leigh and F. Zerbetto, *Angew. Chem. Int. Ed.*, 2007, **46**, 72-191.
5. J. Berná, G. Bottari, D. A. Leigh and E. M. Pérez, *Pure Appl. Chem.*, 2007, **79**, 39-54.
6. C. Cheng, P. R. McGonigal, S. T. Schneebeli, H. Li, N. A. Vermeulen, C. Ke and J. F. Stoddart, *Nat. Nanotech.*, 2015, **10**, 547-553.
7. B. Lewandowski, G. De Bo, J. W. Ward, M. Papmeyer, S. Kuschel, M. J. Aldegunde, P. M. E. Gramlich, D. Heckmann, S. M. Goldup, D. M. D'Souza, A. E. Fernandes and D. A. Leigh, *Science*, 2013, **339**, 189-193.
8. H. Tian and Q.-C. Wang, *Chem. Soc. Rev.*, 2006, **35**, 361-374.
9. K. Zhu, C. A. O'Keefe, V. N. Vukotic, R. W. Schurko and S. J. Loeb, *Nat. Chem.*, 2015, **7**, 514-519.
10. E. A. Neal and S. M. Goldup, *Chem. Commun.*, 2014, **50**, 5128-5142.
11. R. Barat, T. Legigan, I. Tranoy-Opalinski, B. Renoux, E. Peraudeau, J. Clarhaut, P. Poinot, A. E. Fernandes, V. Aucagne, D. A. Leigh and S. Papot, *Chem. Sci.*, 2015, **6**, 2608-2613.
12. M. Franz, J. A. Januszewski, D. Wendinger, C. Neiss, L. D. Movsisyan, F. Hampel, H. L. Anderson, A. Görling and R. R. Tykwinski, *Angew. Chem. Int. Ed.*, 2015, **54**, 6645-6649.
13. L. D. Movsisyan, D. V. Kondratuk, M. Franz, A. L. Thompson, R. R. Tykwinski and H. L. Anderson, *Org. Lett.*, 2012, **14**, 3424-3426.
14. J. Winn, A. Pinczewska and S. M. Goldup, *J. Am. Chem. Soc.*, 2013, **135**, 13318-13321.
15. A. Fernandes, A. Viterisi, F. Coutrot, S. Potok, D. A. Leigh, V. Aucagne and S. Papot, *Angew. Chem. Int. Ed.*, 2009, **48**, 6443-6447.
16. J. M. Baumes, J. J. Gassensmith, J. Giblin, J.-J. Lee, A. G. White, W. J. Culligan, W. M. Leevy, M. Kuno and B. D. Smith, *Nat. Chem.*, 2010, **2**, 1025-1030.
17. E. M. Pérez, D. T. F. Dryden, D. A. Leigh, G. Teobaldi and F. Zerbetto, *J. Am. Chem. Soc.*, 2004, **126**, 12210-12211.
18. F. Cacialli, J. S. Wilson, J. J. Michels, C. Daniel, C. Silva, R. H. Friend, N. Severin, P. Samori, J. P. Rabe, M. J. O'Connell, P. N. Taylor and H. L. Anderson, *Nat. Mater.*, 2002, **1**, 160-164.

19. Q.-C. Wang, D.-H. Qu, J. Ren, K. Chen and H. Tian, *Angew. Chem. Int. Ed.*, 2004, **43**, 2661-2665.
20. A. Mateo-Alonso, C. Ehli, D. M. Guldi and M. Prato, *Org. Lett.*, 2013, **15**, 84-87.
21. A. Mateo-Alonso, C. Ehli, D. M. Guldi and M. Prato, *J. Am. Chem. Soc.*, 2008, **130**, 14938-14939.
22. V. N. Vukotic, C. A. O'Keefe, K. Zhu, K. J. Harris, C. To, R. W. Schurko and S. J. Loeb, *J. Am. Chem. Soc.*, 2015, **137**, 9643-9651.
23. K. Zhu, V. N. Vukotic, C. A. O'Keefe, R. W. Schurko and S. J. Loeb, *J. Am. Chem. Soc.*, 2014, **136**, 7403-7409.
24. V. N. Vukotic, K. J. Harris, K. Zhu, R. W. Schurko and S. J. Loeb, *Nat. Chem.*, 2012, **4**, 456-460.
25. P. R. McGonigal, P. Deria, I. Hod, P. Z. Moghadam, A.-J. Avestro, N. E. Horwitz, I. C. Gibbs-Hall, A. K. Blackburn, D. Chen, Y. Y. Botros, M. R. Wasielewski, R. Q. Snurr, J. T. Hupp, O. K. Farha and J. F. Stoddart, *Proc. Natl. Acad. Sci. U.S.A.*, 2015, **112**, 11161-11168.
26. A. Coskun, M. Hmadeh, G. Barin, F. Gándara, Q. Li, E. Choi, N. L. Strutt, D. B. Cordes, A. M. Z. Slawin, J. F. Stoddart, J.-P. Sauvage and O. M. Yaghi, *Angew. Chem. Int. Ed.*, 2012, **51**, 2160-2163.
27. Q. Li, W. Zhang, O. S. Miljanic, C. B. Knobler, J. F. Stoddart and O. M. Yaghi, *Chem. Commun.*, 2010, **46**, 380-382.
28. Q. Li, C.-H. Sue, S. Basu, A. K. Shveyd, W. Zhang, G. Barin, L. Fang, A. A. Sarjeant, J. F. Stoddart and O. M. Yaghi, *Angew. Chem. Int. Ed.*, 2010, **49**, 6751-6755.
29. X.-Q. Wang, W. Wang, G.-Q. Yin, Y.-X. Wang, C.-W. Zhang, J.-M. Shi, Y. Yu and H.-B. Yang, *Chem. Commun.*, 2015, **51**, 16813-16816.
30. J. Wang and X. Zhang, *ACS Nano*, 2015, **9**, 11389-11397.
31. E. M. Peck, W. Liu, G. T. Spence, S. K. Shaw, A. P. Davis, H. Destecroix and B. D. Smith, *J. Am. Chem. Soc.*, 2015, **137**, 8668-8671.
32. C. Hu, Y. Lan, K. R. West and O. A. Scherman, *Adv. Mater.*, 2015, **27**, 7957-7962.
33. A. Goujon, G. Du, E. Moulin, G. Fuks, M. Maaloum, E. Buhler and N. Giuseppone, *Angew. Chem. Int. Ed.*, 2016, **55**, 703-707.
34. A. Tamura and N. Yui, *Chem. Commun.*, 2014, **50**, 13433-13446.
35. H. W. Gibson, H. Wang, Z. Niu, C. Slebodnick, L. N. Zhakharov and A. L. Rheingold, *Macromolecules*, 2012, **45**, 1270-1280.
36. Z. Niu, F. Huang and H. W. Gibson, *J. Am. Chem. Soc.*, 2011, **133**, 2836-2839.
37. M. Lee, R. B. Moore and H. W. Gibson, *Macromolecules*, 2011, **44**, 5987-5993.
38. H. Dai, *Acc. Chem. Res.*, 2002, **35**, 1035-1044.

39. A. Jorio, G. Dresselhaus and M. S. Dresselhaus, in *Carbon Nanotubes: Advanced Topics in the Synthesis, Structure, Properties and Applications*, Top. Appl. Phys., 2008, vol. 111.
40. Z. Liu, S. Tabakman, K. Welsher and H. Dai, *Nano Res.*, 2009, **2**, 85-120.
41. N. Saito, Y. Usui, K. Aoki, N. Narita, M. Shimizu, K. Hara, N. Ogiwara, K. Nakamura, N. Ishigaki, H. Kato, S. Taruta and M. Endo, *Chem. Soc. Rev.*, 2009, **38**, 1897-1903.
42. J. M. Schnorr and T. M. Swager, *Chem. Mater.*, 2011, **23**, 646-657.
43. S. Park, M. Vosguerichian and Z. Bao, *Nanoscale*, 2013, **5**, 1727-1752.
44. D. Jariwala, V. K. Sangwan, L. J. Lauhon, T. J. Marks and M. C. Hersam, *Chem. Soc. Rev.*, 2013, **42**, 2824-2860.
45. H. Park, A. Afzali, S.-J. Han, G. S. Tulevski, A. D. Franklin, J. Tersoff, J. B. Hannon and W. Haensch, *Nat. Nanotech.*, 2012, **7**, 787-791.
46. A. D. Franklin, M. Luisier, S.-J. Han, G. Tulevski, C. M. Breslin, L. Gignac, M. S. Lundstrom and W. Haensch, *Nano Lett.*, 2012, **12**, 758-762.
47. C. Wang, D. Hwang, Z. Yu, K. Takei, J. Park, T. Chen, B. Ma and A. Javey, *Nat. Mater.*, 2013, **12**, 899-904.
48. Q. Cao, S.-j. Han, G. S. Tulevski, Y. Zhu, D. D. Lu and W. Haensch, *Nat. Nanotech.*, 2013, **8**, 180-186.
49. M. M. Shulaker, G. Hills, N. Patil, H. Wei, H.-Y. Chen, H. S. P. Wong and S. Mitra, *Nature*, 2013, **501**, 526-530.
50. P. Singh, S. Campidelli, S. Giordani, D. Bonifazi, A. Bianco and M. Prato, *Chem. Soc. Rev.*, 2009, **38**, 2214-2230.
51. M. Kanungo, H. Lu, G. G. Malliaras and G. B. Blanchet, *Science*, 2009, **323**, 234-237.
52. J. Zhao, Y. Gao, J. Lin, Z. Chen and Z. Cui, *J. Mater. Chem.*, 2012, **22**, 2051-2056.
53. J. L. Delgado, P. de la Cruz, F. Langa, A. Urbina, J. Casado and J. T. López Navarrete, *Chem. Commun.*, 2004, 1734-1735.
54. R. Martín, F. J. Cespedes-Guirao, M. de Miguel, F. Fernández-Lázaro, H. García and Á. Sastre-Santos, *Chem. Sci.*, 2012, **3**, 470-475.
55. Y.-L. Zhao and J. F. Stoddart, *Acc. Chem. Res.*, 2009, **42**, 1161-1171.
56. A. Wurl, S. Goossen, D. Canevet, M. Sallé, E. M. Pérez, N. Martín and C. Klinke, *J. Phys. Chem. C*, 2012, **116**, 20062-20066.
57. S. D. Stranks, J. K. Sprafke, H. L. Anderson and R. J. Nicholas, *ACS Nano*, 2011, **5**, 2307-2315.
58. A. de Juan, A. López-Moreno, J. Calbo, E. Ortí and E. M. Pérez, *Chem. Sci.*, 2015, **6**, 7008-7014.
59. E. M. Pérez and N. Martín, *Org. Biomol. Chem.*, 2012, **10**, 3577-3583.
60. A. F. M. M. Rahman, F. Wang, K. Matsuda, T. Kimura and N. Komatsu, *Chem. Sci.*, 2011, **2**, 862-867.

61. G. Liu, F. Wang, S. Chaunchaiyakul, Y. Saito, A. K. Bauri, T. Kimura, Y. Kuwahara and N. Komatsu, *J. Am. Chem. Soc.*, 2013, **135**, 4805-4814.
62. G. Liu, Y. Saito, D. Nishio-Hamane, A. K. Bauri, E. Flahaut, T. Kimura and N. Komatsu, *J. Mater. Chem. A*, 2014, **2**, 19067-19074.
63. F. Vialla, G. Delport, Y. Chassagneux, P. Roussignol, J. S. Lauret and C. Voisin, *Nanoscale*, 2016, **8**, 2326-2332.
64. A. López-Moreno and E. M. Pérez, *Chem. Commun.*, 2015, **51**, 5421-5424.
65. A. de Juan, M. Mar Bernal and E. M. Pérez, *ChemPlusChem*, 2015, **80**, 1153-1157.
66. A. de Juan, Y. Pouillon, L. Ruiz-González, A. Torres-Pardo, S. Casado, N. Martín, Á. Rubio and E. M. Pérez, *Angew. Chem., Int. Ed.*, 2014, **53**, 5394-5400.
67. C. Romero-Nieto, R. García, M. Á. Herranz, C. Ehli, M. Ruppert, A. Hirsch, D. M. Guldi and N. Martín, *J. Am. Chem. Soc.*, 2012, **134**, 9183-9192.
68. E. M. Pérez, B. M. Illescas, M. Á. Herranz and N. Martín, *New J. Chem.*, 2009, **33**, 228-234.
69. C. Romero-Nieto, R. García, M. Á. Herranz, L. Rodríguez-Pérez, M. Sánchez-Navarro, J. Rojo, N. Martín and D. M. Guldi, *Angew. Chem. Int. Ed.*, 2013, **52**, 10216-10220.
70. V. Strau, A. Gallego, G. d. l. Torre, T. W. Chamberlain, A. N. Khlobystov, T. Torres and D. M. Guldi, *Faraday Discuss.*, 2014, **172**, 61-79.
71. S. S. Gayathri, M. Wielopolski, E. M. Pérez, G. Fernández, L. Sánchez, R. Viruela, E. Ortí, D. M. Guldi and N. Martín, *Angew. Chem. Int. Ed.*, 2009, **48**, 815-819.
72. A. G. Johnston, D. A. Leigh, A. Murphy, J. P. Smart and M. D. Deegan, *J. Am. Chem. Soc.*, 1996, **118**, 10662-10663.
73. S.-G. Liu, I. Pérez, N. Martín and L. Echegoyen, *J. Org. Chem.*, 2000, **65**, 9092-9102.
74. M. R. Bryce and A. J. Moore, *Synth. Met.*, 1988, **27**, 557-561.
75. R. H. Wopschall and I. Shain, *Anal. Chem.*, 1967, **39**, 1514-1527.
76. M. Chatenet, M. B. Molina-Concha, N. El-Kissi, G. Parrour and J. P. Diard, *Electrochim. Acta*, 2009, **54**, 4426-4435.
77. S. Bruckenstein and G. A. Feldman, *J. Electroanal. Chem.*, 1965, **9**, 395-399.
78. T. A. Halgren and R. B. Nachbar, *J. Comput. Chem.*, 1996, **17**, 587-615.
79. M. J. Frisch, G. W. Trucks, H. B. Schlegel, G. E. Scuseria, M. A. Robb, J. R. Cheeseman, G. Scalmani, V. Barone, B. Mennucci, G. A. Petersson, H. Nakatsuji, M. Caricato, H. P. H. X. Li, A. F. Izmaylov, J. Bloino, G. Zheng, J. L. Sonnenberg, M. Hada, M. Ehara, K. Toyota, R.

Fukuda, J. Hasegawa, M. Ishida, T. Nakajima, Y. Honda, O. Kitao, H. Nakai, T. Vreven, J. A. Montgomery, J. E. P. Jr., F. Ogliaro, M. Bearpark, J. J. Heyd, E. Brothers, K. N. Kudin, V. N. Staroverov, R. Kobayashi, J. Normand, K. Raghavachari, A. Rendell, J. C. Burant, S. S. Iyengar, J. Tomasi, M. Cossi, N. Rega, J. M. Millam, M. Klene, J. E. Knox, J. B. Cross, V. Bakken, C. Adamo, J. Jaramillo, R. Gomperts, R. E. Stratmann, O. Yazyev, A. J. Austin, R. Cammi, C. Pomelli, J. W. Ochterski, R. L. Martin, K. Morokuma, V. G. Zakrzewski, G. A. Voth, P. Salvador, J. J. Dannenberg, S. Dapprich, A. D. Daniels, Ö. Farkas, J. B. Foresman, J. V. Ortiz, J. Cioslowski and G. D. J. Fox, *Gaussian 09 (Revision B.01), Gaussian Inc., Wallingford CT., 2009*

80. K. Momma and F. Izumi, *J. Appl. Crystallogr.*, 2011, **44**, 1272-1276.
81. S. Freddi, L. D'Alfonso, M. Collini, M. Caccia, L. Sironi, G. Tallarida, S. Caprioli and G. Chirico, *J. Phys. Chem. C*, 2009, **113**, 2722-2730.

CHAPTER 4

6. Determination of Association Constants towards Carbon Nanotubes

Single-walled carbon nanotubes (SWNTs) are one of the most promising nanomaterials and their supramolecular chemistry has attracted a lot of attention. However, despite well over a decade of research, there is no standard method for the quantification of their noncovalent chemistry in solution/ suspension. Here, we describe a simple procedure for the determination of association constants (K_a) between soluble molecules and insoluble and heterogeneous carbon nanotube samples. To test the scope of the method, we report binding constants between five different hosts and two types of SWNTs in four solvents. We have determined numeric values of K_a in the range of 1-10^4 M^{-1}. Solvent effects as well as structural changes in both the host and guest result in noticeable changes of K_a. The results obtained experimentally were validated through state-of-the-art DFT calculations. The generalization of quantitative and comparable association constants data should significantly help advance the supramolecular chemistry of carbon nanotubes.

Chem. Sci., 2015, **6**, 7008-7014.

6.1 Introduction

Materials with at least one of their dimensions in the nanometer range, such as graphene,[1-3] carbon nanotubes, [4] quantum dots,[5] metal nanoparticles,[6] few layer transition metal chalcogenides[7] etc., are expected to revolutionize technology[8] and have certainly transformed science already.[†] In particular, the extreme aspect ratio and extraordinary physical properties of single-walled

[†] From a purely bibliometric point of view, there are 73 journals listed under Nanoscience & Nanotechnology in the Journal of Citation Reports, of which the first seven have impact factors larger than 10. Iijima's first report on carbon nanotubes (S. Iijima, *Nature* 1991, **354**, 56) has been cited more than 22 600 times. Data from SciFinder, August 2015.

1. A. K. Geim and K. S. Novoselov, *Nat. Mater.*, 2007, **6**, 183-191.
2. A. K. Geim, *Science*, 2009, **324**, 1530-1534.
3. C. N. R. Rao, A. K. Sood, K. S. Subrahmanyam and A. Govindaraj, *Angew. Chem. Int. Ed.*, 2009, **48**, 7752-7777.
4. D. Tasis, N. Tagmatarchis, A. Bianco and M. Prato, *Chem. Rev.* , 2006, **106**, 1105-1136.
5. J. Y. Kim, O. Voznyy, D. Zhitomirsky and E. H. Sargent, *Adv. Mater.*, 2013, **25**, 4986-5010.
6. M. V. Kovalenko, L. Manna, A. Cabot, Z. Hens, D. V. Talapin, C. R. Kagan, V. I. Klimov, A. L. Rogach, P. Reiss, D. J. Milliron, P. Guyot-Sionnnest, G. Konstantatos, W. J. Parak, T. Hyeon, B. A. Korgel, C. B. Murray and W. Heiss, *ACS Nano*, 2015, **9**, 1012-1057.
7. N. P. Dasgupta, X. Meng, J. W. Elam and A. B. F. Martinson, *Acc. Chem. Res.*, 2015, **48**, 341-348.
8. M. F. L. De Volder, S. H. Tawfick, R. H. Baughman and A. J. Hart, *Science*, 2013, **339**, 535-539.

carbon nanotubes (SWNTs) have attracted a great deal of attention.[9] Chemical modifications are usually necessary to take full advantage of their properties and/or to modulate them.[10,11] A particularly attractive strategy is to utilize noncovalent forces to yield supramolecular constructs, since it guarantees the structural integrity of the nanotube, and changing the structure of the host, its concentration, the solvent, and/or temperature can modulate the stability of the associates.[12,13] In this respect, the quantification of the supramolecular interactions is of paramount importance. From the experimental point of view, skillfully designed atomic force microscopy experiments have allowed for the measurement of interaction forces between single molecules and SWNTs.[14] A kinetic model for the measurement of chirality-specific interactions of SWNTs with hydrogels has also been reported.[15] In silico investigations are far more abundant, and a wide variety of DFT methods have been tested.[16] However, the overwhelming majority of publications on noncovalent chemistry of nanotubes do not report quantitative data.[12,13,17] This is in sharp contrast with the literature on soluble host-guest systems, in which the determination of the association constant (K_a) is hardly ever overlooked, and comparison of the K_a data is the main tool to understand molecular recognition events. Needless to say, the lack of quantitative and comparable information represents a major obstacle in the progress of the supramolecular chemistry of SWNTs.

Here, we describe a simple method for the determination of association constants between insoluble and heterogeneous nanotube samples and soluble molecules. To prove its validity, we have determined the association constants of five molecules towards two types of SWNTs in four different solvents.

9. P. Avouris, Z. Chen and V. Perebeinos, *Nat. Nanotech.*, 2007, **2**, 605-615.
10. P. Singh, S. Campidelli, S. Giordani, D. Bonifazi, A. Bianco and M. Prato, *Chem. Soc. Rev.*, 2009, **38**, 2214-2230.
11. A. Hirsch, *Angew. Chem., Int. Ed*., 2002, **41**, 1853-1859.
12. N. Martín and J.-F. Nierengarten, in *Supramolecular Chemistry of Fullerenes and Carbon Nanotubes*, Wiley-VCH Verlag GmbH & Co. KGaA, 2012.
13. Y.-L. Zhao and J. F. Stoddart, *Acc. Chem. Res.*, 2009, **42**, 1161-1171.
14. S. Iliafar, J. Mittal, D. Vezenov and A. Jagota, *J. Am. Chem. Soc.*, 2014, **136**, 12947-12957.
15. K. Tvrdy, R. M. Jain, R. Han, A. J. Hilmer, T. P. McNicholas and M. S. Strano, *ACS Nano*, 2013, **7**, 1779-1789.
16. D. Umadevi, S. Panigrahi and G. N. Sastry, *Acc. Chem. Res.*, 2014, **47**, 2574-2581.
17. E. M. Pérez and N. Martín, *Chem. Soc. Rev.*, 2015, **44**, 6425-6433.

6.2 Results and Discussion

Due to the heterogeneous nature of most samples and the characteristic insolubility of SWNTs, it is virtually impossible to calculate their molar concentration in solution. This has hampered the determination of association constants in SWNT based supramolecular systems, with a few notable exceptions based on approximations to apply standard spectroscopic titration methods.[18-20] However, it is known that association constants can be calculated from the fraction of occupied binding sites and the concentration of the host-guest complex, the free host, or the free guest species only.[21,22] This method is not usually applied to soluble host-guest systems because the total concentration of host and guest are known quantities and the calculation of the concentration of free species is problematic.[22] We take advantage of the insolubility of the carbonaceous material to measure the concentration of bound and free species.

The experimental procedure is described graphically in Scheme 1 and can be summarized as follows: SWNTs (1 mg mL^{-1}, unless stated otherwise) are suspended in a solution of known concentration of the host molecule in a given solvent, and the mixture stirred for 2 hours to allow it to reach equilibrium. After this time, the suspension is filtered through a 0.2 μm-pore polytetrafluoroethylene membrane, retaining the host-SWNT complex. The solid is analysed through TGA (N_2, 50ºC min^{-1}) to quantify the amount of host in the complex, from which the concentration of free species is calculated by subtraction. Specifically, we measure the weight loss up to 600ºC, where all of the associated host has been desorbed and the nanotubes are still intact. From the degree of functionalization and the mass of the sample analysed, we calculate the total mass of host in the complex, from which its initial concentration in the equilibrium is immediate. Alternatively, the concentration of free species can be directly measured in the filtrate.‡ The same procedure is repeated for several initial concentrations of the host molecule, ranging from 0 to near saturation in

‡ Somewhat counterintuitively, we find the direct measurement of $[H]_{free}$ in the filtrate more problematic experimentally. We believe the main reasons behind this are variations in the volume of solvent during the filtration process and spectral overlap of the hosts with the carbonaceous impurities present in the filtrate.

18. P. Salice, A. Gambarin, N. Daldosso, F. Mancin and E. Menna, *J. Phys. Chem. C*, 2014, **118**, 27028-27038.
19. H. Oh, J. Sim and S.-Y. Ju, *Langmuir*, 2013, **29**, 11154-11162.
20. J. K. Sprafke, S. D. Stranks, J. H. Warner, R. J. Nicholas and H. L. Anderson, *Angew. Chem. Int. Ed.*, 2011, **50**, 2313-2316.
21. K. A. Connors, *Binding Constants: The Measurement of Molecular Complex Stability*, John Wiley & sons, New York, 1987.
22. P. Thordarson, *Chem. Soc. Rev.*, 2011, **40**, 1305-1323.

the solvent under study. A blank experiment to determine the adsorbed/encapsulated solvent was run in all cases, and the data subtracted. All the experiments were performed at room temperature.

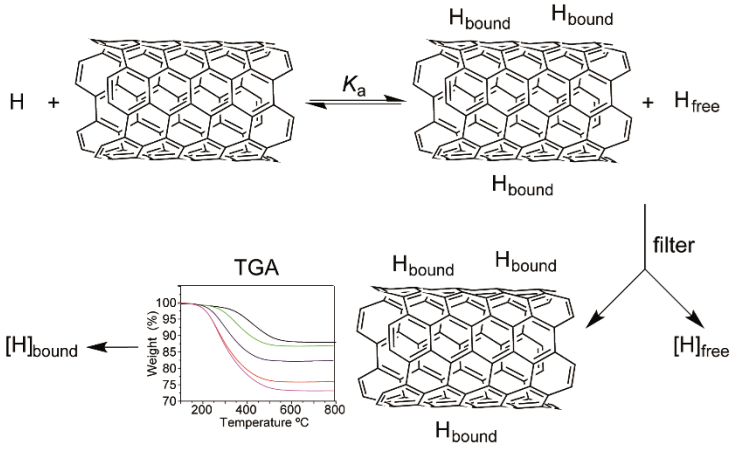

Scheme 1. Procedure for the measurement of $[H]_{bound}$ and $[H]_{free}$. A known concentration of host molecule H and SWNTs are allowed to reach equilibrium, and then complexed and free species are physically separated through filtration. The concentration of $[H]_{bound}$ is measured by TGA (typical results for a titration experiment are shown, see the Experimental Details for full data set). The concentration of $[H]_{free}$ can then be calculated by subtraction or directly measured in the filtrate.

The binding isotherms are obtained by plotting the degree of functionalization against the concentration of free host, and were analyzed using a standard 1:1 isotherm:[22]

$$\theta = \frac{S\ x\ k_a\ x\ [H]_{free}}{1 + k_a\ x\ [H]_{free}}$$

where Θ is the fraction of occupied binding sites and S represents the maximum functionalization at saturation, when Θ equals 1. In this case, the 1:1 stoichiometry does not refer to the host : SWNT molar ratio, but to the number of occupied binding sites on SWNT, so that it is necessarily 1:1. In this respect, the binding isotherm is both formally and conceptually equivalent to the Langmuir isotherm,[23] widely used for the quantification of the adsorption of gases onto solid surfaces.

Pyrene is by far the most widely used supramolecular partner for SWNTs, so we based our investigations on pyrene and its derivatives. Figure 1 shows the

23. I. Langmuir, *J. Am. Chem. Soc.*, 1918, **40**, 1361-1403.

chemical structure of the hosts for SWNTs used in the present work. First, we titrated **1** against plasma-purified SWNTs (pp-SWNTs, 98% purity, 0.8-1.6 nm in diameter) in tetrahydrofuran (THF), dimethylformamide (DMF), tetrachloroethane (TCE), and methanol (MeOH) at room temperature. Figure 2 shows results of these titrations, where each data point is the average of three separate experiments.

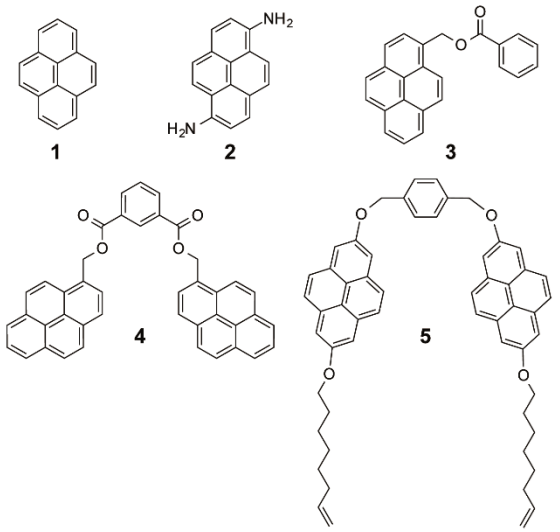

Figure 1. Structure of the hosts for SWNTs used in this work.

As a first test of the experimental validity of our approach, we decided to get data for titrations with significant variations in the concentration of SWNTs. In particular, we used 0.1, 1 and 10 mg mL^{-1} of nanotubes in THF (Figure 2a), which afforded K_a = 16.4 ± 0.8 M^{-1},[‡] 24 ± 6 M^{-1}, and 21 ± 4 M^{-1}, respectively. We were pleased to find that all values for K_a are identical within experimental error. The main variability comes from the degree of functionalization at saturation, which is significantly larger for the more dilute sample. This reflects a more efficient disaggregation of the nanotubes, which in turn results in an increase in the availability of binding sites for **1**. Therefore, the method works correctly for samples with significantly different degrees of aggregation of the SWNTs.

[‡] Considering that each data point consists of three separate experiments, we have reported errors directly as obtained from the fitting software. Based on our previous experience determining association constants, an experimental error within 20% can be expected.

With regards to the effect of the solvent, the association constants increase with decreasing ability to solvate SWNTs, showing that solvophobic interactions play a relevant role in the binding event. In DMF and TCE, solvents commonly used to disperse SWNTs, the binding constants are very small: K_a = 9 ± 3 and 4.5 ± 0.9 M^{-1}, respectively (Figure 2b and c). In THF there is an increase of one order of magnitude, to K_a = 24 ± 6 M^{-1} (Figure 2a), which is further amplified in MeOH, a notoriously bad solvent for SWNTs, to reach millimolar affinity with K_a = (2.6 ± 0.2) x 10^3 M^{-1} (Figure 2d).

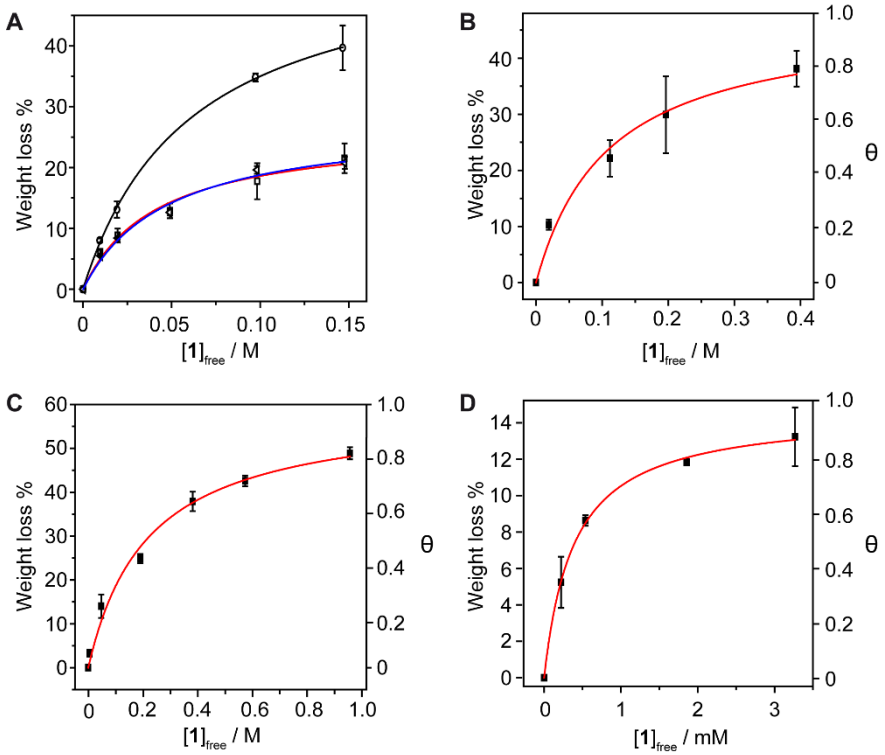

Figure 2. Titrations of pyrene vs. pp-SWNTs in (a) THF at 0.1 mg mL^{-1} of SWNTs (circles and black line, K_a = 16.4 ± 0.8 M^{-1}, r^2 = 0.999); 1 mg mL^{-1} of SWNTs (squares and red line, K_a = 24 ± 6 M^{-1}, r^2 = 0.979); and 10 mg mL^{-1} of SWNTs (triangles and blue line, K_a = 21 ± 4 M^{-1}, r^2 = 0.985); (b) DMF (K_a = 9 ± 3 M^{-1}, r^2 = 0.978); (c) TCE (K_a = 4.5 ± 0.9 M^{-1}, r^2 = 0.987); (d) MeOH (K_a = (2.6 ± 0.2) x 10^3 M^{-1}, r^2 = 0.998). Each data point is the average of three separate experiments, and the error bars represent the standard deviation. Solid lines represent the fit.

In order to investigate whether the method is sufficiently sensitive to detect small changes in the structure of the nanotubes, we carried out titrations of **1** vs. (6,5)-enriched SWNTs (93% purity, 0.7-0.9 nm in diameter) in THF, DMF, TCE and MeOH at room temperature. The association constant towards (6,5)-SWNTs

are: K_a = 41 ± 8 M^{-1} in THF, 1.6 ± 0.4 M^{-1} in DMF, 1.6 ± 0.1 M^{-1} in TCE, and (1.0 ± 0.1) x 10^3 M^{-1} in MeOH (Figure 3). Therefore, with the only exception of THF, in which some unexpected solvent effect takes place, the association constants are smaller than those towards pp-SWNTs. Considering the planar geometry of pyrene, it is expected to establish stronger van der Waals interactions with nanotubes of larger diameter, a tendency that is corroborated by DFT calculations (see below). These results confirm that the method is sensitive enough to such subtle differences in the structure of the nanotube as a decrease in the average diameter of the sample.

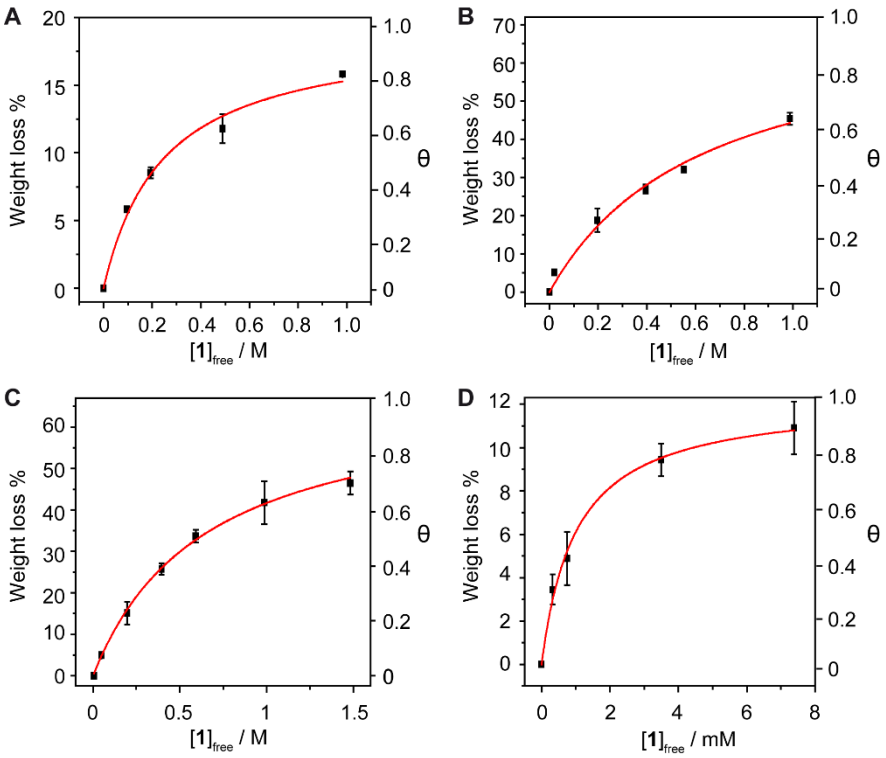

Figure 3. Titrations of **1** vs. (6,5)-SWNTs in (a) THF (K_a = 41 ± 8 M^{-1}, r^2 = 0.987); (b) DMF (K_a = 1.6 ± 0.4 M^{-1}, r^2 = 0.985); (c) TCE (K_a = 1.6 ± 0.1 M^{-1}, r^2 = 0.998); (d) MeOH (K_a = (1.0 ± 0.1) x 10^3 M^{-1}, r^2 = 0.994). Each data point is the average of three separate experiments, and the error bars represent the standard deviation. Solid red lines represent the fit.

The method is also sensitive towards the structure of the host. To get experimental evidence, we designed a collection of hosts composed by 1,6-diaminopyrene (**2**), the benzoic and isophthalic esters of pyrene-1-methanol (**3** and **4**, respectively), and bis-pyrene U-shape molecule **5**, which we have used in

the synthesis of mechanically interlocked derivatives of SWNTs.[24-27] Hosts **3**-**5** were titrated vs. pp-SWNTs in THF at room temperature, while we used DMF for the titration of **2** for solubility reasons.

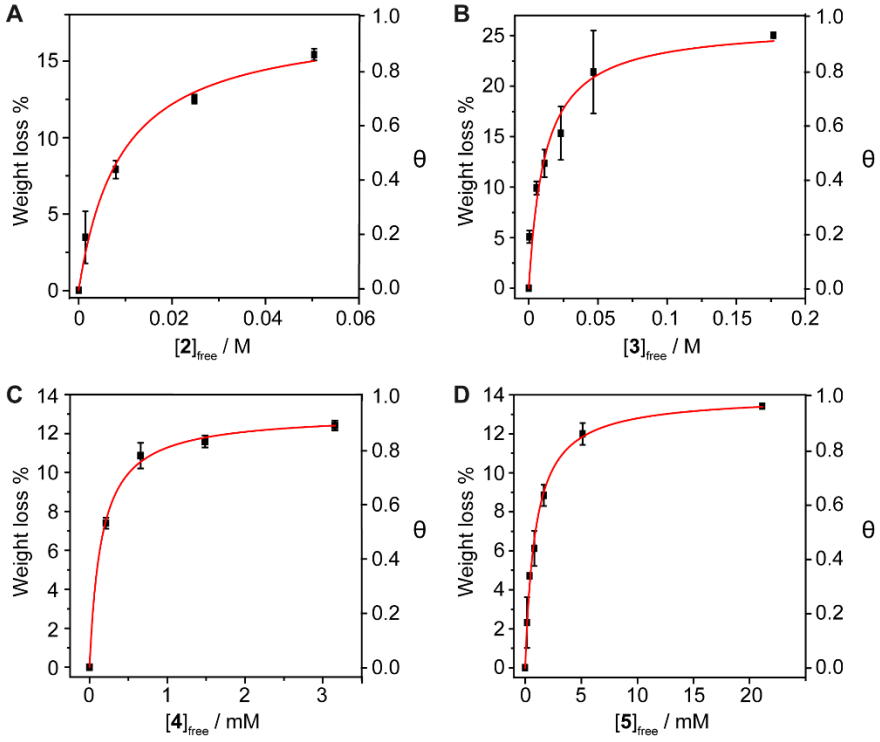

Figure 4. Titrations of the following hosts vs. pp-SWNTs (a) **2** in DMF (K_a = (2.2 ± 0.5) x 10^2 M^{-1}, r^2 = 0.986); (b) **3** in THF (K_a = (9 ± 3) x 10 M^{-1}, r^2 = 0.937); (c) **4** in THF (K_a = (6.5 ± 0.6) x 10^3 M^{-1}, r^2 = 0.998); **5** in THF (K_a = (7 ± 2) x 10^3 M^{-1}, r^2 = 0.951). Each data point is the average of three separate experiments, and the error bars represent the standard deviation. Solid red lines represent the fit.

Both electron-rich conjugated compounds and amines are known to interact strongly with SWNTs, so we expected **2** to show a significantly larger association constant compared to pyrene. This is indeed the case, as we calculated K_a = (2.2 ± 0.5) x 10^2 M^{-1} for the **2**·pp-SWNTs associate (Figure 4a), which is more than two orders of magnitude larger than the K_a of **1** in the same solvent. Addition of an extra aromatic ring in **3** also results in a significant

24. A. de Juan, Y. Pouillon, L. Ruiz-González, A. Torres-Pardo, S. Casado, N. Martín, Á. Rubio and E. M. Pérez, *Angew. Chem., Int. Ed.*, 2014, **53**, 5394-5400.
25. A. de Juan and E. M. Pérez, *Nanoscale*, 2013, **5**, 7141-7148.
26. A. López-Moreno and E. M. Pérez, *Chem. Commun.*, 2015, **51**, 5421-5424.
27. A. de Juan, M. Mar Bernal and E. M. Pérez, *ChemPlusChem*, 2015, **80**, 1153-1157.

increase in binding constant with respect to pyrene, reaching K_a = (9 ± 3) x 10 M^{-1} in THF (Figure 4b). Bivalent tweezers-like hosts are a particularly popular design for the supramolecular association of SWNTs and fullerenes, as they typically show very good affinity at a relatively low synthetic cost.[28] Indeed, **4** shows K_a = (6.5 ± 0.6) x 10^3 M^{-1} towards pp-SWNTs in THF (Figure 4c). Finally, we decided to get an insight into the association of U-shaped molecule **5**, which associates pp-SWNTs with K_a = (7 ± 2) x 10^3 M^{-1} (Figure 4d), slightly larger than that of **4**.

Note that **4** and **5** feature two pyrene binding motifs each, and might show multivalency and/or cooperativity phenomena.[29] Since our method is based on measuring the concentration of the complex by desorbing it completely, it would not be valid to determine stepwise association constants. A possible approach to investigate such issues would be to utilize the Hill equation.[30-32] Considering the clearly hyperbolic shape of the binding isotherms, we have determined average binding constants only.

To validate our experimental results, theoretical calculations were performed for the list of host-guest nanotube assemblies under the density functional theory (DFT) framework. The atom pair-wise Grimme's dispersion correction in its latest version (D3)[33] was coupled to the hybrid density functional of Perdew-Burke-Hernzerhof (PBE0)[34] through the Becke-Johnson damping function[35] and including the three-body dispersion correction (EABC).[36] The double-zeta Pople's 6-31G** basis set[37] was employed throughout and the basis set superposition error (BSSE) was corrected according to the counterpoise (CP) scheme of Boys and Bernardi.[38] The intensity of the interaction between host and guest was calculated by means of two different quantities. The interaction energy (E_{int}) is defined as the energy difference between the host-guest complex (HG)

28. E. M. Pérez and N. Martín, *Pure and Appl. Chem.*, 2010, **82**, 523-533.
29. C. A. Hunter and H. L. Anderson, *Angew. Chem. Int. Ed.*, 2009, **48**, 7488-7499.
30. Y. Baudry, G. Bollot, V. Gorteau, S. Litvinchuk, J. Mareda, M. Nishihara, D. Pasini, F. Perret, D. Ronan, N. Sakai, M. R. Shah, A. Som, N. Sordé, P. Talukdar, D. H. Tran and S. Matile, *Adv. Funct. Mater.*, 2006, **16**, 169-179.
31. E. M. Pérez, L. Sánchez, G. Fernández and N. Martín, *J. Am. Chem. Soc.*, 2006, **128**, 7172-7173.
32. G. Ercolani, *J. Am. Chem. Soc.*, 2003, **125**, 16097-16103.
33. S. Grimme, J. Antony, S. Ehrlich and H. Krieg, *J. Chem. Phys.*, 2010, **132**, 154104.
34. C. Adamo and V. Barone, *J. Chem. Phys.*, 1999, **110**, 6158-6170.
35. S. Grimme, S. Ehrlich and L. Goerigk, *J. Comput. Chem.*, 2011, **32**, 1456-1465.
36. S. Grimme, *Chem. Eur. J.*, 2012, **18**, 9955-9964.
37. M. M. Francl, W. J. Pietro, W. J. Hehre, J. S. Binkley, M. S. Gordon, D. J. DeFrees and J. A. Pople, *J. Chem. Phys.*, 1982, **77**, 3654-3665.
38. S. F. Boys and F. Bernardi, *Mol. Phys.*, 1970, **19**, 553-566.

and the individual moieties separately (H and G), with all of them at the geometry of the complex:

$$E_{int} = E_{HG}^{HG} - E_{H}^{HG} - E_{G}^{HG}$$

where E_X^Y is the energy of fragment X at the geometry of Y.

Otherwise, the binding (or association) energy (E_{bind}) was calculated taking into account the relaxation of the separate monomers and, therefore, considering the deformation energy required to transform the host/guest moieties from their minimum-energy geometries to the geometry acquired in the assembly:

$$E_{bind} = E_{def} + E_{int}$$

where

$$E_{def} = \left(E_{H}^{HG} - E_{H}^{H}\right) + \left(E_{G}^{HG} - E_{G}^{G}\right)$$

As a general model for the pp-SWNTs we have utilized a fragment of a zig-zag (10,0)-SWNT. The effect of the length of the nanotube into the intermolecular interaction was assessed by increasing the SWNT size in a **1**·SWNT complex, showing that the association energy is nearly converged with sizes slightly larger than the host length (see Table S2 and Figure S21).

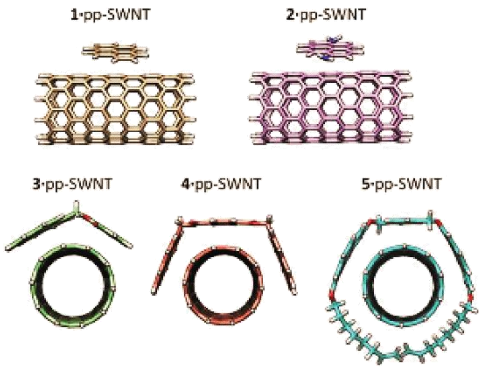

Figure 5. Minimum-energy geometry for the supramolecular assemblies formed by hosts **1**-**5** vs. the pp-SWNTs model calculated at the PBE0-D3/6-31G** level of theory.

Figure 5 displays the minimum-energy geometries for the **1**-**5** hosts assembled with the pp-SWNT model of $C_{160}H_{20}$ computed at the PBE0-D3/6-31G** level of theory in gas phase. Among the different closely energetic conformations of **1** over pp-SWNT, the diagonal arrangement is found to be the most stable, with close π–π contacts in the range of 3.2-3.5 Å. The interaction

energy of **1**·pp-SWNT is computed at -15.24 kcal mol^{-1}, which is slightly reduced to -14.84 kcal mol^{-1} for the binding energy as a consequence of the deformation energy penalty (0.59 kcal mol^{-1}). Moving from the pyrene system to 1,6-diaminopyrene (**2**), additional n–π interactions arise from close nitrogen···nanotube contacts (approximately at 4.0 Å). The E_{int} of **2**·pp-SWNT is calculated 1.3 kcal mol^{-1} larger than for **1**·pp-SWNT, but this difference is not maintained in the binding energy (Table 1). The deformation energy, calculated to be 2.83 kcal mol^{-1} for **2**·pp-SWNT, explains this trend. The inclusion of an extra aromatic ring in **3** results in a significant increase of the interaction energy up to -23.68 kcal mol^{-1}, with close π–π benzene···SWNTs (3.5 Å) and C=O···SWNTs (3.2 Å) contacts. Bivalent tweezers-like hosts further improve the supramolecular affinity vs. pp-SWNT with E_{int} as large as -38.78 and -63.23 kcal mol^{-1} in **4** and **5**, respectively. The binding energy in host **4** (-36.42 kcal mol^{-1}) is indeed approximately the sum of E_{int} for its constituting moieties **1** and **3** (-14.84 + (-21.52) = -36.36 kcal mol^{-1}), which supports the theoretical approach undertaken. Whereas the E_{def} of **4** is computed similar to **2** and **3**, it amounts 20.46 kcal mol^{-1} for **5** due to the accommodation of the alkoxy chains around the nanotube (Figure 5). This disposition confers **5**·pp-SWNT an increased E_{bind} of -42.78 kcal mol^{-1} due to close CH···π contacts calculated in the range of 2.7-3.2 Å, which contribution to the total binding energy amounts 6 kcal mol^{-1}.

Table 1. Energy parameters (kcal mol^{-1}) of the interaction between hosts **1**-**5** and guest SWNTs at the CP-corrected PBE0-D3/6-31G**+EABC level.

System	E_{int}	E_{def}	E_{bind}	CA[a] (Å^2)
1·(6,5)-SWNTs	-11.83	0.81	-13.04	42.20
1·pp-SWNTs	-15.24	0.59	-14.84	42.70
2·pp-SWNTs	-16.53	2.83	-13.70	47.25
3·pp-SWNTs	-23.68	2.16	-21.52	75.30
4·pp-SWNTs	-38.78	2.36	-36.42	126.85
5·pp-SWNTs	-63.23	20.46	-42.78	188.55

[a] The intermolecular contact area (CA) was calculated using the UCSF Chimera 1.7 software according to the formula: (area of the host + area of the guest area of the complex)/2, where the areas used refer to solvent-excluded molecular surfaces, composed of probe contact, toroidal, and reentrant surface.

Finally, the influence of the structure of the nanotube in the stability of the host-guest assembly was assessed by comparing the associates of pp-SWNT and (6,5)-SWNT with pyrene **1**. The E_{int} of **1**·(6,5)-SWNT was computed at -13.85 kcal mol^{-1}, which is 1.4 kcal mol^{-1} smaller than the E_{int} of **1**·pp-SWNT. The minimum energy structures calculated for the supramolecular complexes between pyrene and the two types of nanotubes (Figure S22) reveal subtle differences in terms of intermolecular contacts. The diameter of (6,5)-SWNT is computed at 7.5 Å, slightly smaller than for the pp-SWNT model (7.9 Å), which provokes a less efficient supramolecular assembly with pyrene. The deformation energy of **1**·(6,5)-SWNT is computed somewhat larger than **1**·pp-SWNT (Table 1), suggesting that the pyrene core is required to have a large deformation to accommodate over the more-curved nanotube surface of (6,5)-SWNT. Moreover, the intermolecular contact area for **1**·(6,5)-SWNT is calculated to be 0.5 Å^2 smaller than in **1**·pp-SWNT.

Most remarkably, the calculated E_{bind} energies and the experimentally determined K_a values show excellent quantitative agreement, despite the fact that de-solvation and solvation energies are not included in our calculations. A plot of the ln K_a vs. -E_{bind} for molecules **1**, **3**, **4**, and **5**, towards pp-SWNTs in THF at room temperature, the largest set for which we have extracted comparable K_a data, is shown in Figure 6. Fixing the intercept to 0, the data fit well (r^2 = 0.984) to a straight line of slope 0.22 ± 0.01. Therefore, our analysis shows that the ΔG_{bind} determined experimentally is proportional to the calculated E_{bind}.

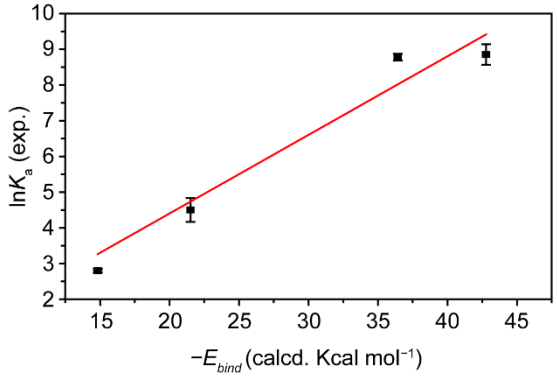

Figure 6. Plot of ln K_a vs. -E_{bind}, comparing the experimental and calculated data.

6.3 Conclusion

In summary, we have described a simple method for the determination of association constants between soluble molecules and insoluble and heterogeneous nanomaterials. The method is based on the measurement of the concentration of free host, and therefore does not require any approximation. The quantitative measurements were carried out using TGA data only, so in principle, any host molecule can be evaluated regardless of its spectroscopic properties.

To illustrate the scope and limitations of this methodology, we have tested five different hosts and two types of SWNTs in four different solvents for a total of 17 binding constant determinations. The data fit well to the binding isotherm in all cases, with a minimum r^2 of 0.937 (Table S1). The method is sensitive to solvent effects, as well as to small structural changes in both the SWNT and the host. The numeric values of K_a span over approximately four orders of magnitude, showing that the method is valid both for very small and large binding constants. Our data were validated by DFT calculations, which correctly reproduce the trends observed experimentally.

Although the main objective of the present work was to develop a standard method for the determination of binding constants towards carbon nanotubes, several interesting observations can be made with the present data set of K_a. Perhaps the most relevant conclusion is that our results back the utilization of a single unit of pyrene as a noncovalent anchor to SWNTs in polar protic solvents,[39] but caution against assuming that it will "adsorb irreversibly" to the nanotubes in any organic solvent,[40] as the association constants can be as low as 1 M^{-1}. This is particularly relevant in cases where the pyrene·SWNT supramolecular construct will be subjected to further modifications after association. In this respect, using two pyrene units connected to form a tweezers-like receptor seems a valid alternative.

Taking into account the simplicity of the methodology described, we sincerely hope that the determination of association constants will become routine for anyone interested in the supramolecular chemistry of carbon

39. N. Nakashima, Y. Tomonari and H. Murakami, *Chem. Lett.*, 2002, **31**, 638-639.
40. R. J. Chen, Y. Zhang, D. Wang and H. Dai, *J. Am. Chem. Soc.*, 2001, **123**, 3838-3839.

nanotubes. The generalization of such quantitative data will undoubtedly produce a significant leap in our understanding of their noncovalent chemistry.

The techniques and methods described here should also be applicable to other insoluble nanomaterials, such as few-layer graphene. We are currently working towards the extension of this method to such nanomaterials.

6.4 Experimental details

6.4.1 Synthesis and Characterization

General. Reagents were used as purchased. All air-sensitive reactions were carried out under argon atmosphere. Flash chromatography was performed using silica gel (Merck, Kieselgel 60, 230-240 mesh, or Scharlau 60, 230-240 mesh). Analytical thin layer chromatographies (TLC) were performed using aluminium-coated Merck Kieselgel 60 F254 plates. The NMR experiments were performed on a Bruker Avance 400 spectrometer (Magnet Ascend 400), operating at a frequency of 400 MHz and Bruker Avance 300 spectrometer (Magnet Ascend 400), operating at a frequency of 300 MHz at 298 K, unless otherwise stated, using partially deuterated solvents as internal standards. Coupling constants (J) are denoted in Hz and chemical shifts (δ) in ppm. Multiplicities are denoted as follows: s = singlet, d = doublet, t = triplet, m = multiplet, b = broad. Fast atom bombardment (FAB) ionization experiments were recorded on a Waters VG AutoSpec spectrometer and Matrix-assisted Laser desorption ionization (coupled to a Time-Of-Flight analyzer) experiments (MALDI-TOF) were recorded on a HP1100MSD spectrometer and a Bruker REFLEX spectrometer, respectively. Thermogravimetric analyses (TGA) were performed using a TA Instruments TGAQ500 with a ramp of 50 °C/min under nitrogen from 100 to 1000 °C.

Synthesis of compound **2**.

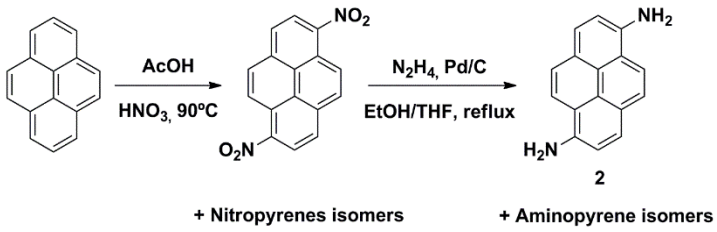

Pyrene (1g, 4.95 mmol) was dissolved in acetic acid and heated at 90ºC. Nitric acid (0.75 mL) was added slowly, and the mixture was stirred at 90ºC for 30 min, then cooled. The resulting yellow precipitated was collected by filtration obtaining a mixture of nitropyrenes. Nitropyrenes (1.45 g) were dissolved in a mixture of ethanol and tetrahydrofuran (2:1, 12 mL) and palladium on activated charcoal (27 mg) was added over the solution. The mixture was refluxed, hydrazine (1.8 mL, 37 mmol) was added and then refluxed for 12 h. The mixture was filtered and the solvent was removed under vacuum. The aminopyrenes were purified by column chromatography (silica gel, 10% Ethyl acetate in dichloromethane).

Rf (10% Ethyl acetate in dichloromethane) values were 0.9 for 1-aminopyrene (Compound **8c**, 20%), 0.6 for 1,6-diaminopyrene (Compound **2**, 25%), 0.4 for 1,3- diaminopyrene and 0.3 for 1,8-diaminopyrene.

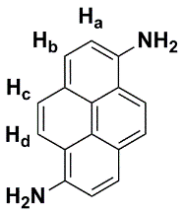

Compound **2** (25% yield). ^{1}H NMR (300 MHz, DMSO-d_6) δ 7.80 (d, *J* = 9.2 Hz, 2H, H_c), 7.75 (d, *J* = 8.2 Hz, 2H, H_b), 7.68 (d, *J* = 9.2 Hz, 2H, H_d), 7.26 (d, *J* = 8.2 Hz, 2H, H_a), 5.92 (s, 4H, NH_2). ^{13}C NMR (75 MHz, DMSO-d_6) δ 142.8, 127.1, 125.5, 124.3, 123.1, 117.3, 116.6, 113.4. MS *m/z* calculated for $C_{16}H_{12}N_2$ [M^+] 232.1 found MALDI-TOF 232.1.

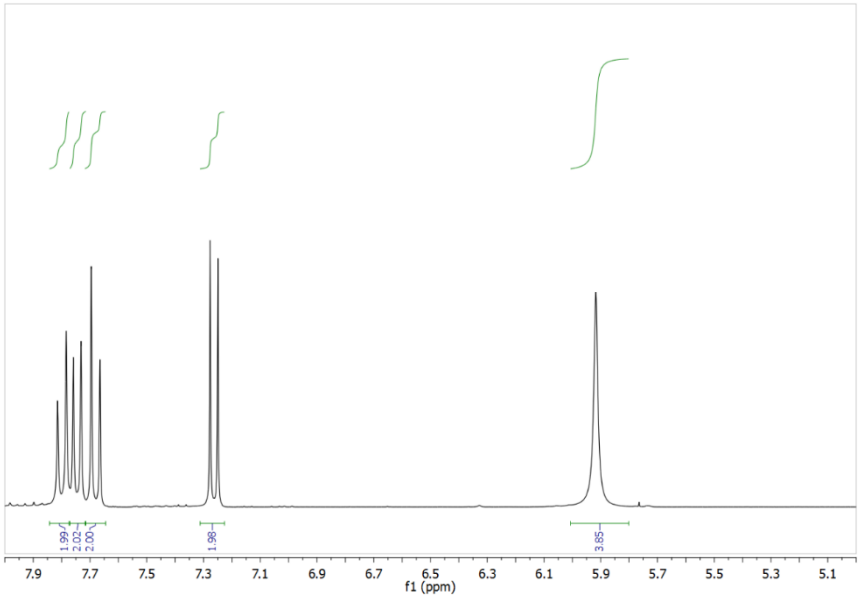
1.99
2.02
2.00
1.98
3.85
7.9
7.7
7.5
7.3
7.1
6.9
6.7
6.5
6.3
6.1
5.9
5.7
5.5
5.3
5.1
f1 (ppm)

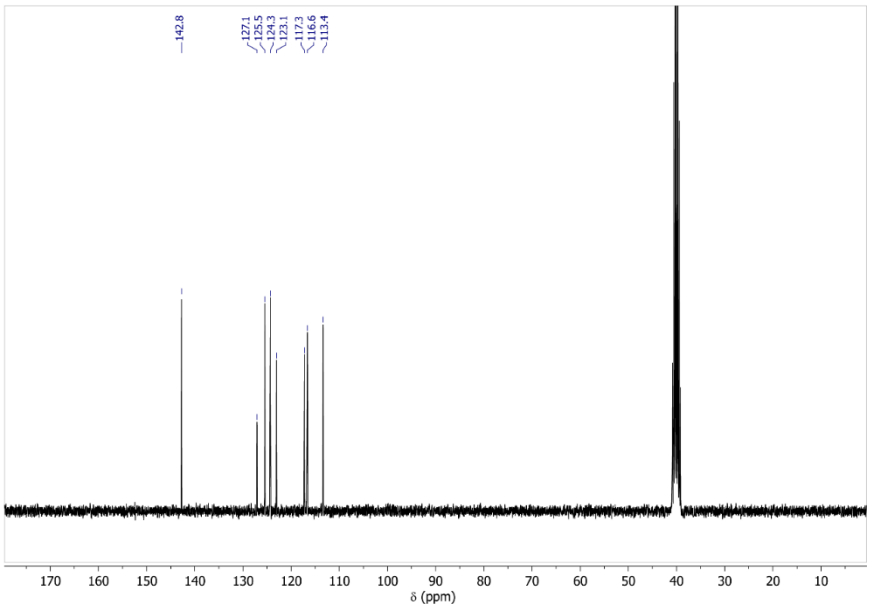
142.8
127.1
125.5
124.3
123.1
117.3
116.6
113.4
170
160
150
140
130
120
110
100
90
80
70
60
50
40
30
20
10
δ (ppm)

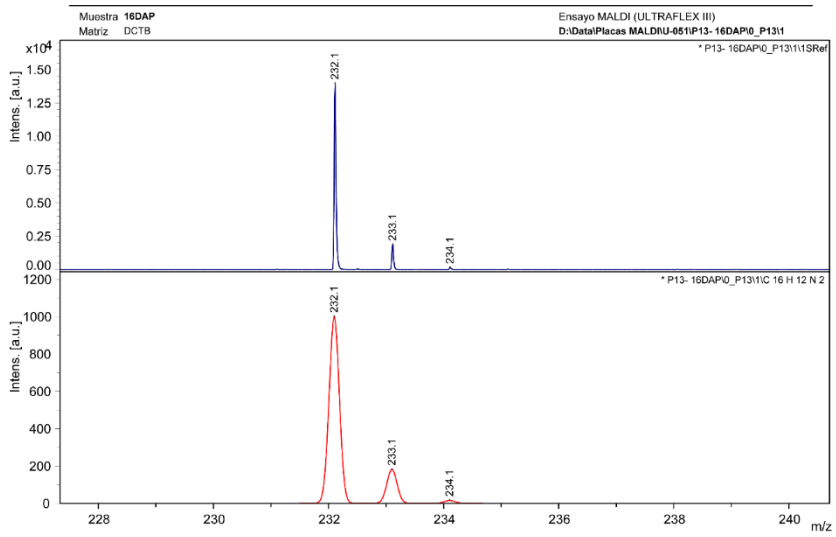

Synthesis of compounds **3** and **4**.

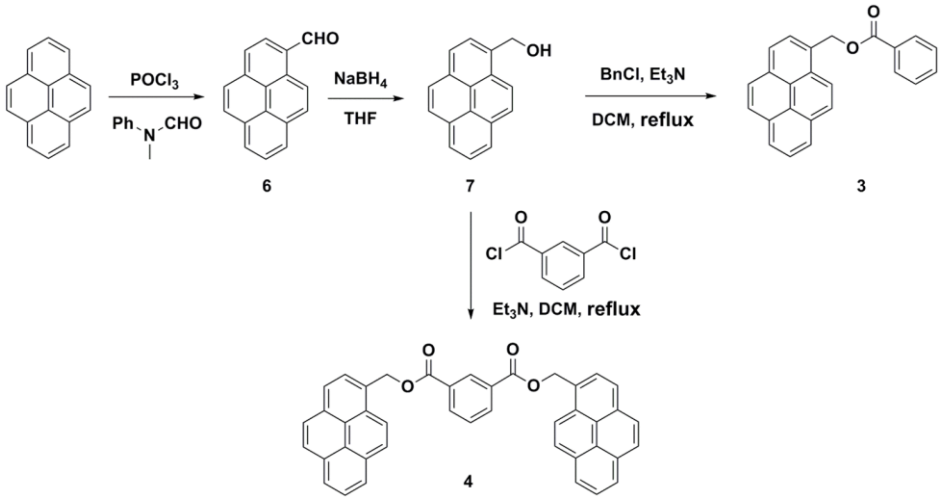

Compound **6**. Pyrene (1.0 g, 4.95 mmol) was added to a mixture of $POCl_3$ and N-methylformanilide at room temperature. The solution was heated to 100ºC under an inert atmosphere for 6 h. The reaction mixture was poured into an ice-water mixture, obtaining a yellow precipitated. The precipitate was collected through vacuum filtration. The solid was purified by recrystallization from methanol to give yellow needles of 1-pyrenecarboxaldehyde (80% yield).

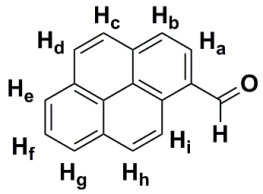

Compound **6** (80% yield). ^{1}H NMR (300 MHz, $CDCl_3$) δ 10.69 (s, 1H, aldehyde), 9.28 (d, *J* = 9.3 Hz, 1H, H_e), 8.38 – 7.90 (m, $8H_{a+b+c+d+f+g+h+i}$).

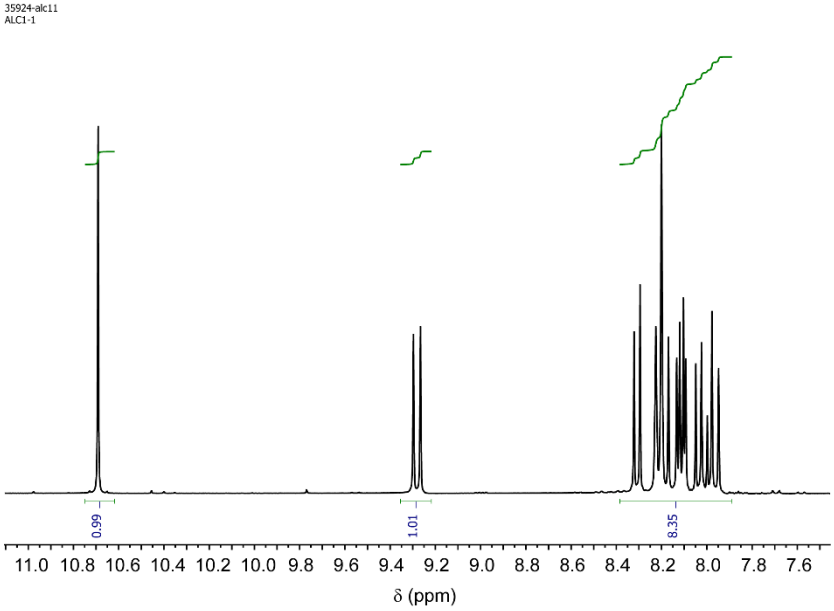

Compound **7**. 1-pyrenecarboxaldehyde (1.15 g, 5.0 mmol) was dissolved in THF (30 mL) and a solution of $NaBH_4$ (210 mg, 5.5 mmol) dissolved in methanol (10 mL) was added dropwise into the 1-pyrenecarboxaldehyde solution at room temperature. After stirring overnight, a few drops of acetic acid were added to the reaction mixture to quench the excess $NaBH_4$. After the organic solvent was removed on a rotary evaporator, the solid was extracted into chloroform twice and washed twice with an aqueous solution. The collected organic solution was dried with sodium sulfate and was concentrated to give yellow solid 1-pyrene-methanol (quantitative yield).

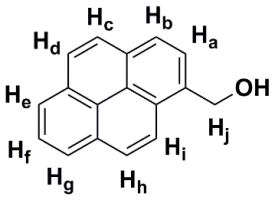

Compound **7** (quantitative yield). ^{1}H NMR (400 MHz, $CDCl_3$) δ 8.39 – 8.01 (m, 9H, $H_{a+b+c+d+e+f+g+h+i}$), 5.43 (s, 2H, H_j), 5.32 (s, 1H, OH).

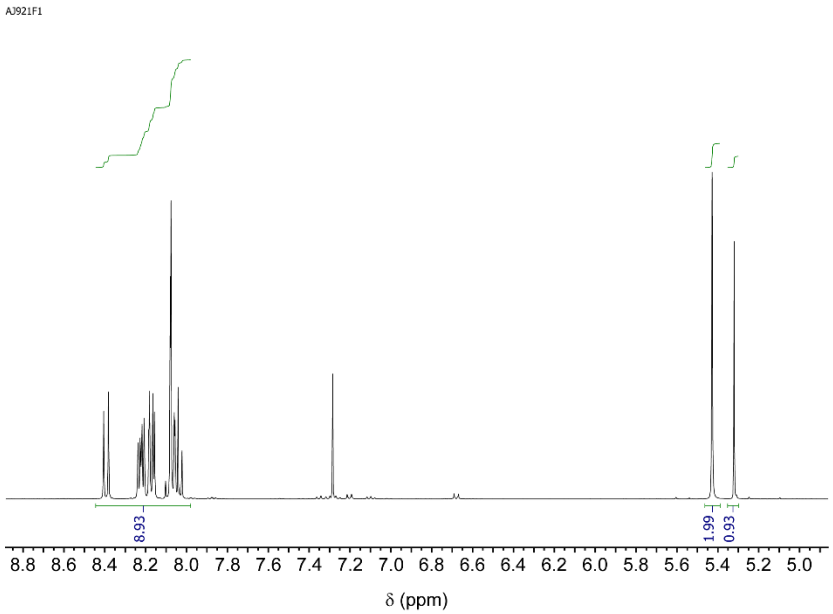

Compound **3**. 1-pyrenemethanol (1.05 g, 4.48 mmol) was dissolved in chloroform (40 mL) and triethylamine (0.93 mL, 6.72 mmol) was added over the solution. Then benzoyl chloride (0.94 g, 6.72 mmol) was added and the mixture was refluxed for 3 h. After this time the solvent was removed under vacuum and hexane was added. The product was recovered by filtration and washed several times with hexane to obtain compound **3** (quantitative yield).

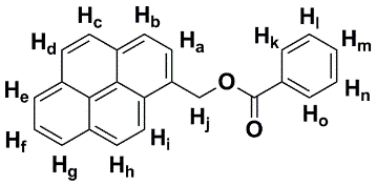

Compound **3** (quantitative yield). ^{1}H NMR (300 MHz, $CDCl_3$) δ 8.38 (d, *J* = 9.2 Hz, 1H, H_e), 8.24 – 8.15 (m, 5H, $H_{b+g+f+k+o}$), 8.10 – 7.99 (m, 5H, $H_{a+c+i+h+d}$), 7.59 – 7.47 (m, 1H, H_m), 7.43 – 7.35 (m, 2H, H_{l+n}) 6.08 (s, 2H, H_j).^{13}C NMR (75 MHz, $CDCl_3$) δ 166.6, 133.1, 131.8, 131.3, 130.8, 130.2, 129.8, 129.7, 129.0, 128.4, 128.4, 127.9, 127.8, 127.4, 126.2, 125.6, 125.5, 125.0, 124.7, 123.0, 65.4. MS *m/z* calculated for $C_{24}H_{16}O_2$ [M^+] 336.1 found MALDI-TOF 336.2.

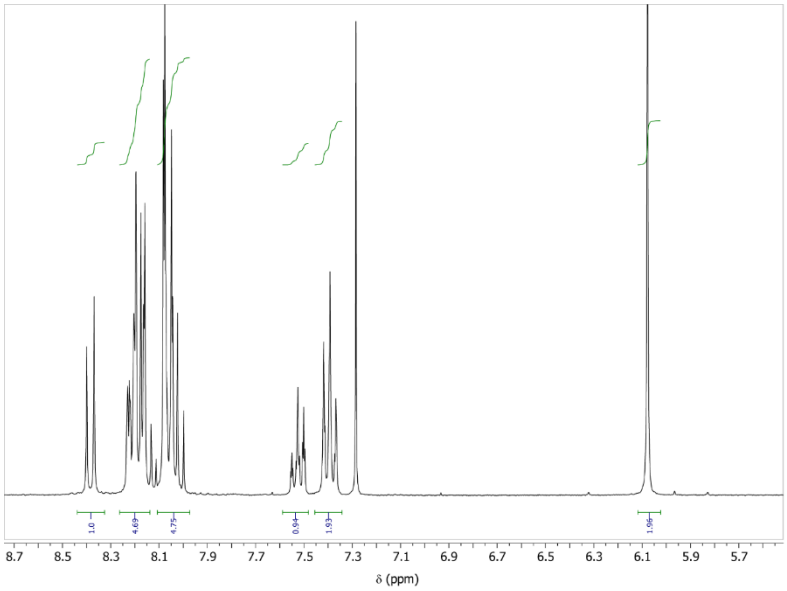

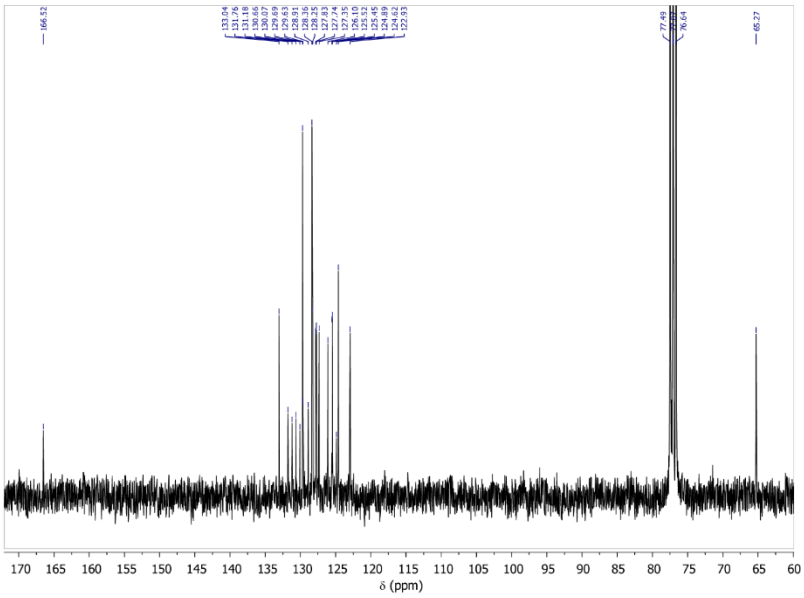

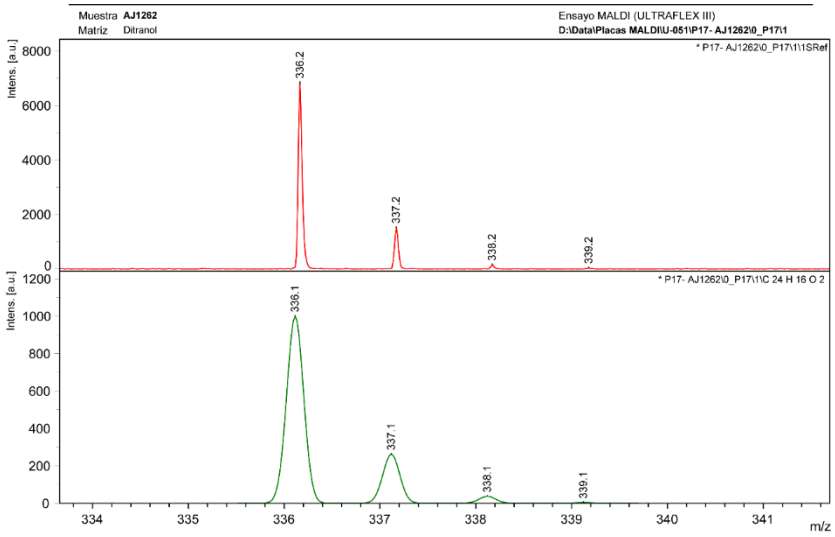

Compound **4**. 1-pyrenemethanol (1 g, 4.27 mmol) was dissolved in chloroform (20 mL) and triethylamine (0.6 mL, 4.27 mmol) was added over the solution. Isophtaloyl chloride (0.21 g, 1.07 mmol) was added and the mixture was refluxed for 4 h. After this time 30 mL of chloroform were added and washed with 50 mL of hydrochloric acid 2N, 50 mL of 5% $NaHCO_3$ aqueous solution and water and then organic layer was dried over Na_2SO_4 and removed

under vacuum to obtain a solid. Compound **4** (65% yield) was purified by column chromatography (silica gel, dichloromethane).

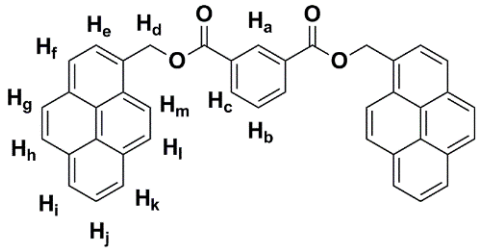

Compound **4** (65% yield).^{1}H NMR (400 MHz, $CDCl_3$) δ 8.80 (t, *J* = 1.2 Hz, 1H, H_a), 8.37-8.34 (m, 2H, H_i), 8.24 – 8.16 (m, 4H, H_{f+c}), 8.18 (d, *J* = 7.6 Hz, 2H, H_k), 8.15 – 8.11 (m, 6H, H_{j+h+g}), 8.11 – 8.09 (m, 2H, H_m), 8.08 – 8.00 (m, 4H, H_{e+l}), 7.45 (t, *J* = 7.8 Hz, 1H, H_b), 6.09 (s, 4H, H_d). ^{13}C NMR (101 MHz, $CDCl_3$) δ 165.7, 134.1, 131.8, 131.2, 131.0, 130.7, 130.6, 129.6, 128.6, 128.6, 128.3, 127.9, 127.8, 127.4, 126.1, 125.6, 125.5, 124.9, 124.6, 124.6, 122.8, 77.3, 65.6. MS *m/z* calculated for $C_{42}H_{26}O_4$ [M^+] 594.2 found FAB 594.2.

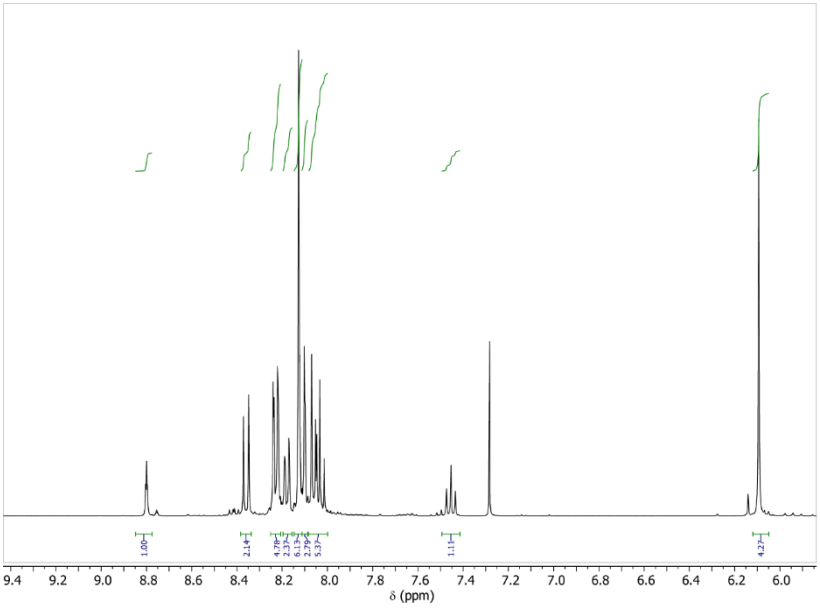

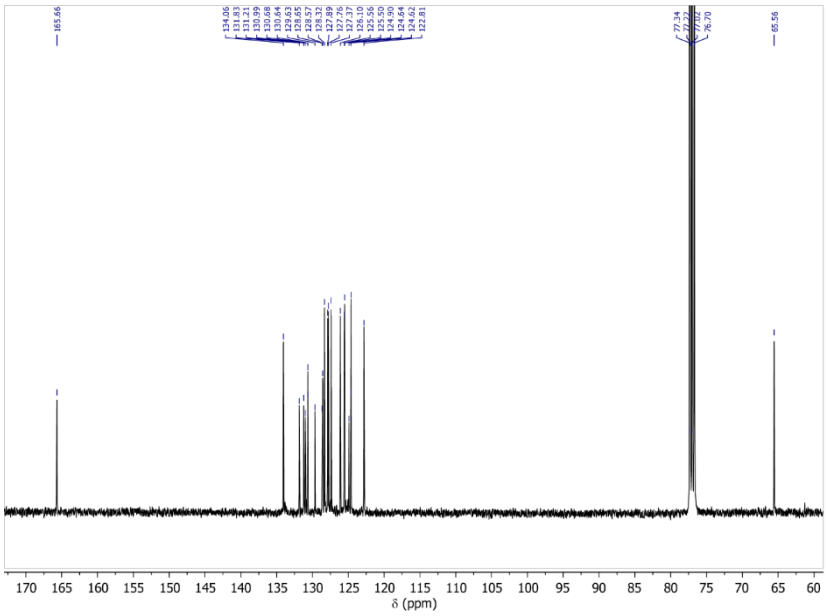
165.66
134.06
131.21
130.99
130.68
130.44
129.63
128.65
128.57
128.32
127.89
127.76
127.73
126.10
125.56
125.50
124.90
124.64
124.62
122.81
77.34
77.22
76.70
65.56
170 165 160 155 150 145 140 135 130 125 120 115 110 105 100 95 90 85 80 75 70 65 60
δ (ppm)

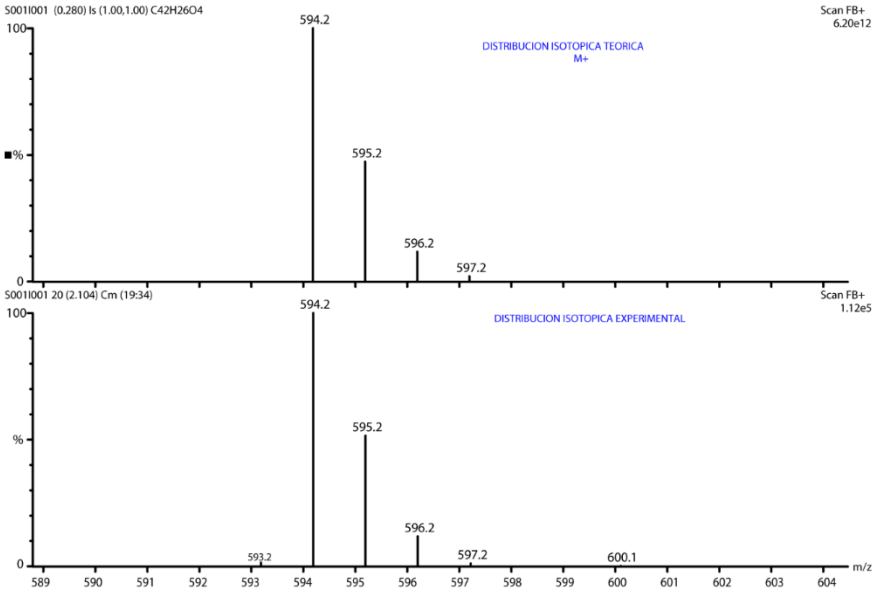
S001I001 (0.280) Is (1.00,1.00) C42H26O4
Scan FB+
6.20e12
100
%
0
594.2
595.2
596.2
597.2
DISTRIBUCION ISOTOPICA TEORICA
M+
S001I001 20 (2.104) Cm (19:34)
Scan FB+
1.12e5
100
%
0
594.2
595.2
596.2
593.2
597.2
600.1
DISTRIBUCION ISOTOPICA EXPERIMENTAL
589 590 591 592 593 594 595 596 597 598 599 600 601 602 603 604
m/z

Synthesis of compound **5**.

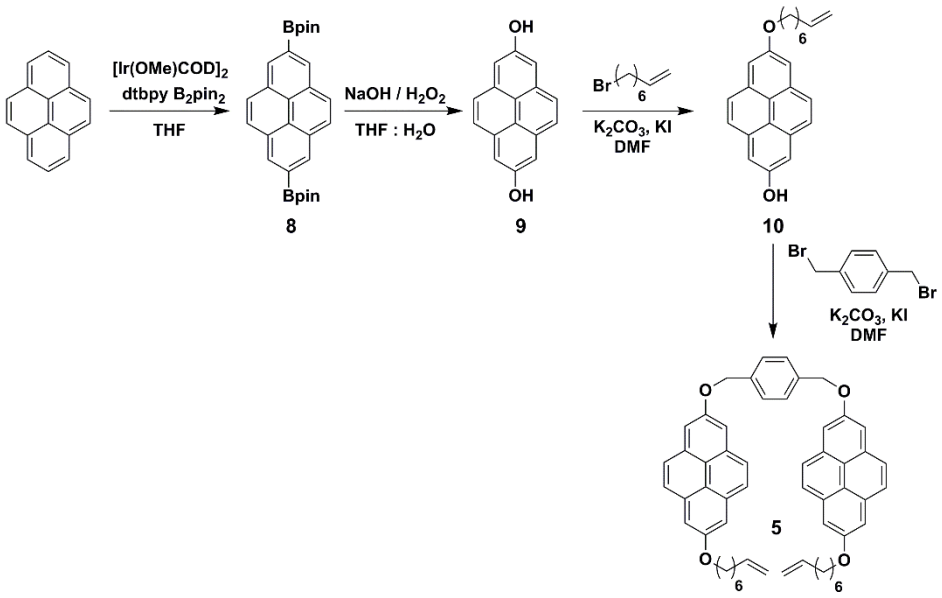

Compound **8**. In a nitrogen-filled glove box, [{Ir (μ-OMe)COD}$_2$] (0.060 g, 0.09 mmol), 4,4'-di-tert-butyl-2,2'-bipyridine (dtbpy, 0.048 g, 0.18 mmol), and B_2pin_2 (0.10 g, 0.39 mmol) were dissolved in THF (5 mL). The mixture was added to pyrene (1.80 g, 8.90 mmol) and B_2pin_2 (4.86 g, 19.1 mmol). After addition of THF (10 mL), the reaction mixture was stirred at 80ºC for 16 h. Then, the reaction mixture was passed through a silica plug (eluent: CH_2Cl_2) and the solvent was removed under reduced pressure. The pale-yellow residue was washed with hexane obtaining compound **8** (quantitative yield)**.**

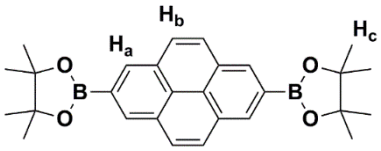

Compound **8** (quantitative yield). ^{1}H NMR (400 MHz, $CDCl_3$) δ 8.62 (s, 4H, H_a), 8.08 (s, 4H, H_b), 1.46 (s, 24H, H_c).

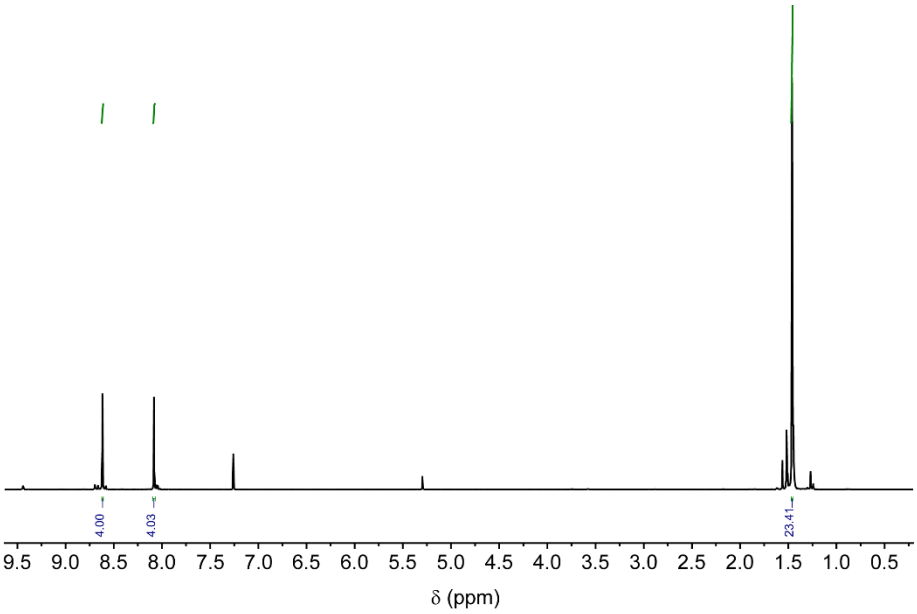

Compound **9**. Molecule **8** (0.50 g, 1.1 mmol) and NaOH (0.26 g, 6.5 mmol) were dissolved in THF (50 mL) and an aqueous solution of H_2O_2 (0.66 g, 6.5 mmol, 35 wt%) was added to this mixture. After stirring at room temperature for 4 h, the solution was acidified to pH 1–2 by using 1M HCl. The product was extracted into Et_2O (3x100 mL) and the organic fractions were dried over $MgSO_4$. (Caution: care must be taken to destroy all peroxides in the aqueous phase by stirring with aqueous H_2SO_4 and CuI). The solvent volume was reduced to about 10 mL under reduced pressure and the product was precipitated by addition of hexane (200 mL). The light-brown solid product **9** (80% yield) was collected by filtration.

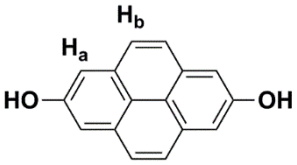

Compound **9** (80% yield). ^{1}H NMR (400 MHz, DMSO) δ 9.88 (s, 2H, OH), 7.94 (d, *J* = 2.6 Hz, 4H, H_b), 7.60 (s, 4H, H_a).

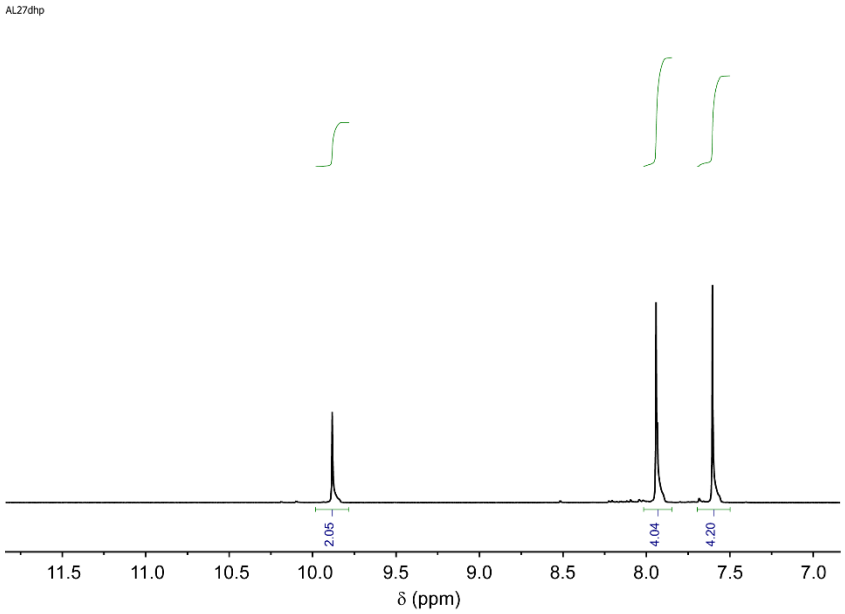

Compound **10**. 2,7-dihydroxypyrene (0.5 g, 2.14 mmol) was dissolved in 20 mL of dry DMF. Then, dry K_2CO_3 (1.65 g, 12 mmol), bromo alkene (2.15 mmol), and a catalytic amount of KI were added and the mixture heated to reflux for 8 h. The crude reaction was poured into ice-cold 1 M aqueous HCl, and filtrated. The solid was redissolved in CH_2Cl_2 and washed twice with water, the organic fraction was dried over $MgSO_4$, the solvent evaporated, and the resulting product subjected to column chromatography (CH_2Cl_2) to obtain the pure product as a light brown solid in 18% yield.

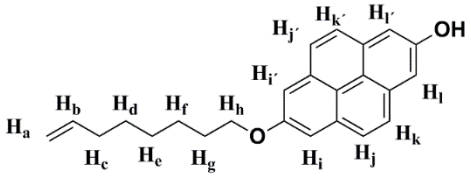

Compound **10** (18% yield). ^{1}H RMN ($CDCl_3$, 300 MHz) δ 7.95 (q, *J* = 9.0 Hz, 4H, $H_{j+j´+k+k´}$), 7.71 (s, 2H, $H_{i+i´}$), 7.62 (s, 2H, $H_{l+l´}$), 5.92 – 5.79 (m, 1H, H_b), 5.27 (s,1H, OH), 5.07 – 4.94 (m, 2H, H_a), 4.26 (t, *J* = 6.5 Hz, 2H, H_h), 2.12 – 2.05 (m, 2H, H_c), 1.99 – 1.90 (m, 2H, H_g), 1.61 – 1.29 (m, 6H, H_{d+e+f}). ^{13}C NMR ($CDCl_3$, 75 MHz) δ 156.7, 153.0, 139.0, 131.8, 131.5, 127.7, 127.1, 120.1, 120.0, 114.3, 111.8, 111.5, 68.6, 33.7, 29.4, 28.9, 28.9, 26.0. MS m/z calculated for $C_{24}H_{24}O_2$ 344.1, found MALDI 344.2.

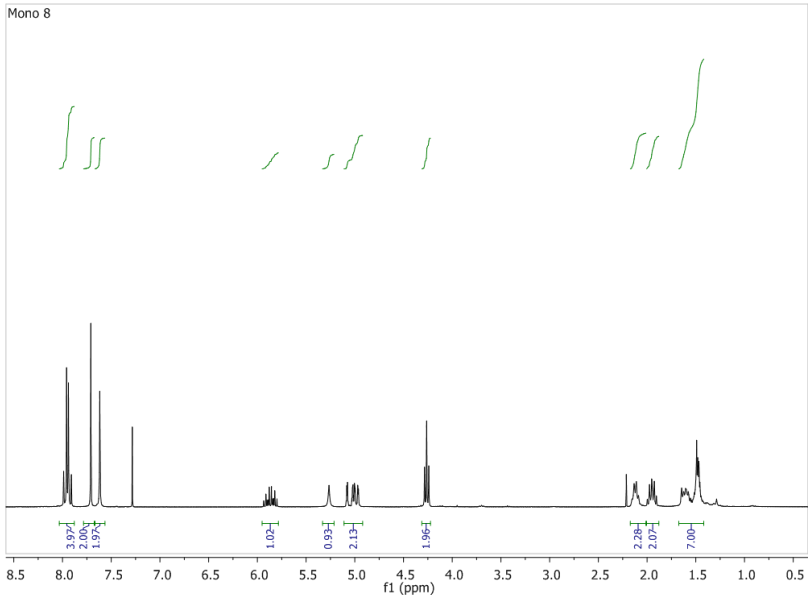
Mono 8
3.97
2.00
1.97
1.02
0.93
2.13
1.96
2.28
2.07
7.00
8.5 8.0 7.5 7.0 6.5 6.0 5.5 5.0 4.5 4.0 3.5 3.0 2.5 2.0 1.5 1.0 0.5
f1 (ppm)

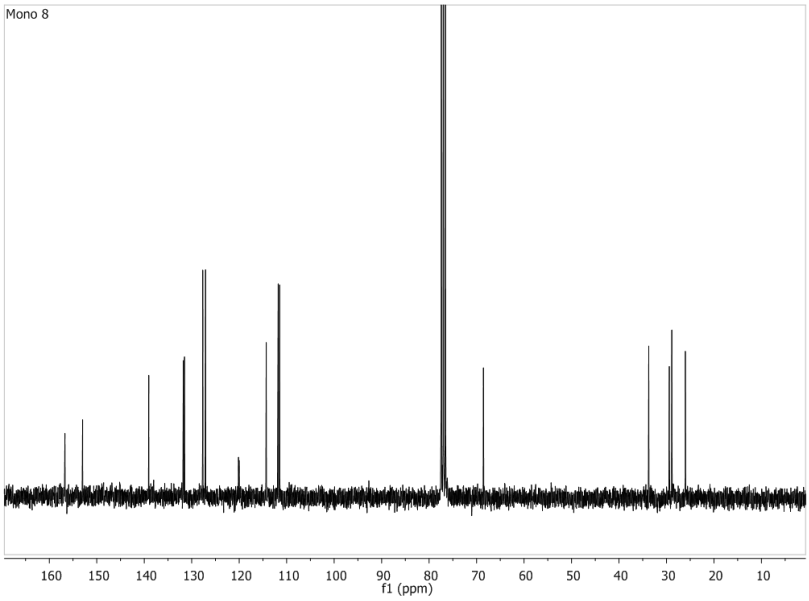
Mono 8
160 150 140 130 120 110 100 90 80 70 60 50 40 30 20 10
f1 (ppm)

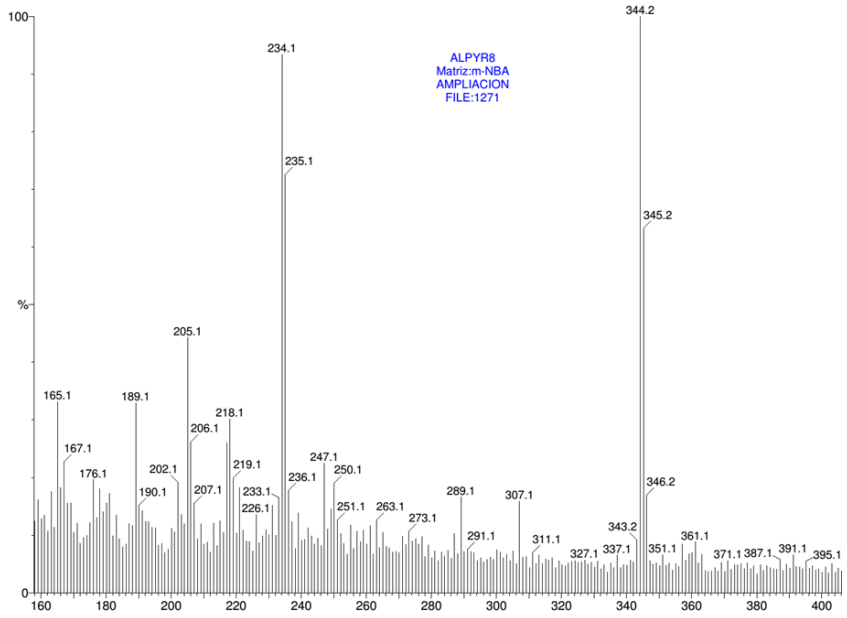

Compound **5**. Dry K_2CO_3 (0.135 g,1.04 mmol), α−α´ dibromo-*p*-xylene (56 mg, 0.21 mmol), and a catalytic amount of potassium iodide were added to a solution of the monoalkylated dihydroxypyrene (0.2 g, 0.52 mmol) in 15 mL of dry N,N-dimethylformamide. The solution was heated to 80 ºC for 4 h. The crude reaction was poured into ice-cold 1 M aqueous HCl, and filtrated. The solid was redissolved in CH_2Cl_2 and washed twice with water, the organic fraction was dried over $MgSO_4$, the solvent evaporated, and the resulting product subjected to column chromatography (CH_2Cl_2) to obtain the pure product as a light brown solid in 59% yield.

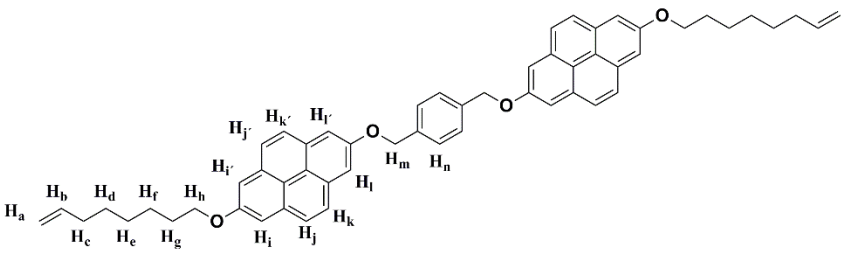

Compound **5** (59% yield). ^{1}H RMN ($CDCl_3$, 300 MHz) δ: 7.97 (s, 8H, $H_{j+j'+k+k'}$), 7.79 (s, 4H, $H_{i+i'}$), 7.71 (s, 4H, $H_{l+l'}$), 7.63 (s, 4H, H_n), 5.93 – 5.80 (m, 2H, H_a), 5.40 (s, 4H, H_m), 5.08 – 4.96 (m, 4H, H_b), 4.27 (t, *J* = 6.5Hz, 4H, H_h), 2.13 – 2.09 (m, 4H, H_c), 2.00 – 1.91 (m, 4H, H_g), 1.63 – 1.58 (m, 4H, H_f), 1.49

– 1.46 (m, 8H, H_{d+e}) ppm. ^{13}C NMR ($CDCl_3$, 75 MHz) δ: 156.8, 156.3, 139.0, 136.9, 131.6, 131.6, 127.8, 127.5, 127.4, 120.3, 120.0, 114.3, 111.6, 111.4, 77.2, 70.3, 68.5, 33.7, 29.7, 29.4, 28.9, 28.9, 26.0 ppm. MS m/z calculated for $C_{56}H_{54}O_4$ 790.4, found MALDI 790.4.

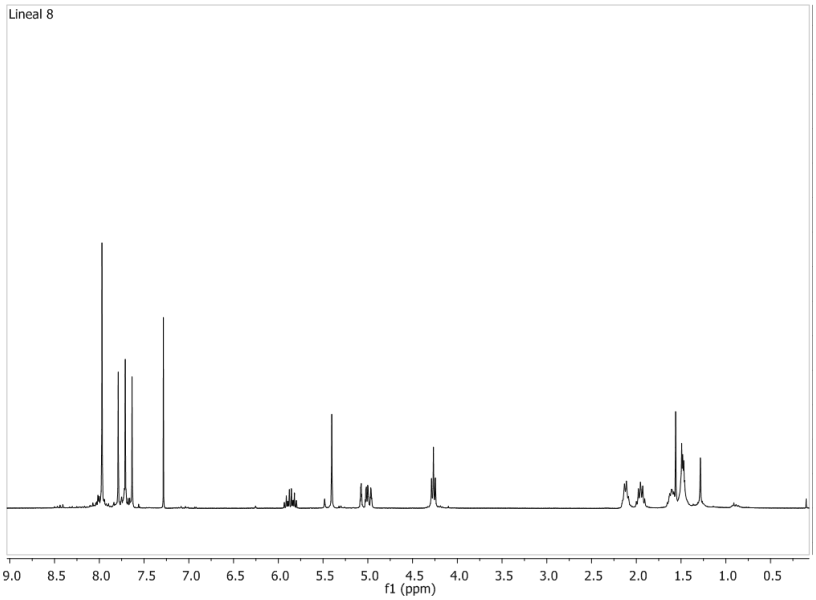

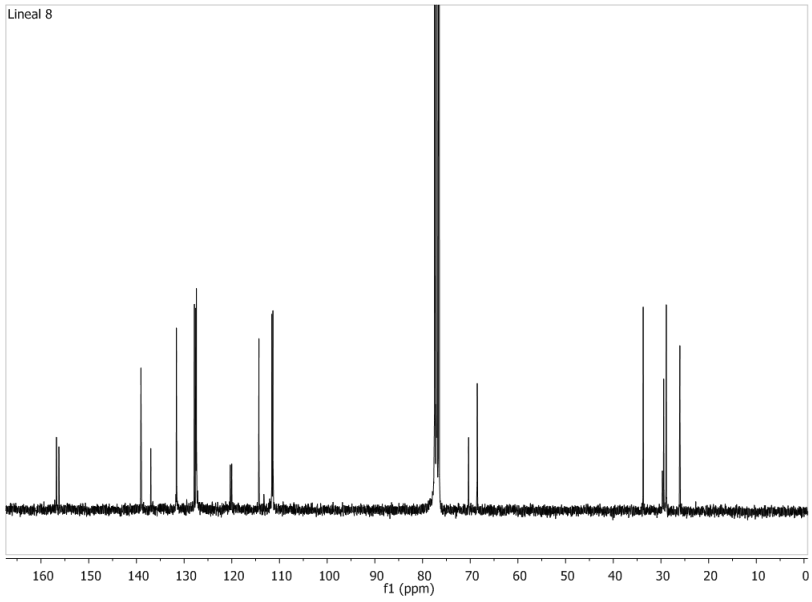

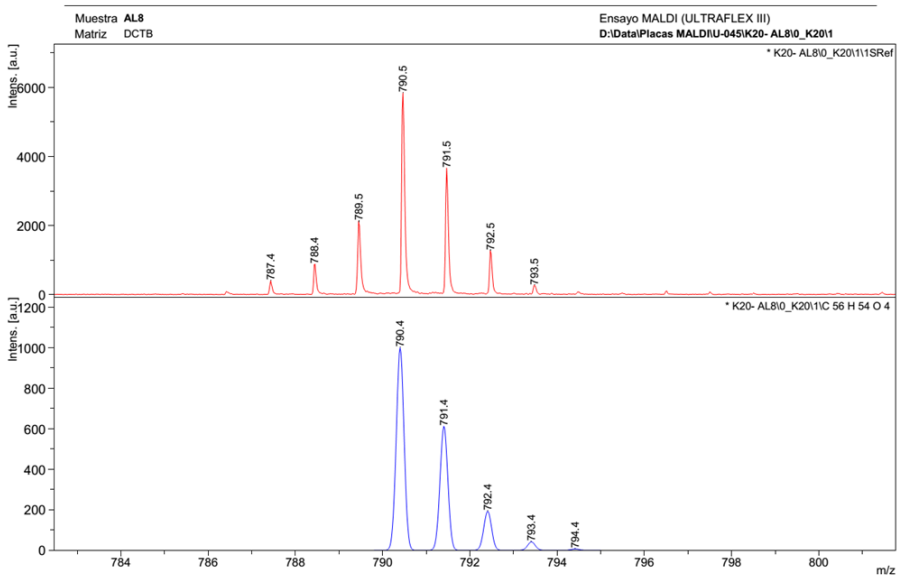

6.4.2 Titration Details

General procedure for titration

The titration curve for each host is formed using the TGA results of independent incubation experiments performed with different host concentration.

Each experiment proceeds as follows: host was dissolved in the corresponding solvent by sonication. Carbon nanotubes were added (mg per mL) and stirred for 2 h at room temperature. Then, the mixture was filtered through a 0.2 µm-pore size polytetrafluorethylene membrane. The solid obtained was dried under vacuum and characterized by thermogravimetric analysis (under N_2, ramp of 50 ºC/min, weight loss was measured from 100 ºC to 600 ºC).

Each independent experiment for each host concentration was repeated 3 times and the different results were averaged. Blank to determine the solvent adsorbed on or encapsulated in the carbon nanotube was carried out, and subtracted in the data analysis.

Table S1. Summary of results obtained from titrations at 298 K.

	Solvent	K_a (M^{-1})	Error (M^{-1})	Saturation	r^2
1·pp-SWNTs	THF[a]	16.4	0.8	56	0.999
1·pp-SWNTs	THF	24	6	26	0.979
1·pp-SWNTs	THF[b]	21	4	28	0.985
1·pp-SWNTs	DMF	9	3	47	0.978
1·pp-SWNTs	TCE	4.5	0.9	59	0.987
1·pp-SWNTs	MeOH	2.6×10^3	0.2×10^3	15	0.998
1·(6,5)-SWNTs	THF	41	8	19	0.987
1·(6,5)-SWNTs	DMF	1.6	0.4	73	0.985
1·(6,5)-SWNTs	TCE	1.6	0.1	67	0.998
1·(6,5)-SWNTs	MeOH	1.0×10^3	0.1×10^3	12	0.994
2·pp-SWNTs	DMF	2.2×10^2	0.5×10^2	18	0.986
2·(6,5)-SWNTs	DMF	29	3	27	0.995
3·pp-SWNTs	THF	9×10	3×10	26	0.937
3·pp-SWNTs	TCE	20	5	24	0.965
4·pp-SWNTs	THF	6.5×10^3	0.6×10^3	13	0.998
4·pp-SWNTs	TCE	4×10^3	1×10^3	9	0.986
5·pp-SWNTs	THF	7×10^3	2×10^3	21	0.951

[a] 0.1 mg/mL of pp-SWNTs.

[b] 10 mg/mL of pp-SWNTs.

Thermogravimetric analysis

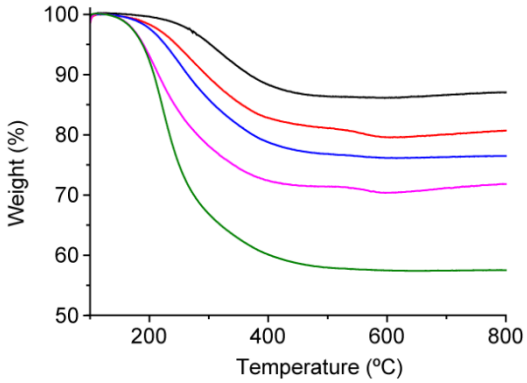

Figure S1. TG analysis of titration of **1** *vs* pp-SWNTs in THF at 0.1 mg/mL of SWNTs.

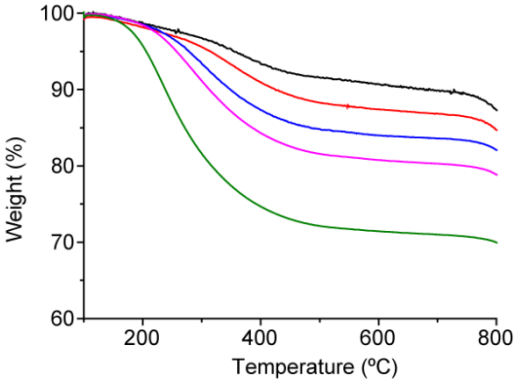

Figure S2. TG analysis of titration of **1** *vs* pp-SWNTs in THF at 1 mg/mL of SWNTs.

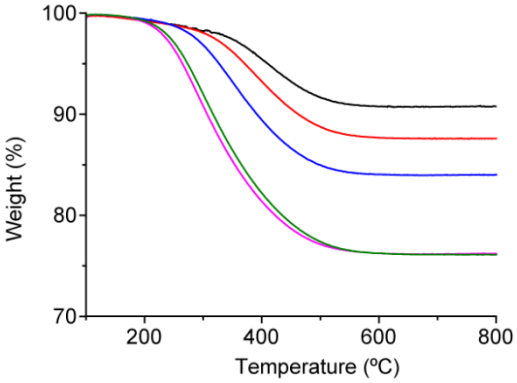

Figure S3. TG analysis of titration of **1** vs pp-SWNTs in THF at 10 mg/mL of SWNTs**.**

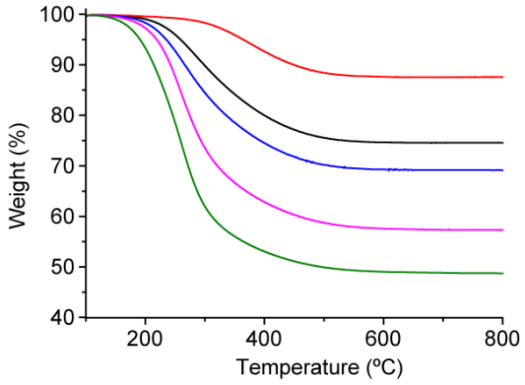

Figure S4. TG analysis of titration of **1** *vs* pp-SWNTs in DMF at 1 mg/mL of SWNTs.

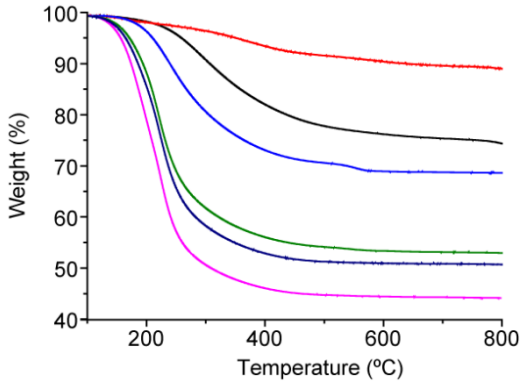

Figure S5. TG analysis of titration of **1** *vs* pp-SWNTs in TCE at 1 mg/mL of SWNTs.

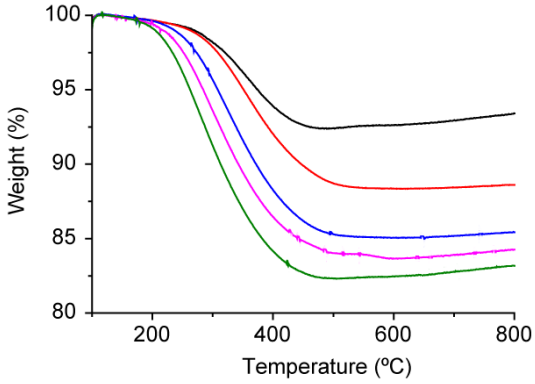

Figure S6. TG analysis of titration of **1** *vs* pp-SWNTs in MeOH at 1 mg/mL of SWNTs.

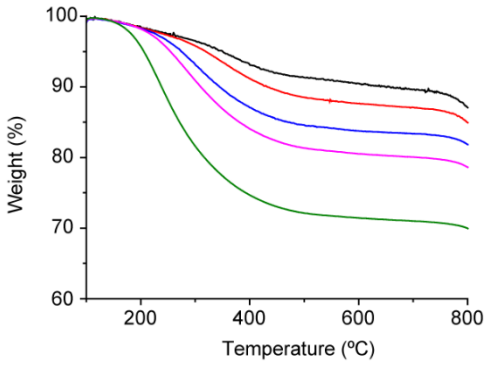

Figure S7. TG analysis of titration of **1** *vs* (6,5)-SWNTs in THF at 1 mg/mL of SWNTs.

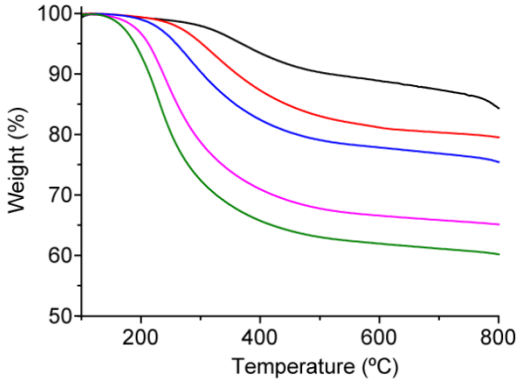

Figure S8. TG analysis of titration of **1** *vs* (6,5)-SWNTs in DMF at 1 mg/mL of SWNTs.

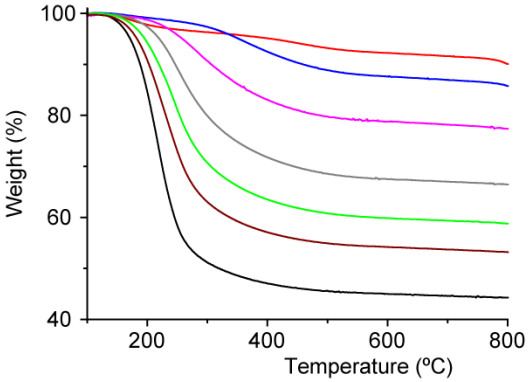

Figure S9. TG analysis of titration of **1** *vs* (6,5)-SWNTs in TCE at 1 mg/mL of SWNTs.

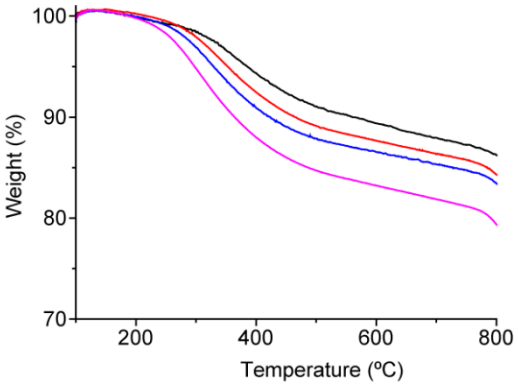

Figure S10. TG analysis of titration of **1** *vs* (6,5)-SWNTs in MeOH at 1 mg/mL of SWNTs.

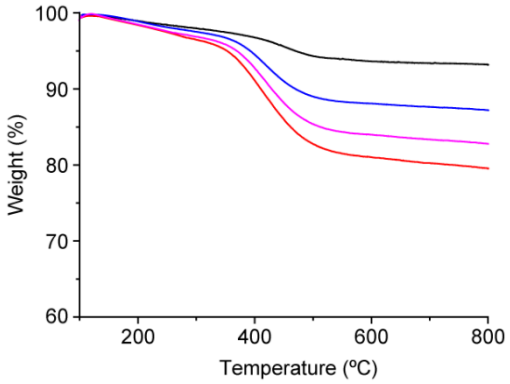

Figure S11. TG analysis of titration of **2** *vs* pp-SWNTs in DMF at 1 mg/mL of SWNTs.

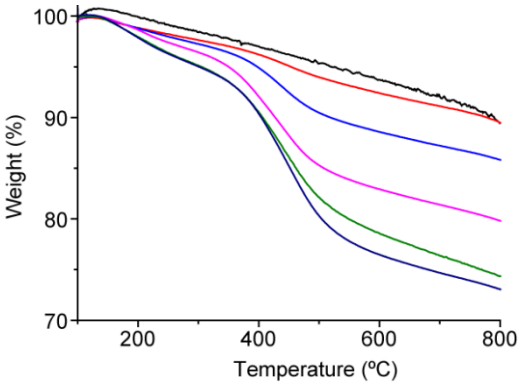

Figure S12. TG analysis of titration of **2** *vs* (6,5)-SWNTs in DMF at 1 mg/mL of SWNTs.

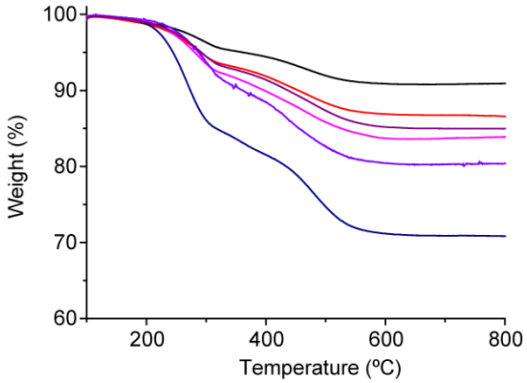

Figure S13. TG analysis of titration of **3** *vs* pp-SWNTs in THF at 1 mg/mL of SWNTs.

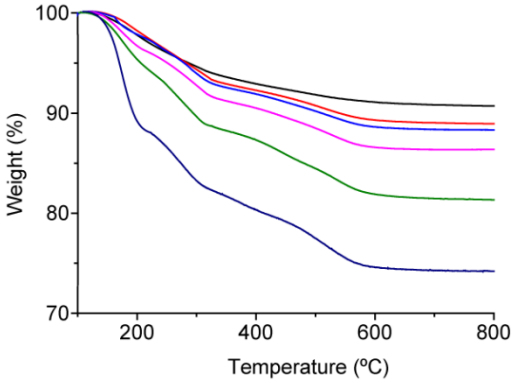

Figure S14. TG analysis of titration of **3** *vs* pp-SWNTs in TCE at 1 mg/mL of SWNTs.

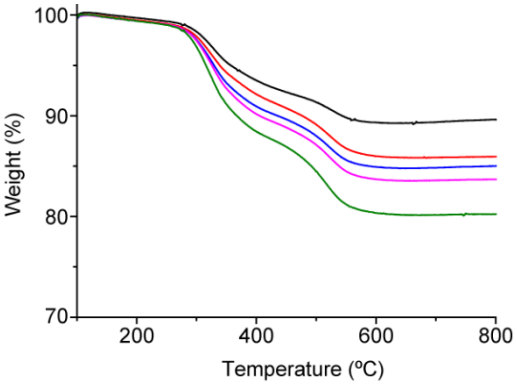

Figure S15. TG analysis of titration of **4** *vs* pp-SWNTs in THF at 1 mg/mL of SWNTs.

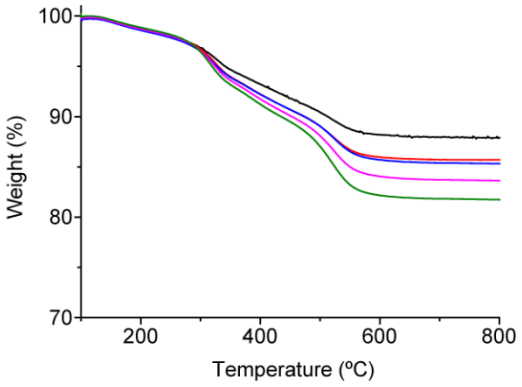

Figure S16. TG analysis of titration of **4** *vs* pp-SWNTs in TCE at 1 mg/mL of SWNTs.

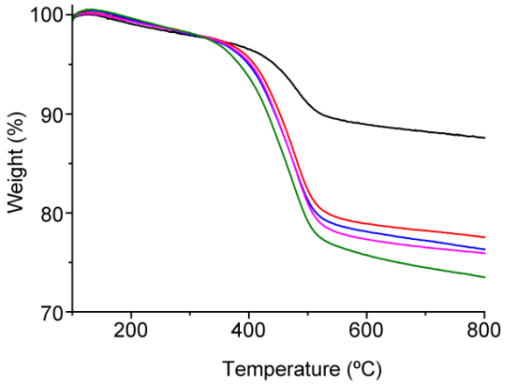

Figure S17. TG analysis of titration of **5** *vs* pp-SWNTs in THF at 1 mg/mL of SWNTs.

Adsorption isotherms

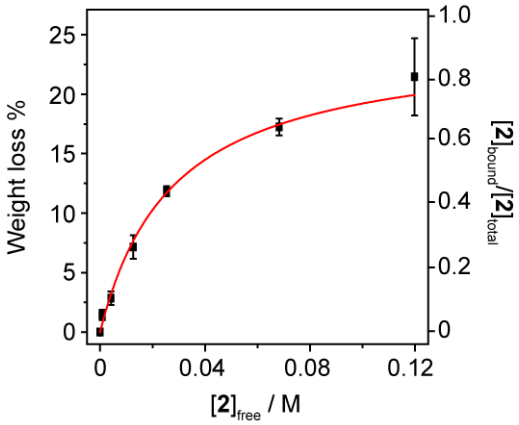

Figure S18. Titration of **2** *vs* (6,5) SWNTs in DMF at 298 K (K_a = 29 ± 3 M^{-1}, r^2 = 0.995)

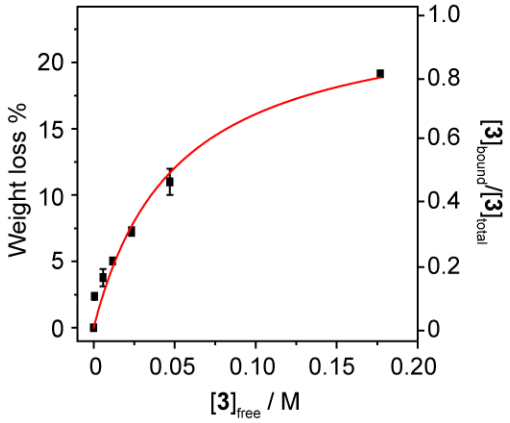

Figure S19. Titration of **3** *vs* pp-SWNTs in TCE at 298 K (K_a = 20 ± 5 M^{-1}, r^2 = 0.965)

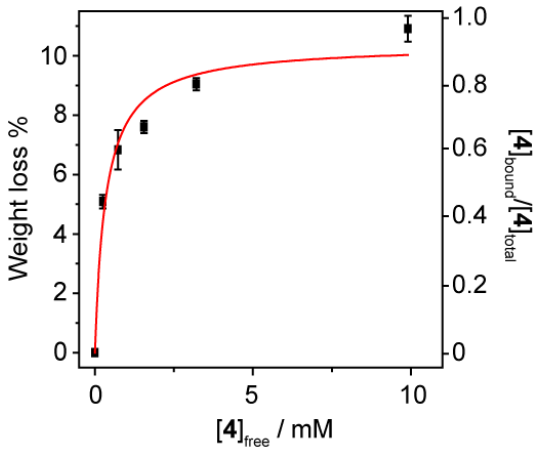

Figure S20. Titrations of **4** *vs* pp-SWNTs in TCE at 298 K (K_a = 2.9± 0.8 × 10^3 M^{-1}, r^2 = 0.960).

6.4.3 Computational Details

Table S2. Binding energy (kcal/mol) depending on the nanotube length for the parallel and perpendicular dispositions of the supramolecular **1**·pp-SWNT complex calculated at the PBE0-D3/6-31G** level of theory.

		Binding energy (kcal/mol)	
		Semi-rigid	**Fully relaxed**
parallel	**1**·$C_{40}H_{20}$	-11.05	-11.25
	1·$C_{80}H_{20}$	-17.80	-18.11
	1·$C_{120}H_{20}$	-21.79	-21.76
	1·$C_{200}H_{20}$	-21.18	-21.42
perpendicular	**1**·$C_{40}H_{20}$	-10.88	-11.12
	1·$C_{80}H_{20}$	-16.40	-17.11
	1·$C_{120}H_{20}$	-19.46	-19.60
	1·$C_{200}H_{20}$	-18.85	-17.97

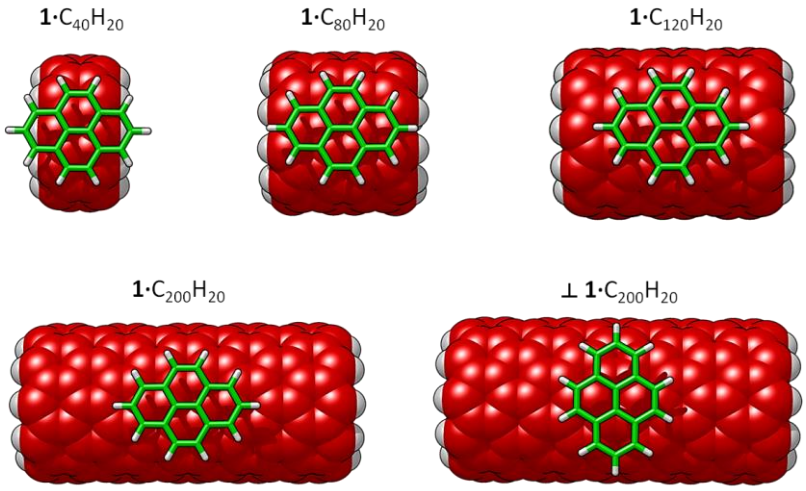

Figure S21. Minimum-energy geometries of parallel **1**·pp-SWNT assemblies and the perpendicular ⊥ **1**·$C_{200}H_{20}$ calculated at the PBE0-D3/6-31G** level from a semi-rigid optimization with fixed intramolecular parameters.

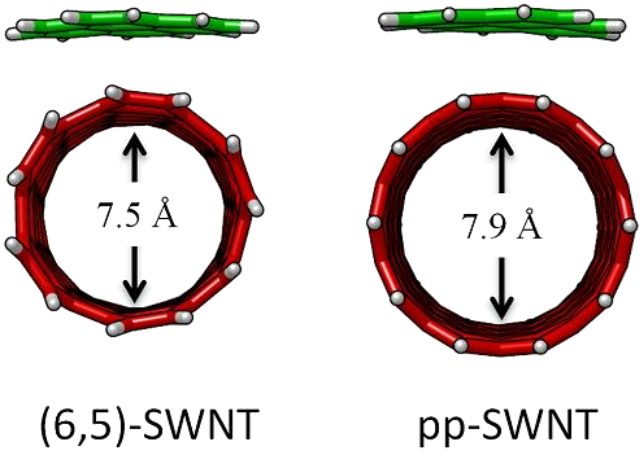

Figure S22. Side view of the supramolecular complex formed by pyrene and two types of SWNTs.

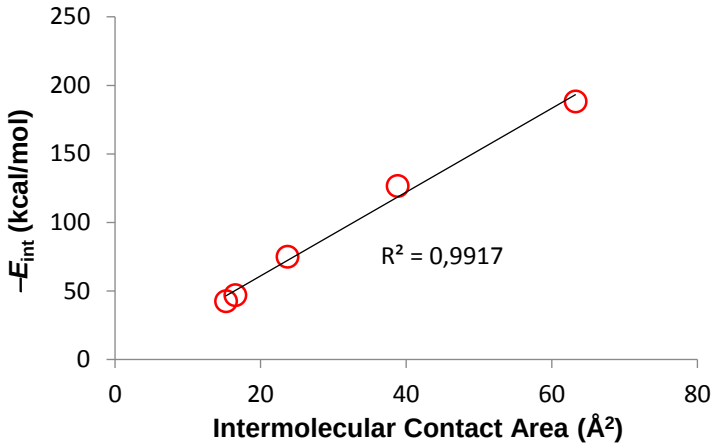

Figure S23. Relationship between the intermolecular contact area and the interaction energy for the **host**·pp-SWNTs assemblies.

6.5 References

1. A. K. Geim and K. S. Novoselov, *Nat. Mater.*, 2007, **6**, 183-191.
2. A. K. Geim, *Science*, 2009, **324**, 1530-1534.
3. C. N. R. Rao, A. K. Sood, K. S. Subrahmanyam and A. Govindaraj, *Angew. Chem. Int. Ed.*, 2009, **48**, 7752-7777.
4. D. Tasis, N. Tagmatarchis, A. Bianco and M. Prato, *Chem. Rev.* , 2006, **106**, 1105-1136.
5. J. Y. Kim, O. Voznyy, D. Zhitomirsky and E. H. Sargent, *Adv. Mater.*, 2013, **25**, 4986-5010.
6. M. V. Kovalenko, L. Manna, A. Cabot, Z. Hens, D. V. Talapin, C. R. Kagan, V. I. Klimov, A. L. Rogach, P. Reiss, D. J. Milliron, P. Guyot-Sionnnest, G. Konstantatos, W. J. Parak, T. Hyeon, B. A. Korgel, C. B. Murray and W. Heiss, *ACS Nano*, 2015, **9**, 1012-1057.
7. N. P. Dasgupta, X. Meng, J. W. Elam and A. B. F. Martinson, *Acc. Chem. Res.*, 2015, **48**, 341-348.
8. M. F. L. De Volder, S. H. Tawfick, R. H. Baughman and A. J. Hart, *Science*, 2013, **339**, 535-539.
9. P. Avouris, Z. Chen and V. Perebeinos, *Nat. Nanotech.*, 2007, **2**, 605-615.
10. P. Singh, S. Campidelli, S. Giordani, D. Bonifazi, A. Bianco and M. Prato, *Chem. Soc. Rev.*, 2009, **38**, 2214-2230.
11. A. Hirsch, *Angew. Chem., Int. Ed.*, 2002, **41**, 1853-1859.

12. N. Martín and J.-F. Nierengarten, in *Supramolecular Chemistry of Fullerenes and Carbon Nanotubes*, Wiley-VCH Verlag GmbH & Co. KGaA, 2012.
13. Y.-L. Zhao and J. F. Stoddart, *Acc. Chem. Res.*, 2009, **42**, 1161-1171.
14. S. Iliafar, J. Mittal, D. Vezenov and A. Jagota, *J. Am. Chem. Soc.*, 2014, **136**, 12947-12957.
15. K. Tvrdy, R. M. Jain, R. Han, A. J. Hilmer, T. P. McNicholas and M. S. Strano, *ACS Nano*, 2013, **7**, 1779-1789.
16. D. Umadevi, S. Panigrahi and G. N. Sastry, *Acc. Chem. Res.*, 2014, **47**, 2574-2581.
17. E. M. Pérez and N. Martín, *Chem. Soc. Rev.*, 2015, **44**, 6425-6433.
18. P. Salice, A. Gambarin, N. Daldosso, F. Mancin and E. Menna, *J. Phys. Chem. C*, 2014, **118**, 27028-27038.
19. H. Oh, J. Sim and S.-Y. Ju, *Langmuir*, 2013, **29**, 11154-11162.
20. J. K. Sprafke, S. D. Stranks, J. H. Warner, R. J. Nicholas and H. L. Anderson, *Angew. Chem. Int. Ed.*, 2011, **50**, 2313-2316.
21. K. A. Connors, *Binding Constants: The Measurement of Molecular Complex Stability*, John Wiley & sons, New York, 1987
22. P. Thordarson, *Chem. Soc. Rev.*, 2011, **40**, 1305-1323.
23. I. Langmuir, *J. Am. Chem. Soc.*, 1918, **40**, 1361-1403.
24. A. de Juan, Y. Pouillon, L. Ruiz-González, A. Torres-Pardo, S. Casado, N. Martín, Á. Rubio and E. M. Pérez, *Angew. Chem., Int. Ed.*, 2014, **53**, 5394-5400.
25. A. de Juan and E. M. Pérez, *Nanoscale*, 2013, **5**, 7141-7148.
26. A. López-Moreno and E. M. Pérez, *Chem. Commun.*, 2015, **51**, 5421-5424.
27. A. de Juan, M. Mar Bernal and E. M. Pérez, *ChemPlusChem*, 2015, **80**, 1153-1157.
28. E. M. Pérez and N. Martín, *Pure and Appl. Chem.*, 2010, **82**, 523-533.
29. C. A. Hunter and H. L. Anderson, *Angew. Chem. Int. Ed.*, 2009, **48**, 7488-7499.
30. Y. Baudry, G. Bollot, V. Gorteau, S. Litvinchuk, J. Mareda, M. Nishihara, D. Pasini, F. Perret, D. Ronan, N. Sakai, M. R. Shah, A. Som, N. Sordé, P. Talukdar, D. H. Tran and S. Matile, *Adv. Funct. Mater.*, 2006, **16**, 169-179.
31. E. M. Pérez, L. Sánchez, G. Fernández and N. Martín, *J. Am. Chem. Soc.*, 2006, **128**, 7172-7173.
32. G. Ercolani, *J. Am. Chem. Soc.*, 2003, **125**, 16097-16103.
33. S. Grimme, J. Antony, S. Ehrlich and H. Krieg, *J. Chem. Phys.*, 2010, **132**, 154104.
34. C. Adamo and V. Barone, *J. Chem. Phys.*, 1999, **110**, 6158-6170.
35. S. Grimme, S. Ehrlich and L. Goerigk, *J. Comput. Chem.*, 2011, **32**, 1456-1465.

36. S. Grimme, *Chem. Eur. J.*, 2012, **18**, 9955-9964.
37. M. M. Francl, W. J. Pietro, W. J. Hehre, J. S. Binkley, M. S. Gordon, D. J. DeFrees and J. A. Pople, *J. Chem. Phys.*, 1982, **77**, 3654-3665.
38. S. F. Boys and F. Bernardi, *Mol. Phys.*, 1970, **19**, 553-566.
39. N. Nakashima, Y. Tomonari and H. Murakami, *Chem. Lett.*, 2002, **31**, 638-639.
40. R. J. Chen, Y. Zhang, D. Wang and H. Dai, *J. Am. Chem. Soc.*, 2001, **123**, 3838-3839.

CONCLUSIONS

7. Conclusions

i) We have introduced the mechanical bond as a new tool for the chemical manipulation of SWNTs through the RCM reaction of a family of U-shaped receptors around SWNTs templates.

ii) Direct threading of SWNT by preformed macrocycle and direct absorption of linear receptor experiments have demonstrated that the threading and de-threading processes present a high energy barrier, so are unlikely to occur. The low loading of organic material attached in the threading assay corresponds to receptor absorbed on the sidewall of the SWNTs.

iii) The stability of MINT products is comparable to SWNTs functionalized covalently.

iv) The structure of the SWNTs is preserved upon modification to form MINTs, as observed in the spectroscopic characterization through UV-vis-NIR, fluorescence and Raman techniques.

v) The MINT forming reaction mechanism follows two steps: formation of U-shaped receptor·SWNTs supramolecular complex followed by RCM reaction, as confirmed by thermodynamic and kinetic experiments.

vi) The optimal conditions to the synthesis of MINTs based on exTTF macrocycles were found.

vii) Efficient charge-transfer in the excited state between the electron donor exTTF macrocycles and electron acceptor SWNTs was observed by transient absorption spectroscopy.

viii) The significantly different charge-transfer rate constants and diffusion coefficients between MINTs and supramolecular models reflect the influence of the mechanical bond on the properties of SWNTs.

ix) Theoretical calculations have helped to understand the structure and properties of the MINT derivatives, such as to find suitable SWNTs for their encapsulation for macrocycles with different sizes.

x) A simple method for the determination of association constants between soluble molecules and SWNTs has been developed. The method is sensitive to solvent effects as well as both structure changes of host or/and guest.